


For Reference

NOT TO BE TAKEN FROM THIS ROOM -

Ex LIBRIS
UNIVERSITATIS
ALBERTAENSIS





Digitized by the Internet Archive
in 2022 with funding from
University of Alberta Library

<https://archive.org/details/Hatzinikolas1978>

THE UNIVERSITY OF ALBERTA

CONCRETE MASONRY WALLS

by



MICHAEL HATZINIKOLAS

A THESIS

SUBMITTED TO THE FACULTY OF GRADUATE STUDIES AND RESEARCH
IN PARTIAL FULFILMENT OF THE REQUIREMENTS FOR THE DEGREE
OF DOCTOR OF PHILOSOPHY IN CIVIL ENGINEERING

DEPARTMENT OF CIVIL ENGINEERING

EDMONTON, ALBERTA

FALL, 1978

ABSTRACT

Previous work and available design methods for load bearing masonry walls are reviewed. The experimental study consisted of tests on sixty-eight full scale concrete masonry walls subjected to a number of combinations of vertical loads and end moments. Variables investigated included slenderness ratio (h/t), vertical reinforcement, horizontal reinforcement, type of construction, and grouting procedures.

Measurements recorded during testing included deflections, strains, and vertical deformations.

Theoretical analyses were developed to predict the buckling load of masonry walls and to evaluate their load bearing capacity using a modified moment magnifier method. The effect of joint reinforcement on the load bearing capacity of masonry has been examined.

A procedure for evaluation of tensile and shear bond strength utilizing the centrifugal force is developed and results using this system are reported.

ACKNOWLEDGEMENTS

This investigation was carried out at the Civil Engineering Department of the University of Alberta.

The writer wishes to convey sincere gratitude to his supervisors, Prof. J. Longworth and Dr. J. Warwaruk, for their guidance and support throughout this program.

The contributions of Mr. J. Dawe in the stability aspects are greatly appreciated.

Preparation of the final manuscript was achieved through the excellent assistance of Mrs. L. Haswell in drafting and Mrs. D. Wyman in typing.

Concluding acknowledgement is given to the Alberta Masonry Institute and the National Research Council of Canada for their financial assistance in the course of this doctoral program.

To the President of the Alberta Masonry Institute, Mr. H. Sims, the Executive Director, M.H. Morstead and to Dr. E. Jessop, I extend sincere gratitude for their interest and support in carrying out this study.

TABLE OF CONTENTS

CHAPTER		PAGE
I	INTRODUCTION	1
	1.1 General Remarks	1
	1.2 Object and Scope	2
II	REVIEW OF PREVIOUS WORK AND CURRENT STRENGTH ANALYSIS THEORIES	3
	2.1 Introduction	3
	2.2 Review of Previous Work	4
	2.2.1 Wall Behaviour	4
	2.2.2 Tensile and Shear Bond	8
	2.2.3 Factors Affecting the Strength of Masonry	11
	2.3 Available Strength Analysis Procedures	11
	2.3.1 General	11
	2.3.2 Elastic Analysis of Plain Masonry Walls Eccentrically Loaded	13
	2.3.3 Elastic Analysis of Reinforced Masonry Walls	19
	2.3.3.1 General	19
	2.3.3.2 Reinforced Masonry Wall with the Steel in Compression .	19
	2.3.3.3 Reinforced Masonry Wall with Steel in Tension	21
	2.3.4 Ultimate Strength Analysis	24
III	CODE DESIGN PROCEDURE	30
	3.1 Introduction	30
	3.2 Load Bearing Masonry Wall Design Procedure According to CSA Standard S-304-1977	30

CHAPTER		PAGE
	3.3 Load Bearing Masonry Wall Design Procedure According to the "Uniform Building Code", 1973 Edition	32
	3.4 Load Bearing Masonry Wall Design Procedure According to the "British Standard Code of Practice CP 111-1970"	33
IV	STABILITY OF MASONRY WALLS	35
	4.1 Introduction	35
	4.2 General	35
	4.3 Walls with Pinned Ends and Triangular Initial Deformations	37
	4.4 Straight Walls with Eccentric Load	42
	4.5 Deflection Curve Approach to Stability of Masonry Walls	46
	4.6 Walls with Initial Double Curvature Imperfections	54
	4.7 Reinforced Masonry Walls	62
	4.8 Effect of Tensile Bond to the Critical Load ..	65
	4.9 Application of the Moment-Magnifier Method to Load Bearing Masonry Walls	66
	4.9.1 General	66
	4.9.2 Element of the Method	68
	4.9.3 Application of the Moment-Amplifier Method to Masonry	70
V	EXPERIMENTAL PROGRAM	74
	5.1 Materials	74
	5.1.1 Concrete Block Units	74
	5.1.2 Mortar	74
	5.1.3 Grout	77
	5.1.4 Reinforcing Steel	77

CHAPTER		PAGE
5.2	Test Specimens	80
5.2.1	Prisms	80
5.2.2	Short Walls	80
5.2.3	Full Scale Walls	83
5.3	Instrumentation	86
5.3.1	Prisms and Short Walls	86
5.3.2	Instrumentation of Walls	86
5.4	Test Procedure	87
5.4.1	Prisms	87
5.4.2	Short Walls	88
5.4.3	Full Scale Walls	88
VI	MATERIAL PROPERTIES AND STRENGTH OF PRISMS AND SHORT WALL SPECIMENS	93
6.1	Introduction	93
6.2	Strength and Modulus of Elasticity of Masonry Units	93
6.2.1	Compressive Strength	93
6.3	Properties of Mortar	96
6.3.1	General	96
6.3.2	Plastic Mortar	96
6.3.3	Hardened Mortar	98
6.4	Grout	103
6.4.1	Compressive Strength	103
6.4.2	Bond Between Grout and Masonry Units ..	103
6.5	Compressive Strength of Prisms	105
6.5.1	General	105

CHAPTER		PAGE
	6.5.2 Analytical Evaluation of Compressive Strength of Masonry Prisms	106
	6.5.3 Test Results	115
	6.5.3.1 Two-Block Prisms	115
	6.5.3.2 Short Walls	115
	6.6 Modulus of Elasticity of Hollow Concrete Masonry	119
	6.6.1 General	119
	6.6.2 Theoretical Considerations for Modulus of Elasticity	119
	6.6.3 Experimental Evaluation of Modulus of Elasticity of Hollow Concrete Block Masonry	123
	6.7 Prism and Short Wall Failures	124
	6.8 Effect of Joint Reinforcement on Vertical Load Carrying Capacity	131
	6.9 Capacity of Short Wall Specimens	134
	6.9.1 Specimens Without Vertical Reinforcement	134
	6.9.2 Partially or Fully Grouted Specimens With Vertical Reinforcement	137
	6.10 Stress Distribution in Axially Loaded Masonry	143
VII	FULL SCALE WALL TEST RESULTS	147
	7.1 Introduction	147
	7.2 Axially Loaded Walls	147
	7.3 Eccentrically Loaded Walls	157
	7.3.1 Plain Walls, Single Curvature Bending	157
	7.3.2 Plain Walls in Double Curvature Bending	161

CHAPTER		PAGE
	7.3.3 Vertically Reinforced Walls, Single Curvature Bending	171
	7.3.4 Vertically Reinforced Walls, Double Curvature Bending	179
	7.4 Effect of Eccentricities on the Load Carrying Capacity of Masonry Walls	184
	7.5 Masonry Strains	188
	7.6 Flexural Rigidity of Masonry	191
VIII	ANALYSIS AND SYNTHESIS OF TEST RESULTS	196
	8.1 Introduction	196
	8.2 Constitutive Relations	196
	8.3 Analysis for Slender Column Effects	198
	8.4 Application of the Moment Magnifier Method to Plain Masonry Walls	199
	8.4.1 Single Curvature Bending, Equal End Eccentricities	199
	8.4.2 Single Curvature Bending, Unequal End Eccentricities	203
	8.4.3 Double Curvature Bending	205
	8.5 Application of the Moment Magnifier Method of Vertically Reinforced Masonry Walls	209
	8.5.1 Single Curvature Bending, Equal End Eccentricities	209
	8.5.2 Double Curvature Bending, Equal End Eccentricities	213
IX	SUMMARY, CONCLUSIONS AND RECOMMENDATIONS	215
	9.1 Summary	215
	9.2 Conclusions	215
	9.3 Recommendations	219
REFERENCES	220

CHAPTER		PAGE
APPENDIX A	SOLUTION OF THE DIFFERENTIAL EQUATIONS FOR WALL WITHOUT TENSILE STRENGTH	224
APPENDIX B	EVALUATION OF INTERPOLATING FUNCTIONS AND COMPUTER PROGRAM FOR EVALUATING THE BUCKLING LOAD FOR STEPPED COLUMNS	230
APPENDIX C	THE USE OF CENTRIFUGAL FORCE FOR DETERMINING THE TENSILE AND SHEAR BOND OF MASONRY	241
	C.1 Introduction	242
	C.2 Existing Methods of Testing	242
	C.3 Development of Centrifugal Testing Procedure	243
	C.4 Limitations	247
	C.5 Testing	247
	C.5.a Test Equipment	247
	C.5.b Test Specimens	250
	C.5.c Test Procedure	252
	C.6 Test Results	256
APPENDIX D	COMPUTER INTERACTION DIAGRAM	262
	D.1 General	263
	D.2 Basic Assumptions for Analysis	263
	D.3 Limitations	264
	D.4 Input Data	265
	D.5 List of Data	265

LIST OF TABLES

TABLE		PAGE
4.1	Buckling Coefficients for Step Columns or Walls	63
5.1	Dimensions and Physical Properties of Concrete Block Units	76
5.2	Particle Size Distribution of Masonry Sand	76
5.3	Short Wall Specimens	82
5.4	Full Scale Walls	85
6.1	Compressive Strength of Mortar 2 x 2 x 2 in. Cubes...	102
6.2	Test Results for Axially Loaded Two Block Prisms	116
6.3	Test Results for Axially Loaded Short Walls	117
6.4	Test Results for Eccentrically Loaded Short Walls ..	118
6.5	Test Results for Axially Loaded Reinforced Short Walls and Grouted Short Walls	120
6.6	Coefficient "a" of Apparent Increase in Strength Due to Flexure	136
7.1	Test Results for Axially Loaded Walls	148
7.2	Test Results for Plain Walls Tested in Single Curvature Bending	159
7.3	Test Results for Walls Without Vertical Reinforce- ment and Tested in Double Curvature Bending	165
7.4	Test Results for Vertically Reinforced Walls Tested in Single Curvature Bending	172
7.5	Test Results for Reinforced Walls Tested in Double Curvature	181
C.1	Tensile Bond Strength of Type S Mortar and Concrete Block	257
C.2	Tensile Bond Strength of Grout and Concrete Block ..	259
C.3	Results from a Statistical Analysis of Test Results	260
C.4	Tensile Bond Test Data	261

LIST OF FIGURES

FIGURE	PAGE
2.1 Shear Box Test Arrangement	10
2.2 Bond Tension Test Arrangement	12
2.3 Stress Distribution at Failure Under Various Vertical Load and Moment Combinations	14
2.4 Stress Distribution for a Solid Cross-Section Having Zero Tensile Strength and the Load Applied Outside the kern	17
2.5 Stress Due to Axial Load and Moment Acting on a Reinforced Wall Section with Total Cross-Section in Compression	20
2.6 Compression on Part of Cross-Section of Reinforced Wall with Steel in Compression	22
2.7 Stress Distribution for Reinforced Wall Section with Steel in Tension	23
2.8 Strains and Stresses in Reinforced Masonry for Ultimate Condition	26
2.9 Strain and Strain Distribution for Reinforced Section in Compression	29
4.1 Concentrically Loaded Wall with Triangular Initial Deflection	39
4.2 Maximum Load for Wall with Initial Triangular Deflection	43
4.3 Deflected Shape of Eccentrically Loaded Wall	44
4.4 Maximum Load for Eccentrically Loaded Wall	47
4.5 Cracked and Effective Cross-Section of Eccentrically Loaded Wall	48
4.6 Equilibrium Conditions on Cross-Section	49
4.7 Deflection Curve of Deformed Compression Face	51
4.8 Curvature of Deflected Wall	51

FIGURE	PAGE
4.9 Wall Bent in Double Curvature	56
4.10 Extent of Cracking of Wall with Double Curvature Imperfections Bend in the First Buckling Mode	57
4.11 Equivalent Stepped Column Section for Evaluation of the Buckling Load	59
4.12 Effect of Tensile Bond to the Uncracked Section	67
4.13 Deflections of Eccentrically Loaded Masonry Walls	72
5.1 Masonry Units	75
5.2 Idealized Stress-Strain Relation for Reinforcing Steel	78
5.3 Truss Type Joint Reinforcement	79
5.4 Prism and Short Wall Specimens	81
6.1 Stress-Strain Relation for Solid Concrete Masonry Units	97
6.2 Schematic Diagram of Bond Test Apparatus	99
6.3 Tensile and Shear Bond Test Specimens	101
6.4 Stress-Strain Relation for Type S Mortar Cylinders ...	104
6.5 Block and Mortar Stresses Due to Applied Compressive Load	107
6.6 Relation Between Tensile and Compressive Stresses in a Masonry Unit at Failure	108
6.7 Relation Between Prism Strength and Thickness of Components	114
6.8 Test Specimen for Evaluation of the Elasticity Modulus	121
6.9 Stress Strain Relation for Hollow Concrete Block Masonry	125
6.10 Stress Distribution in a Uniformly Loaded Plate with Rigid Inclusion	132
6.11 Capacity of Short Wall	135

FIGURE	PAGE
6.12 Forces Acting on the Cross-Section of an Eccentrically Loaded Wall Portion	138
6.13 Forces Acting on Eccentrically Loaded Wall Segment	139
6.14 Grid Used in Finite Element Analysis	144
6.15 Lateral Stresses in Axially Loaded Masonry	145
7.1 Deflected Shape of Wall A1	151
7.2 Deflected Shape of Wall C2	153
7.3 Reinforcement Strain vs Load for Wall C2	154
7.4 Reinforcement Strain vs Load for Wall I1	155
7.5 Deflected Shape of Wall A2	162
7.6 Axial Deformation vs Load for Series A	163
7.7 Center-Line Deflection vs Vertical Load for Series A .	164
7.8 Deflected Shape of Wall E1	168
7.9 Deflected Shape of Wall E5	169
7.10 Axial Deformation vs Vertical Load for Series E	170
7.11 Deflected Shape of Wall L3	173
7.12 Reinforcement Strains at Mid-Height for Wall C3	177
7.13 Reinforcement Strains at Mid-Height for Wall H2	178
7.14 Influence of Location of Strain Gauge on the Measured Strain	180
7.15 Deflected Shape of Wall J4	185
7.16 Reinforcement Strains in Wall J4	186
7.17 Vertical Load vs Eccentricity for Plain and Reinforced Walls in Double and Single Curvature	187
7.18 Masonry Strains for Wall B5	189
7.19 Masonry Strains for Wall F1	190

FIGURE	PAGE
7.20 Masonry Strains for Wall H1	192
7.21 Variation of Flexural Rigidity with Eccentricity	194
8.1 Effects of Slenderness on the Strength of Masonry Walls in Single Curvature Bending	201
8.2 Effects of Slenderness on the Strength of Masonry Walls in Single Curvature Eccentricity	204
8.3 Effect of Slenderness on the Strength of Masonry Walls in Double Curvature Bending	206
8.4 Interaction Diagram Modified for Slenderness for a Cross-Section Reinforced with 3-#3 Bars	210
8.5 Interaction Diagram Modified for Slenderness for a Cross-Section Reinforced with 3-#9 Bars	212
A.1 Instability Failure of Column Without Tensile Strength	229
B.1 Interpolating Functions	232
C.1 Schematic Diagram of Test Apparatus	245
C.2 Test Specimens	251
D.1 Input Dimensions	267

LIST OF PLATES

PLATE		PAGE
5.1	Typical Wall Construction	84
5.2	Test Wall Support	89
5.3	Device Used to Transport Wall and Prism Specimens	91
5.4	Wall in Position for Testing	92
6.1	Test Set-up for Determining Compressive Strength And Load Deformation Characteristics of Solid Concrete Masonry Units	95
6.2	Failure Mode of a Two-Block Fully-Bedded Prism	126
6.3	Typical Failures of Prisms with No. 9 Gauge Wire Joint Reinforcement	127
6.4	Failure Mode of Axially Loaded Concrete Block Masonry Specimen	128
6.5	Detailed View of Tensile Splitting Failure	129
6.6	Failures of Short Walls Tested with Pinned Ends	130
6.7	Failure of Short Wall Specimen with 3-#9 Vertical Bars	141
6.8	Failure of Short Wall Specimens with 3-#3 Vertical Bars	142
7.1	Failures of Axially Loaded Plain Walls	150
7.2	Failures of Axially Loaded Reinforced Walls	152
7.3	Grouted Core Showing Mortar Penetration	158
7.4	Wall A2 During Tests	160
7.5	Wall A3 at Failure	160
7.6	Failure of Plain Wall in Loaded in Double Curvature	166
7.7	Wall F2 After Failure	166
7.8	Failure of Wall Loaded in Double Curvature	167

PLATE	PAGE
7.9 Wall L5 During Testing	174
7.10 Typical Failure of Reinforced Wall Tested in Single Curvature with Eccentricities Larger than $t/3$	175
7.11 Failure of Wall B2	176
7.12 Failure of Wall B3	176
7.13 Failure of Wall J1 (Crushing at Mid-Height)	182
7.14 Failure of Wall J2 (Bending in Upper Portion)	182
7.15 Failure of Wall J3 (Bending in Upper Portion)	183
7.16 Failure of Wall K1 (Bending in Upper Portion)	183
C.1 View of the Testing Machine	248
C.2 Compartment for Tensile Bond Test	249
C.3 Tensile Bond Specimen After Failure	253
C.4 Specimen for Tensile Bond Strength Test	254
C.5 Specimen for Grout Tensile Bond After Testing	255

List of Symbols

Dimensions and Section Properties

A	= gross section area
a	= depth of the equivalent rectangular block = $k_b C$
A_h	= area of horizontal steel per unit length of wall
A_n	= net area of cross-section
A_s	= area of reinforcing steel
A_v	= area of vertical steel per unit length of wall
b	= width of section under consideration
c	= depth to the neutral axis
e	= eccentricity
e'	= $t'/6$ eccentricity of the line of thrust
e_b	= eccentricity at bottom of wall
e_c	= initial deflection
e_k	= kern eccentricity
e_p	= eccentricity of applied load
e_t	= eccentricity at top of wall
h	= height of wall
I	= moment of inertia
I_n	= net moment of inertia about the centroidal
I_o	= gross moment of inertia
I_t	= reduced moment of inertia of top section
ℓ	= length of a section
t	= thickness of cross-section
t'	= reduced depth

t_b	= height of block
t_m	= height (thickness) of mortar joint
u	= distance from line of thrust to the compression face
u_o	= minimum distance from the line of thrust to the compression face
ζ	= distance from location of zero stress to the point where the stress is equal to the tensile strength
ξ	= distance from compression fiber to the location of zero stress

Material Properties

E	= elastic modulus
E_b	= modulus of elasticity of concrete blocks
E_j	= modulus of elasticity of mortar joint
E_m	= elastic modulus of masonry
E_s	= elastic modulus of steel
ν_b	= Poisson's ratio of block
ν_j	= Poisson's ratio

Forces and Moments

M	= moment
M_b	= smaller end moment
M_{max}	= maximum moment
M_t	= larger end moment
M_u	= ultimate moment
P	= applied load
P_a	= allowable vertical load
P_{cr}	= critical or buckling load

P_u = ultimate vertical load

Stresses and Strains

F = centrifugal force

f = stress at outer fiber

f_a = stress due to applied axial load

f_b = stress due to applied moment

f'_b = ultimate compressive strength of concrete block unit

f_m = allowable stress in masonry

f'_m = ultimate uniaxial compressive strength in masonry

f_{max} = maximum stress at outer fiber

f_{min} = minimum stress at outer fiber

f_s = steel stress

f_y = yield stress of reinforcing steel

ϵ = strain

ϵ_m = masonry strain at failure

ϵ_{max} = maximum strain in masonry

ϵ_{min} = minimum strain in masonry

ϵ_s = steel strain

ϵ_{xb} = extensional strain in X direction in block

ϵ_y = yield strain of steel

ϵ_{zb} = extensional strain in Y direction in block

σ_o = average stress at the face of the element

σ_{cb} = uniaxial compression strength of block

σ_{cm} = uniaxial compression strength of mortar

σ_{tb} = uniaxial tensile strength of block

σ_x = tensile stress in X direction

σ_{xm}	= lateral compressive stress in the mortar joint
σ_{xyo}	= shearing resistance of mortar for zero normal stress
σ_{xy}	= maximum shearing stress
σ_y	= normal stress on cross-section
σ_z	= tensile stress in Z direction

Miscellaneous

C_e	= eccentricity coefficient
C_s	= slenderness coefficient
C_m	= $0.6 + 0.4 (M_b/M_t)$
g	= factor relating to the depth of cracked section
k_b	= factor relating to equivalent compressive rectangular block = 0.8 for $f_m \leq 4000$ psi
m	= mass
R	= radius of rotation or of curvature
ω	= angular velocity
X	= distance from the center of the wall towards the support
X_c	= distance from support to the point of inflection
y	= the buckled shape
w	= unit weight
α	= $e_t/(e_t + e_b)$
α_m	= $h\sqrt{P/EI}$
λ	= buckling coefficient
Δ, δ	= deflection
η	= E_s/E_m
κ	= $1/t$ distance from the compression face to the centroid of steel

ρ = percent of reinforcing steel = A_s/b_t

μ = coefficient of friction

π_B = total potential energy

CHAPTER I

Introduction

1.1 General Remarks

The use of concrete blocks as a building material has increased at a constant rate over the last fifteen years in almost every large city in Canada. The use of blocks is not a new idea. It is as old as the ancient megalithic structures of Egypt, Greece and Mesopotamia. The interest in masonry is increasing because of the economy of construction and the pleasing appearance presented by masonry structures.

However, today's structures are complicated and economic reasons demand a clear understanding of the behavior of the structure. The thickness of load bearing masonry walls has decreased over the years and where very thick walls were once used an eight inch wall may now perform the same function.

Progress in the design and construction of modern masonry buildings has resulted in the creation of a number of outstanding projects. Masonry buildings varying in size and architectural aspect have been designed and erected in many parts of the world. These structures include a 23-storey apartment building in Winnipeg, Manitoba; a 20-storey apartment in Denver, Colorado; an 18-storey building in Zurich, Switzerland and many more throughout Europe, the U.S.A., Canada and South America.

A considerable amount of experimental and theoretical work has been carried out with emphasis on the behavior of plain masonry walls under combined vertical load and moment. However, little research has been carried out on the behavior of reinforced masonry walls under similar load conditions. It is hoped that the theoretical findings and experimental data presented in this study will complement other current research programs and assist in the formulation of design rules comparable with those existing for concrete and steel.

1.2 Object and Scope

The main objectives of this study are:

- a) To examine the commonly used theories for evaluating the strength of plain and reinforced concrete block masonry.
- b) To observe the behavior, cracking pattern, and ultimate strength of plain and reinforced masonry.
- c) To examine factors affecting the behavior of plain and reinforced masonry, such as tensile bond and horizontal joint reinforcement.
- d) To examine the stability of masonry walls.
- e) To develop analysis for predicting the ultimate strength of masonry walls under various combinations of loading.

CHAPTER II

Review of Previous Work and Current Strength Analysis Theories

2.1 Introduction

The design of load bearing masonry walls in North America is based on codes containing empirical values for allowable stresses and other factors. These conservative and somewhat arbitrary values have been carried over from the time when the structural behavior of masonry wall construction was not as well understood as it is today. However, some of these building codes now permit the design of masonry walls by rational methods, such as working stress. Only quite recently has any progress been made in the use of structural masonry. Traditionally, masonry has not been treated as an engineered material and its use has been hampered by outmoded regulations, resulting in buildings with excessively thick walls; totally uneconomical beyond a two or three storey structure. However, research work started in a number of countries in Europe and North America and by the 1950's the Swiss had demonstrated the potential of engineered masonry.

Since then, similar developments have taken place in many other countries and a substantial amount of research work has resulted in the evolution of increasingly sophisticated design guides and codes of practice. Current procedures for the design of

masonry walls and a brief review of research work, in the same related areas, are presented in this chapter.

2.2 Review of Previous Work

2.2.1 Wall Behavior

Research on plain masonry walls under axial and eccentric loads has been carried out over the years in many institutions. A series of tests at the Swiss Federal Institute for Testing Materials and Research in Dübendorf, extending over twenty years, has yielded a better understanding of the behaviour of masonry walls. This work made possible the construction of buildings up to 18 storeys high and of a 16-storey building with bearing walls measuring 5-7/8" in thickness.

The fundamentals of the behaviour of masonry walls under combined loading were established by Angervo¹ in 1954 and by Chapman and Slatford² in 1957 with the solution of the basic differential equation for a column with no tensile strength. Factors affecting the strength of masonry walls, such as the strengths of the masonry unit and the media connecting the units, have been the subject of studies carried out by many investigators. Most notable are the works of Hilsdorf³, Francis⁴ *et al* and Hendry⁵. Hilsdorf expressed the failure criterion for masonry by means of a straight line relationship between lateral tension and local compression. The second attempt to quantitatively predict the compressive strength of masonry prisms by Francis *et al* was based on strain considerations. Both Hilsdorf and Francis related the strength of the assembly to the strength of the unit and the mortar. Their relations include

the effects of the unit height and the thickness of the joint. The effects of the loading condition on the strength of the assembly have been the subject of an extensive study carried out by Hendry.⁶ The effects of slenderness on the capacity of brick masonry walls have been experimentally investigated by Hendry⁶, Fattal⁷ and Yokel⁸. In 1971 Shahlin⁹ suggested that for normal strength materials and a ratio of effective height to least lateral dimension (h/t) of less than 30, the axial load capacity of masonry walls becomes a stress problem whereas buckling is a failure mode in masonry for slenderness ratios greater than 30. The effect of slenderness ratio on the lateral tensile stresses within the wall was examined by Smith¹⁰ using a finite element method.

In 1971 Yokel¹¹ *et al* carried out a series of tests on a number of masonry walls, using both brick and concrete masonry. They suggested that the load carrying capacity of masonry walls can be predicted using the moment magnifier method. The work also concluded that rational analysis can be used to determine a lower-limit for the strength of a shear masonry wall under eccentric vertical load. The range of eccentricities in their experimental program carried from zero to the kern. A small number of 4 inch thick concrete masonry walls were tested by Drysdale¹² *et al* who concluded that the present method of designing walls had a very high safety factor. The study concluded that the slenderness coefficients recommended for use by CSA Standard S-304-M¹³, do not provide a consistent means of accounting for strength reduction as it is influenced by slenderness. According to the above study, formulation of a more rational design procedure is required to permit the

advantage of the extra capacity which exists in many loading conditions. Drysdale¹² assumed that the curvature of an eccentrically loaded wall can be approximated by a sine curve. However, the actual curvature is a function of many factors; the most important ones being the initial imperfections, type of loading, and crack formation.

The behavior of concrete block masonry was the subject of an experimental program carried out by Cranston and Roberts.¹⁴ In their work, tests on eccentrically-loaded non-reinforced walls and couplet specimens are reported and a simple theoretical approach for solid block masonry is derived; the same study presents a method of predicting wall strength. Also described are additional tests on reinforced masonry sections subjected to lateral loading only and the simple ultimate load theory used for reinforced concrete is shown to give a good indication of the ultimate strength of the sections. The effect of employing different values of the partial factor of safety for strength of the masonry is considered by Cranston and Roberts¹⁴. Some of their studies indicated that present design procedures using allowable stresses result in uneconomical design and a variable factor of safety.

There is a lack of experimental data on the compressive strength of masonry walls especially of concrete masonry walls with eccentricities greater than one-third the wall thickness measured from the centroidal axis. Consequently, in current recommended design procedures and building code requirements for engineered masonry, such as CSA Standard S-304-M, eccentricities up to one-third of the wall thickness are treated by one method, while eccentricities

exceeding one-third are covered by a special provision. Yorkdale and Allen¹⁵ reported on tests at the Brick Institute of America on 12 brick walls tested with eccentricities $1/2$ and $5/12$ the wall thickness. They concluded that tensile stresses at the top quarter point of both short and tall walls, loaded with an eccentricity of $5/12$ of the thickness, were sufficiently large to create cracks in the bed joints at relatively low loads.

Walls tested with load eccentricity of $t/2$ and slenderness ratio of 10 reported by Yorkdale and Allen developed tensile strains and cracking at relatively low loads at the top quarter point of the height. For walls with larger slenderness ratios cracks were formed in the top four courses. Yorkdale and Allen recommended the use of steel reinforcement in the top quarter of the wall height for walls loaded at eccentricities in excess of $1/3$ the wall thickness. No justification of their recommendation is given; however, it is obvious from their testing procedure (zero eccentricity at the bottom of the wall) that maximum moment occurs at the top of the specimens.

The overall behavior of masonry walls is, as stated previously, a function of the properties of the elements that make up the wall, namely masonry units and mortars. The most important parameter is the modulus of elasticity. There seems to be some confusion in existing literature about this important parameter. For the same type of construction and materials, values of modulus of elasticity quoted in literature vary from 600 - 1000 times the compressive strength. Shahlin⁹ presented an analytical approach for evaluating the modulus of elasticity based on elastic considerations.

Turkstra¹⁶ used a regression analysis to express the modulus of elasticity as a function of measured strains and uniaxial strength, the same approach was used by Drysdale *et al*¹².

Yokel and Dikkers¹¹ recommended a rigidity factor (product of moment of inertia and modulus of elasticity) defined by a function of the applied axial load in a similar manner as used in reinforced concrete columns. This approach however is limited to eccentricities within the kern.

2.2.2 Tensile and Shear Bond

The bond between unit and mortar is a complex parameter depending on such factors as surface roughness, initial rate of absorption, workmanship, type of mortar, (as it relates to cement content), time elapsed between mixing, curing and usage of mortar. The interaction between masonry units and the bonding agent is a subject that has been investigated using a variety of testing procedures.

The most common procedure used to evaluate tensile bond is the modulus of rupture test, which utilizes a small beam tested under third point loading. The modulus of rupture is calculated by assuming a linear stress distribution. However, finite element analysis indicates that the stress distribution is not linear. In testing cross brick couplets* involving one mortar joint, Polyakov¹⁷ found difficulties in fixing the application of load in the center of the couplet, and also in laying the bricks. He

* Test specimen consisting of two masonry units and one mortar joint.

made the assembly in the form of a cube of two halves mortared together and then pulled apart by special clamps.

Other research workers, Pearson¹⁸ and Cumpf¹⁹, found the couplet test quite satisfactory, and it is now generally accepted that cross-brick couplets give satisfactory results for bond in tension. In calculating the bond from this type of test, uniform stress distribution is assumed over the bonded area. However, this may not be valid, especially when the specimen is short as in the case of specimens involving two bricks and one mortar joint. Small misalignment of the load will introduce a moment which will further alter the stress distribution. A cross brick couplet test therefore is not entirely reliable in evaluating the tensile bond strength.

The resistance of masonry to shearing forces is a function of the precompressive force acting on the masonry. To determine the effect of precompression on the shear strength of couplets Hendry^{20,21} *et al* performed a series of tests with equipment shown in Figure 2.1, using varying compressive load. The authors assumed that the total shear strength of the couplets consisted of bond shear and frictional resistance and may be represented by:

$$\sigma_{xy} = \sigma_{xy_0} + \mu\sigma_y$$

where

μ = the coefficient of friction

σ_{xy_0} = the shearing resistance of mortar joint for zero normal stress.

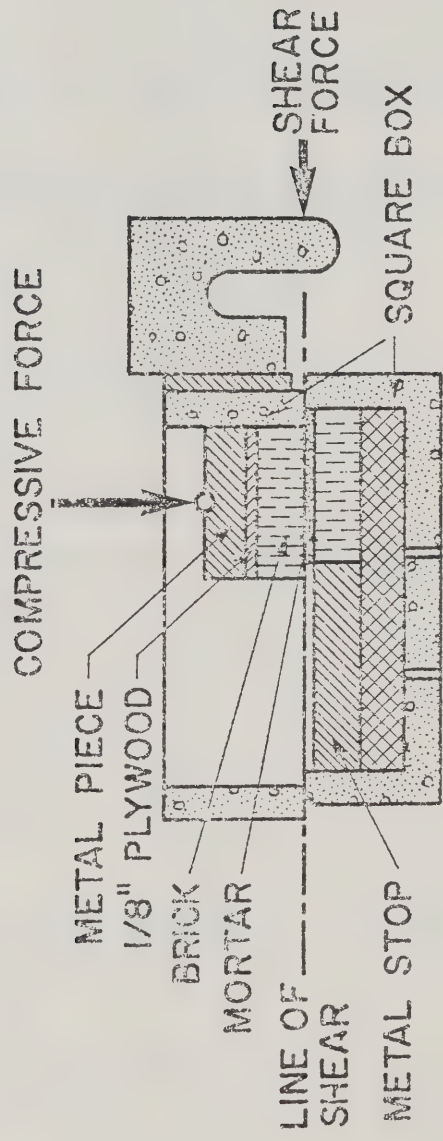


FIG. 2.1 Shear Box Test Arrangement

σ_{xy} = the maximum shearing stress

σ_y = the normal stress

Results of tests carried out by the writer at the University of Manitoba were in agreement with the results obtained by Hendry^{20,21}. Test results for bond tension tests obtained using the apparatus shown in Figure 2.2 were also obtained by Hendry *et al.*

2.2.3 Factors Affecting the Strength of Masonry

Experimental results are meagre with regard to other factors affecting the strength of masonry assemblages, such as masonry unit strength, mortar, joint thickness, and workmanship. As with other building materials, the strength of masonry is affected by workmanship. The deep furrowing of bed joints and the partial filling of vertical head and collar joints are practices that reduce strength to some degree. Thick joints will also lower strength. There is little or no data available from which to derive definite functional relations by statistical methods for the influence of the above parameters.

2.3 Available Strength Analysis Procedures

2.3.1 General

Masonry buildings are, at present, designed in western countries by working or permissible stress analysis. Walls are normally designed for allowable stress by accepted principles of mechanics, with no allowance for moment transfer at floor to wall connection. Loads acting on the walls include live and dead floor loads and self-weight and lateral wind load. Additional stresses

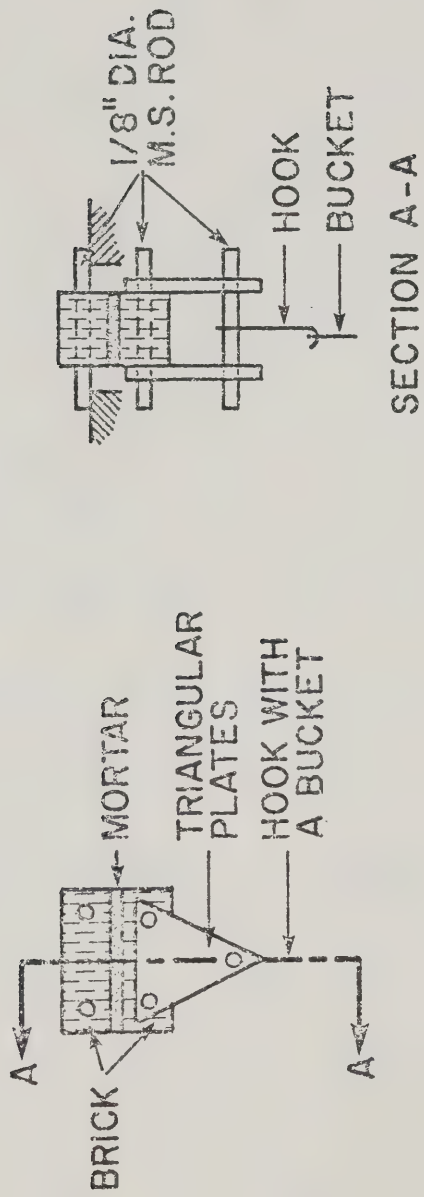


FIG. 2.2 Bond Tension Test Arrangement

result from temperature variations, characteristic dimensional changes of the materials, deflection and rotational components in contact or built into the masonry, foundation movements, and other specific conditions of loading. The net result is a wall with axial and eccentric loads applied at their ends, combined with lateral loads. All these stress conditions are superimposed to establish statically equivalent loads at an approximate eccentricity. Component dimension are then assumed and the stresses calculated. The stresses are then checked against the allowable values based on a combination of unit strength and mortar type, or based on actual prism tests of masonry. The decision to use plain or reinforced masonry depends on the magnitude of the loads. The available design theories for plain and reinforced walls are examined in the following section.

2.3.2 Elastic Analysis of Plain Masonry Walls Eccentrically Loaded

The load-carrying capacity of a plain masonry wall cross-section subjected to an eccentric load can be determined if the tensile and compressive strength of the masonry, as well as the stress distribution on the cross-section at failure, are known. The stress distribution, in turn, depends on the stress-strain properties of the masonry. If the assumption is made that the wall does not warp in flexure and that a linear stress-strain relationship exists for masonry up to failure, then the stress distribution under the action of the eccentric load will be as shown in Figure 2.3 for various vertical load and moment combinations.

From this figure it is obvious that failure will occur when either the compressive or the tensile strength of the masonry

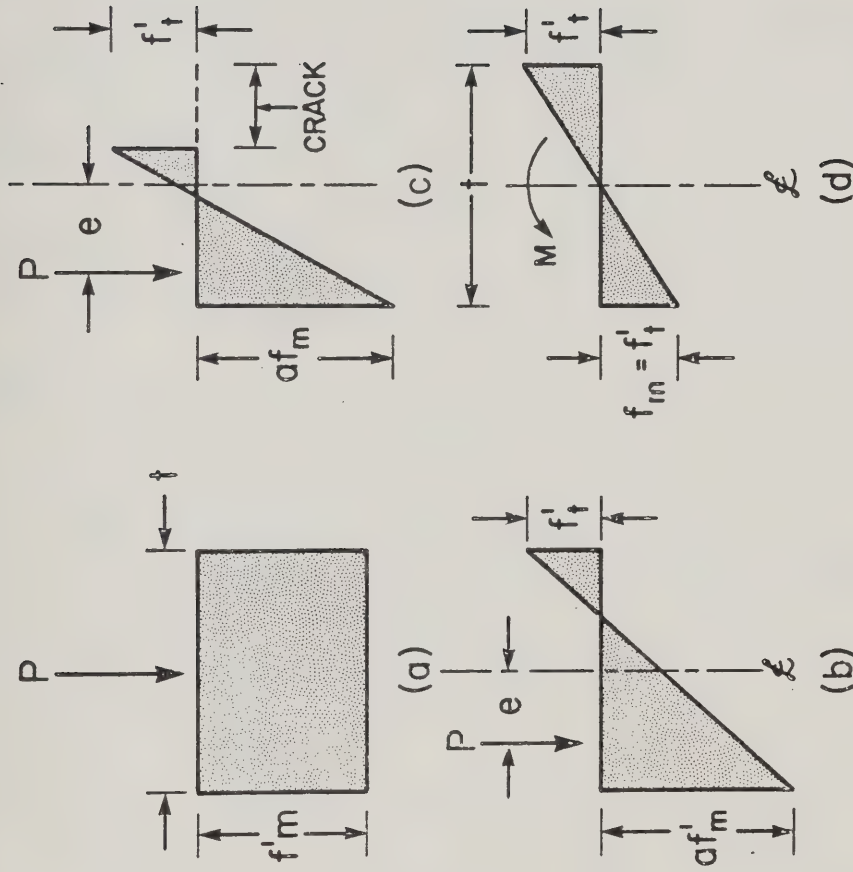


FIG. 2.3 Stress Distributions at Failure Under
Various Vertical Load and Moment Combinations

is reached. These types of failures are illustrated in Figure 2.3. Figure 2.3c shows a condition where the tensile strength is reached over a portion of the wall which then becomes ineffective. This case will not be included in this analysis for, at that stage, the wall will be cracked extensively and, if unreinforced, will not satisfy serviceability.

The stresses at the opposite faces of a cross-section can be obtained using superposition of the flexural and axial stresses using the relation:

$$f = \frac{P}{A_n} + \frac{Pet}{2I_n} \dots\dots\dots 2.1$$

where

f = stress at outer fiber

A_n = net area of cross-section

I_n = moment of inertia about the centroidal axis of net cross-section

e = eccentricity of applied load

P = applied load

t = thickness of cross-section

In Equation 2.1, f and P are assumed positive when compressive. If the tensile strength of the masonry is assumed zero, then Equation 2.1 is valid only when the eccentricity of the load is less or equal to the kern eccentricity, since a load applied at the kern point produces zero stress in one of the outer fibers of the section.

The magnitude of the eccentricity can be obtained from equation 2.1 as:

$$e_K = \frac{2I_n}{A_n t} \dots\dots\dots 2.2$$

For solid rectangular sections Equations 2.1 and 2.2 assume the simpler form:

$$f_{\max} = \frac{P}{A} \left[1 + \frac{6e}{t} \right] \dots\dots\dots 2.3$$

$$f_{\min} = \frac{P}{A} \left[1 - \frac{6e}{t} \right] \dots\dots\dots 2.4$$

$$e_K = \frac{t}{6} \dots\dots\dots 2.5$$

where

f_{\max} = maximum stress at outer fiber

f_{\min} = minimum stress at outer fiber

For vertical loads applied at eccentricities greater than the kern eccentricity and for zero tensile strength, the stress distribution will be as shown in Figure 2.4. In this case the maximum stress for a solid rectangular cross section and linear stress distribution is given by:

$$f_{\max} = \frac{4}{3} \frac{P}{A(1 - 2e/t)} \dots\dots\dots 2.6$$

Equation 2.6 is derived by considering equilibrium as follows:

Consider a wall section of length ℓ and thickness t such that

$$A = \ell t$$

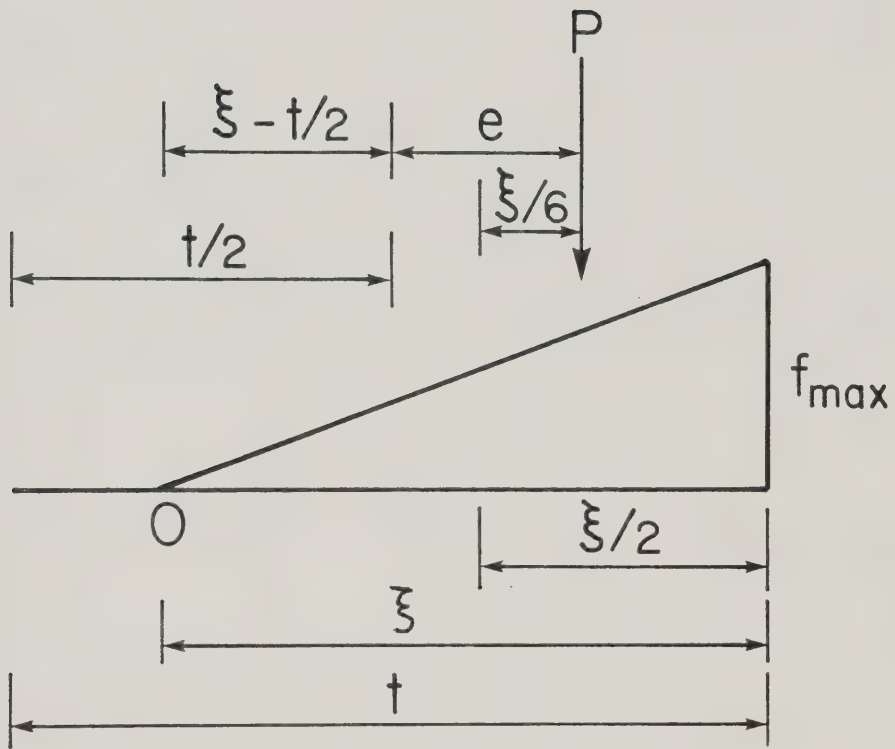


FIG. 2.4 Stress Distribution for a Solid Cross-Section Having Zero Tensile Strength and the Load Applied Outside the kern

Moment equilibrium about point 0 of Figure 2.4 yields the following relations:

$$P \left(e + \xi - \frac{t}{2} \right) = \frac{2}{3} \xi f_{\max} \frac{1}{2} b \frac{A}{t} \dots\dots\dots 2.7$$

By considering force equilibrium and referring to Figure 2.4

$$\frac{1}{2} t \xi A f_{\max} = P \quad \text{or}$$

$$\xi = \frac{2tP}{Af_{\max}} \dots\dots\dots 2.8$$

substituting ξ from Equation 2.8 into Equation 2.7 the following relations are obtained

$$P \left(e + \frac{2tP}{Af_{\max}} - \frac{t}{2} \right) = \frac{4}{3} \frac{tP^2}{Af_{\max}} \quad \text{or}$$

$$e + \frac{2tP}{Af_{\max}} - \frac{t}{2} = \frac{4}{3} \frac{t}{A} \frac{P}{f_{\max}} \quad \text{or}$$

$$f_{\max} \left[e - \frac{t}{2} \right] = \frac{4}{3} t \frac{P}{A} - \frac{2tP}{A} \quad \text{or}$$

$$f_{\max} = \frac{P}{A} \left[\frac{-2/3 t}{e - t/2} \right]$$

which is an alternative form of Equation 2.6.

2.3.3 Elastic Analysis of Reinforced Masonry Walls

2.3.3.1 General

Many applications arise in practice where masonry walls must be reinforced in order to improve their load bearing capacity, to alter their load deformation characteristics, to improve ductility, or to increase their moment resistance. Walls are often subjected to bending moment in addition to axial load. In analyzing such walls by elastic theory there are two separate cases to be considered: firstly, where the eccentricity of the load is so small that no tensile stress is developed in the member and secondly where the eccentricity produces significant tension on a portion of the cross-section and the wall is assumed to be cracked. If P is the axial load and M is the applied moment, it is convenient to express the effect as equivalent to a load P acting at an eccentricity e from the center or the centroid of the wall such that $e = \frac{M}{P}$. The same assumptions as for plain walls are made in deriving the relations for reinforced walls, namely: at any cross-section, plane sections remain plane and the reinforcement is the only effective tensile component.

2.3.3.2 Reinforced Masonry Wall with the Steel in Compression

Two stress conditions exist within this loading case:

- a) compression on total cross-section,
- b) compression on part of the cross-section.

Figure 2.5 shows the stress distribution on the cross-section for condition (a). From this figure the following equations can be obtained:

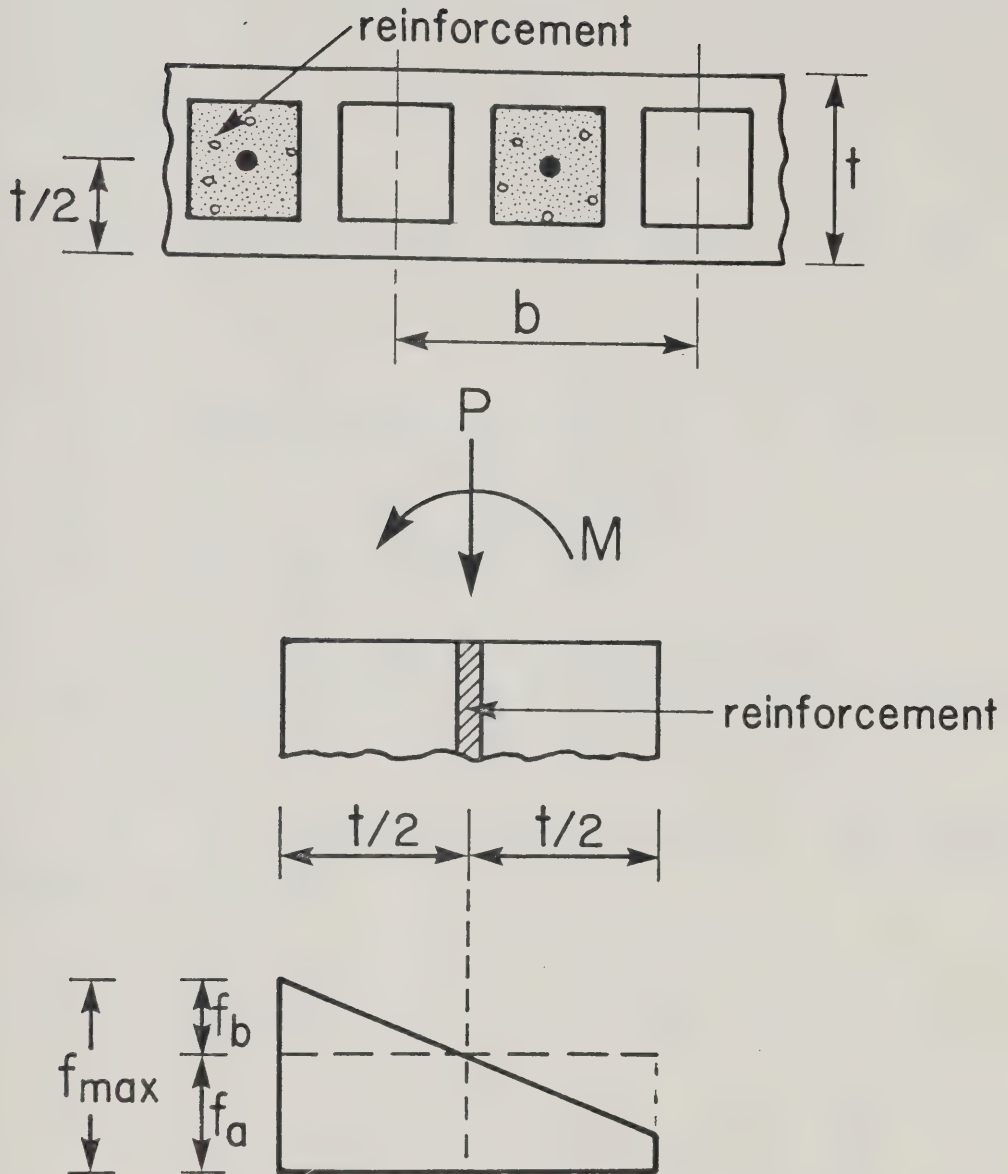


FIG. 2.5 Stress Due to Axial Load and Moment Acting on a Reinforced Wall Section with Total Cross-Section in Compression

$$P = b t f_a \dots\dots\dots 2.9$$

$$M = \frac{1}{2} t b (f_{\max} - f_a) \left(\frac{t}{2} - \frac{t}{3} \right)$$

$$= \frac{1}{12} b t^2 (f_{\max} - f_a) \dots\dots\dots 2.10$$

where

b = distance between reinforcing bars

f_a = stress due to applied axial load

f_b = stress due to applied moment

In Equations 2.9 and 2.10 the effect of reinforcement has been neglected. This simplification does not alter the results significantly.

Assuming that the stress distribution resulting from the applied axial load and moment is as shown in Figure 2.6 the following relations can be derived:

$$P = \frac{1}{2} f_{\max} b g t \dots\dots\dots 2.11$$

$$M = \frac{1}{2} f_{\max} b g t \left(\frac{t}{2} - g \frac{t}{3} \right) = \frac{1}{12} f_{\max} b g t^2 (3 - 2g)$$

$$\dots\dots\dots 2.12$$

where

g = factor relating to the depth of the cracked section.

2.3.3.3 Reinforced Masonry Wall with Steel in Tension

If the applied loads are such as to produce tension in the steel, the stress distribution will be as shown in Figure 2.7.

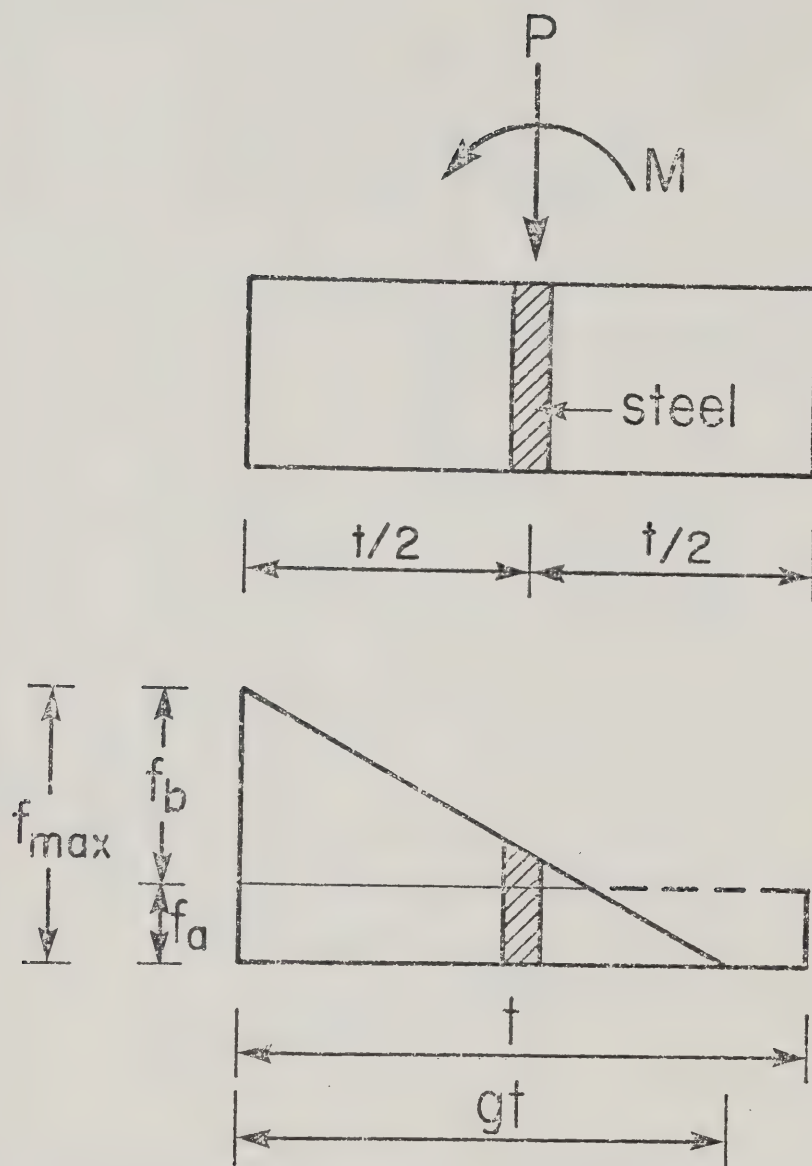


FIG. 2.6 Compression on Part of Cross-Section of Reinforced Wall with Steel in Compression

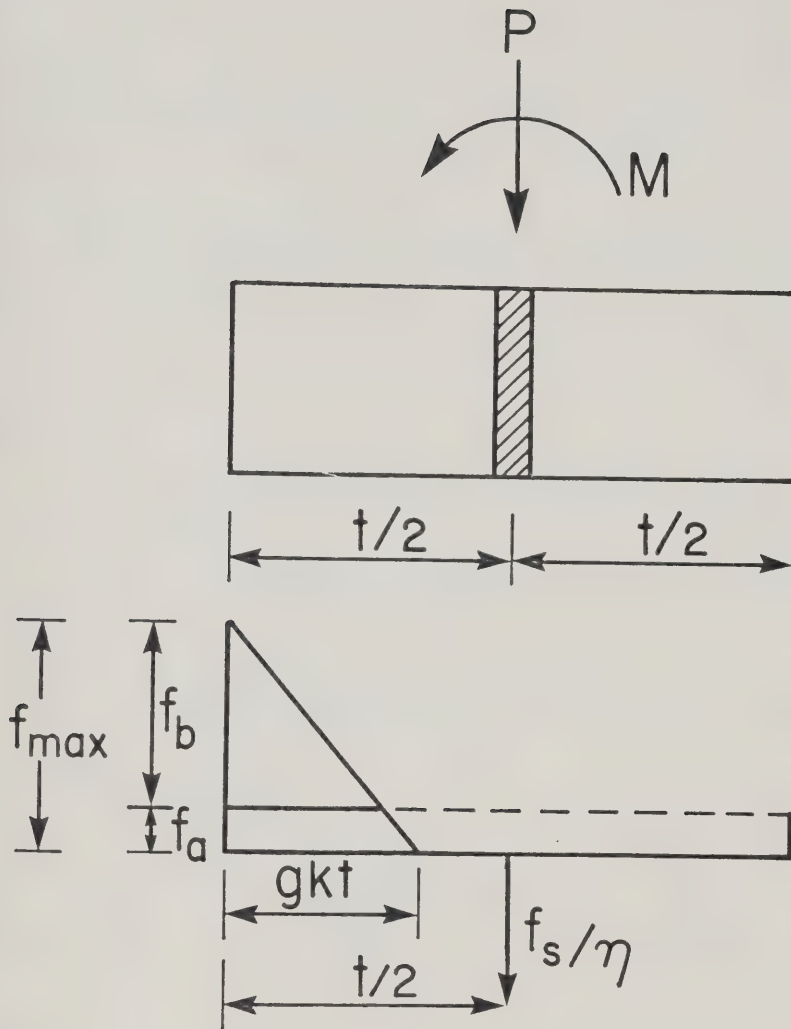


FIG. 2.7 Stress Distribution for Reinforced Wall Section with Steel in Tension

From basic equilibrium considerations the following equations can be obtained relating the stresses in the wall section and the reinforcing steel.

$$P = \frac{1}{2} f_{\max} bKgt - \frac{1}{2} \rho t \eta f_{\max} \left(\frac{1-g}{g} \right) \dots\dots\dots 2.13$$

$$M = \frac{1}{2} f_{\max} bKgt \left(\frac{t}{2} - \frac{K}{3} gt \right) + \frac{1}{2} \rho bKt \eta f'_m \left(\frac{1-g}{g} \right) \left(Kt - \frac{t}{2} \right) \dots\dots\dots 2.14$$

where

$\rho = A_s/bt$ the percent of reinforcing steel

$K = \frac{1}{t}$ (distance (from the compression face) to the centroid of steel)

$\eta = E_s/E_m$ where

E_s, E_m the modulus of elasticity of the steel and masonry, respectively.

In this case,

$$g = \sqrt{\left(\eta\rho - \frac{f_a}{f_{\max}K} \right)^2 + 2\eta\rho - \left(\eta\rho - \frac{f_a}{f_{\max}K} \right)} \dots\dots\dots 2.15$$

where

$$f_a = \frac{1}{2} f_{\max} Kg - \eta\rho Kf \left(\frac{1-g}{g} \right) \dots\dots\dots 2.16$$

2.3.4 Ultimate Strength Analysis

The principles of ultimate strength design for reinforced concrete members can be used to evaluate the ultimate capacity of reinforced masonry walls. For reinforced masonry walls, as for reinforced concrete, there are four possible modes of failure:

- a) balanced failure (simultaneous failure of masonry and yielding of steel),
- b) yielding of the steel in tension,
- c) masonry failure before the steel reaches its yield strength,
- d) steel in compression and crushing failure of masonry.

a) Balanced Failure.

Referring to Figure 2.8, the expressions for the ultimate load and moment are obtained from equilibrium considerations.

$$P_u = 0.85 f'_m ab - A_s f_y \quad \dots\dots\dots 2.17$$

$$M = P_u e = 0.85 f'_m ab \left(\frac{t}{2} - \frac{a}{2} \right) \quad \dots\dots\dots 2.18$$

where

P_u = ultimate axial load

e = eccentricity of ultimate load from the centroid of the tension steel

A_s = area of steel in tension

a = depth of the equivalent rectangular block = $K_b c$

f_y = yield stress for reinforcing steel

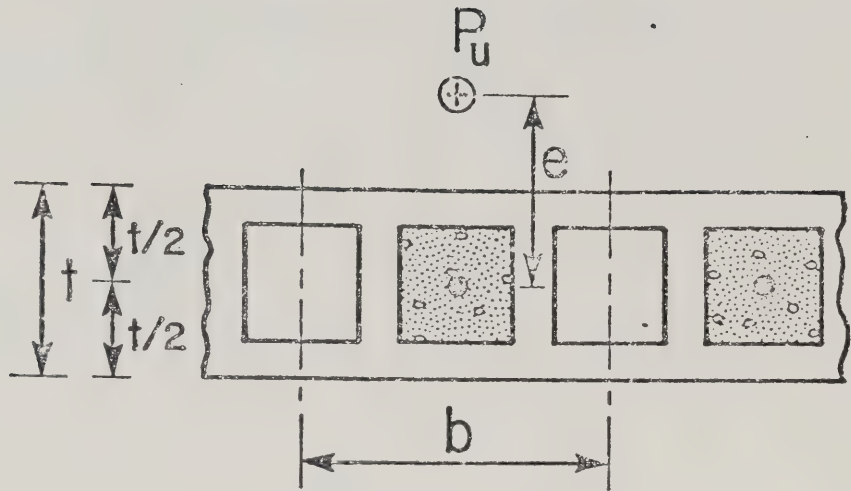
$c = \epsilon_m E_s t / 2(f_y + \epsilon_m E_s) =$ depth to the neutral axis

$K_b = 0.85$ for $f'_m \leq 4000$ psi

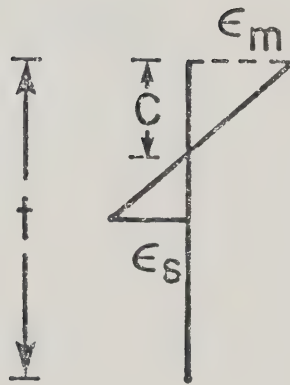
ϵ_m = masonry strain at ultimate load

b) Tension Failure.

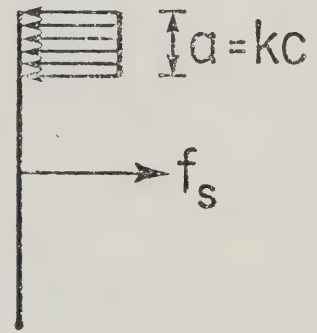
A tension failure occurs when the ultimate load is less than the balanced load ($P_u < P_b$). In this case the distance from the compression face to the neutral axis is smaller than it is for



(a) cross section



(b) strains



(c) stresses

FIG. 2.8 Strains and Stresses in Reinforced
Masonry for Ultimate Condition

the balanced load, and the strain in the reinforcing steel is larger than the yield strain. The ultimate load and moment can be found using equations 2.17 and 2.18 by trial and error in conjunction with relation:

$$\frac{\epsilon_s}{t/2 - c} = \frac{\epsilon_m}{c} \dots\dots\dots 2.19$$

where

$$\epsilon_s = \text{strain in steel} > \frac{f_y}{E_s}$$

c) Compression Failure.

If the ultimate load is larger than the balanced load then, as shown in Figure 2.8, the depth to the neutral axis from the compression side is larger than for the balanced condition and the steel strain is less than the yield strain ($\epsilon_s < f_y/E_s$). If the steel is in tension the stress in the steel can be found from the strain compatibility relations as:

$$f_s = \epsilon_s E_s = \frac{\epsilon_m (\frac{t}{2} - c)}{c} \times E_s = \epsilon_m E_s \frac{[K_b \frac{t}{2} - a]}{a} \dots\dots\dots 2.20$$

The ultimate load can be found using Equations 2.17 and 2.18 in conjunction with Equation 2.20.

d) Steel in Compression.

If the moment acting on the wall is small then the steel will be in compression. The strain in the reinforcement is a function

of the ultimate masonry strain and the cross-sectional properties.

If the entire cross-section is in compression as shown in Figure 2.9, the steel is the strain in

$$\epsilon_s = \epsilon_{\min} + \frac{1}{2} [\epsilon_{\max} - \epsilon_{\min}] \quad \dots\dots\dots 2.21$$

where

ϵ_{\min} = minimum strain in masonry

ϵ_{\max} = maximum strain in masonry.

The force in the steel can be now included in the calculation of the ultimate load using $f_{\max} = f'_m$ the ultimate strength of the masonry and f_{\min} as calculated by Equation 2.1.

$$P_u = \frac{1}{2} [f'_m + f_{\min}] bt + A_s f_s \quad \dots\dots\dots 2.22$$

$$M_u = \frac{1}{2} bt \left[f'_m - \frac{P_u}{A_n} \right] \left[\frac{t}{2} - \frac{t}{3} \right] = \frac{1}{12} bt^2 \left[f'_m - \frac{P_u}{A_n} \right] \quad \dots\dots\dots 2.23$$

For cases of partial compression on the cross-section and the steel in compression the procedure is similar.

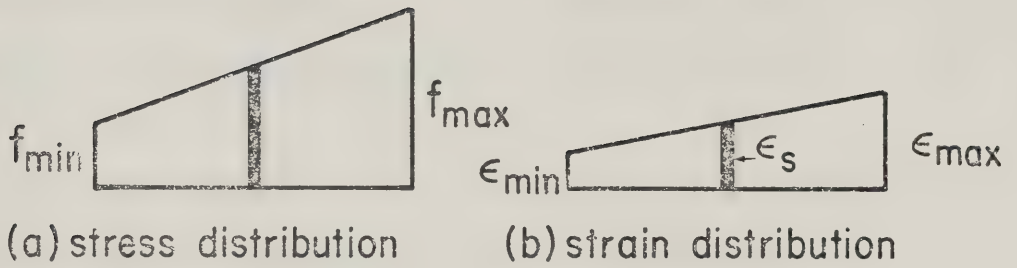


FIG. 2.9 Stress and Strain Distribution for Reinforced Section in Compression

CHAPTER III

Code Design Procedures

3.1 Introduction

In the previous chapter, the capacity of plain and reinforced masonry walls was examined with regard to strength. When designing masonry structures other factors such as slenderness effects, workmanship, construction procedures, etc., must be taken into account.

In this chapter the procedures for designing load bearing masonry walls under three codes of practice are examined. These building codes are:

- a) Canadian CSA Standard S-304-1977, "Masonry Design and Construction".¹³
- b) "Uniform Building Code", International Conference of Building Officials, 1973 edition.²³
- c) "British Standard Code of Practice, CP 111-1970".²⁴

3.2 Load Bearing Masonry Wall Design Procedure According to CSA Standard S-304-1977¹³

The load bearing capacity of a masonry wall is calculated using an allowable stress, the net area of the cross-section and reduction factors which account for the eccentricity of load, and wall height to thickness ratio.

The basic formula for evaluating the vertical load capacity is given in Article 4.6.7.1 as:

$$P_a = C_e C_s f_m A_n \dots\dots\dots 3.1$$

$$P_a = C_s f_m A_n \dots\dots\dots 3.2$$

where

P_a = allowable vertical load

C_e = eccentricity coefficient

C_s = slenderness coefficient

f_m = allowable stress

A_n = net cross-section area

Values of C_e and C_s may be taken from tables in the Standard or they may be calculated using the expressions:

$$C_s = 120 - \frac{h/t}{300} \left[5.75 + \left(1.5 + \frac{e_t}{e_b} \right)^2 \right] \leq 1.0 \dots\dots 3.3$$

$$C_e = 1.95 \left(\frac{1}{2} - \frac{e}{t} \right) + \frac{1}{2} \left[\frac{e}{t} - \frac{1}{20} \right] \left[1 - \frac{e_t}{e_b} \right] \dots\dots\dots 3.4$$

$$C_e = \frac{1.3}{1 + 6 \frac{e}{t}} + \frac{1}{2} \left(\frac{e}{t} - \frac{1}{20} \right) \left(1 - \frac{e_t}{e_b} \right) \dots\dots\dots 3.5$$

Equation 3.4 is used for $t/6 < e \leq t/3$. Equation 3.5 is to be used for $t/20 < e \leq t/6$. Equation 3.2 is used for $e < t/20$

where

e = virtual eccentricity; the eccentricity of the vertical load plus the value calculated by dividing the moment at the cross-section by the axial load.

e_t = eccentricity at top of wall.

e_b = eccentricity at bottom of wall.

The procedure in designing reinforced concrete masonry walls is the same as for plain walls. The allowable masonry stress is the same as for plain walls for axially loaded reinforced walls and is increased by 10% for the case of combined loading.

For virtual eccentricity less than $t/10$ no reduction in load carrying capacity is introduced in the case of reinforced walls as a result of the introduced moment. If the virtual eccentricity is larger than $t/3$ or a value which will produce tension in the reinforcement, the allowable load is calculated on the basis of transformed section and a linear stress distribution. The load calculated using this procedure is modified by applying a slenderness coefficient to account for load-deflection effects. The slenderness coefficient being the same as described previously.

3.3 Load Bearing Masonry Wall Design Procedure According to the "Uniform Building Code"²³, 1973 Edition

The procedure to be followed in designing load bearing masonry walls in accordance with the above document is summarized in the following paragraphs:

1) Plain Masonry Walls

Design and construction of elements of plain masonry shall

be such that the unit stresses do not exceed those set in tables in this division for the various masonry units.

2) Reinforced Masonry

All reinforced masonry shall be so designed and constructed that the unit stresses do not exceed those set forth in tables of this division. The design and construction of reinforced masonry shall be based on the assumptions, requirements and methods of stress determination specified for reinforced concrete.

To account for slenderness effects the axial stress is limited to a value determined by the expression:

$$f_m = 0.2 f'_m \left[1 - \left(\frac{h}{40t} \right)^3 \right] \dots\dots\dots 3.6$$

where

f_m = allowable compressive stress

f'_m = ultimate strength

h = height of wall in inches

t = thickness of wall in inches

3.4 Load Bearing Masonry Wall Design Procedure According to the "British Standard Code of Practice CP 111-1970"²⁴

The British approach to masonry design is based on allowable stress for a given masonry unit strength and the strength of a given mortar type. This basic stress is multiplied by a reduction factor for slenderness for h/t ratios larger than six. With reasonable standard of workmanship and axially loaded walls of

normal storey height this process gives load factors which range between 4 and 7 for 9-inch thick walls and between 6 and 14 for 12-inch thick walls. The assessment of the amount of loading eccentricity at a wall/slab junction is complex and is influenced by the degree of fixity at the junction as well as by the floor loading and relative stiffness of slab and wall. No guidance is given by the code, and it is usual to consider all walls as being axially loaded when the floor slab is stiff and passes over the full width of the wall. The decision rests with the designer and depends, obviously, on his assessment of slab thickness. The code provides combined stress reduction factors for slenderness and eccentric loading.

CHAPTER IV

Stability of Masonry Walls

4.1 Introduction

Masonry walls behave elastically in compression, but are brittle in tension. The strength of masonry in tension is limited to that of tensile bond between the mortar and the masonry units. This bond is usually small (less than 100 psi for common mortars) and for all practical purposes it can be assumed to be zero. In this chapter the mechanism of failure of walls with zero tensile strength is examined. The buckling load of eccentrically loaded slender masonry walls is evaluated, and the principles of the moment magnifier method, as it applies to masonry, are examined.

4.2 General

A slender wall, initially straight and concentrically loaded, will fail in buckling if the compressive strength of the material is not exceeded by the critical stress.

However, the load is normally eccentrically applied and there are imperfections in the wall. These imperfections may be represented as additional eccentricity of loading or as initial transverse deformation. If the wall has a limited tensile strength the theoretical treatment is more difficult than if the tensile strength were zero. Although the tensile strength of masonry is variable, it should be included in a theoretical analysis in

order to correlate observed experimental behavior.

When a wall without tensile strength is eccentrically loaded outside the core boundary, tensile cracks will appear in a portion of its height. The extent of the cracked portion is dependent on the end eccentricities of the applied load, the magnitude of the load and the lateral deflection. As the load increases, the wall deflects and the eccentricity of the load in the central portion of the wall increases while the compressed and active section decreases. An eccentrically loaded reinforced masonry wall will exhibit the same behavior until the crack reaches the location of the reinforcement.

To arrive at a theoretical basis for the design of nominally straight and concentrically loaded walls, an imperfection must be included in the analysis. This may be present either as an eccentricity of loading or as initial displacement of the wall.

For a purely elastic wall it is convenient to assume that the deflected shape is sinusoidal or parabolic, while for a brittle wall it is simpler for analysis to assume that the deflected shape is triangular. If the load is applied with a deliberate and known eccentricity there seems to be no necessity to consider an additional effect of column imperfection. As a result of these considerations three bases can be made for theoretical analysis.

- 1) The wall is pinned at each end, has a triangular initial deformation, and is concentrically loaded,

or

- 2) The wall is initially straight and eccentrically loaded in single curvature bending,

or

- 3) The wall is initially bent in double curvature.

4.3 Walls with Pinned Ends and Triangular Initial Deformations

For zero initial deformations instability occurs when the Euler load is reached. This results in complete collapse of the wall, provided that the material strength is not exceeded before collapse occurs. Where the initial deformation is finite but less than $t/6$ the load/deflection curve for the wall is that for a purely elastic wall, until the third point of the cross-section coincides with the line of thrust. On one side of the wall cracks then form and the load/deflection curve deviates from the elastic curve. If the initial deformation is greater than one sixth of the wall thickness, cracking occurs immediately load is applied if the tensile strength is zero. After cracking has occurred the effective depth of the section decreases with load and the height over which cracking occurs increases. The effective depth varies along the length of the wall and the effective eccentricity of the load at any section depends on the deflection of the wall. At final collapse, the effective depth at the center of the wall is reduced to zero so that a hinge is formed. At this instant the two parts of the wall become straight. Cracking never extends over the entire height of the wall because the thrust line remains concentric at the ends. Different deflection equations govern in the cracked and uncracked portions of the wall, but they must yield the same values of deflection and slope at the boundary between cracked and uncracked portions.

Figure 4.1 shows the deflected shape of a wall concentrically loaded with initial triangular deflection.

Assume that the initial deflection is given by:

$$y_o = e_c \left(1 - \frac{2x}{h}\right)$$

where

e_c = initial deflection at mid-height

x = distance measured from mid-height

h = height of the wall

If the additional deflection due to applied load is y_1 , the total deflection is given by:

$$y = y_o + y_1$$

As the wall deflects; a portion cracks and a portion remains uncracked.

For the uncracked portion, the basic relation between load and deformation is given by:

$$EI_o \frac{d^2 y_1}{dx^2} + Py = 0$$

Since

$$\frac{d^2 y_o}{dx^2} = 0$$

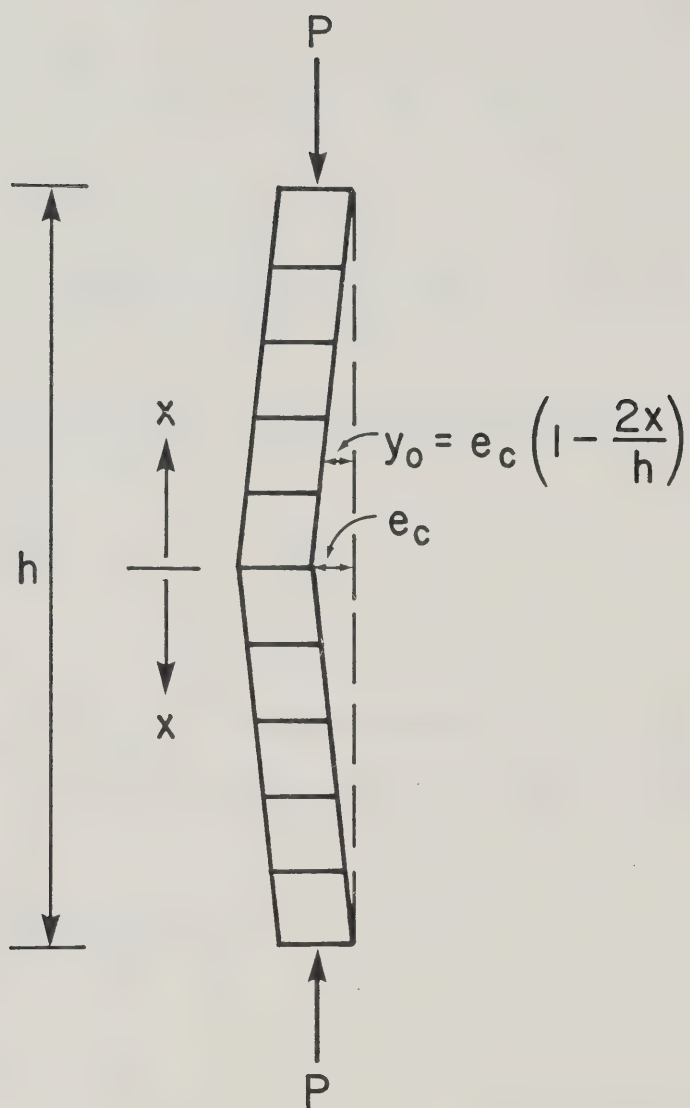


FIG. 4.1 Concentrically Loaded Wall with
Triangular Initial Deflection

$$EI_o \frac{d^2y}{dx^2} + Py = 0 \quad \dots\dots\dots 4.1$$

The line of thrust with respect to the cracked section is:

$$e' = \frac{t'}{6}$$

where

$$t' = \text{reduced depth} = 3 \left(\frac{t}{2} - y \right)$$

The moment of inertia of the cracked section is given by:

$$I_o \left(\frac{t'}{t} \right)^3$$

where

I_o = the moment of inertia of the uncracked section.

At any cracked section the following relation holds:

$$EI_o \left(\frac{t'}{t} \right)^3 \frac{d^2y}{dx^2} + Pe' = 0$$

Since $d^2y_o/dx^2 = 0$

$$EI_o \left(\frac{t'}{t} \right)^3 \frac{d^2y}{dx^2} + Pe' = 0$$

or

$$EI_o \left(\frac{t'}{t} \right)^3 \frac{d^2y}{dx^2} + P \frac{t'}{6} = 0$$

or

$$EI_o \frac{d^2 y}{dx^2} + \frac{Pt'}{6 \left(\frac{t'}{t} \right)^3} = 0$$

Substituting $t' = 3(t/2 - y)$ the following expression is obtained:

$$EI_o \frac{d^2 y}{dx^2} + \frac{Pt^3}{54 \left(\frac{t}{2} - y \right)^2} = 0 \quad \dots\dots\dots 4.2$$

Let

$$z = \left(\frac{t}{2} - y \right)$$

then

$$\frac{d^2 z}{dx^2} = - \frac{d^2 y}{dx^2}$$

Substituting back in Equations 4.1 and 4.2, the following equations are obtained for the uncracked and cracked sections respectively:

$$EI_o \frac{d^2 z}{dx^2} + P \left(z - \frac{t}{2} \right) = 0 \quad \dots\dots\dots 4.3$$

$$EI_o \frac{d^2 z}{dx^2} - \frac{Pt^3}{54z^2} = 0 \quad \dots\dots\dots 4.4$$

Equations 4.3 and 4.4 are coupled differential equations governing the load deflection characteristics of an axially loaded wall with initial triangular deformation. Solution of these equations gives the maximum load that can be carried by a wall as a function of the initial imperfection. Figure 4.2 is a graphical representation of the solution of the differential equations and can be used to evaluate the buckling load for walls with no tensile strength and triangular initial imperfections. Chapman and Slatford² developed a detailed solution to this problem.

4.4 Straight Walls with Eccentric Load

If a straight wall is eccentrically loaded and the load is gradually increased, part or all of the wall will crack. Figure 4.3 shows the deflected shape of such a wall. For the uncracked portion of the wall the governing differential equation is:

$$EI_o \frac{d^2y}{dx^2} + P(e_p + y) = 0 \quad \dots\dots\dots 4.5$$

where

e_p = eccentricity of the load

The eccentricity of the line of thrust with respect to the cracked section is:

$$e' = \frac{t'}{6}$$

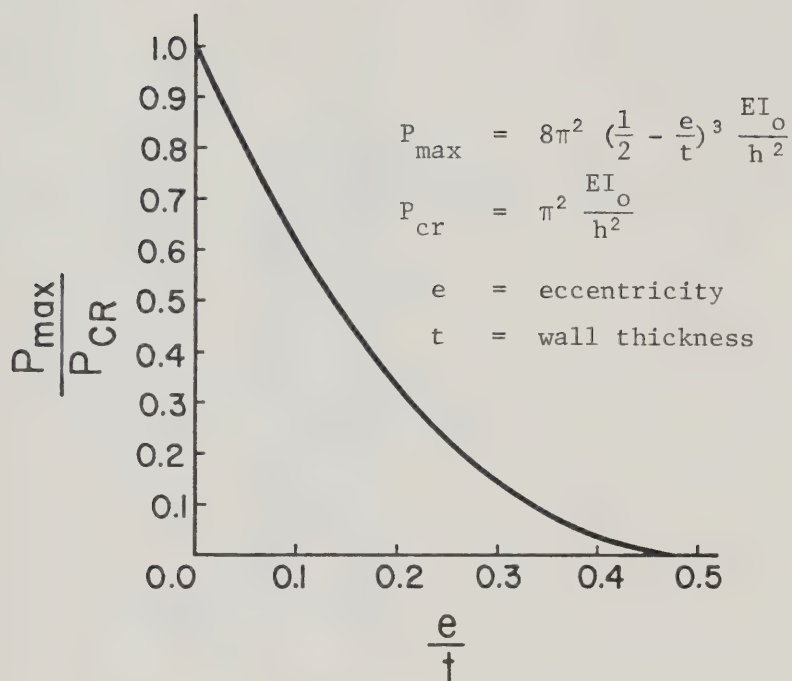


FIG. 4.2 Maximum Load for Wall with Initial Triangular Deflection

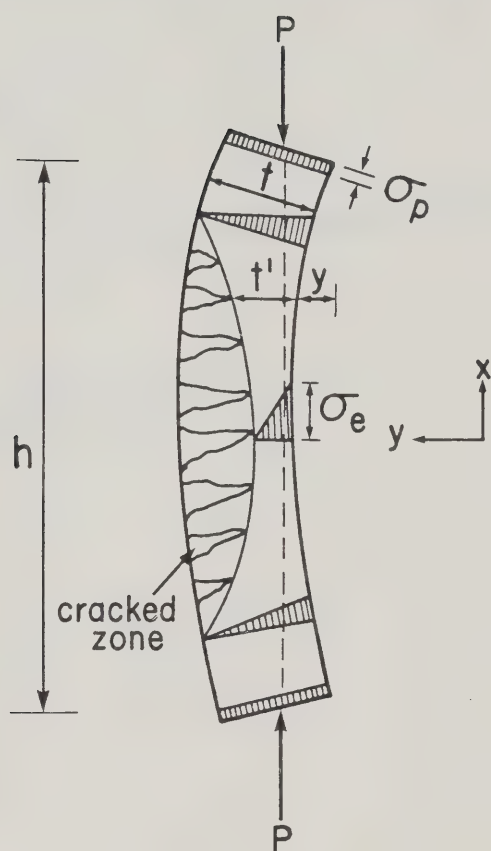


FIG. 4.3 Deflected Shape of Eccentrically Loaded Wall

and the reduced thickness is

$$t' = 3 \left(\frac{t}{2} - y - e_p \right)$$

The reduced moment of inertia is given by:

$$I_o \left(\frac{t'}{t} \right)^3$$

At any cracked section the governing differential equation is written as:

$$EI_o \left(\frac{t'}{t} \right)^3 \frac{d^2 y}{dx^2} + Pe' = 0$$

or

$$EI_o \frac{d^2 y}{dx^2} + \frac{Pt^3}{54 \left(\frac{t}{2} - y - e_p \right)} = 0 \dots\dots\dots 4.6$$

Let

$$z = \frac{t}{2} - y - e_p$$

then

$$\frac{d^2 z}{dx^2} = - \frac{d^2 y}{dx^2}$$

Substituting in Equations 4.5 and 4.6 the following equations are obtained:

$$EI_o \frac{d^2 z}{dx^2} - P \left(\frac{t}{2} - z \right) = 0 \dots\dots\dots 4.7$$

$$EI_o \frac{d^2z}{dx^2} - \frac{Pt^3}{54z^2} = 0 \dots\dots\dots 4.8$$

Equations 4.7 and 4.8 are coupled differential equations, and they can be solved to obtain the maximum load. A solution to these equations was presented by Chapman and Slatford², and a plot of this solution is shown in Figure 4.4, in which the ratio of P_{cr}/P_{max} versus e/t is plotted. In this plot P_{cr} is the Euler buckling load and P_{max} is the load obtained by the solution of Equations 4.7 and 4.8.

4.5 Deflection Curve Approach to Stability of Masonry Walls

An approach to the stability of masonry walls may be developed from the deflection curve. The results obtained using this approach compare favorably with those obtained by Chapman and Slatford².

Consider the wall shown in Figure 4.5 loaded at an eccentricity $e > t/6$, and having a deflected shape and cracked zone as shown. Equilibrium at any point must be satisfied. Assuming that plane sections remain plane the stress distribution on any cross-section will be as shown in Figure 4.6. Maximum stress occurs at the compression face and is given as a function of the distance from the line of thrust to the compression face by:

$$\sigma_o = \frac{2P}{3bu} \dots\dots\dots 4.9$$

where

P = applied load

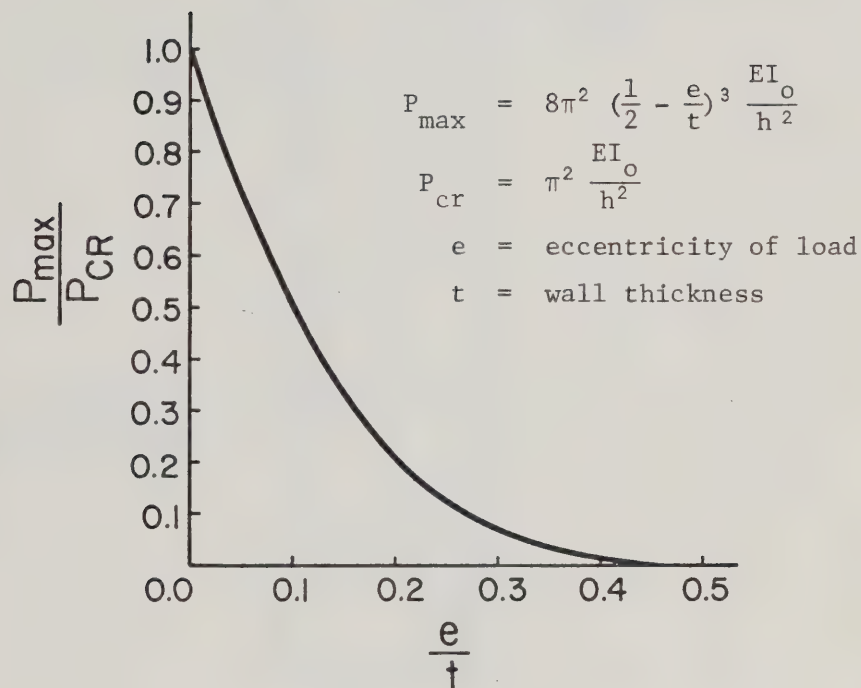


FIG. 4.4 Maximum Load for Eccentrically Loaded Wall

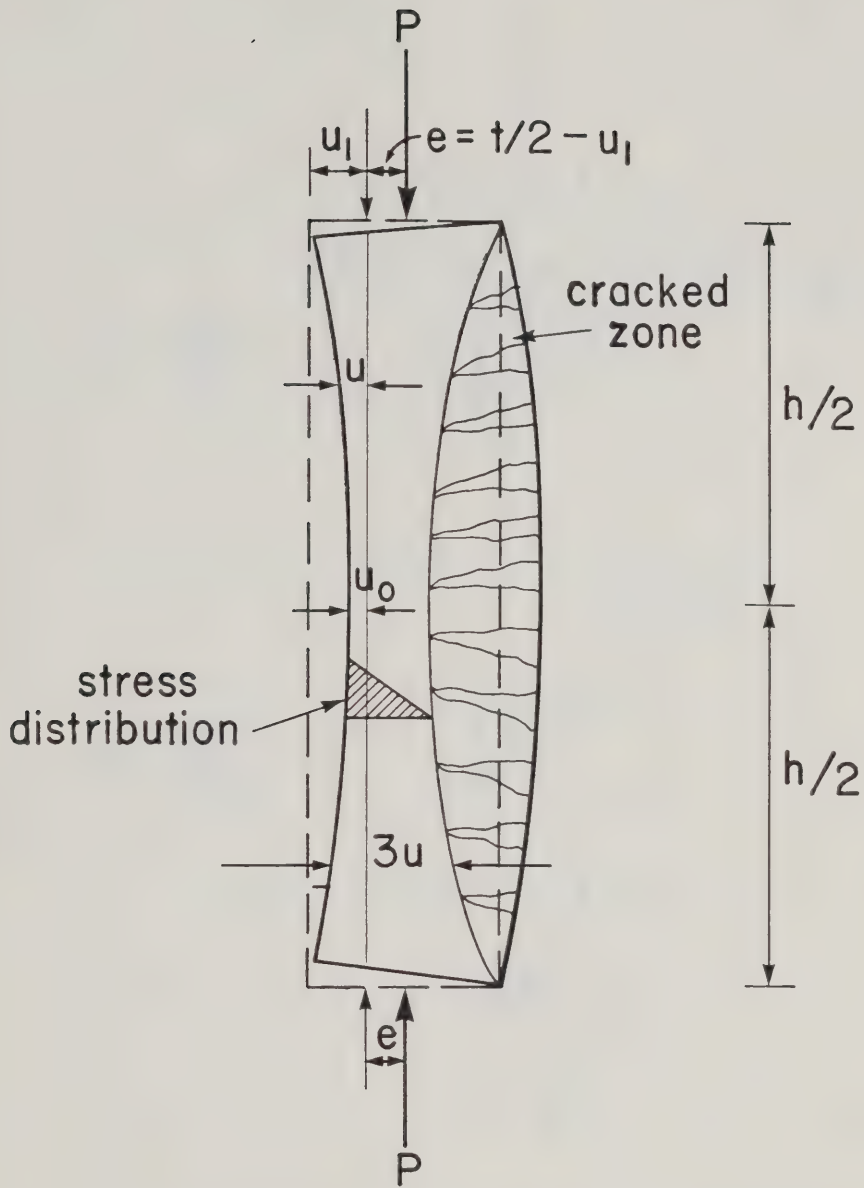


FIG. 4.5 Cracked and Effective Cross-Section of Eccentrically Loaded Wall

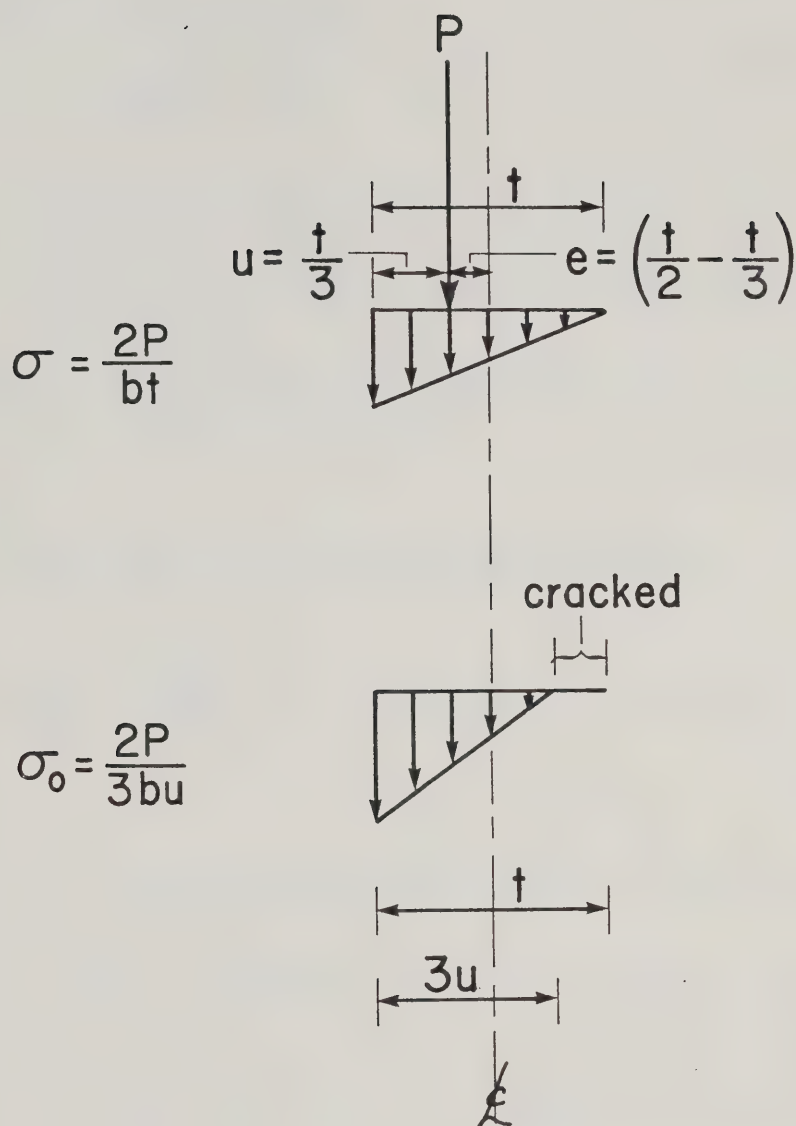


FIG. 4.6 Equilibrium Conditions on Cross-Section
for Stresses

b = width of the wall

u = distance from line of thrust to the compression force

At any section along the wall the uncracked thickness is $t - 3u$, and therefore Equation 4.9 is valid for $t/2 > e \geq t/6$ where t = the thickness of the wall. Maximum stress occurs at mid-height of the wall where due to deflection ($P-\Delta$ effect) the depth of the crack will be a maximum and the uncracked section a minimum.

At this point the maximum stress is given by:

$$\sigma_{\max} = \frac{2P}{3bu_0} \dots\dots\dots 4.10$$

where

u_0 = minimum distance from the line of thrust to the compression face

Consider the deflected wall as shown in Figure 4.7.

The x -axis is parallel to the thrust line of the load P and is tangent to the deflection curve at the origin. At any point $y = u - u_0$ and at $x = h/2$, $y = u_1 - u_0$.

Consider now an element of the deflection curve as shown in Figure 4.8. The curvature of the compression face is caused by the shortening of the face under compressive stress relative to the length of the boundary of the uncracked zone, which does not change in length since the stress is zero at this boundary.

As $d\ell \rightarrow 0$ the change in slope of the deflection curve over the length of the element is:

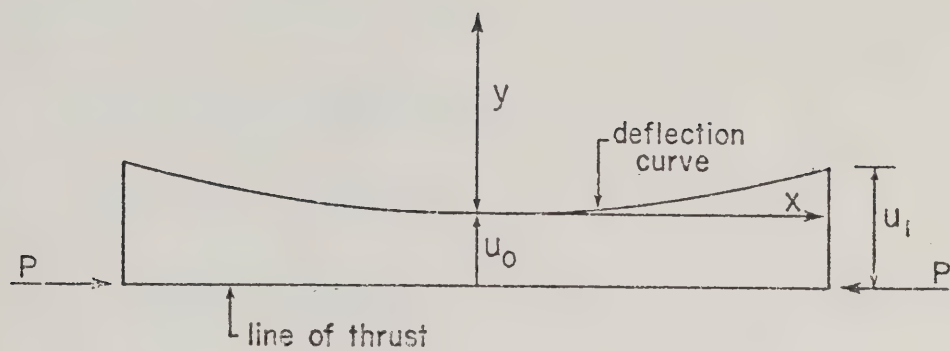


FIG. 4.7 Deflection Curve of Deformed Compression Face

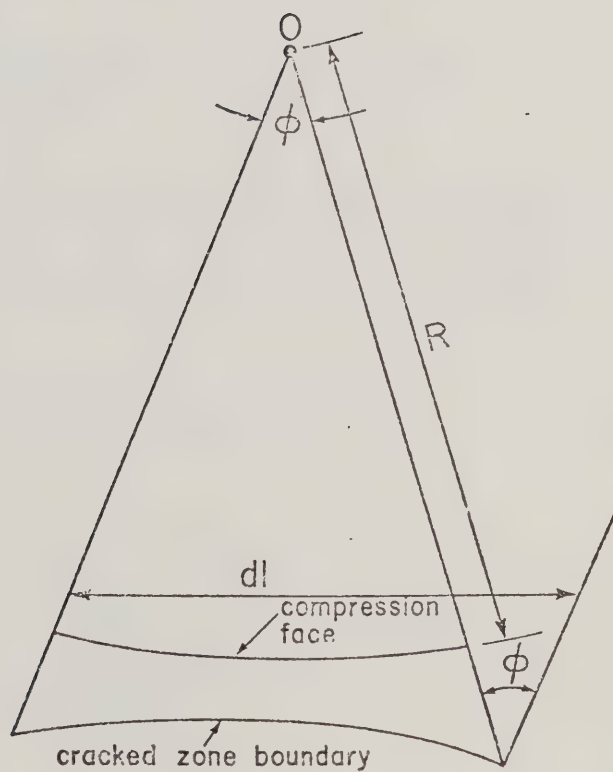


FIG. 4.8 Curvature of Deflected Wall

$$\phi = \frac{\epsilon d\ell}{3u} \dots\dots\dots 4.11$$

where

ϵ = strain in element $d\ell$

The strain however is given by

$$\epsilon = \frac{\sigma_o}{E} = \frac{Pu}{3bu} \left(\frac{1}{E} \right) \dots\dots\dots 4.12$$

where

σ_o = average stress at the face of the element

E = modulus of elasticity

Substituting Equation 4.12 in Equation 4.11

$$\phi = \frac{2P}{9Ebu^2} d\ell \dots\dots\dots 4.13$$

The length of the compression face is given by $d\ell(1 - \epsilon)$ and it can be expressed in terms of the radius of curvature R as:

$$\frac{1}{R} = \frac{\phi}{d\ell(1 - \epsilon)} = \frac{2P}{3Eb} \frac{1}{u^2(1 - \epsilon)}$$

In general

$$\frac{1}{R} = \frac{\frac{d^2y}{dx^2}}{\left[1 + \left(\frac{dy}{dx} \right)^2 \right]^{3/2}}$$

Therefore

$$\frac{d^2y}{dx^2} = \frac{2P}{3Eb} \frac{\left[1 + \left(\frac{dy}{dx}\right)^2\right]^{3/2}}{u^2 (1 - \epsilon)} \dots\dots\dots 4.14$$

for small strains it can be assumed that $(1 - \epsilon) \approx 1$ and

$$\frac{\left[1 - \left(\frac{dy}{dx}\right)^2\right]^{3/2}}{1 - \epsilon} \approx 1$$

Equation 4.14 then becomes

$$\frac{d^2y}{dx^2} = \frac{2P}{9Eb} \frac{1}{u^2} \dots\dots\dots 4.15$$

Let

$$\frac{2P}{9Eb} = K$$

then

$$\frac{d^2y}{dx^2} = K \frac{1}{u^2} \dots\dots\dots 4.16$$

The distance from the line of thrust to the compression face as a function of the deflection curve is given by:

$$u = u_o + y$$

Substituting the above expression in 4.15 the following expression is obtained.

$$\frac{d^2y}{dx^2} = \frac{K}{(u_o + y)^2} \dots\dots\dots 4.17$$

which is the differential equation for the deflection curve for walls with no tensile strength.

A solution to this differential equation, presented in Appendix A, yields:

$$P_{cr} = 0.64125\pi^2 Eu_1^3/h^2 \dots\dots\dots 4.18$$

This solution is approximated by:

$$P_{cr} = 8\pi^2 \left(\frac{1}{2} - \frac{e}{t}\right)^3 EI_o/h^2 \dots\dots\dots 4.19$$

within an accuracy of 4%.

Equation 4.19 is simpler to apply than Equation 4.18 and the error of 4% is considered acceptable for all practical design applications. This solution compares very favorably with the one given by Yokel²⁵ and Chapman and Slatford².

4.6 Walls with Initial Double Curvature Imperfections

When a wall is bent in double curvature due to eccentricities of the vertical load, or initial imperfections, the critical load is influenced by the location of the point of inflection. Neglecting

self-weight, the point of inflection as a function of the end eccentricities is given by:

$$x_c = h \left(\frac{e_t}{e_t + e_b} \right) = \alpha h \dots\dots\dots 4.19$$

where

x_c = distance from support to the point of inflection

h = height of the wall

e_t, e_b = the eccentricities of the load at top and bottom

Under these loading conditions there is a strong possibility that the wall will buckle in a shape approaching the first mode which is the lower-bound case. If the wall is to buckle in its first mode the cracks created by one of the end moments will close as it buckles, and, in effect, the rigidity will increase. At the limit, the wall becomes member with a cracked portion and an uncracked portion.

Figure 4.9 shows a wall bent initially in double curvature due to the applied loads. It is safe to assume that the wall will buckle in the direction of the larger moment and therefore it can be further assumed that the shape of the cracked portion will be similar to that for a wall in single curvature bending as shown in Figure 4.10. It was shown in Section 4.5 that the moment of inertia of a cracked wall section can be approximated by the expression:

$$I = 8 \left(\frac{1}{2} - \frac{e_t}{t} \right)^3 I_o$$

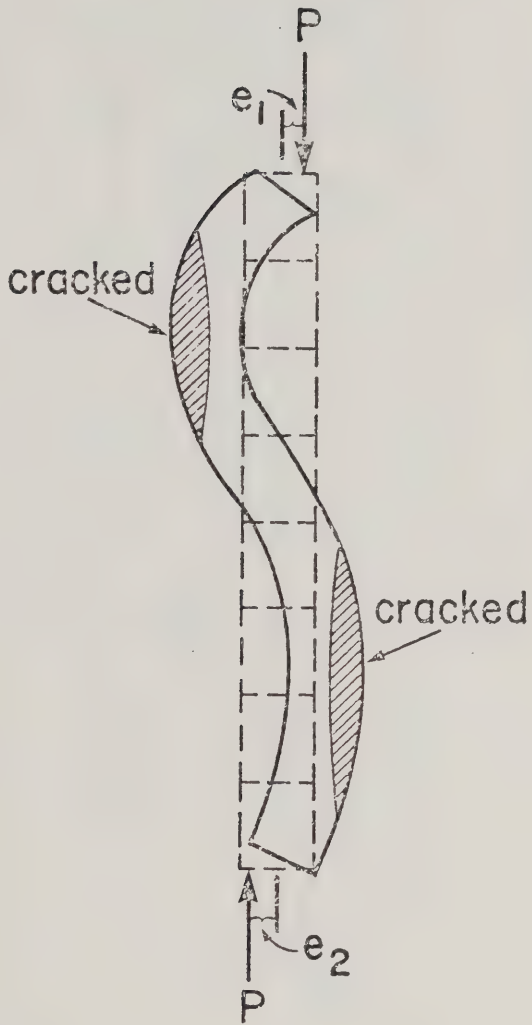


FIG. 4.9 Wall Bent in Double Curvature

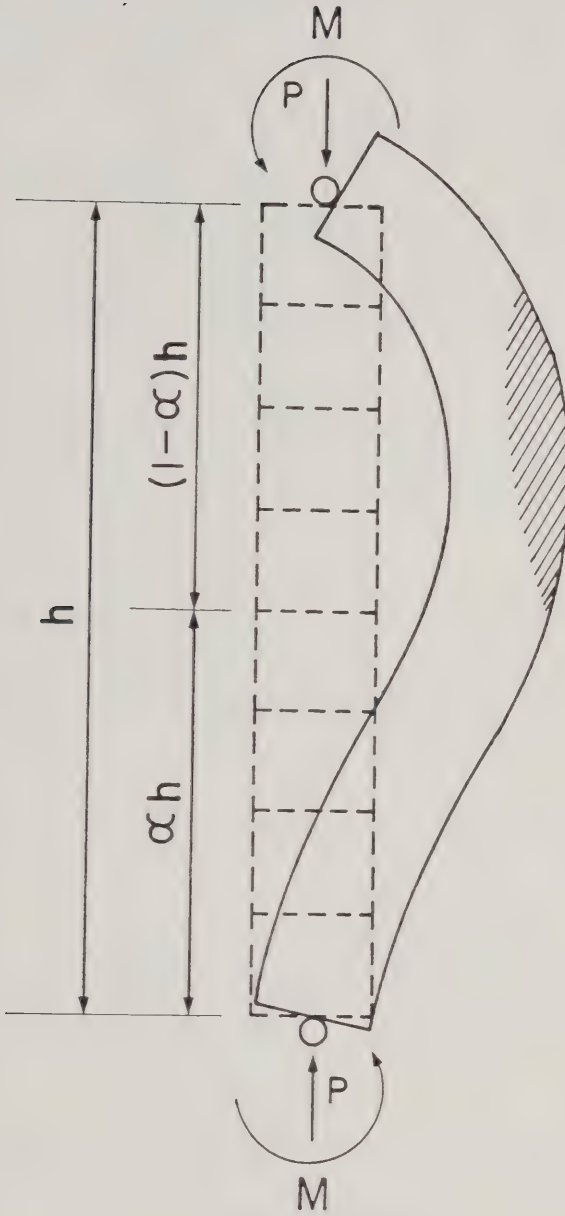


FIG. 4.10 Extent of Cracking for Wall With
Double Curvature Imperfections Bend
in the First Buckling Mode

The equivalent stepped column shown in Figure 4.11 can be analyzed using an energy method. For an elastic structure the total potential energy Π_B is composed of the strain energy and the potential of the applied load.

The total potential energy at buckling for any member subjected to combined bending and axial load is given by:

$$\Pi_B = \frac{1}{2} \int_0^h EI_o (y'')^2 dx - \frac{1}{2} P_{cr} \int_0^h (y')^2 dx \dots \quad 4.20$$

where

y = the buckled shape

The equilibrium condition is expressed mathematically as:

$$\delta \Pi_B = 0 \dots\dots\dots 4.21$$

To determine the buckling load for the stepped column a suitable buckled shape is selected and the condition of Equation 4.21 is imposed.

To obtain the best possible shape for the buckling configuration, a finite element approach may be used with a fifth order interpolating function. Equation 4.20 is rewritten to account for the different section properties in the two segments as follows:

$$\begin{aligned} \Pi_B = & \frac{1}{2} \int_0^{\alpha h} EI_o (y'')^2 dx + \frac{1}{2} \int_{\alpha h}^h EI (y'')^2 dx \\ & - \frac{1}{2} P_{cr} \int_0^h (y')^2 dx \dots\dots\dots 4.22 \end{aligned}$$

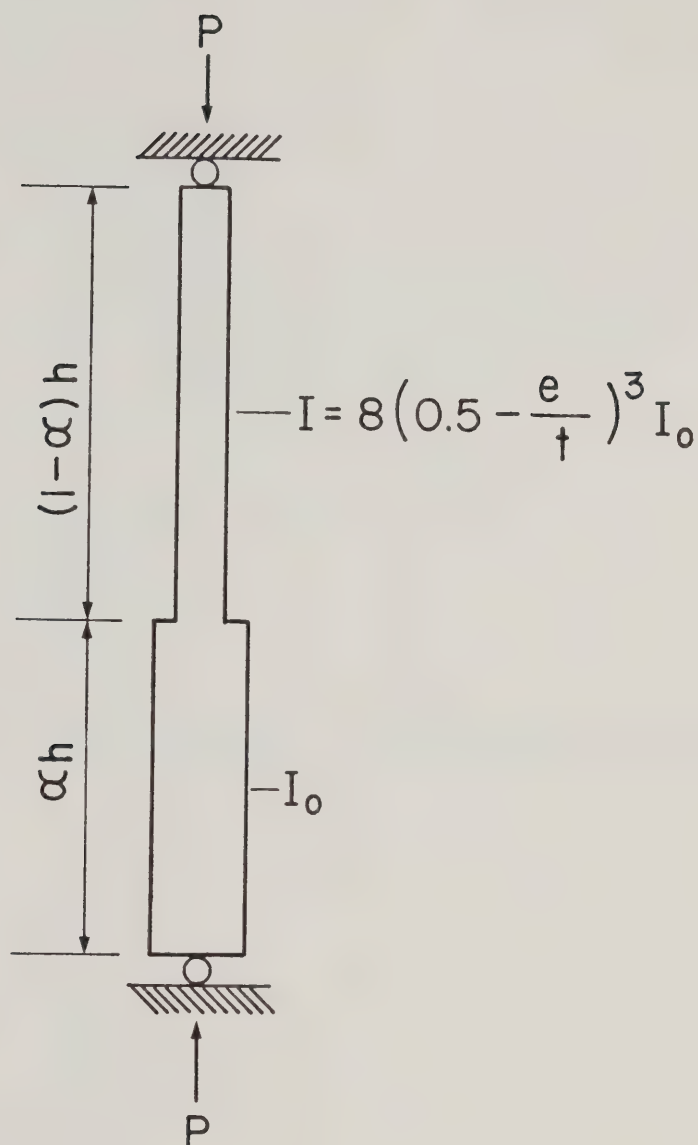


FIG. 4.11 Equivalent Stepped Column Section
for Evaluation of the Buckling Load

Letting

$$y = \langle \phi \rangle \{ \theta \}$$

Then

$$y' = \langle \phi' \rangle \{ \theta \}$$

$$y'' = \langle \phi'' \rangle \{ \theta \}$$

$$(y')^2 = \langle \phi' \rangle \{ \theta \} \langle \phi' \rangle \{ \theta \} = \{ \theta \} [\phi'] \{ \theta \}$$

$$(y'')^2 = \langle \phi'' \rangle \{ \theta \} \langle \phi'' \rangle \{ \theta \} = \{ \theta \} [\phi''] \{ \theta \}$$

where

$$y = \text{deflection}$$

$$y' = \text{slope}$$

$$y'' = \text{curvature}$$

$$\langle \phi \rangle = \langle \phi_1 \phi_2 \phi_3 \phi_4 \phi_5 \phi_6 \rangle, \text{ the interpolating functions,}$$

and

$$\{ \theta \} = \begin{bmatrix} y_1 \\ y_1' \\ y_1'' \\ y_2 \\ y_2' \\ y_2'' \end{bmatrix}$$

Since end deflections y_1 and y_2 are zero, the interpolating functions ϕ_1 and ϕ_4 must be zero

Changing the limits of integration and substituting for y'' and y' in Equation 4.22, the following relation is obtained for the total potential

$$\begin{aligned} \Pi_B = & \frac{1}{2} \frac{EI_0}{h} \int_0^\alpha \{\theta\} [\Phi''] \{\theta\} dn + \frac{1}{2} \frac{EI_1}{h} \int_\alpha^1 \{\theta\} [\Phi''] \{\theta\} dn \\ & - \frac{1}{2} P_{cr} h \int_0^1 \{\theta\} [\Phi'] \{\theta\} dn \end{aligned}$$

Applying Equation 4.21 to the above, the expression for the equilibrium condition may be expressed as

$$\begin{aligned} \delta \Pi_B = & \frac{EI}{h} \int_0^\alpha [\Phi''] \{\theta\} dn + \frac{EI_1}{h} \int_\alpha^1 [\Phi''] \{\theta\} dn \\ & - P_{cr} h \int_0^1 [\Phi'] \{\theta\} dn = 0 \end{aligned}$$

or,

$$\int_0^\alpha [\Phi''] \{\theta\} dn + \beta \int_\alpha^1 [\Phi''] \{\theta\} dn = \frac{P_{cr} h^2}{EI_0} \int_0^1 [\Phi'] \{\theta\} dn$$

where

$$\beta = I_t/I_0$$

The above relation can be reduced to:

$$[K] \{\theta\} = \lambda [Kg] \{\theta\} \dots\dots\dots 4.23$$

where

$[K]$ = bending stiffness matrix

$[K_g]$ = geometric stiffness matrix

This equation is solved as an Eigen value problem to find λ .

For $h^2/EI_o = 1$ the above relation can be solved to obtain the coefficients which will give the buckling load for values of α and β as $P_{cr} = \lambda EI_o/h^2$. Table 4.1 is a tabulation of λ values as found using this method. The interpolating functions and the boundary conditions used are given in Appendix B. The critical load (P_{cr}) may be evaluated for any stepped column of constant modulus of elasticity by entering Table 4.1 with values of α and β , finding λ and multiplying λ by EI_o/h^2 .

The advantages of using this method are:

- a) High order polynomials will approximate very closely the actual shape that a stepped column may assume as a result of initial bending and variations in the geometric properties. It is found that a fifth order polynomial is quite adequate in this case.
- b) Using the determinate search method will assure the selection of the best shape to minimize the energy stored in the system.

4.7 Reinforced Masonry Walls

The behavior of slender reinforced masonry walls is more complex than the behavior of slender unreinforced walls, since the cross-section contains three materials at any cross-section and four

TABLE 4.1 Buckling Coefficients for Step Columns or Walls

$\beta \backslash \alpha$	0.0	0.05	0.10	0.15	0.20	0.25	0.30	0.35	0.40	0.45	0.50	0.55	0.60	0.65	0.70	0.75	0.80	0.85	0.90	0.95	1.00
0.05	0.49	0.50	0.52	0.54	0.57	0.61	0.66	0.76	0.92	1.18	1.52	1.94	2.42	2.98	3.74	4.92	6.81	8.84	9.71	9.87	9.88
0.10	0.99	0.99	1.02	1.06	1.11	1.18	1.26	1.33	1.58	1.89	2.35	2.95	3.67	4.50	5.47	6.63	7.99	9.17	9.74	9.87	9.88
0.15	1.48	1.48	1.51	1.57	1.64	1.72	1.83	1.98	2.20	2.54	3.03	3.70	4.52	5.45	6.45	7.51	8.54	9.35	9.70	9.87	9.88
0.20	1.98	1.98	2.01	2.07	2.18	2.26	2.39	2.55	2.79	3.15	3.66	4.34	5.17	6.11	7.08	8.02	8.85	9.46	9.78	9.87	9.88
0.25	2.47	2.47	2.50	2.57	2.66	2.78	2.93	3.11	3.37	3.73	4.24	4.91	5.73	6.63	7.53	8.36	9.04	9.53	9.79	9.87	9.88
0.30	2.98	2.97	2.99	3.06	3.18	3.29	3.45	3.65	3.92	4.28	4.78	5.43	6.20	7.05	7.88	8.81	9.18	9.59	9.80	9.87	9.88
0.35	3.48	3.46	3.49	3.55	3.66	3.80	3.97	4.17	4.45	4.81	5.29	6.90	6.63	7.41	8.15	8.80	9.29	9.03	9.81	9.87	9.88
0.40	3.95	3.95	3.98	4.04	4.15	4.29	4.47	4.68	4.95	5.31	5.77	6.35	7.02	7.72	8.39	8.95	9.36	9.66	9.82	9.87	9.88
0.45	4.44	4.45	4.47	4.53	4.64	4.78	4.96	5.18	5.45	5.79	6.23	6.78	7.37	8.00	8.59	9.08	9.45	9.09	9.83	9.87	9.88
0.50	4.94	4.94	4.96	5.02	5.12	5.27	5.44	5.66	5.92	6.25	6.66	7.14	7.69	8.25	8.76	9.19	9.51	9.72	9.88	9.87	9.88
0.55	5.43	5.43	5.45	5.51	5.81	5.74	5.91	6.12	6.38	6.69	7.06	7.50	7.99	8.47	8.92	9.29	9.56	9.76	9.84	9.87	9.88
0.60	5.93	5.93	5.95	6.00	6.09	6.22	6.38	6.58	6.82	7.10	7.44	7.84	8.26	8.68	9.06	9.38	9.61	9.76	9.84	9.87	9.88
0.65	6.42	6.42	6.44	6.48	6.57	6.69	6.84	7.02	7.24	7.50	7.81	8.15	8.51	8.87	9.19	9.46	9.65	9.78	9.86	9.87	9.88
0.70	6.91	6.91	6.93	6.97	7.04	7.15	7.29	7.46	7.65	7.89	8.15	8.44	8.75	9.05	9.31	9.53	9.89	9.80	9.85	9.87	9.88
0.75	7.41	7.41	7.42	7.46	7.52	7.61	7.73	7.88	8.05	8.25	8.48	8.72	8.97	9.21	9.42	9.60	9.73	9.81	9.86	9.87	9.88
0.80	7.90	7.90	7.91	7.94	7.99	8.07	8.17	8.30	8.44	8.60	8.79	8.98	9.17	9.36	9.53	9.66	9.78	9.83	9.86	9.87	9.88
0.85	8.39	8.39	8.40	8.43	8.47	8.53	8.61	8.70	8.81	9.94	0.08	9.22	9.37	9.50	9.62	9.72	9.79	9.84	9.80	9.87	9.88
0.90	8.89	8.89	8.89	8.91	8.94	8.98	9.03	9.10	9.16	9.26	9.36	9.45	9.55	9.63	9.71	9.77	9.82	9.65	9.87	9.87	9.88
0.95	9.38	9.38	9.38	9.39	9.41	9.43	9.46	9.49	9.53	9.58	9.62	9.67	9.72	9.76	9.80	9.83	9.85	9.86	9.87	9.87	9.88
1.00	9.88	9.88	9.88	9.88	9.88	9.88	9.88	9.88	9.88	9.88	9.88	9.88	9.88	9.88	9.88	9.88	9.88	9.88	9.88	9.88	9.88

materials overall, namely, concrete block, grout, steel and mortar. The buckling load may also be influenced by variations in the grouted core caused by mortar penetration into the core along the height of the wall. Another factor influencing the buckling load is the incomplete compaction of the grout due to the difficulty in ramming or vibrating the grout in the presence of reinforcement. Since it is impossible to account for the above factors, an exact mathematical approach to buckling of reinforced masonry walls will be at best heavily dependent on the assumptions. The behavior of reinforced masonry walls is similar to the behavior of plain masonry walls for those loading combinations which produce compressive stresses in the reinforcing steel. For loading conditions which produce tensile stresses in the reinforcement, the behavior of a reinforced masonry section is similar to that of a reinforced concrete section. If the assumption is made that a reinforced wall has no tensile strength and if the effect of the reinforcement in increasing the rigidity is ignored the buckling load for a reinforced wall will be the same as for a plain wall.

The buckling load for a reinforced wall loaded in single curvature can be evaluated using Equation 4.18 for eccentricities smaller than $t/3$. For eccentricities larger than $t/3$ the steel will be in tension and the behavior of the wall will be a function of the extent of cracking and the transformed moment of inertia. MacGregor *et al*²⁶ recommend the use of the following relation for flexural rigidity of wall panels with a single layer of reinforcement:

$$E_m I = E_m I_o \left(\frac{1}{2} - \frac{e}{t} \right) \geq 0.10 E_m I_o \quad \dots\dots\dots 4.24$$

For double curvature bending the analysis is similar to that of plain walls. The effects of the reinforcement will be to allow the use of a limiting value for EI as given by Equation 4.24 instead of a value equal to zero as for the case of plain walls.

4.8 Effect of Tensile Bond on the Critical Load

In the previous sections the buckling load was evaluated assuming zero tensile strength. The presence of tensile bond strength will influence the critical load by increasing the uncracked section, which in turn will increase the moment of inertia and thus the critical load. It was shown in Section 2.3.2 that, assuming linear stress distribution the depth of the uncracked section is given by:

$$\zeta = \frac{2tP}{A f_{\max}}$$

The minimum distance from the point of zero stress to the location where the tensile stress is equal to the tensile bond is given by:

$$\zeta = \frac{\xi f'_t}{f_{\max}} \dots\dots\dots 4.25$$

where

- f'_t = tensile bond strength
- f_{\max} = maximum compressive stress
- ζ = distance from point of zero stress to the point where the tensile stress is equal to f'_t

Figure 4.12 illustrates the effort of limited tensile strength on the extent of cracking on the cross-section. The additional uncracked section, due to $f'_t \neq 0$, which is approximately given by Equation 4.25, can be incorporated in the evaluation of P_{cr} from Equation 4.18 by including ζ in the relation as follows:

$$P_{cr} = \frac{\pi^2 E}{12h^2} \left[\left(1 - \frac{2e}{t} \right) t + \zeta \right]^3 b \dots\dots\dots 4.26$$

(see also Figure 4.12)

where

$$\frac{b}{12} \left[\left(1 - \frac{2e}{t} \right) t + \zeta \right]^3 \text{ is the reduced moment of inertia.}$$

4.9 Application of the Moment-Magnifier Method to Load Bearing Masonry Walls

4.9.1 General

The moment-magnifier method was originally developed to predict the ultimate strength of steel beam columns. McGuire²⁸ gives a detailed derivation of the method. The procedure has been extended for use in design of intermediate length reinforced concrete columns by MacGregor *et al*²⁹. The method is based on the concept that, in a column, bending moments determined by elastic analysis are amplified by a factor dependent on:

- a) effective length of the member
- b) material properties
- c) magnitude of vertical load

To obtain the resulting moment, the first order moment is multiplied by the amplification factor. The column is then designed on the

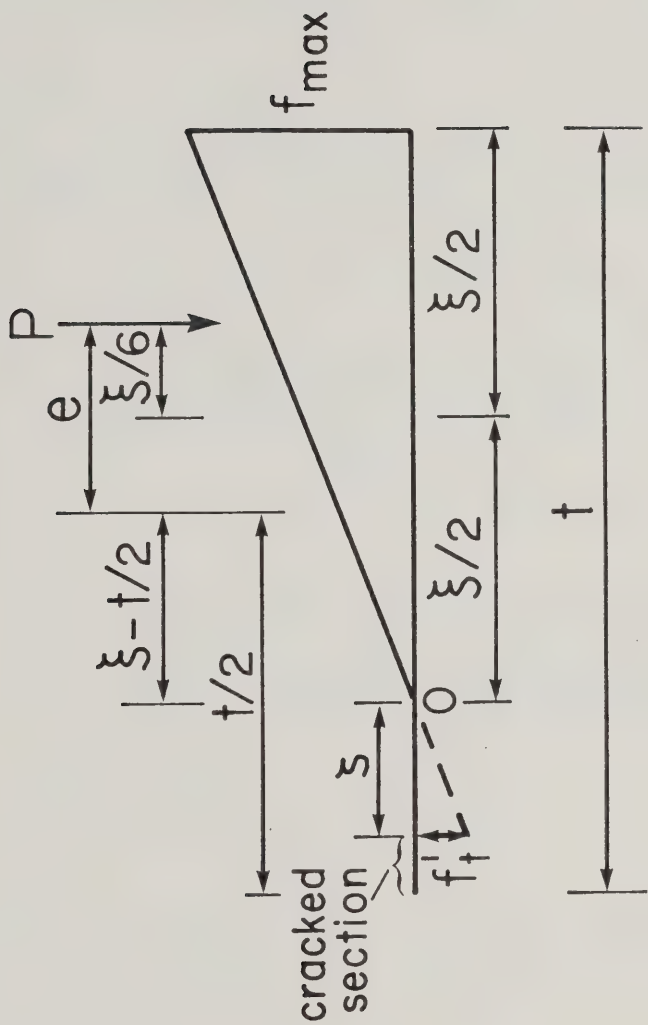


FIGURE 4.12 Effect of Tensile Bond to the Uncracked Section

basis of an interaction diagram for a short column.

4.9.2 Elements of the Method

The maximum moment in an elastic beam-column loaded with an axial load (P), and end moments (M_t, M_b) is shown by Galambos³⁰ to be

$$M_{\max} = \delta M_t \dots\dots\dots 4.27$$

where

$$\delta = \frac{\sqrt{1 + (M_b/M_t)^2 - (M_b/M_t) \cos \alpha_m}}{\sin \alpha_m} \dots\dots\dots 4.28$$

where

M_t = larger end moment in the column, always positive

M_b = smaller end moment in the column, positive if column is bent in single curvature

$$\alpha_m = h\sqrt{P/EI} = \pi\sqrt{P/P_E}$$

$$P = \text{Euler Load} = \pi^2 EI/h^2$$

To evaluate the maximum moment on a beam column ACI Building Code Requirements for Reinforced Concrete (ACI 318-71)³¹ uses Equation 4.27 with δ given by:

$$\delta_m = \frac{C_m}{1 - \frac{P_u}{P_{cr}}} > 1.0 \dots\dots\dots 4.29$$

where

δ_m = moment magnifier factor

P_u = the ultimate load on the column

P_{cr} = the critical buckling load of the column

$$C_m = 0.6 + 0.4 (M_b/M_t) \dots\dots\dots 4.30$$

The positive algebraic sign in Equation 4.30 applies when both end moments induce compression on the same face of the column. The ratio of the moments indicates the shape of the deformed column. If the end moments are equal, C_m is unity; if one end of the column is pin-ended, C_m reduces to 0.6. If the base of the column is fixed then the carry-over moment is minus one-half the top moment, and C_m becomes 0.4.

For columns subjected to transverse loading, the maximum moment can occur at a section away from the end of the member. In this case the value of the largest calculated moment occurring anywhere along the member is used for the value of M_t in Equation 4.27 and C_m is taken as 1.0.

In Equation 4.29 the critical load relates to the buckling load of an equivalent axially loaded column. In applying the method in the design of concrete and steel columns it has been customary to account for the end conditions that may exist in a particular situation, thus allowing for fixity provided by bracing beams or slabs. This in effect increases the buckling load and as a result the magnification factor was reduced. MacGregor and Mathews³² showed that by equating relations 4.28 and 4.29 with $P_{cr} = \pi^2 EI_o / (Kh)^2$ and solving for the effective length factor (K), the following relation is obtained:

$$K = \frac{\pi}{\alpha_m} \sqrt{1 - \frac{C_m \sin \alpha_m}{\sqrt{1 + \left(\frac{M_b}{M_t}\right)^2 - \left(\frac{M_b}{M_t}\right) \cos \alpha_m}}} \dots\dots 4.31$$

Solving Equation 4.31 for values of M_b/M_t from -1 to +1 and P_u/P_E from 0.03 to 0.63 MacGregor and Mathews found that the values of the effective length factor ranged from 0.999 to 1.265. They concluded that the values of K greater than 1.10 corresponded to cases where C_m is underestimated by the ACI equation (columns with α and M_b/M_t both low). If these values are excluded the average K value was equal to 1.05. The absence of values less than 1.0 indicates that the effective lengths of columns in a braced frame, should not be used if the column end moments are known from a second-order analysis.

4.9.3 Application of the Moment-Amplifier Method to Masonry

It was shown in previous sections that the critical or buckling load for slender walls without tensile strength is a function of the magnitude and direction of the applied end moments. The dependence of the critical load on the loading condition must be recognized in applying the moment-magnifier method to the design of masonry.

The magnification factor in the case of masonry must account for the reduction in rigidity resulting from cracking. As the load increases cracks propagate resulting in a reduced moment of inertia. This produces a non-linear increase in deflections. To account for the dependence of rigidity on the stress level on all cross-sections along the height of the wall the critical load to be used

in the moment magnifier equation must be calculated using the procedures developed previously in this chapter. Figure 4.13 illustrates the non-proportionality of deflections to the eccentricities.

It was shown that, for plain masonry walls in single curvature bending, the critical load is given by

$$P_{cr} = 8\pi^2 \left[\frac{1}{2} - \frac{e}{t} \right]^3 \frac{EI_o}{h^2}$$

This relation is used in Equation 4.29 to evaluate the moment magnifier δ_m . For plain walls the bending stress obtained from a first order analysis is multiplied by the magnification factor, δ_m , and added to the stress resulting from the axial load. The first order bending stress is obtained using the equations derived in Chapter II.

For walls with initial double curvature imperfections, or walls bent in double curvature, the procedure is similar to that for walls in single curvature with the critical load evaluated using the procedures described in Section 4.6. Table 4.1 lists coefficients used to evaluate critical loads for walls in double curvature bending. These coefficients are functions of the applied end moments, and values of moment of inertia for cracked and uncracked sections. For a reinforced wall the critical load used in evaluating the moment magnifier factor is a function of the end eccentricities, and Table 4.1 can be used in a manner similar to that for plain walls.

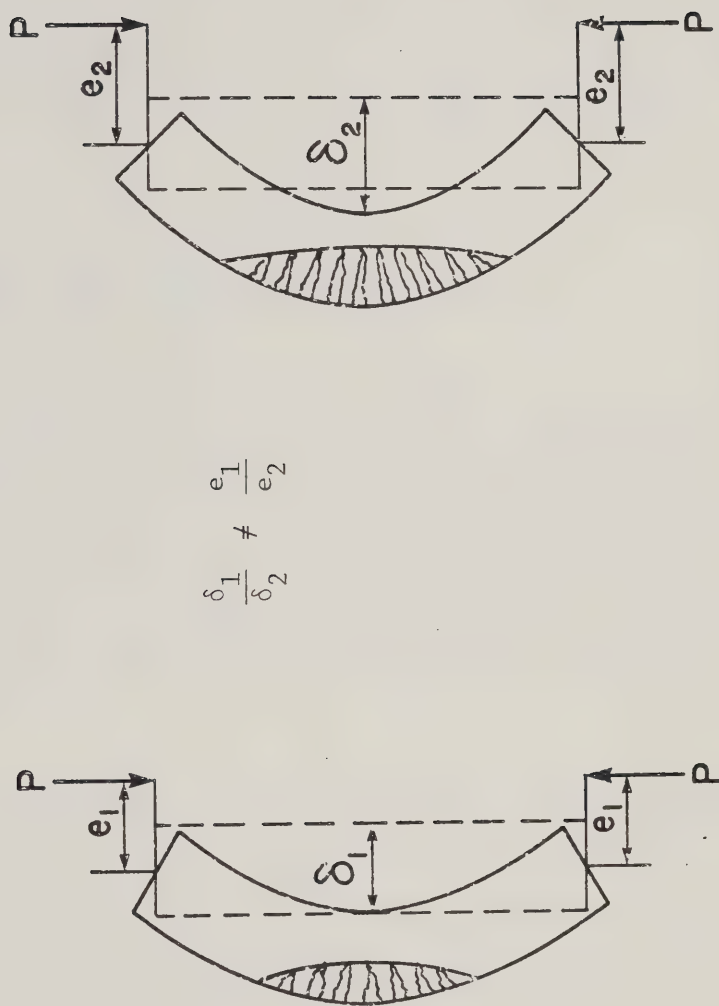


FIG. 4.13 Deflections of Eccentrically Loaded Masonry Walls

For reinforced walls in single curvature the eccentricities smaller than $t/3$, the critical load is the same as that for plain walls having the same moment of inertia. For eccentricities larger than $t/3$ the steel is in tension and the cracked zone will advance beyond the location of the steel. For this case MacGregor²⁷ showed that the moment of inertia of the section can be approximated by the equation:

$$EI = EI_o \left[0.5 - \frac{e}{t} \right] \geq 0.10 EI_o \quad \dots\dots\dots 4.31$$

For reinforced walls in double curvature, the limiting value for the moment of inertia to be used in conjunction with Table 4.1 is that given by Equation 4.31. The concepts discussed briefly in this chapter are used in Chapter VIII where the moment magnifier method is applied to the experimental data obtained in this study.

For design purposes the rigidity of the member is reduced by a factor depending on the ratio of the dead to live load in order to account for creep which in long term loading will increase deflections and amplify the moment acting on the section. MacGregor²⁹ recommends the use of the following equation for evaluating rigidity:

$$EI = \frac{1}{1 + \beta_d} [EI_o] \quad \dots\dots\dots 4.32$$

where

β_d = ratio of dead to live load

CHAPTER V

Experimental Program

5.1 Materials

All materials used in the construction of the test specimens are commercially available and typical of those commonly used in masonry building construction in the Edmonton area.

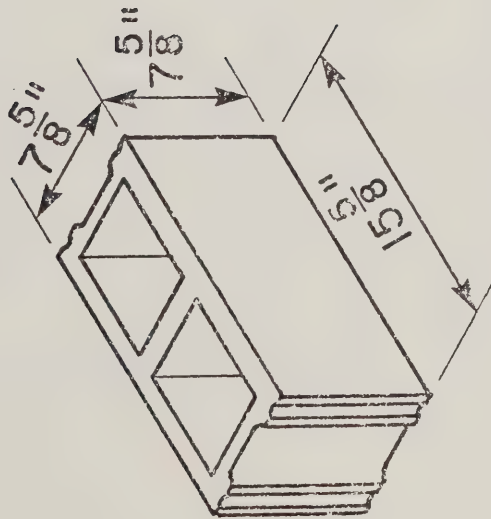
5.1.1 Concrete Block Units

The basic units used for constructing all test specimens were the 8 x 8 x 16 in. stretcher block, the 8 x 8 x 16 in. end block and the 8 x 8 x 8 in. half block. The units are shown schematically in Figure 5.1. The physical properties of the units are listed in Table 5.1.

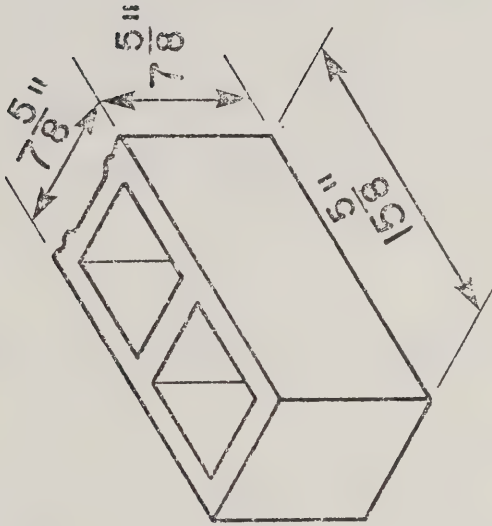
5.1.2 Mortar

Type S mortar was used throughout the experimental program. The mortar was mixed in accordance with the CSA-A179M-1976 standard³³. Normal cement (type III, CSA-A5-1961)³⁴, type S hydrated lime (CSA-A82.43-1950)³⁵ and masonry sand were proportioned by volume in accordance with 1 part cement, 1/2 part lime and 4-1/2 parts sand.

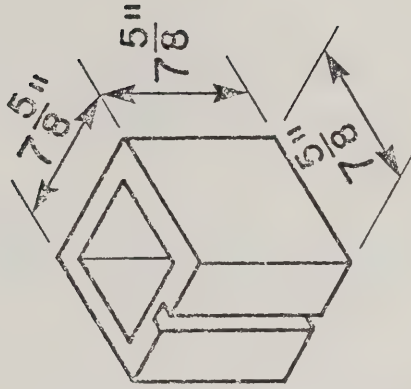
The sieve analysis of the sand, as shown in Table 5.2, indicated that its fineness of 2.34 conformed to the requirements of CSA-A82.56M-1976³⁶. The mortar was mixed in an electrically driven mixer with blades on a vertical axis. From every batch of



(a) stretcher



(b) single corner



(c) half block

FIG. 5.1 Masonry Units

TABLE 5.1 Dimensions and Physical Properties of
Concrete Block Units

Masonry Unit	Width in.	Length in.	Height in.	Gross Area in. ²	Effective Net Solid* Area %	Compressive Strength ksi	
						Gross Area	Net Area
Stretcher	7 5/8	15 5/8	7 5/8	119.15	54.45	1.34	2.46
End Block	7 5/8	15 5/8	7 5/8	119.15	54.45	1.40	2.57
Half	7 5/8	15 5/8	7 5/8	58.15	67.00	1.58	2.35
Solid	3 5/8	15 5/8	7 5/8	56.65	100.00	2.45	2.45

* Based on volume measurements of the cores

TABLE 5.2 Particle Size Distribution of Masonry Sand

Sieve Size	Weight Retained Grams	% Retained	% Cumulative Retained
#4	0	0	0
#8	4.0	0.25	0.25
#16	15.5	1.0	1.25
#30	649.0	42.0	43.25
#50	729.0	47.20	90.45
#100	132.0	8.55	99.0
pan	15.5	1.0	
Total	1545.0	100.0	234.2
Fineness Modulus	2.34		

mortar four - 2 x 2 x 2 in. cubes and two standard cylinders were cast and cured in accordance with CSA-A23.3-1973³⁷.

5.1.3 Grout

A mixture of normal weight crushed gravel (1/4 in. maximum particle size) and natural sand was used to grout the reinforced walls. The two materials were proportioned in such a way as to produce a blend that conformed with ASTM-C595-74³⁸. The mix was proportioned by volume using type III normal cement, in accordance with requirements of CSA Standard A 179M-1976³³. The proportions were 1 part Portland Cement, 2-1/2 parts sand, and 1-1/2 parts coarse aggregate. From every batch of grout two standard cylinders were cast and cured according to

5.1.4 Reinforcing Steel

No. 3, #6 and #9 deformed bars were used for vertical reinforcement. The average yield stress of nine specimens tested was 59.50 ksi. The idealized stress strain relationship for the reinforcing steel is shown in Figure 5.2. A number of test specimens were reinforced in the horizontal direction with #9 gauge wire reinforcement placed in the mortar joints. The joint reinforcement was of a continuous truss design and consisted of two parallel longitudinal wires welded to perpendicular wires as shown in Figure 5.3. In selected cases the joint reinforcement was flattened by passing the wire through rollers which reduced the diameter by 40%.

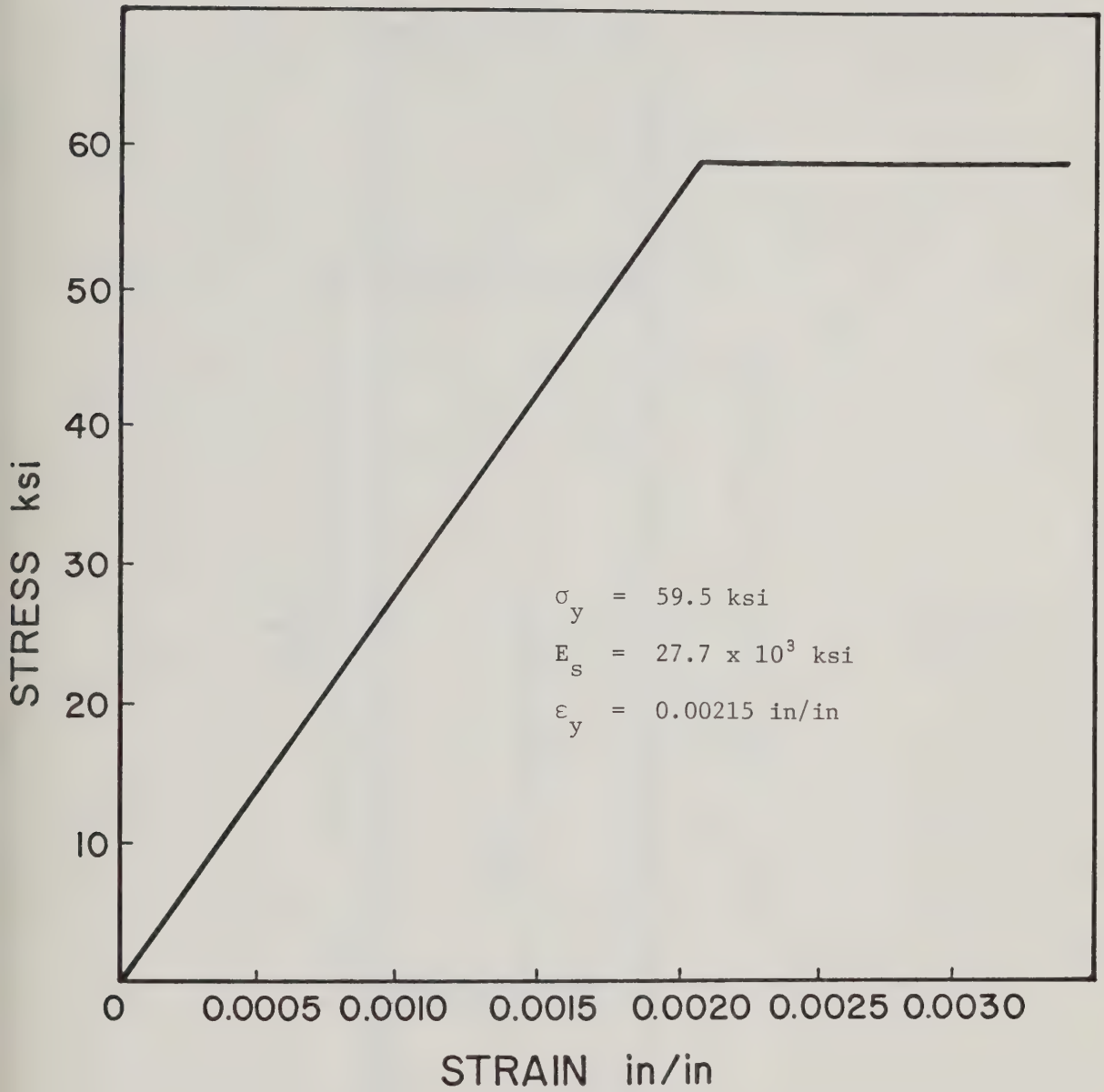


FIG. 5.2 Idealized Stress-Strain Relation for Reinforcing Steel

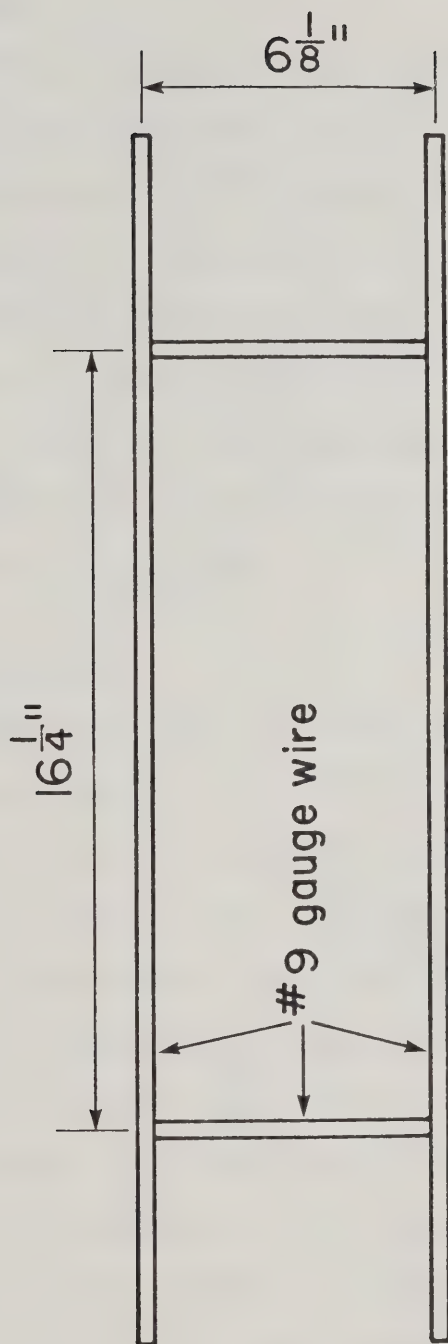


FIG. 5.3 Truss Type Joint Reinforcement

5.2 Test Specimens

5.2.1 Prisms

Thirty two-block, one mortar joint, prisms were built. Twenty of these prisms were plain and ten contained #9 gauge wire joint reinforcement. Of the twenty plain prisms, ten were fully bedded, and ten were constructed with face-shell mortar only. Five of the reinforced prisms were reinforced with joint reinforcement which had been flattened by passing it through rollers reducing the diameter by about 40%. The remaining five contained normal type joint reinforcement. The dimensions of these prisms are shown schematically in Figure 5.4.

5.2.2 Short Walls

Short walls were the control specimens in the experimental part of this study. A total of forty short walls, five blocks in height, were built in running bond with blocks overlapping by 50% in adjacent courses. Ten of the short walls were 1-1/2 blocks in length and the remaining thirty were 2-1/2 blocks in length. Figures 5.4a and 5.4b illustrate schematically the dimensions of the short walls. The specimens 1-1/2 blocks in length were plain and were constructed with face shell mortar. For the other specimens the variables introduced were: full bedding or face-shell bedding, normal or flattened joint reinforcement, completely or partially grouted, and varying amounts of vertical reinforcement. Table 5.3 summarizes the number of short walls and the incorporated variables. The specimens were constructed and air cured in a laboratory environment maintained at 72°F and 34 percent relative humidity.

TABLE 5.3 Short Wall Specimens

Number of Short Walls	Mortar Bed		Grouted			Reinforcement					
	Fully Bedded	Face Shell Mortar	Fully	Partially	UngROUTED	Joint		Plain	Vertical		
						#9 Gauge Wire	Flattened #9 Gauge Wire		3#3	3#6	3#9 Plain
6		✓			✓	✓		✓			✓
7		✓			✓		✓				✓
2		✓			✓						✓
2	✓										✓
2	✓		✓								✓
2	✓			✓							✓
3		✓		✓					✓		
3		✓		✓				✓			
3		✓		✓				✓			

5.2.3 Full Scale Walls

All walls were constructed in running bond. Each course contained one stretcher, one end block and one half block. The bed and head joint mortar was applied only to the face shells, this practice being the most common in the construction industry. The height of the walls varied from 12 to 22 blocks and all walls were 39.60 inches wide. The wall specimens were constructed and air cured in a laboratory environment maintained at 72°F and 34 percent relative humidity.

All specimens were constructed by experienced masons using techniques typical of good workmanship and supervision. Plate 5.1 shows walls under construction. The mortar joints on both faces were cut flush and then tooled. In all wall specimens the first course was laid directly on a polyethylene sheet placed on the laboratory floor. The thickness of the mortar joints was 3/8 in., and the mason kept the outer face of the wall in alignment using horizontal line and level.

The first and last courses in all walls were fully grouted in order to avoid local failures in testing with large eccentricities. In walls designated to be reinforced, clean out holes were provided in the first course. The reinforced walls were grouted in one lift, and vibrated using a one inch diameter vibrator.

The variables introduced were similar to those for short walls. Table 5.4 gives a summary of the full scale walls.



PLATE 5.1 Typical Wall Construction

TABLE 5.4 Full Scale Walls

Wall Designation	Number of Walls	Slenderness Ratio (Nominal)	Reinforcement					
			Vertical				Horizontal	
			Plain	3#3	3#6	3#9	#9 Gauge Wire	Plain
A	5	12	✓					✓
B	5	12				✓		✓
C	1	14	✓					✓
	5	14				✓		
D	1	16	✓					✓
	5	16				✓		✓
E	1	16	✓					✓
	1	14	✓					✓
	3	12	✓					✓
F	5	16					✓	
G	3	16					✓	
	6	16	✓					✓
H	5	16			✓			✓
I	5	16		✓				✓
J	4	16		✓				✓
K	1	16		✓				✓
L	5	22				✓		✓
M	2	22	✓					✓
N	5	16	✓				✓	✓
Total	68							

5.3 Instrumentation

5.3.1 Prisms and Short Walls

For prisms and short walls tested in vertical compression, vertical deformations were monitored by the movement of the head of the testing machine with an accuracy of 1/10000 inches. Deformations were also measured using mechanical gauges over specified lengths in an attempt to measure deformations taking place in the block and the mortar joint.

5.3.2 Instrumentation of Walls

Transverse deflections were measured at every two block height using linear variable differential transducers (LVDT's), calibrated to read increments of ± 0.0001 in. The LVDT's were attached to an independent frame and connected to the wall with thin wires in such a way as to compensate for the vertical deformations. Strains at the face of the wall were measured using 4 in. long concrete strain gauges attached at midheight. Total axial deformation was measured by the movement of the piston of the testing machine.

The strains in the reinforcing steel were measured by strain gauges mounted on the reinforcement. The lead wires from these strain gauges came out of the wall at the level of the position of the gauge, in order to avoid interference with grouting, and bond, and also to avoid possible damage to the wiring during vibration. The procedure involved drilling 3/8" holes in the wall at the level of the strain gauge. Wire was placed through the hole, led to the top of the wall and connected to the strain gauge on the reinforcing bar. The bar was then slowly lowered into position and at the same

time the lead wire was pulled back through the hole. In those cases where more than one strain gauge was used, all wires were placed through the corresponding holes and pulled simultaneously.

Vertical load, vertical deformation, transverse deflections, transverse strains and reinforcement strains were measured, recorded, and partially processed automatically. The measuring devices, (strain gauges, load cells, and linear variable differential transducers) were powered by a common six volt power supply that produced output in the range of ± 6 volts. The analog signals were converted into digital form by a digital voltmeter controlled by a program in the NOVA computer. An interactive Fortran program written for the NOVA provided the capacity to monitor load and deflections during load application and to request output of a set of readings, which were further recorded on a 1.2 million word disc. The processing and recording of data at a particular level of load application was completed in five seconds. After completion of the test, the data was printed on a hard copy terminal, stored on a digital cassette tape, and transmitted to the AMDAHL 470 computer for further processing.

5.4 Test Procedure

5.4.1 Prisms

All two-block prisms were tested in axial compression. The prisms were capped top and bottom with high strength plaster. One-quarter (1/4) inch steel plates were placed at top and bottom and the load was applied over the total area of the prisms.

5.4.2 Short Walls

Short walls were tested in axial compression or combined axial load and bending. All short walls were capped with high strength plaster.

Ten short walls of one and one half blocks in length were tested in axial compression with flat end conditions. The remaining 30 short walls were tested with pin-ended conditions using the arrangement shown in Plate 5.2. The vertical load was applied by the head of a 1.4 million lb. capacity hydraulic testing machine through a 6 in. deep steel channel section which consisted of 3/4 in. side plates and 2 in. base. A two inch diameter round bar, resting on a 2 in. thick, 2 in. wide plate with a cylindrical groove, was placed on top of the channel. A similar plate was placed on top of the roller. The width of the channel was 7.75 inches. The same support was provided at the top and bottom of the walls.

High strength plaster was used to achieve even bearing surfaces on top and bottom. By allowing the plaster to flow on the sides of the channel total support and a tight fit was provided.

To provide for application of eccentric loads the rollers were moved to predetermined positions by means of bolts and threaded holes in the channel, roller and plates. To maintain the walls in vertical alignment, temporary wedges were used. These wedges were removed when the loading head was brought into contact with the loading assembly and as a small precompressive force was applied to the wall.

5.4.3 Full Scale Walls

The walls were moved into the testing machine using the

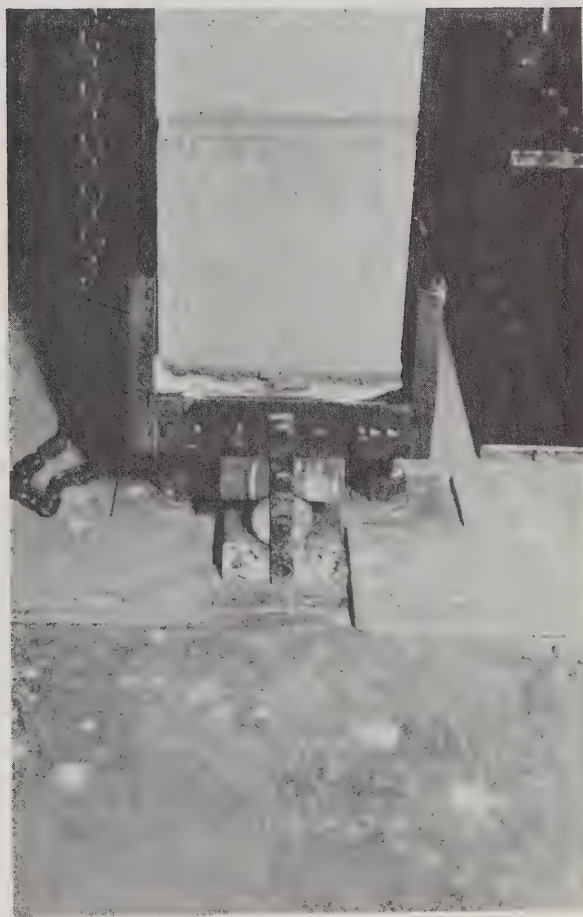


PLATE 5.2 Test Wall Support

device shown in Plate 5.2. The device consisted of two channel sections connected with threaded steel rods. The channels were placed on the two sides of the wall and compressive force was introduced by tightening a set of bolts. To avoid damaging the specimens, rubber pads were placed in three locations on each side of the wall as shown in Plate 5.3. The walls were lifted by a 10-ton overhead crane and moved into position for testing.

Plate 5.4 shows a wall specimen positioned and ready to be tested. The load was applied using the same procedure and arrangement as for short wall specimens.



PLATE 5.3 Device Used to Transport the
Wall and Prism Specimens

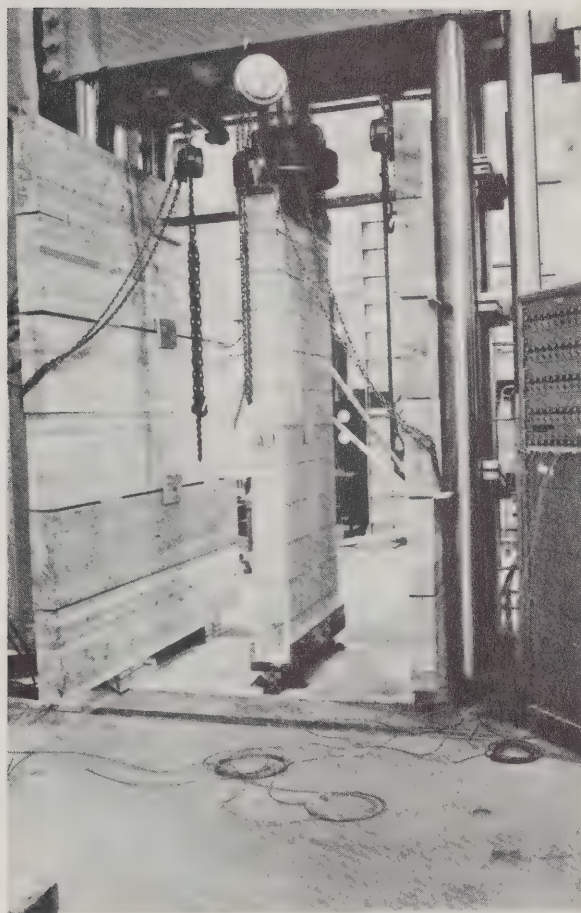


PLATE 5.4 Wall in Position for Testing

CHAPTER VI

Material Properties and Strength of
Prisms and Short Wall Specimens

6.1 Introduction

In this chapter the properties of the individual materials are examined experimentally. The properties of the composite material are then studied both theoretically and experimentally and theoretical relations which predict these properties are developed. Failure mechanisms for masonry are discussed and the state of stress of loaded masonry is examined by means of a finite element analysis in an attempt to explain the mechanisms of failure.

6.2 Strength and Modulus of Elasticity of Masonry Units

6.2.1 Compressive Strength

One of the most difficult aspects of testing masonry units is the determination of their compressive strength. Normally the masonry units are capped prior to testing and are subjected to compressive stresses in a standard testing machine. Compressive strength values of masonry units are affected by dimensions, testing procedure, and support conditions.

Because of the restraining effect provided by the bearing plates during testing, masonry units of different dimensions, particularly of different height to width ratios, yield different

compressive strength values for a given type of material. Such uncertainties in the determination of the compressive strength of a masonry unit are, at least in part, responsible for the wide scatter in experimental data relating masonry strength to the compressive strength of a single unit. In addition, the state of stress developed in a standard compression test of a masonry unit differs from the stress state in a masonry assembly. The masonry unit in an assembly, is subjected to stresses in the direction of the external load and lateral tensile stresses resulting from differences in material properties. This aspect is further examined in Section 6.4 of this chapter.

In this study, the compressive strength of the masonry units was determined by testing 30 solid blocks with nominal dimensions of 4 x 8 x 16 in. Plate 6.1 shows the test set up for evaluating the compressive strength and the load deformation characteristics of the solid blocks.

The maximum and minimum observed stresses at failure were 3890 psi and 1850 psi respectively with a mean value of 2350 psi. The coefficient of variation was 9.7% and the 95% confidence limits on the mean were 2270 and 2420 psi. Excluding 5% of the test data the expected strength was 1950 psi with 95% confidence limits equal to 1900 and 2000 psi.

Compressive strains for a number of specimens were measured by monitoring the travel of the piston of the testing machine and by 4 inch strain gauges attached to the face of the block.

Figure 6.1 is a plot of measured stresses and strains for a number of specimens. Applying the ACI formula for the modulus

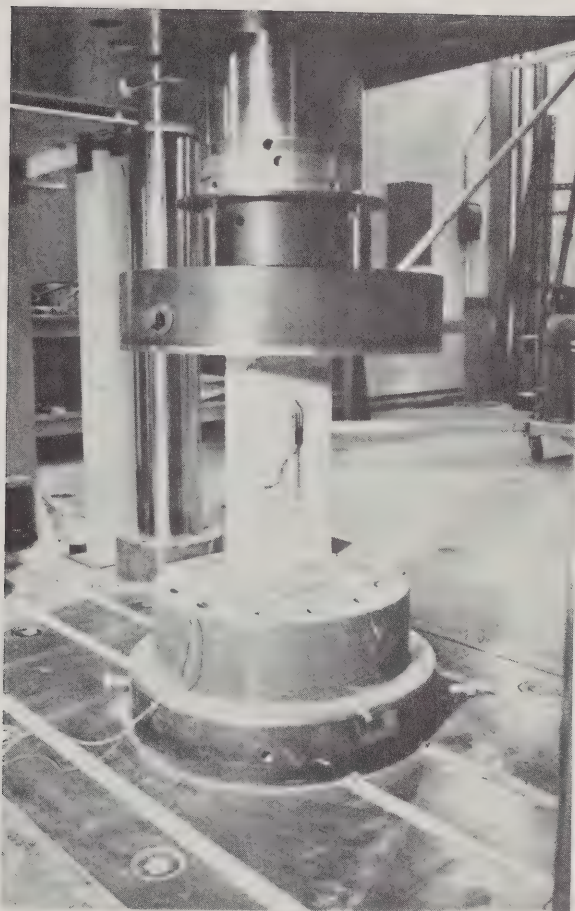


PLATE 6.1 Test Set-up for Determining Compressive
Strength End Load Deformation
Characteristics of Solid Concrete Masonry
Units

of elasticity of concrete and using 95 lb/ft³ for the unit weight and 1950 psi for strength, the modulus of elasticity for the concrete block unit is:

$$E_b = w^{1.5} 33\sqrt{f'_b} \text{ psi} = 95^{1.5} \times 33\sqrt{1950}$$

$$= 1.35 \times 10^6 \text{ psi}$$

This value, plotted in Figure 6.1, is in good agreement with the observed data.

6.3 Properties of Mortar

6.3.1 General

The prime function of the mortar is to bond masonry units into a monolithic mass ensuring a barrier to the entry of wind-driven rain and providing required structural integrity. This requires a complete "extent" of bond. Masonry mortar and concrete blocks contain the same basic ingredients - cementitious material, aggregate and water. As a result, it is commonly assumed that mortar and concrete block perform similar functions. This is not the case. In a masonry wall the mortar essentially acts as the binder to unite the units that provide the strength. The properties of mortar fall into two distinct groups: those of plastic mortar, and those of hardened mortar.

6.3.2 Plastic Mortar

Workability is the most important property of plastic

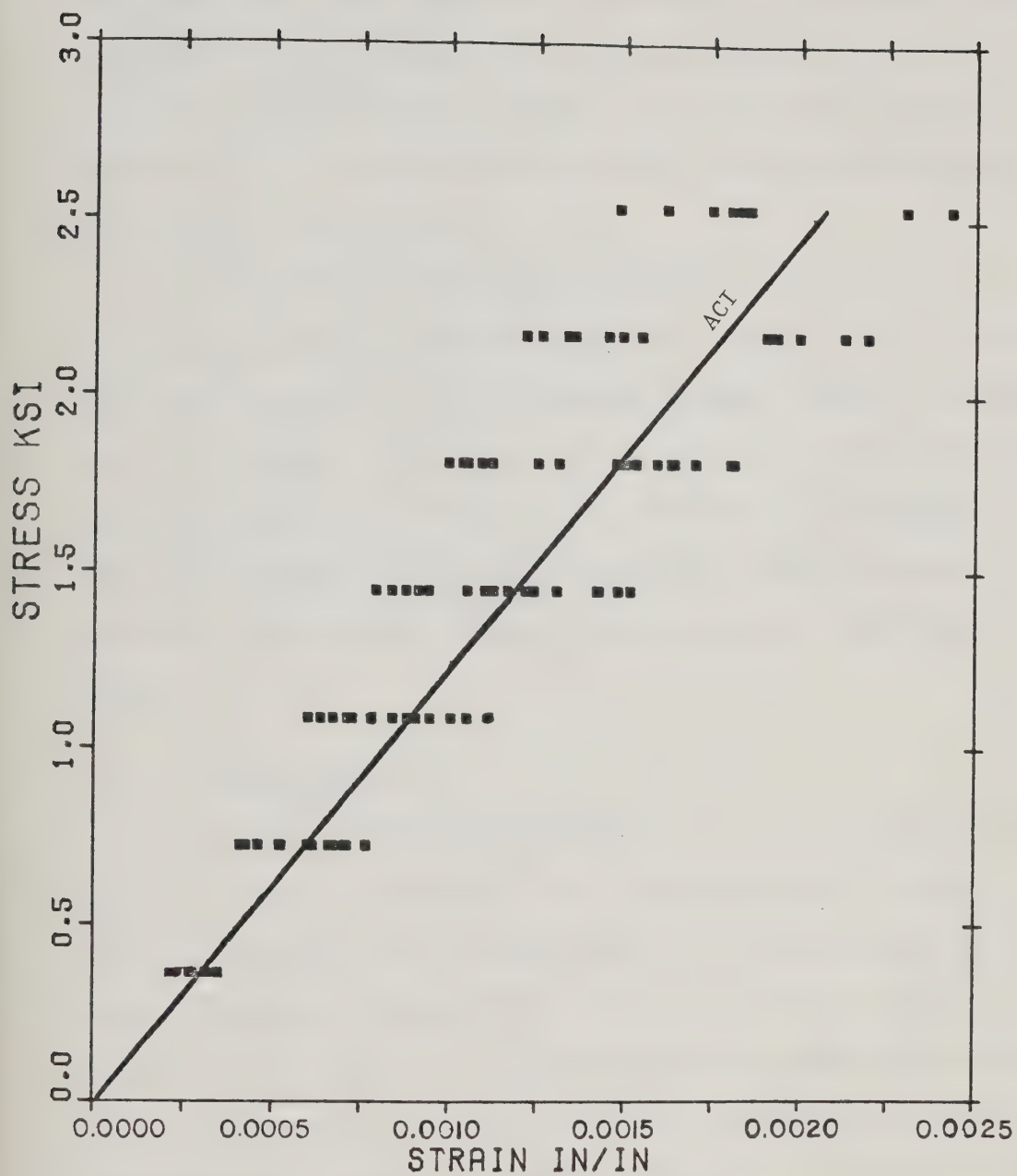


FIG. 6.1 Stress-Strain Relation for Solid
Concrete Masonry Units

mortar. It can be defined as the ability of the mortar to spread, under the trowel, into the cracks and crevices of the masonry unit. In reality it is a combination of several properties including plasticity, consistency and cohesion. It defies exact laboratory measurement, but the mason can assess it by observing the response of the mortar to his trowel.

Workability is the result of a roller-bearing effect of the aggregate particles lubricated by the cementing slurry. Factors affecting workability include aggregate grading, material proportions and water content. The capacity of the mortar to retain satisfactory workability under the influence of the suction of the concrete block unit depends on its water retentivity. Good workability and good water retention are essential for maximum bond with masonry units.

6.3.3 Hardened Mortar

A number of strength properties are of prime importance in hardened mortar. First among these is the strength of the bond between the mortar and the masonry unit. The bond strength is usually assessed on the basis of compressive strength values obtained from 2-inch cubes cast and cured under conditions reflecting construction practice. A new method which utilizes centrifugal force to apply uniform tensile or shearing stresses on a masonry specimen was developed during the course of the experimental part of this study. The system consists of a rotating disc as shown schematically in Figure 6.2 to which the test specimens are attached, as shown. Specimens used for determining tensile bond and shear bond strength

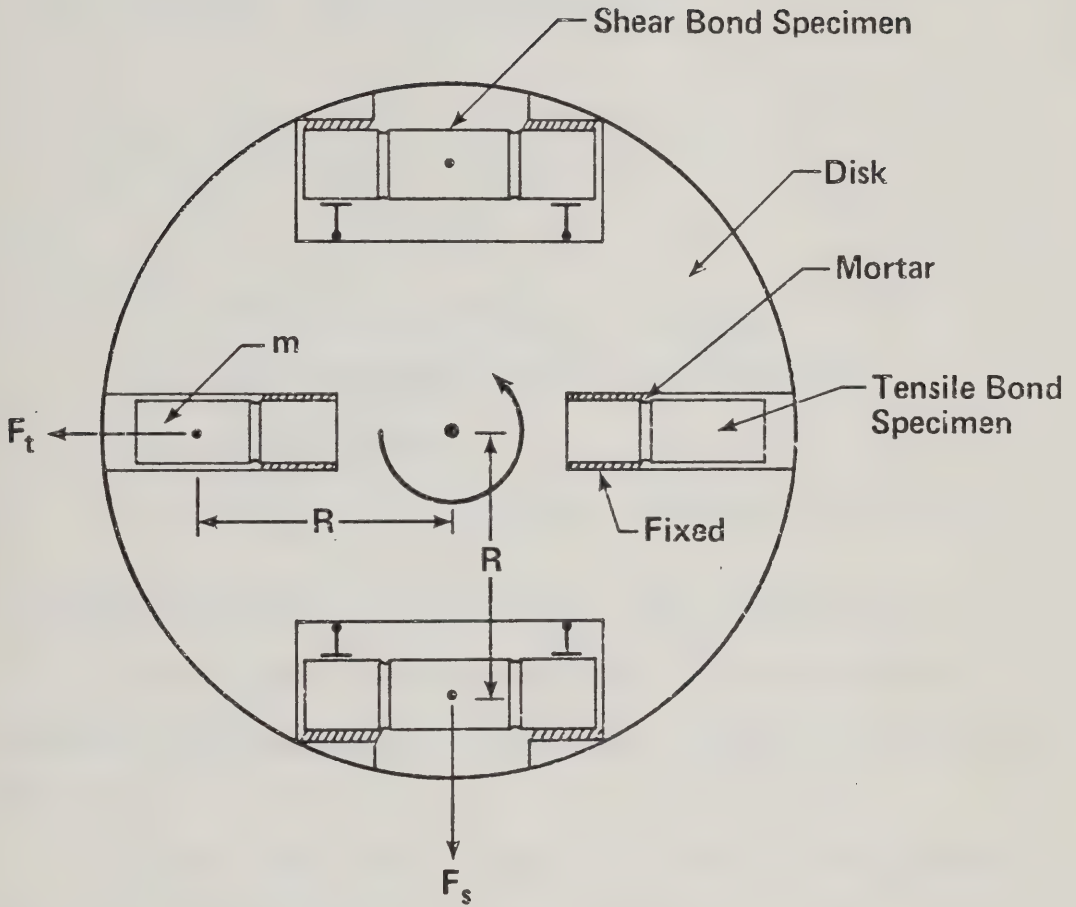


FIG. 6.2 Schematic Diagram of Bond Test Apparatus

are shown in Figure 6.3. As the system is rotated at increasing angular velocity with a small constant acceleration, the force in the radial direction increases and at a particular velocity the force is large enough to break the bond. The force causing failure is then calculated, using the relationship:

$$F = m\omega^2 R$$

where

F = radial force acting on the specimen

m = mass of separated portion of the specimen

ω = angular velocity

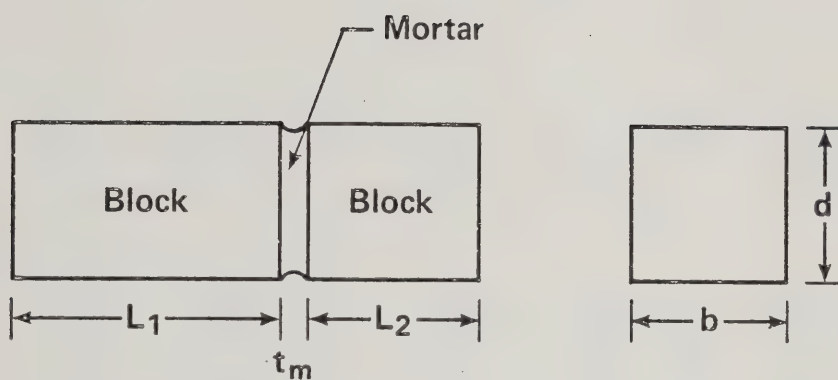
R = distance from the center of rotation to the center of mass.

A complete description of the system is given in Appendix C.

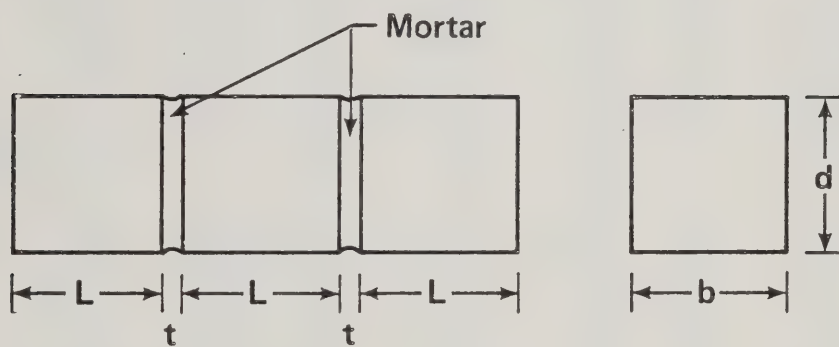
The mean tensile bond strength for 90 specimens tested using this new system was 42 psi and with a standard deviation of 20.0 psi.

The mean shear bond strength of the fourty-five specimens tested was 40.4 psi with a standard deviation of 21.7 psi. A complete set of the data from tensile bond tests is given in Table C.1 in Appendix C.

Fifty 2 x 2 x 2 in. cubes were tested in compression. The mean compressive strength was 2540 psi with a coefficient of variation of 8.3% and a standard deviation of 210 psi. The 9% confidence limits based on 5% exclusion were 2280 and 2210 psi. A complete set of cube strength results is given in Table 6.1.



a) Tensile bond specimen



b) Shear bond specimen

FIG. 6.3 Tensile and Shear Bond Test Specimens

TABLE 6.1
Compressive Strength of Mortar
2 x 2 x 2 in. Cubes

No.	Load (kips)	Stress (psi)	No.	Load (kips)	Stress (psi)	No.	Load (kips)	Stress (psi)
<u>7 Day Test:</u>								
1	6.00	1500	9	10.60	2650	30	10.10	2520
2	5.80	1450	10	11.50	2870	31	11.05	2760
3	6.45	1610	11	10.20	2550	32	11.30	2820
4	5.70	1430	12	9.50	2370	33	11.30	2820
5	5.90	1480	13	10.80	2700	34	11.00	2750
6	6.00	1500	14	11.50	2870	35	9.10	2270
7	4.60	1500	15	11.90	2970	36	10.40	2600
8	4.10	1030	16	10.60	2650	37	10.90	2720
9	7.00	1750	17	9.90	2470	38	10.70	2670
10	5.20	1300	18	10.40	2600	39	10.20	2550
<u>28 Day Test:</u>			19	8.75	2180	40	10.80	2700
			20	8.80	2200	41	10.50	2620
1	10.25	2560	21	9.80	2450	42	9.60	2400
2	9.30	2320	22	9.45	2360	43	10.40	2600
3	9.00	2250	23	11.20	2800	44	9.80	2450
4	10.90	2720	24	8.40	2100	45	10.65	2660
5	10.10	2520	25	10.40	2600	46	9.80	2450
6	11.40	2850	26	8.75	2180	47	8.50	2120
7	10.18	2540	27	9.90	2470	48	10.20	2550
8	10.90	2720	28	9.60	2400	49	9.10	2270
			29	9.80	2450	50	9.90	2470

Fifty standard 6 x 12 in. mortar cylinders were tested in axial compression. The mean compressive strength was 1600 psi with a coefficient of variation of 26.9% and a standard deviation of 430 psi. The load deformation characteristics of the mortar cylinders is shown in Figure 6.4. A straight line passing through the average stress-strain data yields a modulus of elasticity of 0.7×10^6 psi.

6.4 Grout

6.4.1 Compressive Strength

The compressive strength of the grout used in grouting the reinforced short walls and full scale walls, was evaluated experimentally by testing thirty specimens prepared in accordance with CSA Standard A179M-1976³³. The mean compressive strength was 2380 psi, with a standard deviation of 280 psi, and a coefficient of variation of 10.6%.

6.4.2 Bond Between Grout and Masonry Units

The bond between the concrete block units and the grout was evaluated experimentally using the centrifugal testing machine previously described. Eighteen test specimens were manufactured by pouring grout into a 4 x 4 x 12 in. form on the bottom of which was a 4 x 4 x 4 in. concrete block specimen cut from a 4 x 8 x 16 in. solid block. Care was taken to ensure that the face on which the grout was poured was an original rather than a cut face. The mean bond value was 145 psi, with a standard deviation 7.0 psi and a coefficient of variation of 5%. The complete test results are given in Table C.2, in Appendix C.

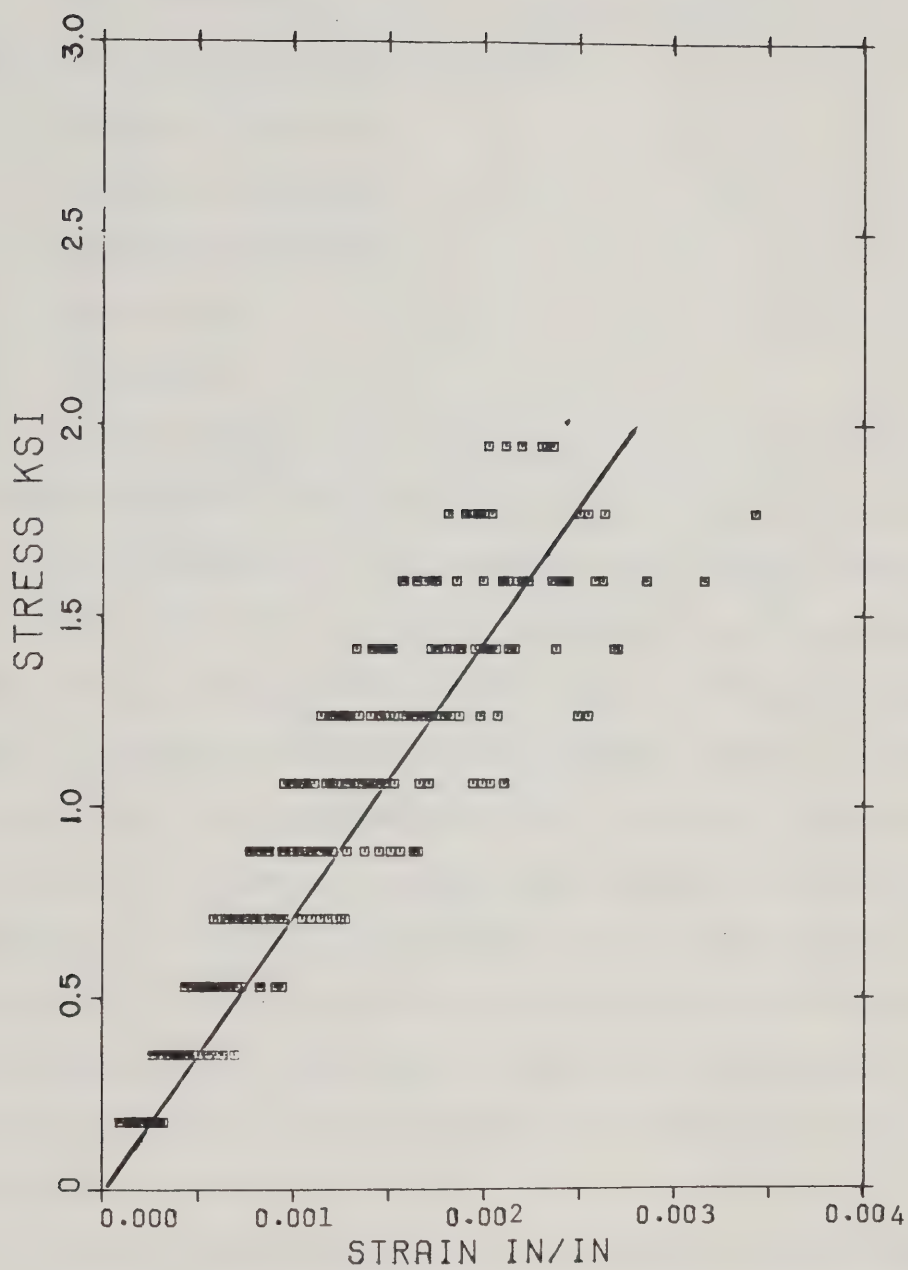


Fig. 6.4 Stress-Strain Relation for Type S Mortar Cylinders

6.5 Compressive Strength of Prisms

6.5.1 General

The compressive strength of a masonry assembly is a function of many factors, the most important being:

- a) strength of the unit
- b) strength of the mortar
- c) thickness of the joint
- d) reinforcement
- e) workmanship

The compressive strength of an assemblage usually lies between the compressive strength of the mortar and that of the masonry unit. The modulus of elasticity of the mortar is usually smaller than that of the masonry unit and, as a result, the free lateral deformation of the mortar is substantially greater than that of the concrete block. If there is a difference in the Poisson's ratio of the two materials, the lateral strains will differ even more. Because the masonry unit, at the mortar interface, must undergo the same lateral expansion as the mortar due to friction and bond, the lateral expansion of the mortar is restrained, producing tensile strains in the masonry units. These lateral strains introduce tensile stresses and tensile failure occurs before the compressive strength of the unit is reached.

Assuming that the prime mode of failure in concrete block masonry assemblages is tensile splitting it is now in order to summarize the variables affecting this phenomenon. The physical properties of mortar and masonry units, together with their geometric relationships, control the compressive strength. Past investigators

have tried to relate the compressive strength, the modulus of rupture, the tensile strength and the shearing strength of the masonry unit to the compressive strength of the assemblage. Studies of physical properties for mortar have usually been confined to compressive and splitting strengths.

Studies concerning the geometric relationships have included the effects of slenderness ratio of the assemblage, joint thickness, net area, and core patterns. In addition to these variables there is the influence of workmanship to be considered.

6.5.2 Analytical Evaluation of Compressive Strength of Masonry Prisms

Based on a stress analysis Hilsdorf³ in 1967 presented an analytical procedure to predict the compressive strength of masonry. His work is based on solid masonry units fully bedded by mortar. In applying the method as developed by Hilsdorf one must recognize that in hollow concrete block construction practice, mortar is placed only on the face shells. It has been observed, however, that the mortar penetrates into the web by 25 to 50 percent. Figure 6.5 shows the stress conditions in a prism of solid blocks. Hilsdorf's theoretical approach of compressive strength of masonry assemblages is based on the assumptions that masonry units behave in accordance with a modification of Mohr's theory of failure, that there is a perfect bond between the block and mortar interfaces and that the distribution of lateral and vertical stresses is uniform. Figure 6.6 shows the theoretical envelope relating the tensile and compressive stresses in a block at failure.

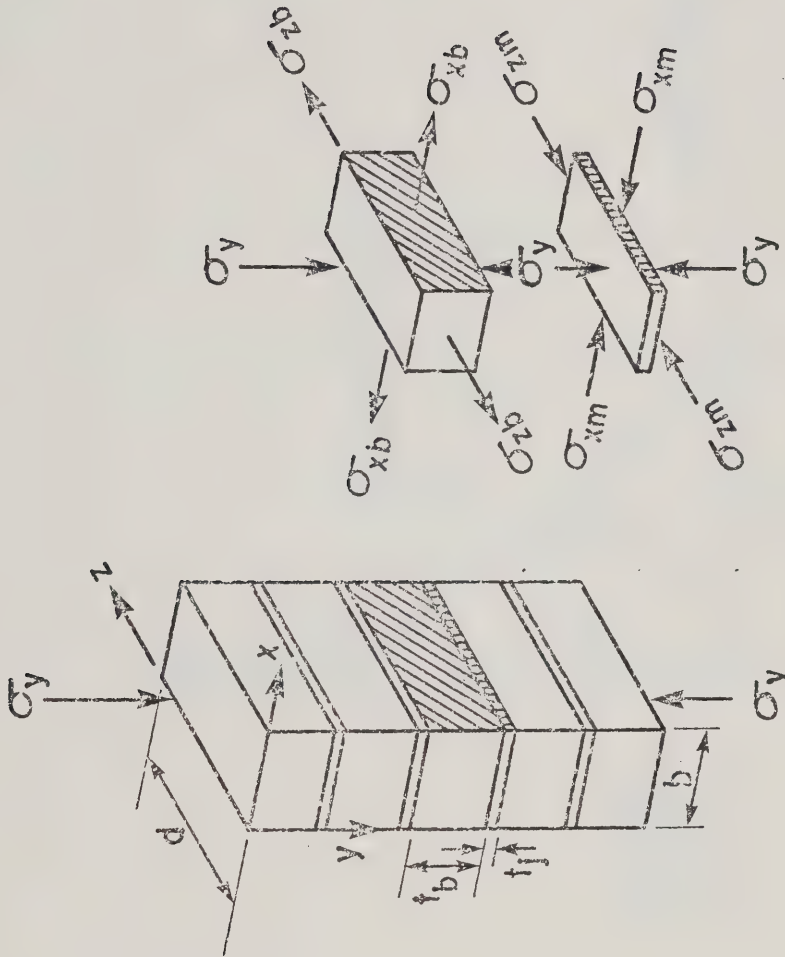


FIG. 6.5 Block and Mortar Stresses Due to Applied Compressive Load

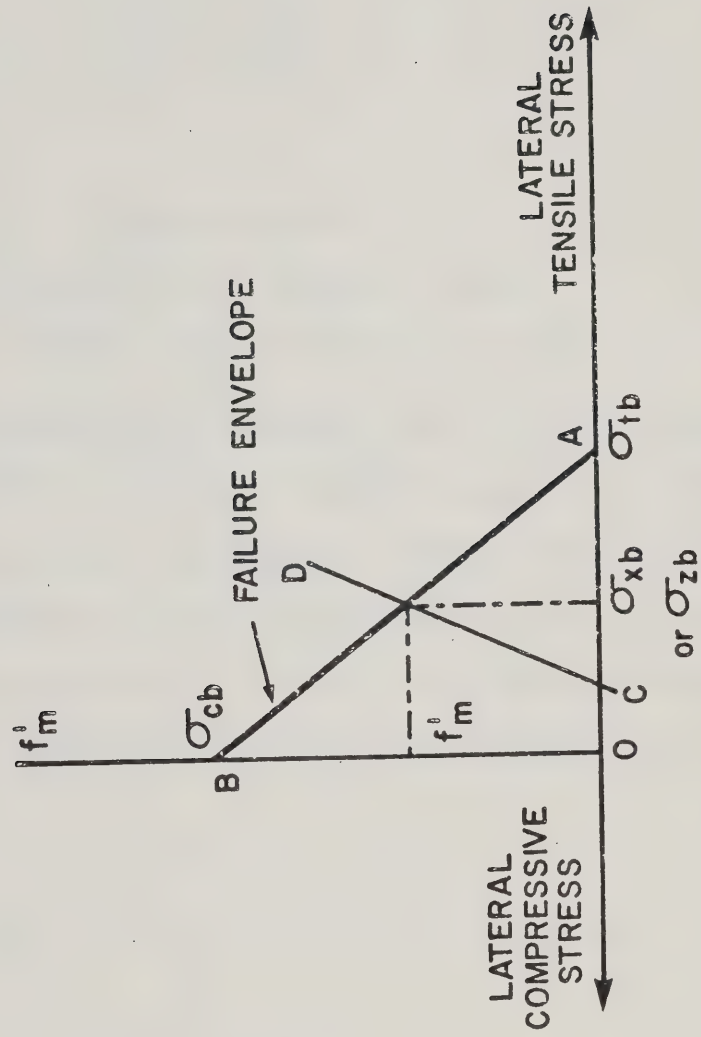


FIG. 6.6 Relation Between Tensile and Compressive Stresses in a Masonry Unit at Failure

If it is further assumed that the tensile stresses are equal in the x and z directions, then line AB in Figure 6.6 can be represented by

$$\sigma_x = \sigma_z = \sigma_{tb} \left[1 - \frac{\sigma_y}{\sigma_{cb}} \right] \dots\dots\dots 6.1$$

where

- $\sigma_x = \sigma_z =$ tensile stresses
- $\sigma_{tb} =$ uniaxial tensile strength of block
- $\sigma_{cb} =$ uniaxial compressive strength of block

As the vertical load increases, the mortar has a tendency to expand laterally. The mortar is however assumed to be in perfect bond with the block and it is therefore confined. The strength of the mortar increases due to the confinement and if the results from triaxial compression tests for concrete are applied to mortar, this strength can be approximated by the following relation suggested by Richart *et al*³⁹:

$$\sigma_y = \sigma_{cm} + 4.1 \sigma_{xm} \dots\dots\dots 6.2$$

where

- $\sigma_y =$ local stress in the vertical direction
- $\sigma_{cm} =$ uniaxial compressive strength of mortar
- $\sigma_{xm} =$ lateral compressive strength in the mortar joint

From Equation 6.2 the minimum lateral confinement of the mortar joint is given by:

$$\sigma_{xm} = \frac{1}{4.1} (\sigma_y - \sigma_{cm}) \dots\dots\dots 6.3$$

If the lateral tensile stress in the block and the compressive lateral stresses in the mortar joint are uniformly distributed over the height of the block and mortar joints then for equilibrium:

$$\sigma_{xb} t_b = \sigma_{xm} t_j \dots\dots\dots 6.4$$

where

- t_b = height of block
- t_j = height (thickness) of joint

Substituting Equation 6.4 into Equation 6.3, the equation for line CD in Figure 6.6 is:

$$\sigma_{xb} = \frac{t_j}{4.1 t_b} (\sigma_y - \sigma_{cm}) \dots\dots\dots 6.5$$

From Equations 6.1 and 6.2 the intersection of line AB and CD, or the failure stress σ_y , can be evaluated as:

$$\sigma_y = \sigma_{cb} \left[\frac{4.1 \sigma_{tb} + \alpha \sigma_{cm}}{4.1 \sigma_{tb} + \alpha \sigma_{cb}} \right] \dots\dots\dots 6.6$$

where

$$\alpha = t_j/t_b$$

Hilsdorf suggested a coefficient of non-uniformity to be applied to Equation 6.6. This factor is not a constant but depends on such parameters as geometric relations and strength.

The compressive strength of masonry prisms can also be quantitatively predicted by strain compatibility. The lateral stresses produce lateral strains and, if all the assumptions made previously hold, then

$$\begin{aligned}\epsilon_{xb} &= \frac{1}{E_b} \left[\sigma_{xb} + \nu_b (\sigma_y - \sigma_{zb}) \right] \\ \epsilon_{zb} &= \frac{1}{E_b} \left[\sigma_{zb} + \nu_b (\sigma_y - \sigma_{xb}) \right] \dots\dots\dots 6.7\end{aligned}$$

where

$$\begin{aligned}\epsilon_{xb}, \epsilon_{zb} &= \text{the extensional strains in the x and z} \\ &\quad \text{directions in the block} \\ E_b &= \text{modulus of elasticity of concrete block} \\ \nu_b &= \text{Poisson's ratio for the concrete block}\end{aligned}$$

Similarly the strains in the same directions at the mortar joint are given by

$$\begin{aligned}\epsilon_{xj} &= \frac{1}{E_j} \left[-\sigma_{xj} + \nu_j (\sigma_y + \sigma_{zj}) \right] \\ \epsilon_{zj} &= \frac{1}{E_j} \left[-\sigma_{zj} + \nu_j (\sigma_z + \sigma_{xj}) \right] \dots\dots\dots 6.8\end{aligned}$$

where

$$\epsilon_{xj}, \epsilon_{zj} = \text{the extensional strains in the mortar in the x and y direction}$$

E_j = modulus of elasticity of mortar joint

ν_j = Poisson's ratio for mortar joint

For compatibility

$$\epsilon_{xb} = \epsilon_{xj}$$

..... 6.9

$$\epsilon_{zb} = \epsilon_{zj}$$

For equilibrium, the total lateral tensile force on the block must be equal to the compressive force in the mortar. In the x-direction equilibrium requires that:

$$\sigma_{xb} t_b = \sigma_{xj} t_j$$

..... 6.10

$$\sigma_{zj} = \frac{t_b}{t_j} \sigma_{zb}$$

By setting ϵ_{xb} equal to ϵ_{xj} and substituting for σ_{xj} and σ_{zj} , the following equation is obtained:

$$\sigma_{xb} = \sigma_{zb} = \frac{\sigma_y (\phi \nu_j - \nu_b)}{1 + \alpha \phi - \nu_b - \psi \phi \nu_j}$$

..... 6.11

where

$$\psi = t_b / t_j$$

$$\phi = E_b / E_j$$

Equation 6.11 suggests that lateral stresses will reduce the effective value of f'_m , (the value of σ_y at which failure occurs). The limiting case from Equation 6.11 occurs when σ_{xb} and σ_{zb} are equal to the uniaxial tensile strength of the block and σ_y is zero. The other extreme is when the compressive stress (σ_y) is equal to the strength of the block and the tensile stresses are zero.

If the two extreme points are connected by a straight line by assuming Mohr's theory of failure as suggested by Hilsdorf, then the relationship between the tensile and compressive stress in the block can be expressed by:

$$\sigma_{xb} = \frac{1}{k} (\sigma_{cb} - f'_m) \quad \dots\dots\dots 6.13$$

where

$$k = \sigma_{cb} / \sigma_{tb}$$

By substituting the above expression for σ_{xb} in Equation 6.11 the following relation between f'_m and σ_{cb} is obtained:

$$\frac{f'_m}{\sigma_{cb}} = \frac{1}{1 + \frac{k(\phi v_m - v_b)}{(1 - v_b) + \psi \phi (1 - v_m)}} \quad \dots\dots\dots 6.14$$

A comparison of the two methods for predicting the compressive strength of masonry prisms is shown in Figure 6.7. The comparison is made for $\sigma_{cb} = 4000$ psi; $\sigma_{tb} = 400$ psi; $\sigma_{cm} = 2000$ psi; $v = v_b = v_m = 0.15$; $\phi = E_b / E_m = 2$.

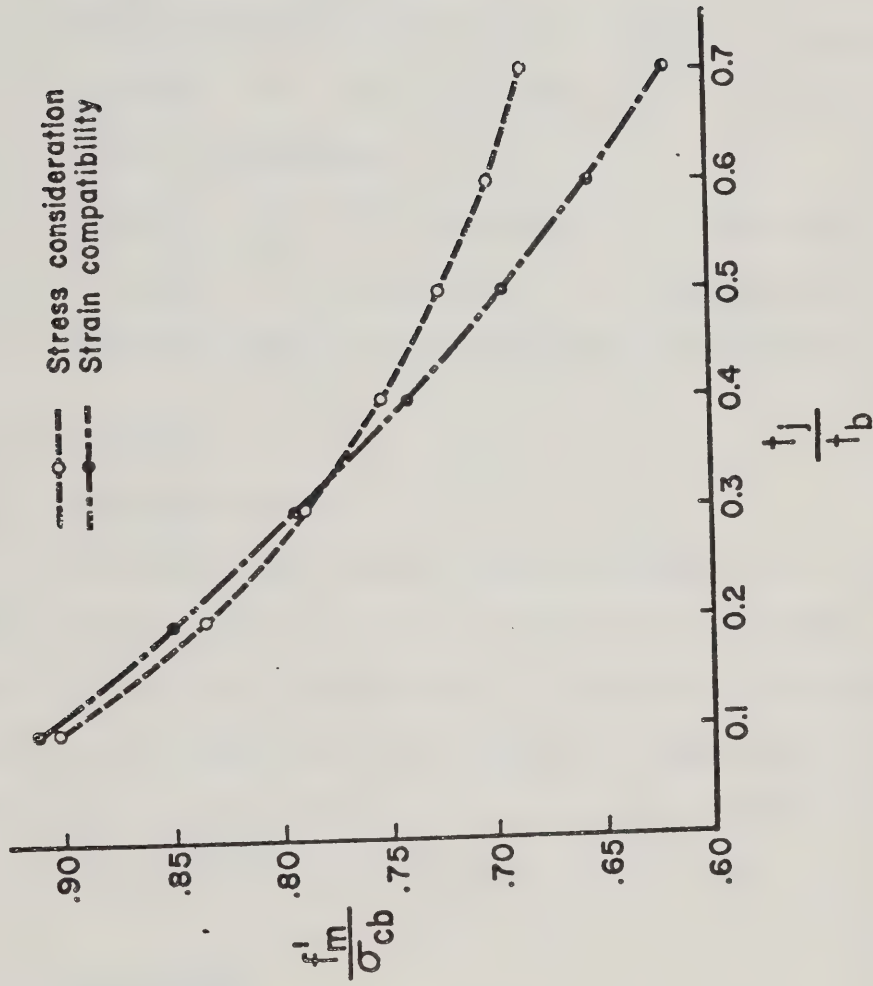


FIG. 6.7 Relation Between Prism Strength and Thickness of Components

The two methods presented are both approximate and subject to limitations, especially when applied to hollow concrete block assemblages. The most important limitations are:

- a) Assumption that $\sigma_x = \sigma_z$.
- b) Assumption that extent of mortar bedding has no effect on the behavior of the assembly.
- c) Assumption that vertical joints do not affect the strength.
- d) Assumption that shear at the block mortar interface has no effect on behavior.
- e) Assumption that failure initiates at the centroidal axis.
- f) Assumption that failure initiates at the masonry unit.
- g) Assumption that bond provides adequate confinement.

6.5.3 Test Results

6.5.3.1 Two-Block Prisms

The failure loads and the resulting stresses for the axially loaded two-block prisms are given in Table 6.2. The average failure stress for plain fully bedded prisms was 2090 psi and for plain prisms with face-shell mortar was 2010 psi. Prisms with flattened joint reinforcement failed at an average stress of 1840 psi and prisms with #9 gauge wire reinforcement failed at 1690 psi.

6.5.3.2 Short Walls

The results of tests on plain ungrouted short walls are summarized in Table 6.3 for axially loaded specimens and in Table 6.4 for eccentrically loaded specimens.

Sixteen short walls, nine of which were reinforced in one or two directions and seven of which had no vertical reinforcement

TABLE 6.2 Test Results for Axially Loaded

Two Block Prisms

Prism	Mortar Bedded Area in. ²	Joint Reinforcement	Load at Failure kips	Stress at Failure Based on Mortar Bedded Area psi	Stress Based on Gross Area in. ²
* 1	58	Plain	132.4	2270	1110
2	"		117.5	2010	990
3	"		112.9	1930	940
4	"		150.1	2570	1260
5	"		106.6	1830	890
6	"		127.9	2190	1070
7	"		129.8	2230	1090
8	"		136.0	2330	1140
9	"		90.0	1540	750
10	"		115.7	1980	970
Average			121.9	2090	1020
**11	39	Plain	75.7	1940	640
12	"		100.0	2560	840
13	"		68.9	1760	580
14	"		78.8	2010	660
15	"		94.3	2410	790
16	"		90.0	2300	750
17	"		60.0	1530	500
18	"		65.5	1670	550
19	"		87.5	2240	730
20	"		65.0	1660	550
Average			78.5	2010	660
21	"	Flattened #9 Gauge Wire	90.0	2300	840
22	"		98.5	2520	830
23	"		60.4	1540	510
24	"		60.6	1550	510
25	"		50.8	1300	430
Average			72.0	1840	620
26	"	#9 Gauge Wire	60.5	1550	510
27	"		45.8	1170	380
28	"		55.2	1410	460
29	"		60.1	1540	500
30	"		70.0	2790	840
Average			58.3	1690	540

* Specimens 1 to 10 were fully bedded.

** For specimens 11 to 30 mortar was placed at the face shells only.

TABLE 6.3 Test Results for Axially Loaded Short Walls

Specimen	Mortar Bedded Area in. ²	Joint Reinforcement	Load at Failure kips	Stress at Failure Based on Mortar Bedded Area psi	Stress Based on Gross Area in. ²
* 1	152.5	plain	275.4	1690	550
2	152.5	plain	260.0	1700	560
Average			258.7	1690	560
** 3	122.3	plain	215.5	1760	710
4	122.3	plain	249.1	2040	820
Average			232.3	1900	760
5	122.3	flattened	234.8	1920	770
6	122.3	#9 gauge wire	191.1	1560	630
Average			212.9	1740	700
7	122.3	#9 gauge	200.0	1640	660
8	122.3	wire	171.2	1340	560
Average			185.6	1490	610

* Specimens 1 and 2 were fully bedded.

** For specimens 3 to 8 mortar was placed at the face shells only.

TABLE 6.4 Test Results for Eccentrically Loaded Short Walls

Specimen	Mortar Bedded Area in. ²	Joint Reinforcement	Eccentricity in.	Load at Failure kips	Moment at Failure kip-in.	Stress at Failure Based on Mortared Area psi
* 1	152.5	plain	t/6 = 1.27"	180.0	228.0	2630
2	122.3	"	t/6 = 1.27"	196.9	250.0	3190
3	"	"	t/6 = 1.27"	150.1	190.0	2430
4	"	"	t/3 = 2.54"	119.3	303.0	2890
5	"	"	t/3 = 2.54"	158.7	403.0	3850
Average						3000
6	"	#9 gauge	t/6 = 1.27"	160.0	203.0	2590
7	"	wire	t/6 = 1.27"	149.1	189.0	2420
8	"	"	t/3 = 2.54"	92.7	235.0	2250
9	"	"	t/3 = 2.54"	105.5	264.0	2540
10	"	"	t/3 = 2.54"	92.7	235.0	2250
Average						2410

* Specimen fully bedded.

and were fully or partially grouted, were tested in axial compression in an attempt to establish the contribution of vertical reinforcement and grout in carrying axial loads. The experimental results for these specimens are listed in Table 6.5. Analysis of results described in this chapter are presented in Chapter IX.

6.6 Modulus of Elasticity of Hollow Concrete Masonry

6.6.1 General

In masonry design, the modulus of elasticity is a factor affecting strength calculations and deflection calculations. Evaluation of this important strength parameter is a complicated task since the modulus of elasticity of masonry is affected by the modulus of both the masonry constituents, namely the mortar and block. Other factors which influence this parameter include the effect of vertical joints the thickness of the horizontal joints, stress levels and the shape of the block. Experimental information on the modulus of elasticity of masonry is lacking. In this section the elastic modulus of masonry is examined both theoretically and experimentally.

6.6.2 Theoretical Considerations for Modulus of Elasticity

Assuming that both mortar and concrete blocks obey Hooke's law and that there is a lack of fit at the interfaces, the following relations can be derived with reference to Figure 6.8.

The total deformation of one block plus one joint is:

$$\Delta t = \Delta t_j + \Delta t_b \dots\dots\dots 6.15$$

TABLE 6.5 Test Results for Axially Loaded Reinforced Short Walls and Grouted Short Walls

Specimen	Type of Construction	Number of Cores Filled	Vertical Reinforcement	Horizontal Reinforcement	Load at Failure kips	Loaded Area in. ²	Stress at Failure psi
1	fully bedded	5	plain	plain	317.9	302.1	1050
2	"	5	"	"	368.4	302.1	1220
Average							1130
3	phace shell	5	"	"	342.4	302.1	1130
4	mortar	5	"	#9 gauge wire	344.6	302.1	1140
5	fully bedded	3	"	plain	297.4	271.8	1090
6	phace shell	3	"	"	303.7	271.8	1120
7	mortar	3	"	"	303.8	271.8	1120
Average							1120
8	"	3	3#9	"	386.6	271.8	1420
9	"	3	3#9	"	275.3	271.8	1380
Average							1400
10	"	3	3#6	"	334.1	271.8	1230
11	"	3	3#6	"	265.3	271.8	1340
Average							1280
12	"	3	3#3	"	348.3	271.8	1280
13	"	3	3#3	"	280.3	271.8	1030
Average							1150
14	"	3	3#9	#9 gauge wire	311.5	271.8	1140
15	"	3	3#6	"	366.9	271.8	1350
16	"	3	3#3	"	201.2	271.8	1110

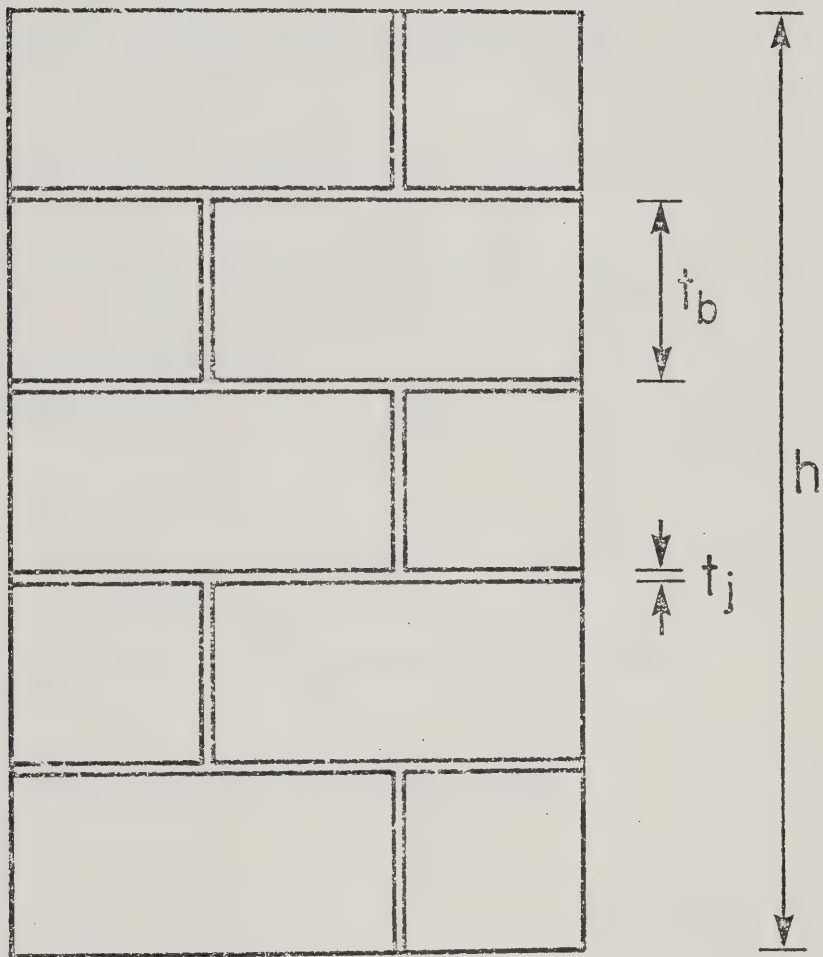


FIG. 6.8 Test Specimen for Evaluation of the Elasticity Modulus

where

Δt = total deformation

Δt_j = joint deformation

Δt_b = block deformation

The deformation of the joint with thickness t_j is:

$$\Delta t_j = \epsilon_j t_j \dots\dots\dots 6.16$$

where ϵ_j is the strain caused by the stress σ in the joint which has modulus of elasticity E_j .

By Hooke's Law

$$\Delta t_j = \frac{\sigma}{E_j} t_j \dots\dots\dots 6.17$$

similarly for the block and the assembly we can write:

$$\Delta t_b = \frac{\sigma}{E_b} t_b \dots\dots\dots 6.18$$

$$\Delta t = \frac{\sigma}{E_m} t \dots\dots\dots 6.19$$

where

$$t = t_j + t_b$$

E_m = modulus of elasticity of the assembly

Substituting in Equation 6.15 the following relation is obtained:

$$\frac{\sigma}{E_m} t = \frac{\sigma}{E_j} t_j + \frac{\sigma}{E_b} t_b \dots\dots\dots 6.20$$

From this relation the modulus of elasticity of the masonry system is:

$$E_m = \frac{t}{\frac{t_j}{E_j} + \frac{t_b}{E_b}} \dots\dots\dots 6.21$$

Letting

$$\frac{t_b}{t_b + t_j} = \frac{t_b}{t} = \delta \dots\dots\dots 6.22$$

and substituting in Equation 6.21, the following expression is obtained:

$$E_m = \frac{1}{\frac{1-\delta}{E_j} + \frac{\delta}{E_b}} \dots\dots\dots 6.23$$

Substituting into Equation 6.23 the values for the modulus of elasticity of the block and mortar as found experimentally in previous sections of this chapter, the theoretical modulus for the assembly is:

$$E_m = \frac{8}{\left[\frac{0.375}{0.70} + \frac{7.625}{1.35} \right]} \times 10^6 \approx 1.3 \times 10^6 \text{ psi}$$

6.6.3 Experimental Evaluation of Modulus of Elasticity of Hollow Concrete Block Masonry

The stress-strain relationship derived from tests of ten, one and one-half block wide, five block high specimens in axial compression

with flat end conditions is shown in Figure 6.9. The average stress at failure was 2056 psi. A straight line passing through the average values of the data obtained, suggests a value for the modulus of elasticity of 1.12×10^6 psi. This value is 86% of the theoretical value. The CSA Standard S-304 M¹³ recommends a modulus of elasticity equal to 1000 times ultimate compressive strength of the masonry. The ultimate strength for the units and mortar used in this study, computed in accordance with CSA Standard S-304-M¹³ is 1490 psi, resulting in a modulus of elasticity of 1.49×10^6 psi. This value is much higher than that obtained experimentally. Experimental results suggest a value of $750 f'_m$ to be more conservative for use in the CSA Standard S-304-M¹³ relation for modulus of elasticity. Factors affecting the modulus of elasticity of masonry are discussed in Chapter IX.

6.7 Prism and Short Wall Failures

The two-block prisms, tested in axial compression with flat ends, failed by vertical splitting in the web and face shells as shown in Plate 6.2. This type of failure was also observed in short wall specimens tested with flat or pinned ends with vertical loads applied axially or at small eccentricities. As vertical load eccentricity was increased, failure by web splitting was accompanied almost simultaneously by cracking in the horizontal mortar joints on the tensile face of the specimen. Typical failures of prisms and short wall specimens tested in axial compression are shown in Plates 6.3, 6.4, 6.5 and 6.6.

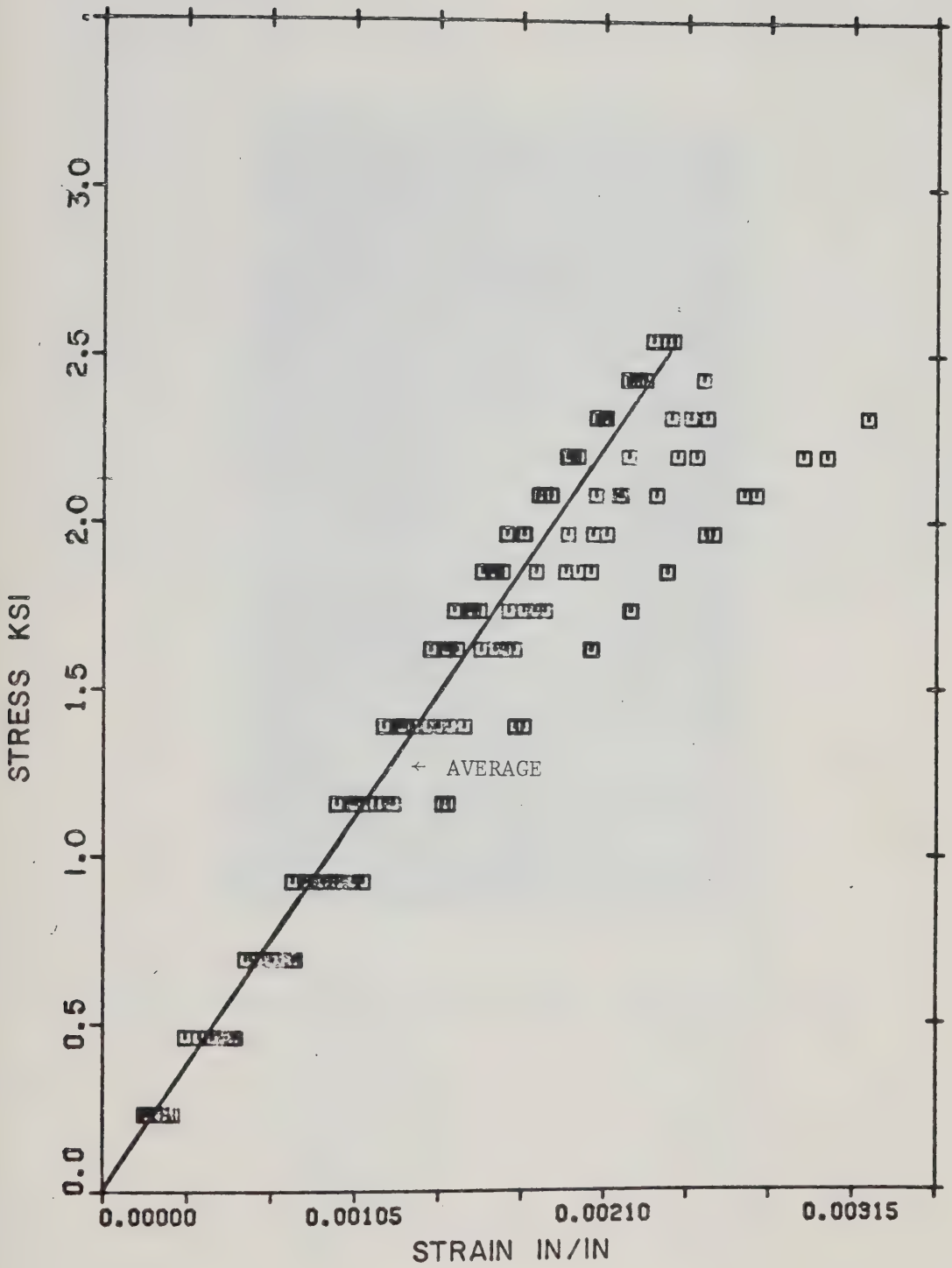


FIG. 6.9 Stress Strain Relation for Hollow Concrete Block Masonry

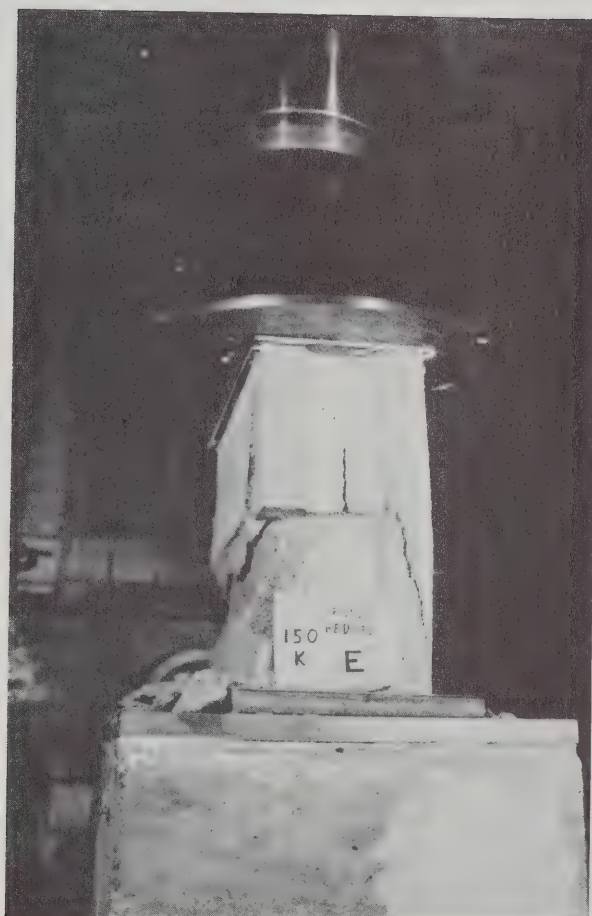


PLATE 6.2 Failure Mode of a Two-Block Fully-Bedded Prism

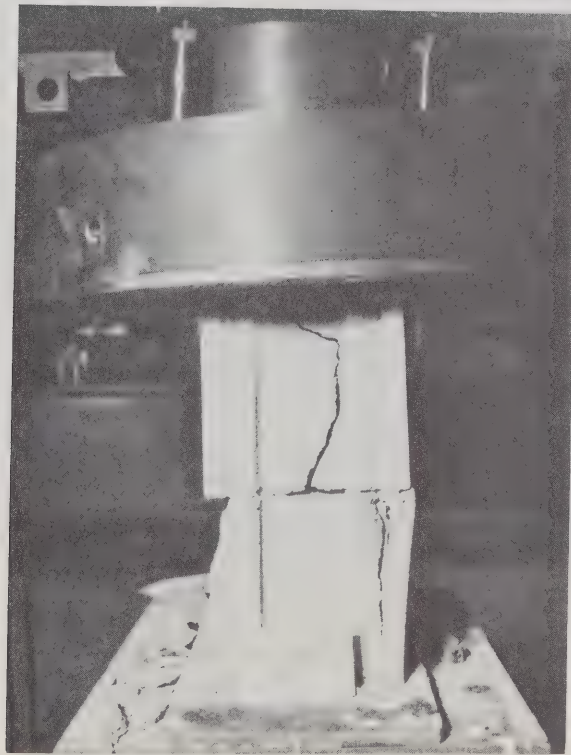


PLATE 6.3 Typical Failures of Prisms with No. 9
Gauge Wire Joint Reinforcement



PLATE 6.4 Failure Mode of Axially Loaded Concrete
Block Masonry Specimen



PLATE 6.5 Detailed View of Tensile Splitting Failure

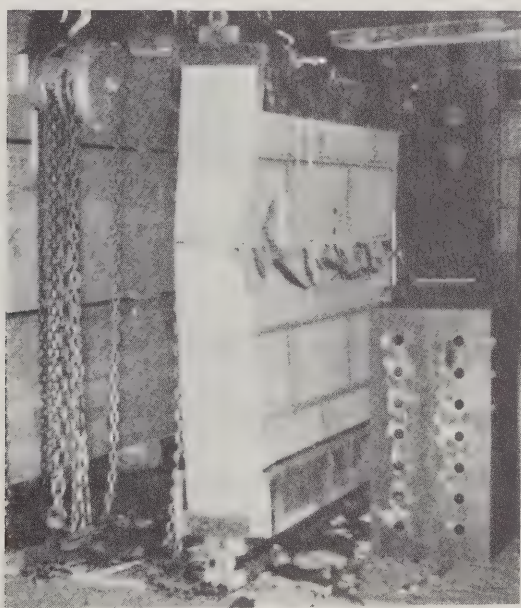
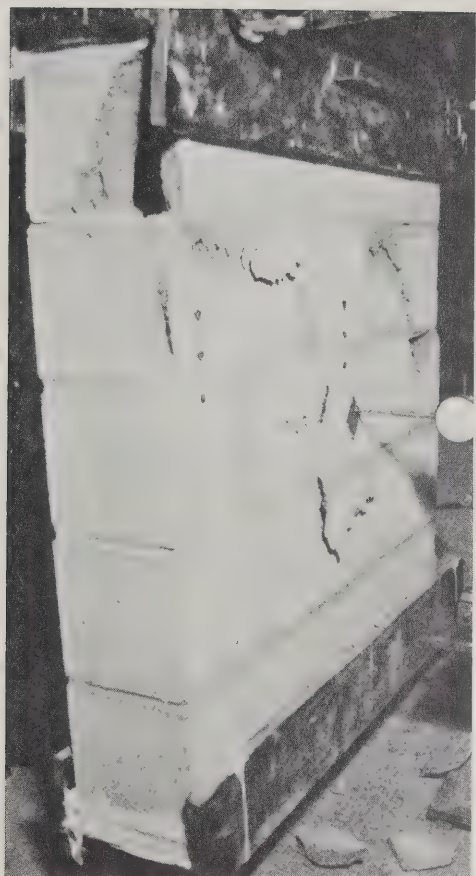


PLATE 6.6 Failures of Short Walls Tested with Pinned Ends

6.8 Effect of Joint Reinforcement on Vertical Load Carrying Capacity

Most codes specify a certain minimum percentage of steel to be placed in the joint of reinforced masonry walls. The CSA Standard S-304-M¹³ specifies that reinforced masonry load-bearing and shear walls shall be reinforced horizontally and vertically with steel having a minimum area calculated in conformance with the following formulae:

$$A_v = 0.002 A_g \alpha$$

$$A_h = 0.002 A_g (1 - \alpha)$$

where

A_v = area of vertical steel per unit of length of wall

A_h = area of horizontal steel per unit length of wall

A_g = gross section area per unit length of wall

α = reinforcement distribution factor varying from 0.33 to 0.67 as determined by the designer.

The basis of this requirement is to provide two-way action for resisting lateral loads. Theoretically, there is no reason to expect that joint reinforcement will increase the load bearing capacity of concrete masonry walls, especially with the construction procedures commonly used in Canada.

As a result of the substantial difference in the elastic properties of steel and mortar it can be assumed that the stress distribution in the mortar joint will be similar to that for a plate with a rigid inclusion. Figure 6.10 shows the distribution

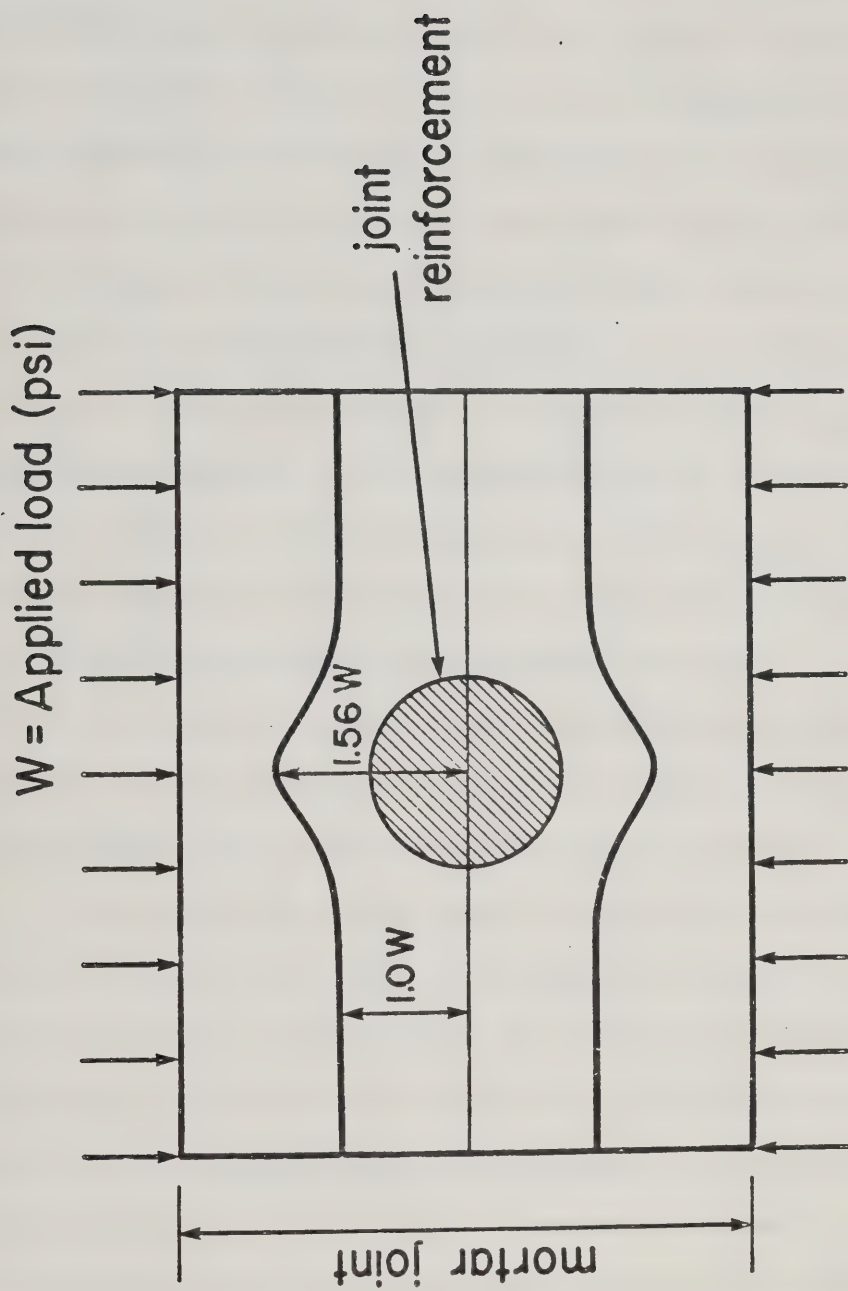


FIG. 6.10 Stress Distribution in a Uniformly Loaded Plate with Rigid Inclusion

of stress in a reinforced mortar joint uniformly loaded. This stress distribution has a peak of at least $1.56 W$, where W is the uniformly distributed load acting on the joint. The distribution is based on the assumption that the steel is infinitely stiffer than the mortar which is a realistic assumption considering that the ratio of modulus of elasticity of steel to that of mortar is of the order of 40 to 1. In reality the stress distribution is more complex because of the presence of confinement stresses and inelastic action. Exact analytical evaluation of the stress distribution in anisotropic plates is complex and beyond the scope of this thesis. Lekhniskii⁴⁰ gives a complete detailed account of stress patterns created in anisotropic plates under various loading conditions.

The average failure stresses for prisms with normal joint reinforcement was 18% lower than for plain prisms. For prisms with flattened joint reinforcement the reduction was 8%.

Axially loaded short walls failed in a similar manner to that for prisms. Short walls with normal joint reinforcement failed at average stresses 20% less than plain walls and specimens with flattened joint reinforcement at 8% less than plain walls. Fully bedded specimens carried only 10% additional load to that for specimens with face shell mortar. Eccentrically loaded short wall specimens with round joint reinforcement failed at an average stress 22% less than plain walls. Tests on full scale walls with and without joint reinforcement found the trend to be similar. Reinforced short wall specimens containing joint reinforcement failed at an average stress 6% lower than reinforced specimens without joint reinforcement.

6.9 Capacity of Short Wall Specimens

6.9.1 Specimens Without Vertical Reinforcement

A total of sixteen 8 x 40 x 40 in. short wall specimens with pinned support conditions were tested under vertical loads applied at equal top and bottom eccentricities of 0, $t/6$ and $t/3$.

Figure 6.11 shows plots of test results for eccentrically loaded short walls loaded to failure based on data in Tables 6.2 and 6.3. It is evident from Figure 6.11 and Tables 6.2 and 6.3 that a significant increase in "apparent" compressive strength occurs as a result of flexure. A similar behavior has been reported by Yokel and Mathey⁴¹ who introduced a coefficient "a" to distinguish compressive strength in flexure, designated by af'_m , from the compressive strength f'_m obtained from axial load tests on prisms with flat supports. The values of "a" given in Table 6.6 have been calculated by taking the ratio of flexural compressive strength to axial compressive strength. The curve shown in Figure 6.11 is a theoretical interaction curve developed using a computer program capable of analyzing plain and reinforced sections partially or fully grouted, fully bedded or face-shell bedded. The program and the material properties used in developing the interaction diagram are given in Appendix D.

The theoretical interaction diagram of Figure 6.11 was obtained using average compressive strength under kern point loading (i.e. $a f'_m = 1.45 \times 1900 \approx 2750$ psi). The difference in failure stresses under axial and eccentric loads is attributed to the mode of failure. Under axial load the failure mode is the well known critical splitting of the blocks in the webs and flanges. In

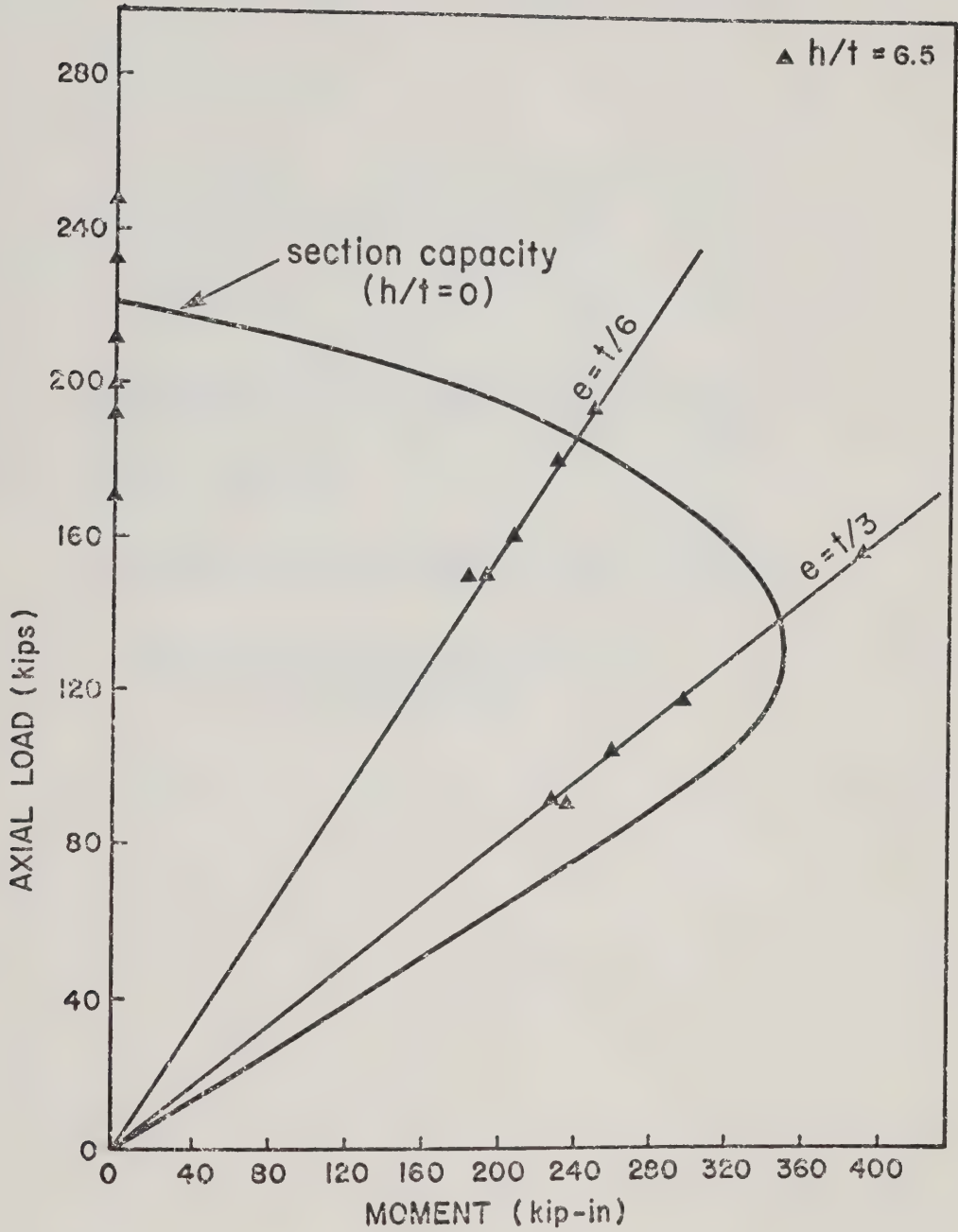


FIG. 6.11 Capacity of Short Wall

TABLE 6.6 Coefficient "a" of Apparent Increase of
Strength Due to Flexure

e/t	0	$t/6$	$t/3$
a for $f'_m = 1900$ psi	1.0	1.38	1.52
	1.0	1.68	2.02
	1.0	1.44	--
Average	1.00	1.45	1.80
a for $f'_m = 1650^*$ psi	1.0	1.57	1.36
	1.0	1.46	1.53
	1.0	--	1.36
Average	1.00	1.50	1.40

* Specimens reinforced with #9 gauge
wire joint reinforcement.

eccentrically loaded walls shear is introduced as shown in Figure 6.12. The shearing force opposes the splitting force on the compression side.

Due to the difference in material properties, most of the rotation in an eccentrically loaded wall takes place in the mortar joints resulting in the formation of a wedge. The forces acting on the block and mortar joint are shown qualitatively in Figure 6.13. The horizontal component of the force acting on the joint reduces the splitting force. Another factor contributing to the change in failure mode is the variation in confinement resulting from the variation in stress level across the joint.

As a result of the above factors the section fails when its compressive capacity is reached. For normal joint thicknesses this corresponds to the compressive strength of the masonry unit.

6.9.2 Partially or Fully Grouted Specimens with Vertical Reinforcement

The test results for axially loaded reinforced short walls and grouted short walls are presented in Table 6.5. For fully bedded and fully grouted plain specimens the average load at failure was 343 kips corresponding to an average stress of 1130 psi. Only one specimen, face-shell bedded and fully grouted, was tested. This specimen failed at 342.4 kips corresponding to a stress of 1130 psi. For a fully grouted specimen with #9 gauge wire joint reinforcement the failure stress 1140 psi. It appears from this data that there is no substantial difference in load carrying capacity among the three types of specimens.

The type of construction (fully bedded or face-shell bedded) had no effect on the strength of the assembly for walls built in

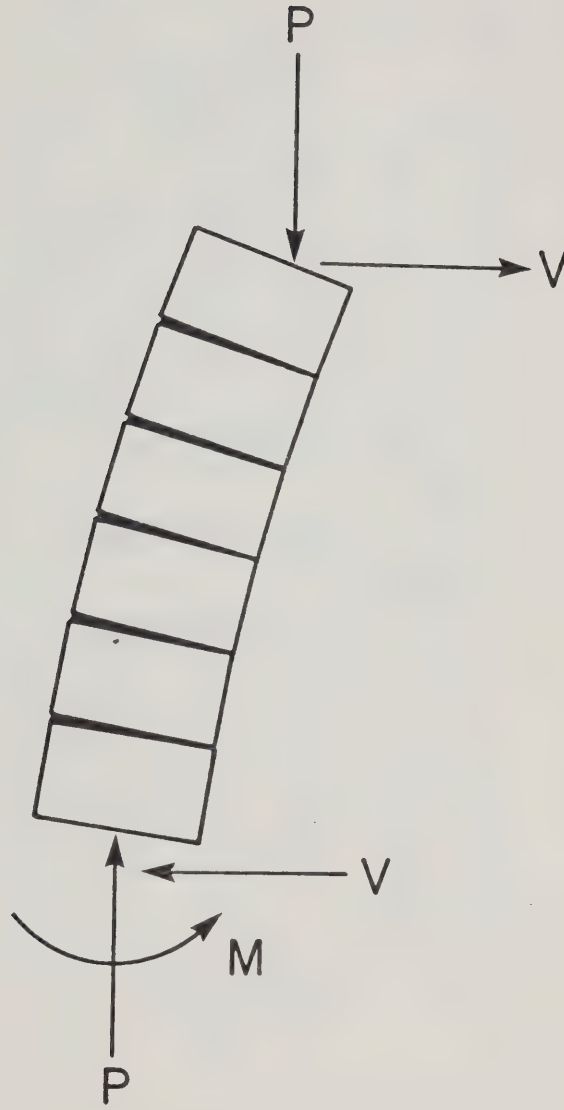


FIG. 6.12 Forces Acting on the Cross-Section of an Eccentrically Loaded Wall Portion

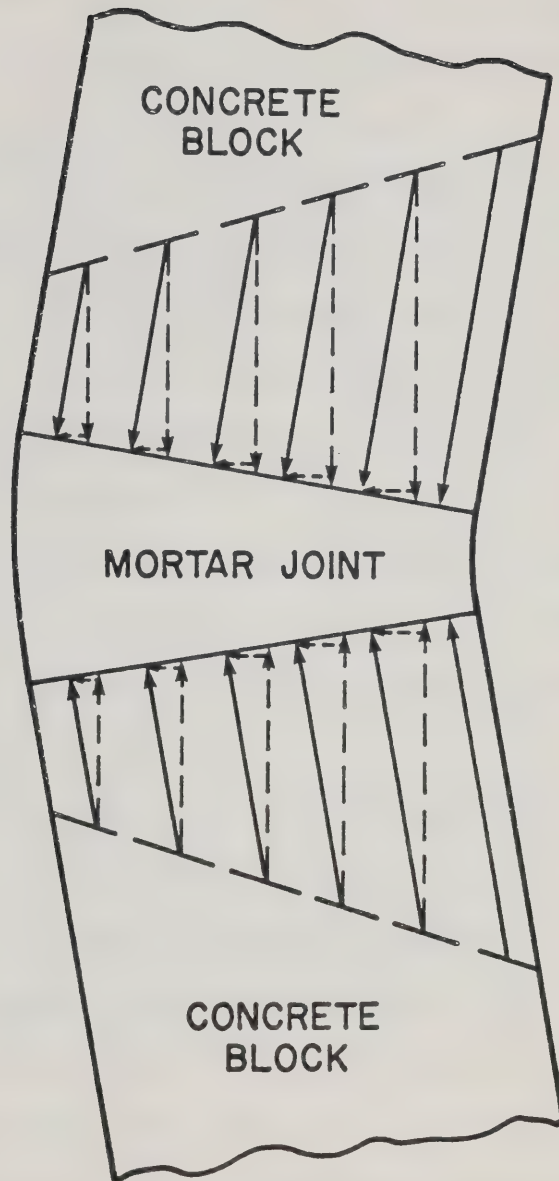


FIG. 6.13 Forces Acting on Eccentrically Loaded Wall Segment

running bond because the webs are not in vertical alignment. This non-alignment caused the mortar placed on the cross webs to be ineffective. Mortar penetration into the cores caused reduction of the grouted cross-sectional area at the joint, with the net result that only part of the grout is effective.

Assuming 25% active mortar penetration, an active mortar bedded area of 122.3 in.^2 and the stress at failure equal to 1900 psi for axially loaded ungrouted walls, the contribution of the grout for the four walls was 110.9 kips. For a grout compressive strength of 2380 psi, this yields an effective grout area of 46.6 in.^2 or 9.30 in.^2 per core.

Walls with only three cores filled failed at an average load of 301.6 kips. The theoretical load based on the analysis for fully grouted walls was 298.9 kips, which is in very close agreement with the test values.

For specimens with vertical reinforcement the contribution of the steel in resisting axial loads was found to be 82.0 kips for specimens with 3-#9 bars, 50.8 kips for specimens with 3-#6 and 15.4 kips for specimens with 3-#3 bars. The percent utilization of steel in the three groups of specimens with vertical reinforcement was therefore 46%, 64.1% and 77.7%, respectively.

The presence of joint reinforcement in three specimens with vertical reinforcement had no significant effect on the capacity of the section.

Typical failures of specimens with vertical reinforcement are shown in Plates 6.7 and 6.8.

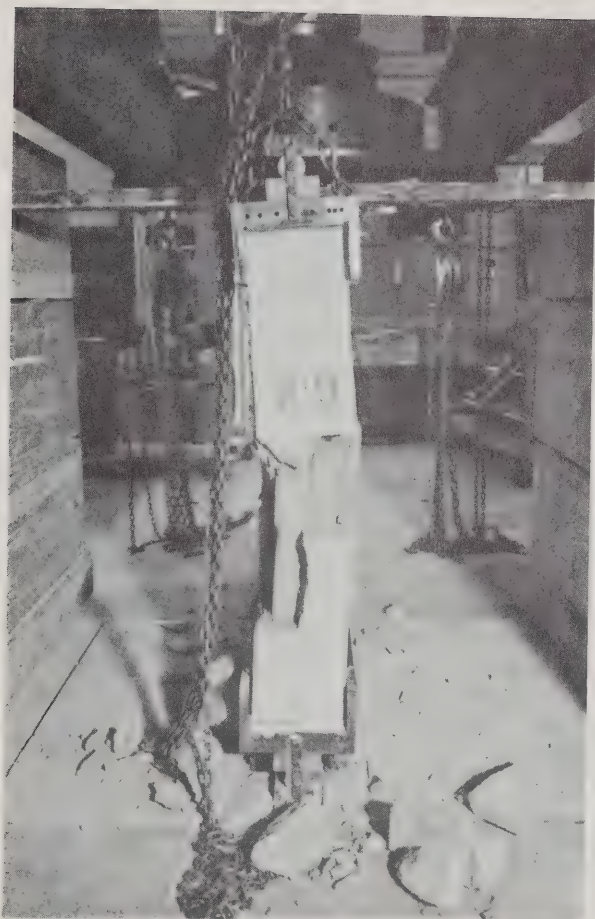


PLATE 6.7 Failure of Short Wall Specimen with 3-#9
Vertical Bars

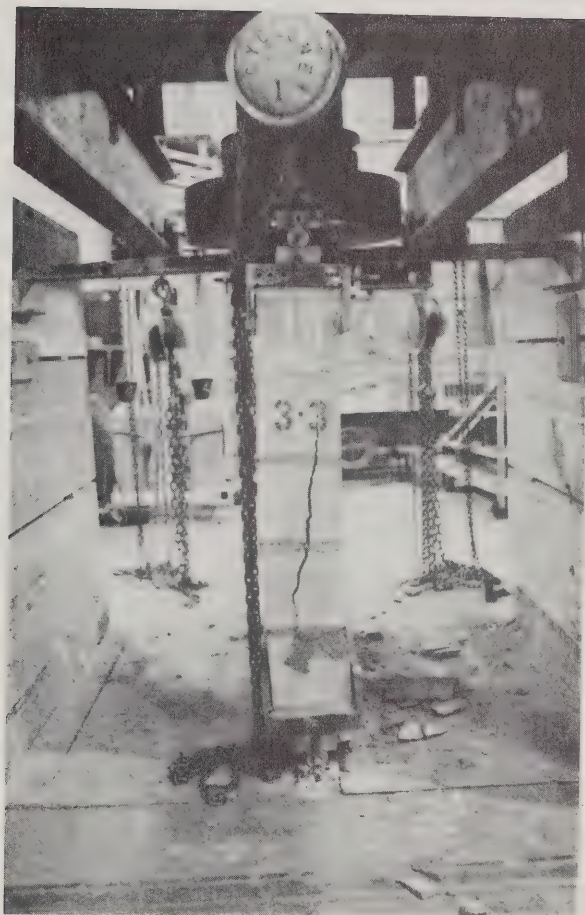


PLATE 6.8 Failure of Short Wall Specimens with 3-#3
Vertical Bars

6.10 Stress Distribution in Axially Loaded Masonry

Failure criteria were examined in Section 6.5 and relations predicting the ultimate capacity of masonry were developed. The derivations were based on a uniform tensile stress distribution along the height of the block. To account for the variation in the stress along the height and other uncertainties, Hilsdorf³ suggested the use of a "uniformity" coefficient. The stress distribution of axially loaded masonry was evaluated by finite element using a program developed by Dr. D.W. Murray, of the Department of Civil Engineering, University of Alberta. This program makes use of quadratic serendipity elements. The loading conditions and the grid used in the analysis are shown in Figure 6.14. The analyzed portion consisted of one block and two mortar joints. The material properties used in the analysis were: 1.30×10^6 psi for modulus of elasticity, 0.2 for Poisson's ratio for the block, and for the mortar 0.7×10^6 psi for elastic modulus and 0.4 for Poisson's ratio. The results obtained from the analysis are shown in Figure 6.15. The computed maximum tensile stress is approximately 400 psi. The tensile strength of the block material, estimated using the relation $f'_{bt} = 7.5 \sqrt{f'_b}$, with mean compressive strength as obtained experimentally is of the order of 350 psi. This analysis indicates that the tensile strength of the block material is exceeded by 12.5%, which suggests a uniformity coefficient equal to 0.875. Substituting the mean strength parameters obtained experimentally and the above value for the coefficient of uniformity in Equation 6.6 the expected stress at failure for axially loaded masonry is:

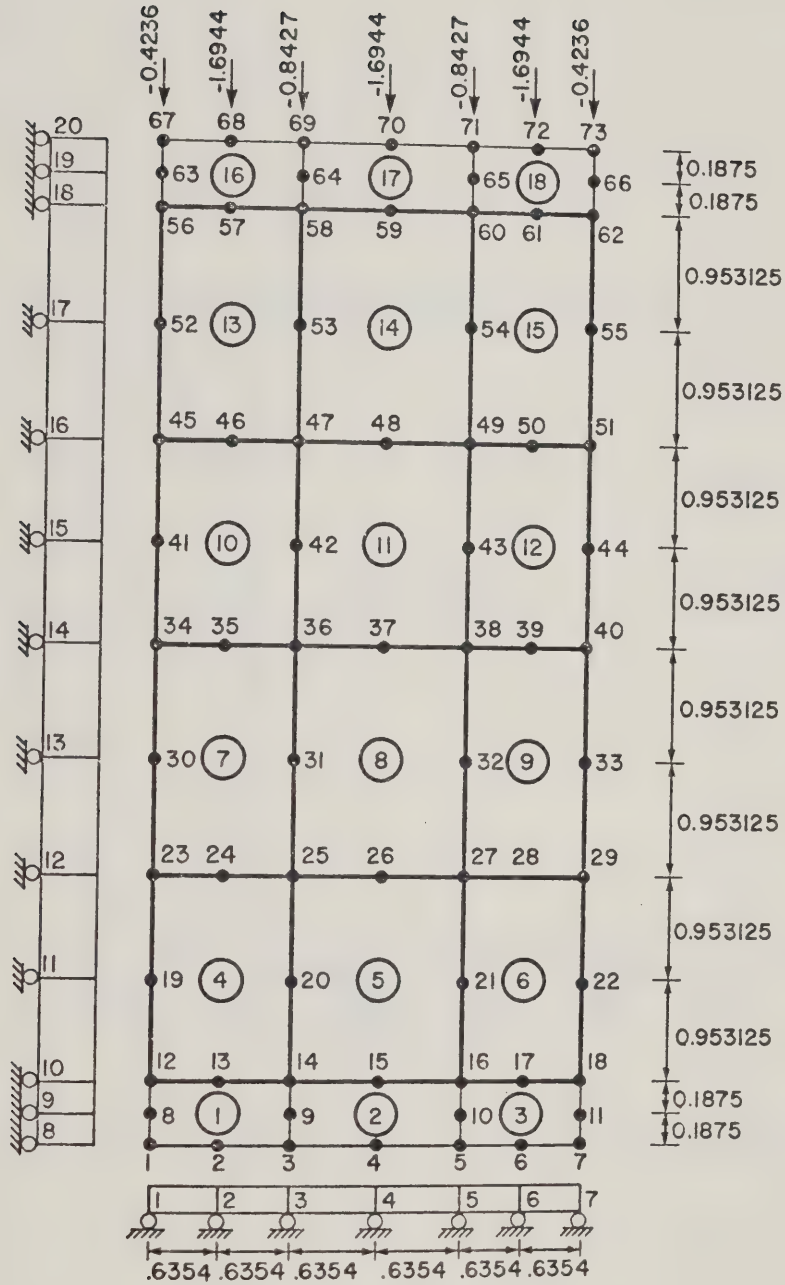


FIG. 6.14 Grid Used in Finite Element Analysis

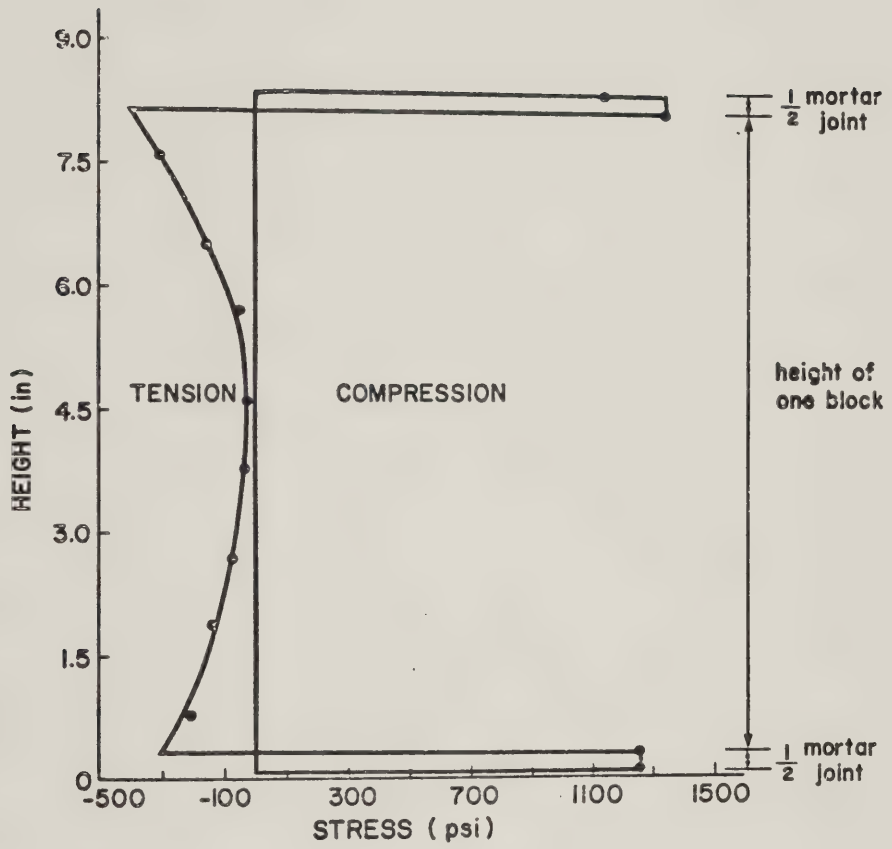


FIG. 6.15 Lateral Stresses in Axially Loaded Masonry

$$f'_m = 0.875 \left[2350 \left(\frac{350 + 0.011995 \times 2545}{350 + 0.011991 \times 2350} \right) \right] =$$

$$= 0.875 [2364] = 2068 \text{ psi}$$

which is in good agreement with the experimental evidence.

CHAPTER VII

Full Scale Wall Test Results

7.1 Introduction

The experimental program involved tests on sixty-eight full scale walls, which were subjected to various axial loads and moments. A description of the walls tested is given in tabulated form in Table 5.4 of Chapter V. The test results are presented in two groups, namely results for axially loaded specimens, and those for specimens subjected to eccentric loading. A complete set of experimental data is given in Structural Engineering Report No. 71 of the Civil Engineering Department, University of Alberta

7.2 Axially Loaded Walls

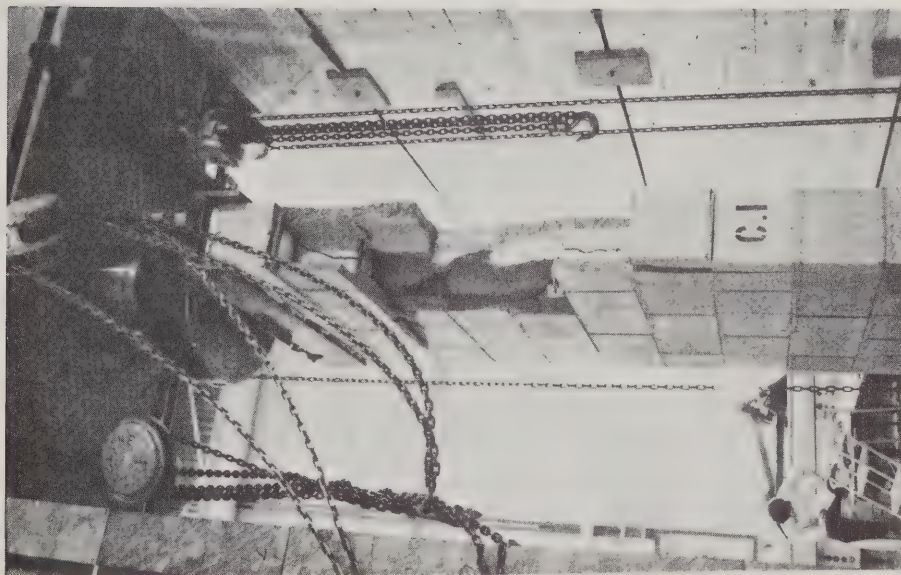
Data reported in this section include tests on plain and vertically reinforced walls with slenderness ratios varying from 12 to 22 (nominal). The actual slenderness ratios calculated on the basis of the test set-up and actual wall thicknesses are given in the tables of test results. All walls were tested with pin-ended conditions. Table 7.1 gives a summary of test results for axially loaded walls. These results were found to be in good agreement with those obtained in tests of small specimens. The average compressive strength of plain walls was 1830 psi. The strength calculations are based on mortared area and 25% active mortar penetration. Failures of plain walls were sudden and in some cases explosive.

TABLE 7.1 Test Results for Axially Loaded Walls

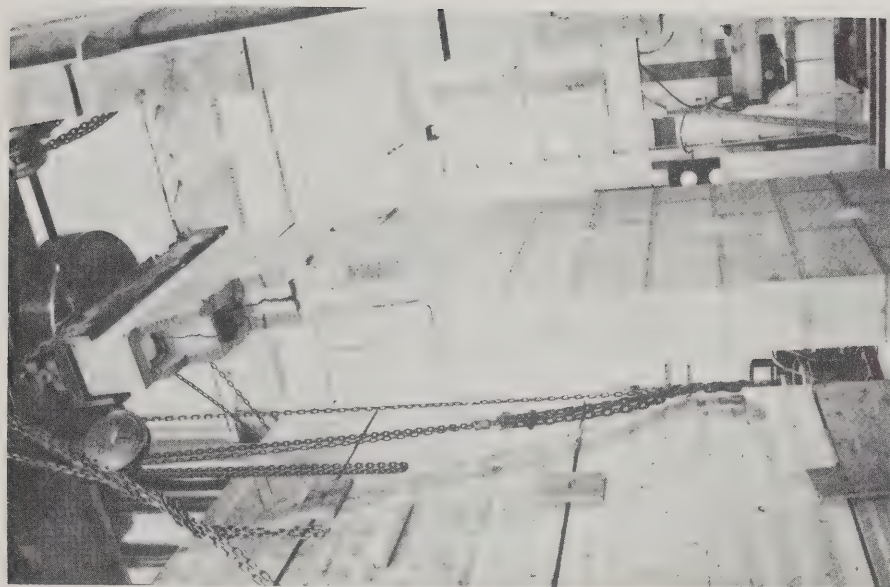
Wall Designation	h/t Nominal	h/t Actual	Reinforcement		Number of Cores Filled	Failure Load kips	Stress at Failure Based on	
			Vertical	Horizontal			Gross Cross Section Area psi	Mortared and Grouted Area psi
A1	12	13.77	--	--	--	262.5	870	2150
A4	12	13.77	--	--	--	238.6	790	1950
C1	14	15.87	--	--	--	190.0	630	1550
D1	16	17.97	--	--	--	218.3	720	1780
M1	22	24.24	--	--	--	207.8	690	1700
Average						219.6	740	1830
F1	16	17.97	--	#9 gauge wire	--	160.0	530	1310
I1	16	17.97	3#3	--	3	305.0	1010	1120
H1	16	17.97	3#6	--	3	375.2	1240	1380
C2	14	15.87	3#9	--	3	315.0	1040	1120
D2	16	17.97	3#9	--	3	400.0	1320	1470
L1	22	24.24	3#9	--	3	383.5	1270	1410
Average						355.7	1180	1300

Plate 7.1 shows Walls C1 and D1 after failure. Lateral deflections monitored during the tests showed that the walls remained almost straight until failure occurred. Maximum deflection at mid-height was of the order of 0.075 inches for all plain walls. Figure 7.1 shows the deflected shape of Wall A1 at different load levels. Specimens with vertical reinforcement failed at stress levels close to those of short wall specimens with similar reinforcement. Partially grouted walls with vertical reinforcement failed with vertical cracks forming through the ungrouted cores. Formation of vertical cracks occurred without warning; however, complete failures occurred after additional load was applied and the cracks propagated from the point of origin to almost the ends of the walls. In most cases cracks were first formed at mid-height of the walls. In examining the walls after failure it was found that the grout was split parallel to the reinforcement. The vertical cracks in the walls are considered to be tension cracks resulting from the difference in stress levels in the grouted and ungrouted portions of the cross-section.

Plate 7.2 shows failures of axially loaded walls with vertical reinforcement. A typical deflected shape for a reinforced wall at various load levels is shown in Figure 7.2. Steel strains monitored at mid-height are plotted in Figures 7.3 and 7.4. The average steel strain at failure for Wall C2, reinforced with three #9 bars, was 5.1×10^{-4} in/in. For Wall I1, reinforced with three #3 bars, the average steel strain at failure was 9×10^{-4} in/in. The maximum steel strain observed was 1.2×10^{-3} in/in. which is approximately 60% of the yield strain. The efficiency of the



a) Wall C1



b) Wall D1

PLATE 7.1 Failures of Axially Loaded Plain Walls

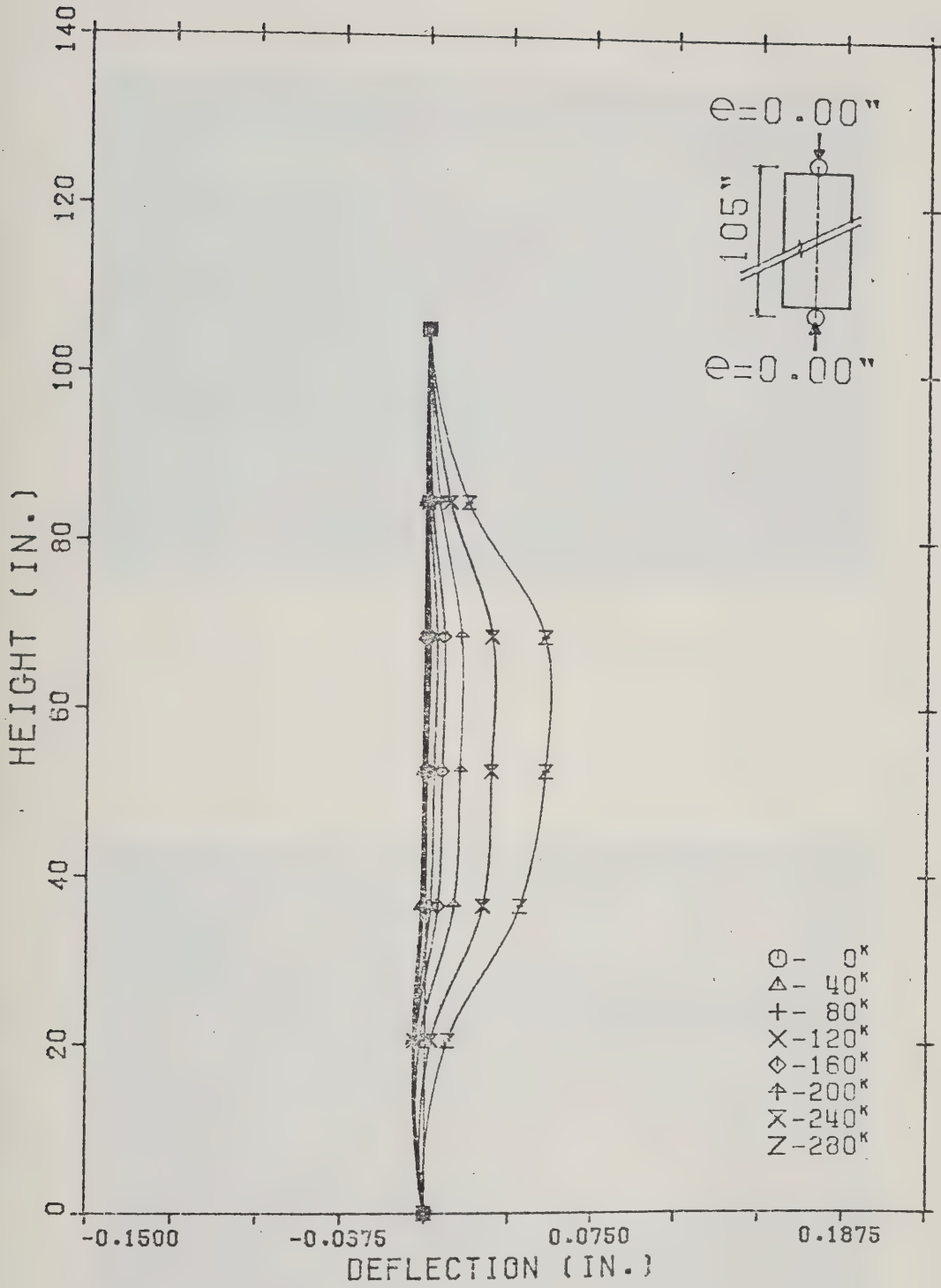
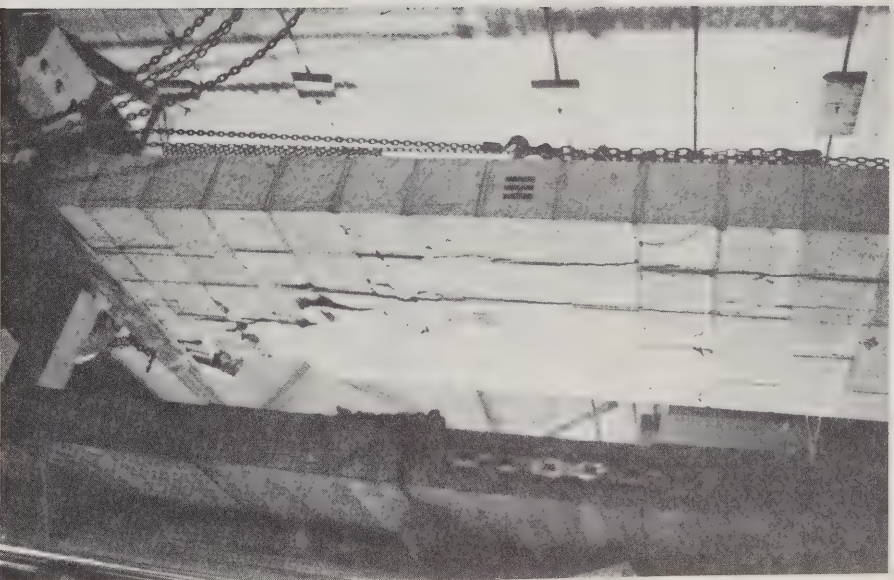


FIG. 7.1 Deflected Shape of Wall A1



a) Wall C2



b) Wall H1

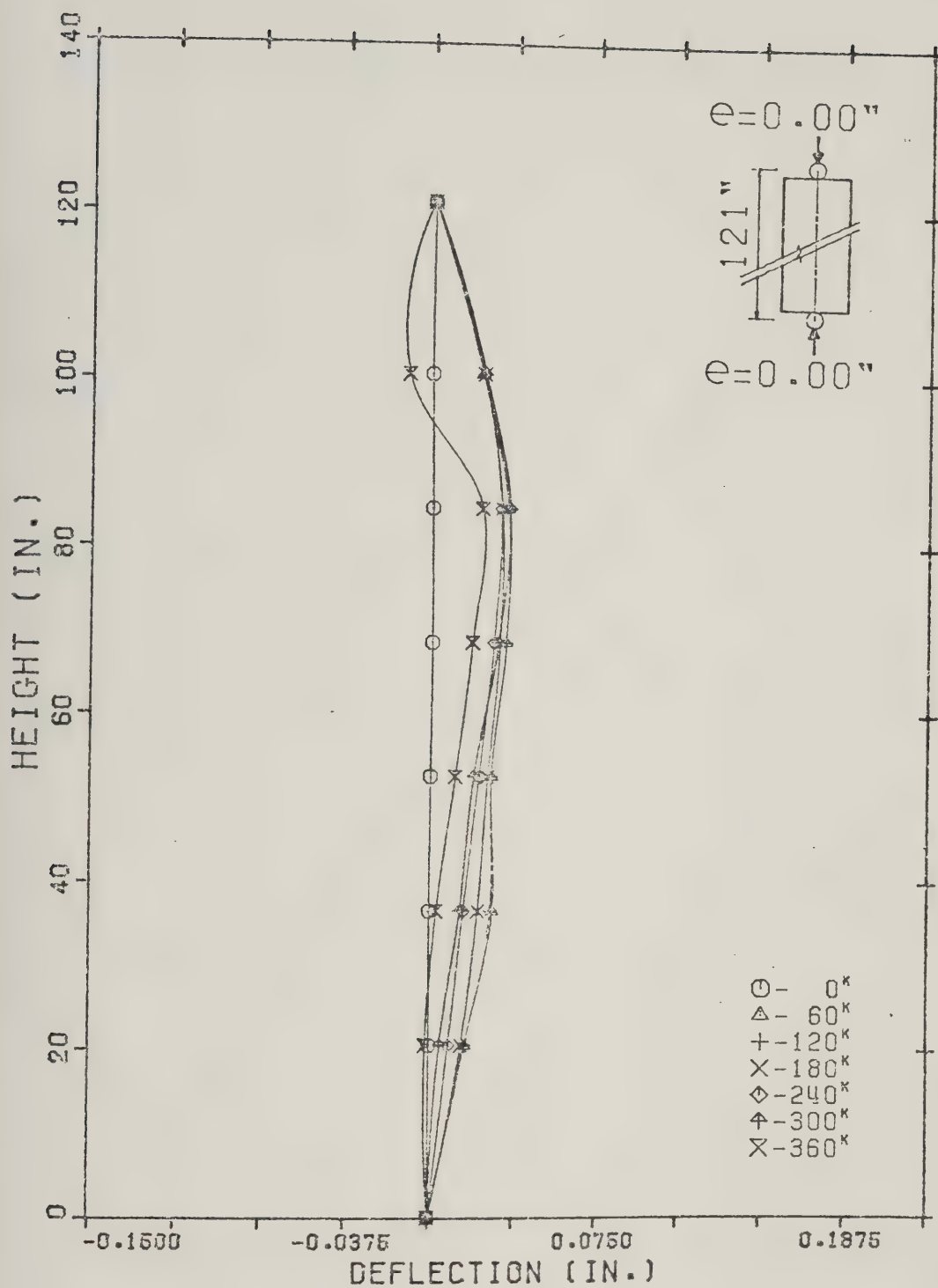


FIG. 7.2 Deflected Shape of Wall C2

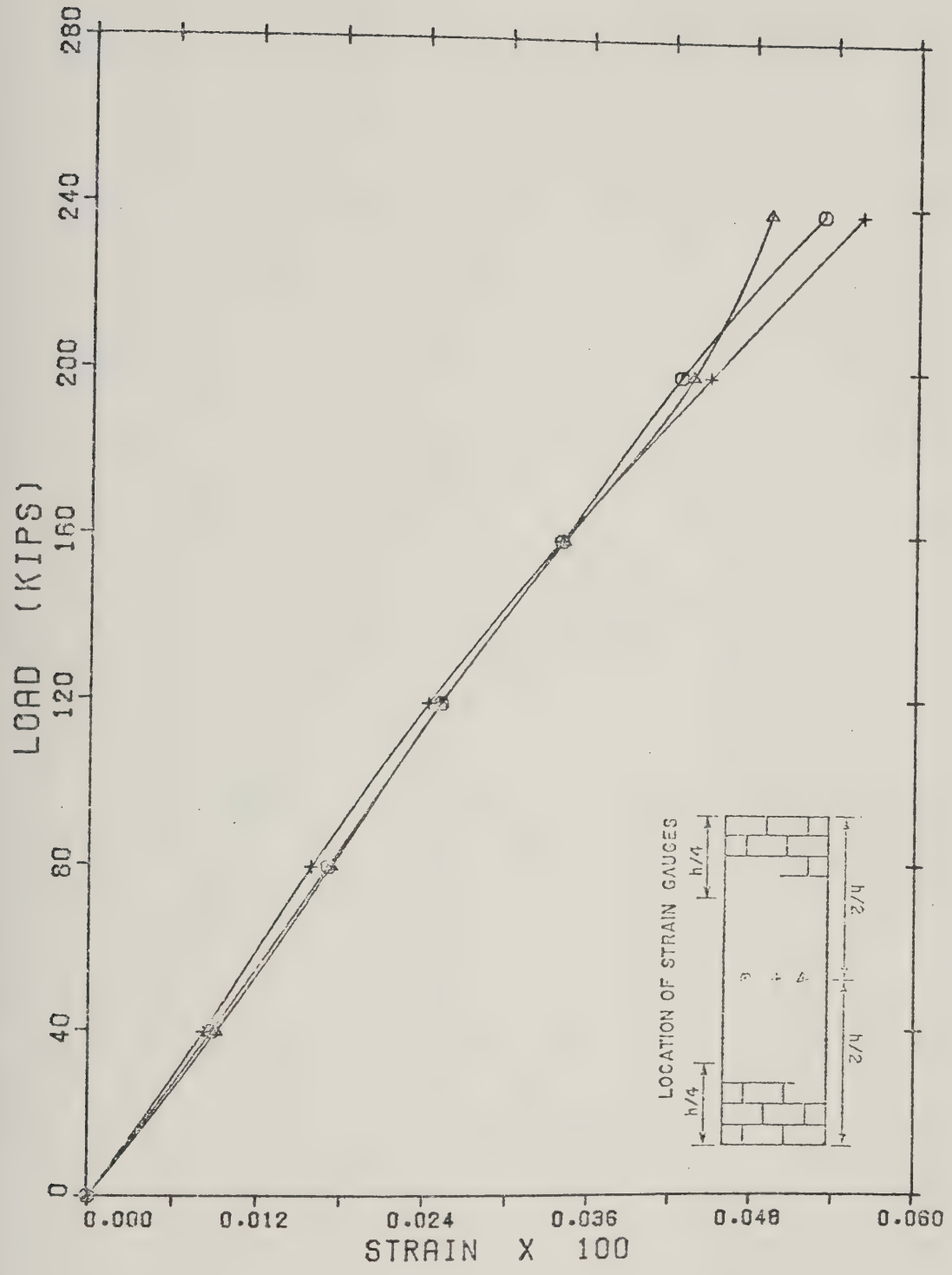


FIG. 7.3 Reinforcement Strain vs Load for Wall C2

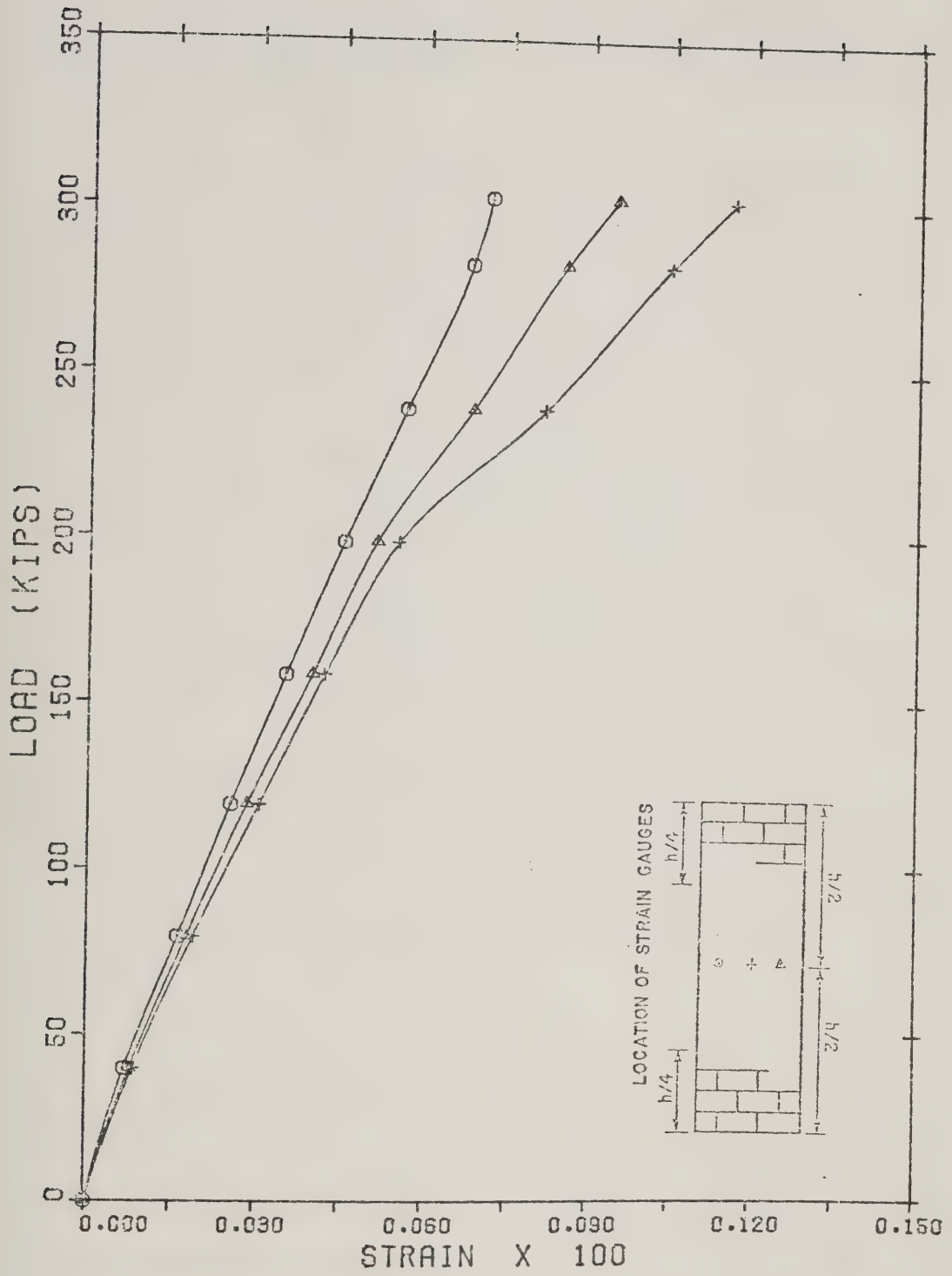


FIG. 7.4 Reinforcement Strain vs Load for Wall II

vertical steel as a function of the area (size), calculated in Chapter VI from short wall tests, is in agreement with the results of this part of the study.

The difference in Poisson's ratio and the absence of confinement reinforcement are two possible factors contributing to the decrease of steel efficiency with increasing bar size. As load increases the vertical reinforcement expands laterally more than the surrounding concrete due to the difference in Poisson's ratio, giving rise to horizontal tensile stresses. Another adverse effect is the slip between reinforcing bars and the grout. The deformations in the reinforcement cause pressures on the contact surface between steel and concrete perpendicular to the direction of the bars. Similar conclusions were reached by Larson⁴² in a study of concrete walls. The effects of the above factors are functions of the bar size, an observation confirmed by the test results. From the results obtained in this part of the study and those of Chapter VI, it appears that for axially loaded wall segments where the position of the reinforcement within the wall is not critical, smaller size bars produce better steel utilization.

For both plain and reinforced walls the results indicated that for axially loaded walls there was no reduction in capacity that could be attributed to slenderness effects. The walls failed when the stress levels reached the strength of one or more of the materials involved. These results strengthen the statement made by Shahlin⁹ indicating that, for slenderness ratios less than 30, masonry fails when the capacity of the cross-section is reached.

Wall F1 contained joint reinforcement in the form of #9 gauge wire. This wall failed at a load 27% lower than the average load of the five plain walls tested.

All reinforced walls were examined after failure in order to observe the effectiveness of one lift grouting procedure; no voids were found. Plate 7.3 shows a #9 bar fully surrounded by grout when removed from a specially prepared specimen which was not tested. On the same plate the penetration of the mortar into the core and the reduction of the core area at the joint levels are clearly shown.

7.3 Eccentrically Loaded Walls

7.3.1 Plain Walls, Single Curvature Bending

Eight walls were tested in single curvature bending. Four were tested with equal load eccentricities at both ends, and the remaining four were tested under load which was eccentric at one end and axial at the other. The walls tested with load eccentricity at one end only contained joint reinforcement in the form of 9-gauge wire. Failure loads and resulting stresses are given in Table 7.2.

All walls, except A5 and G4, failed when the stress on the compression side reached the strength of the materials. The average stress at failure for these walls was 3150 psi. Although failures were complete, sufficient warning was given by crack formation on the tension side. Cracks were formed at low loads in walls with large eccentricities; however, these walls were able to sustain additional load. Plates 7.4 and 7.5 show Wall A2 during the test



PLATE 7.3 Grouted Core Showing Mortar Penetration

TABLE 7.2 Test Results for Plain Walls Tested
in Single Curvature Bending

Wall Designation	h/t Nominal	h/t Actual	Eccentricity of Load		Load at Failure kips	Moment at Failure kip-in.	Moment Adjusted to Include P-Δ Effects k-in.	Maximum Mortar Stress at Failure psi
			Top in.	Bottom in.				
A2	12	13.77	t/6=1.27	1.27	159.2	202.1	245.2	2670
A3	12	13.77	t/3=2.54	2.54	80.3	202.9	262.1	2065
A5	12	13.77	3.00	3.00	26.1	78.3	87.9	740
G1	16	17.97	t/6=1.27	0.00	160.0	203.2	203.2	2510
G2	16	17.97	t/3=2.54	0.00	124.8	314.0	314.0	2710
G3	16	17.97	3.00	0.00	15.3	255.0	255.0	2070
G4	16	17.97	3.50	0.00	49.0	171.5	171.5	1420
M2	22	24.20	t/3=1.27	1.27	120.0	152.4	295.4	2741
N1	16	17.97	t/3=1.27	0.00	183.5	232.4	232.4	2750

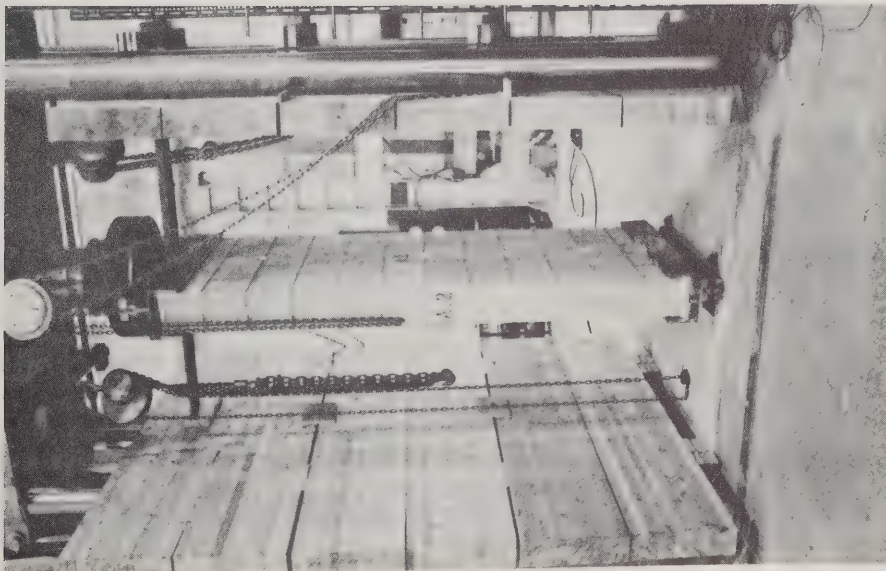


PLATE 7.4 Wall A2 During Tests

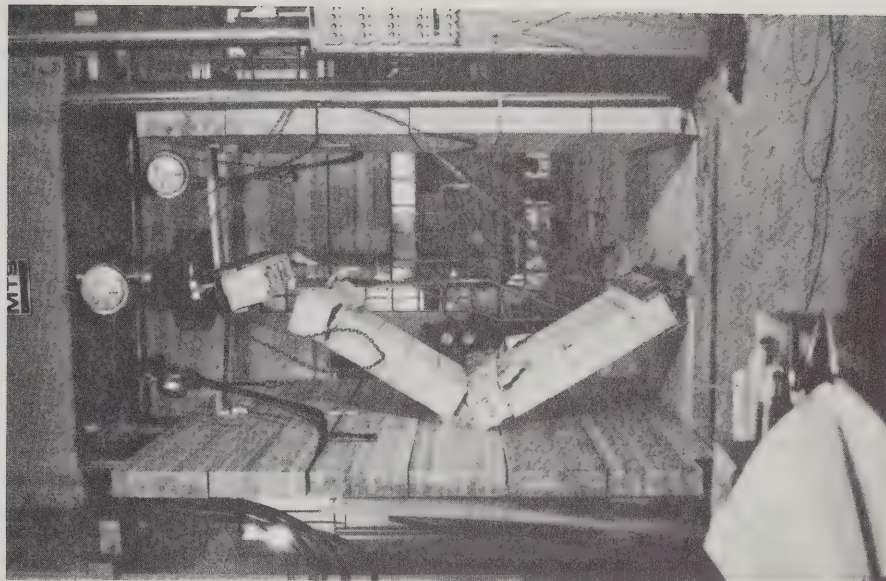


PLATE 7.5 Wall A3 at Failure

and Wall A3 at the instant of failure. The deflected shape of Wall A2 at various load levels is shown in Figure 7.5. Graphs of load versus axial deformation for walls in Series A is given in Figure 7.6. The centerline deflection as a function of the load for the same group of walls is given in Figure 7.7.

7.3.2 Plain Walls in Double Curvature Bending

Data reported in this section was obtained from tests on eighteen walls. The variables investigated included slenderness ratio, unequal end eccentricities and joint reinforcement.

Table 7.3 presents a summary of the test results and testing conditions. The average stress at failure was 3480 psi calculated on the basis of mortared area and 25% active mortar penetration (bearing area equal to 122.3 in.²). Failures of walls loaded in double curvature were explosive and complete, as demonstrated in Plates 7.6, 7.7 and 7.8. Deflections measured during the application of the loads indicated that the point of inflection moved to one end, and the walls tended to assume their first buckling mode shape. Figures 7.8 and 7.9 show the deflected shapes of walls E1 and E5 during the test. The failure load, for walls with large eccentricities was close to the buckling loads as calculated using the procedure developed in Chapter IV.

Axial deformations versus axial load plotted for Series E in Figure 7.10, showed a linear relation. Maximum axial deformations were of the same order regardless of eccentricities.

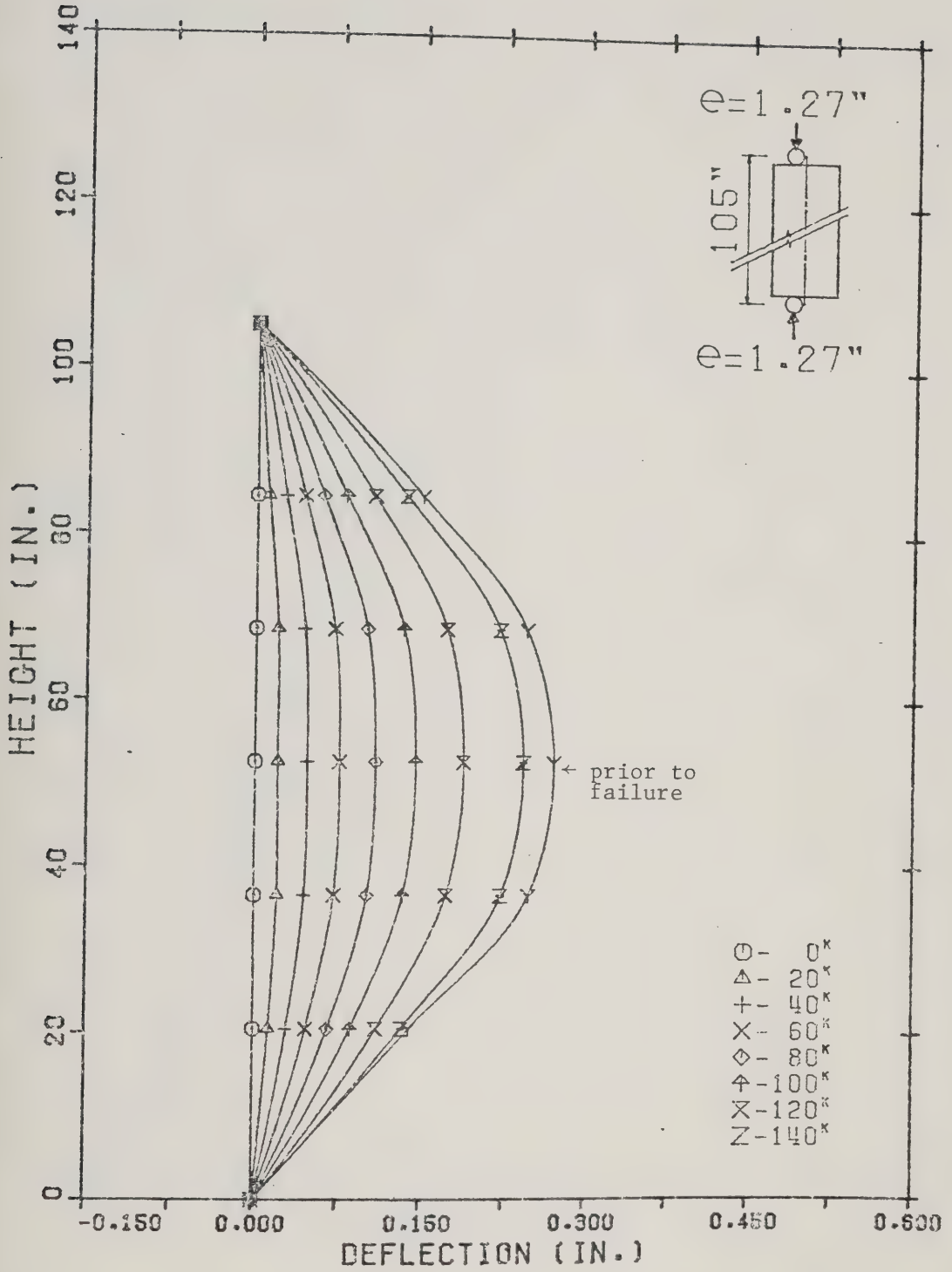


FIG. 7.5 Deflected Shape of Wall A2

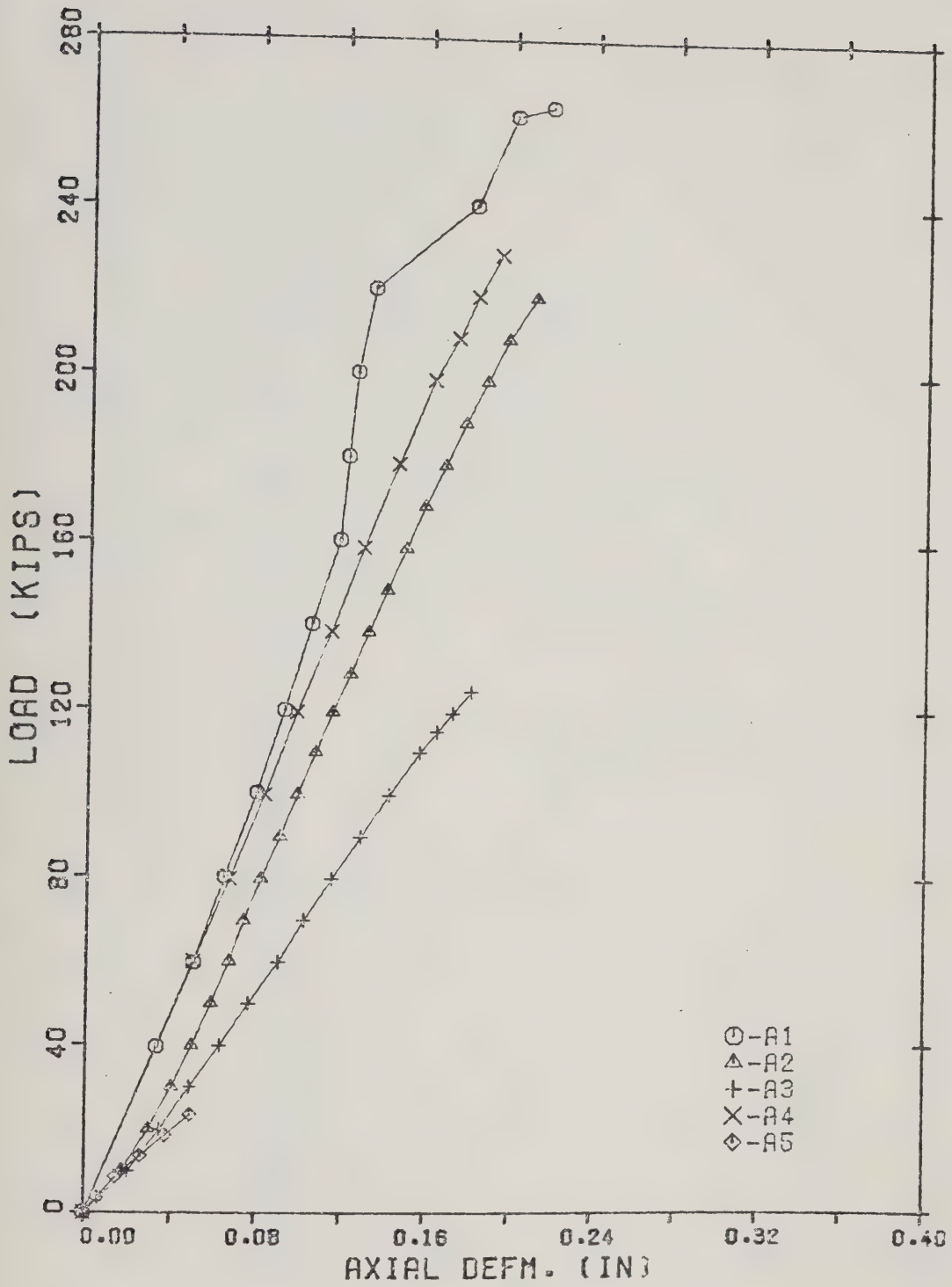


FIG. 7.6 Axial Deformation vs Load for Series A

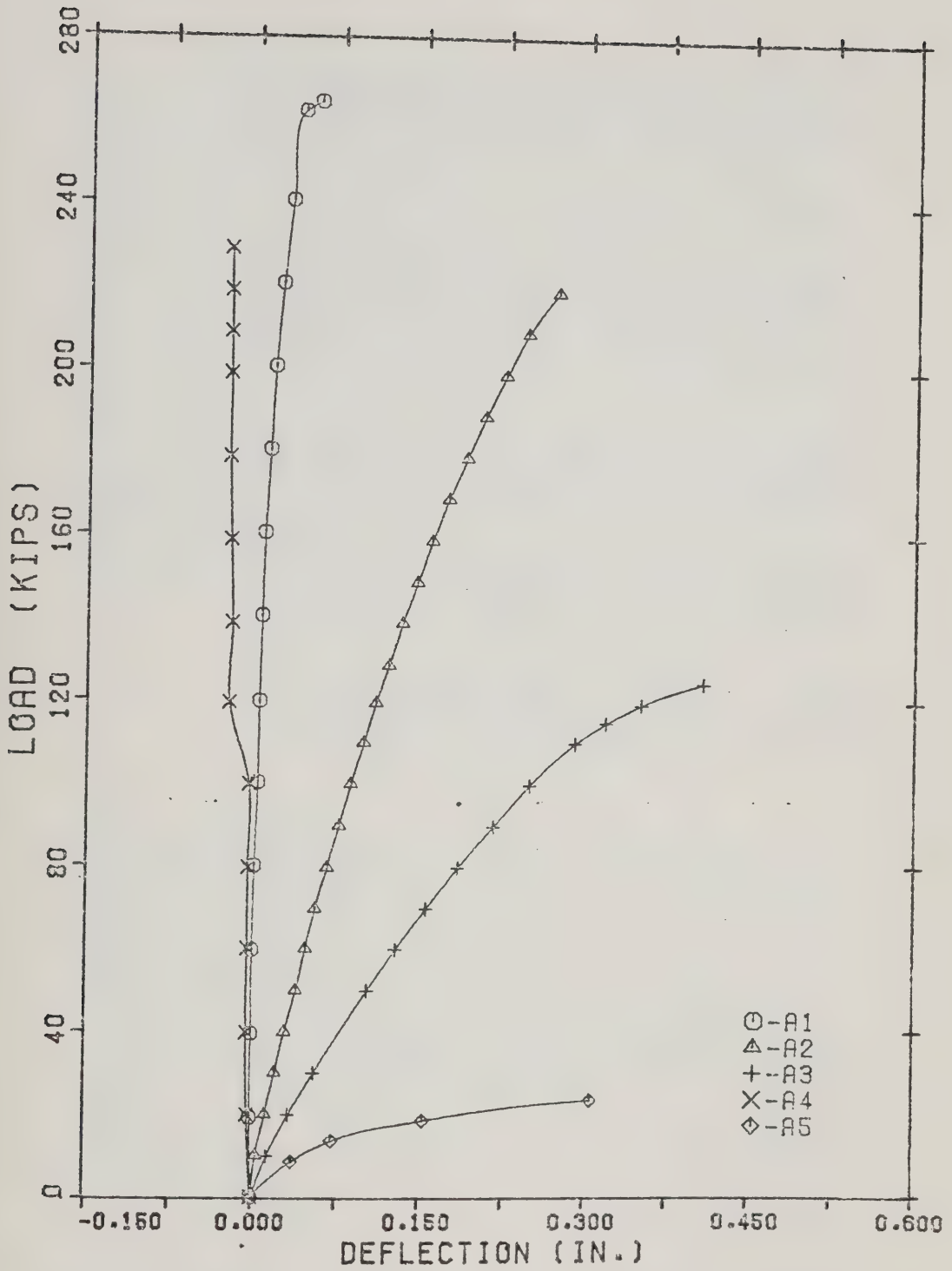


FIG. 7.7 Center-Line Deflection vs Vertical Load for Series A

TABLE 7.3 Test Results for Walls Without Vertical Reinforcement and Tested in Double Curvature Bending

Wall Designation	h/t Nominal	h/t Actual	Joint Reinforcement	Eccentricity		Failure Load kips	Moment at Failure kip-in.	Failure Stress psi
				Top in.	Bottom in.			
E1	16	17.97	plain	+3.54	-3.54	85.0	300.9	2490
E2	14	15.87	"	+3.54	-3.54	115.0	407.1	3370
E3	12	13.77	"	+3.54	-3.54	135.0	477.9	3950
E4	12	13.77	"	+2.54	-2.54	156.6	397.8	3650
E5	12	13.77	"	+1.27	-1.27	220.4	279.9	3470
F2	16	17.97	#9 gauge wire	+1.27	-1.27	160.0	203.2	2520
F3	16	17.97	"	+2.54	-2.54	144.6	365.8	3360
F4	16	17.97	"	+3.00	-3.00	124.6	373.8	3250
F5	16	17.94	"	+3.50	-3.50	78.8	275.8	2150
G5	16	17.97	"	+3.00	-2.54	150.6	451.8	3920
G6	16	17.97	"	+3.50	-2.54	144.4	505.4	4190
G7	16	17.97	"	+1.27	-1.27	196.6	249.7	3090
G8	16	17.97	"	+3.00	-3.56	117.0	409.5	3400
G9	16	17.97	"	+3.00	-3.00	148.2	444.6	3800
N2	16	17.97	"	+1.27	-1.27	191.3	242.9	3130
N3	16	17.97	"	+2.54	-2.54	158.6	402.8	3700
N4	16	17.97	"	+3.00	-3.00	114.9	344.7	3820
N5	16	17.97	"	+3.50	-3.50	75.4	263.9	2060

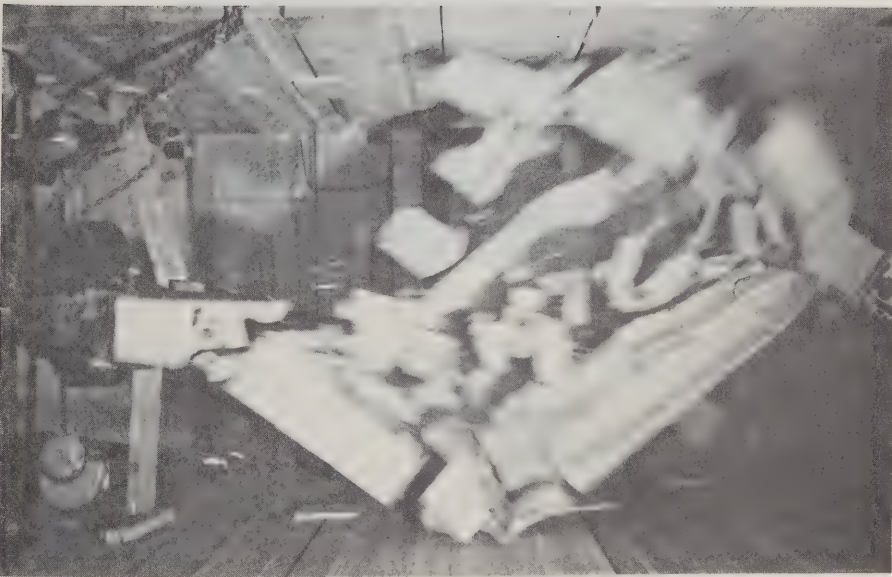


PLATE 7.6 Failure of Plain Wall in
Loaded in Double Curvature

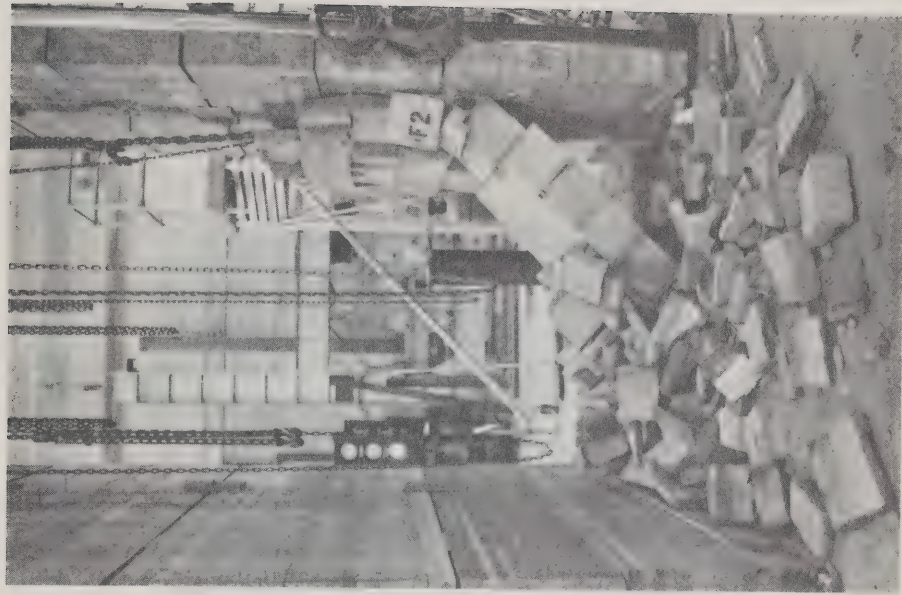


PLATE 7.7 Wall F2 After Failure

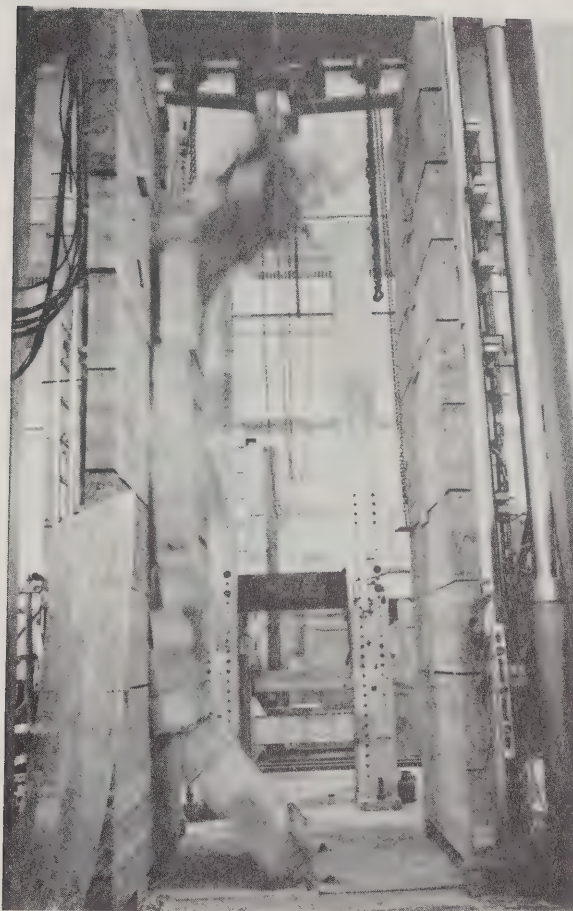


PLATE 7.8 Failure of Wall Loaded in
Double Curvature

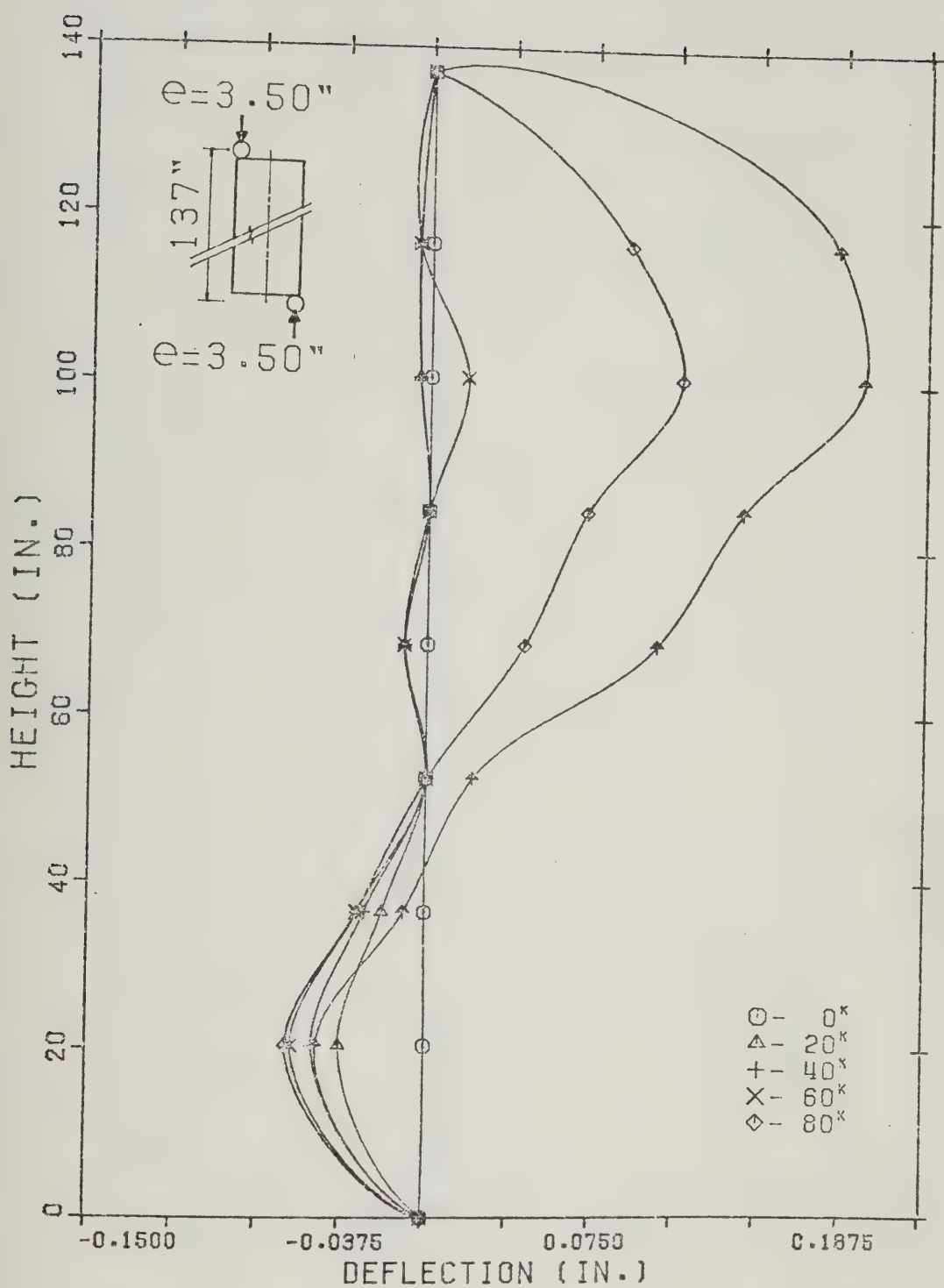


FIG. 7.8 Deflected Shape of Wall E1

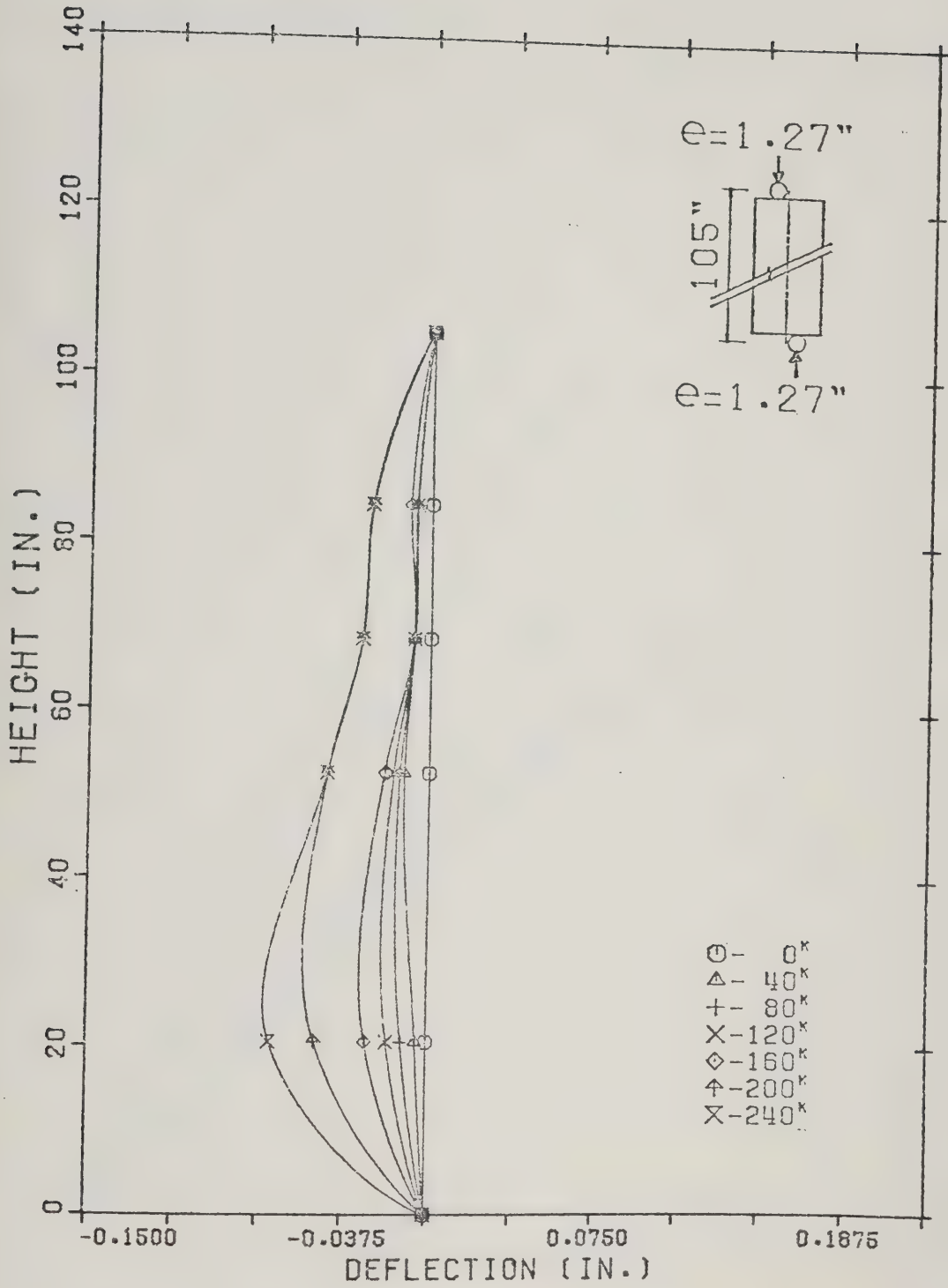


FIG. 7.9 Deflected Shape of Wall E5

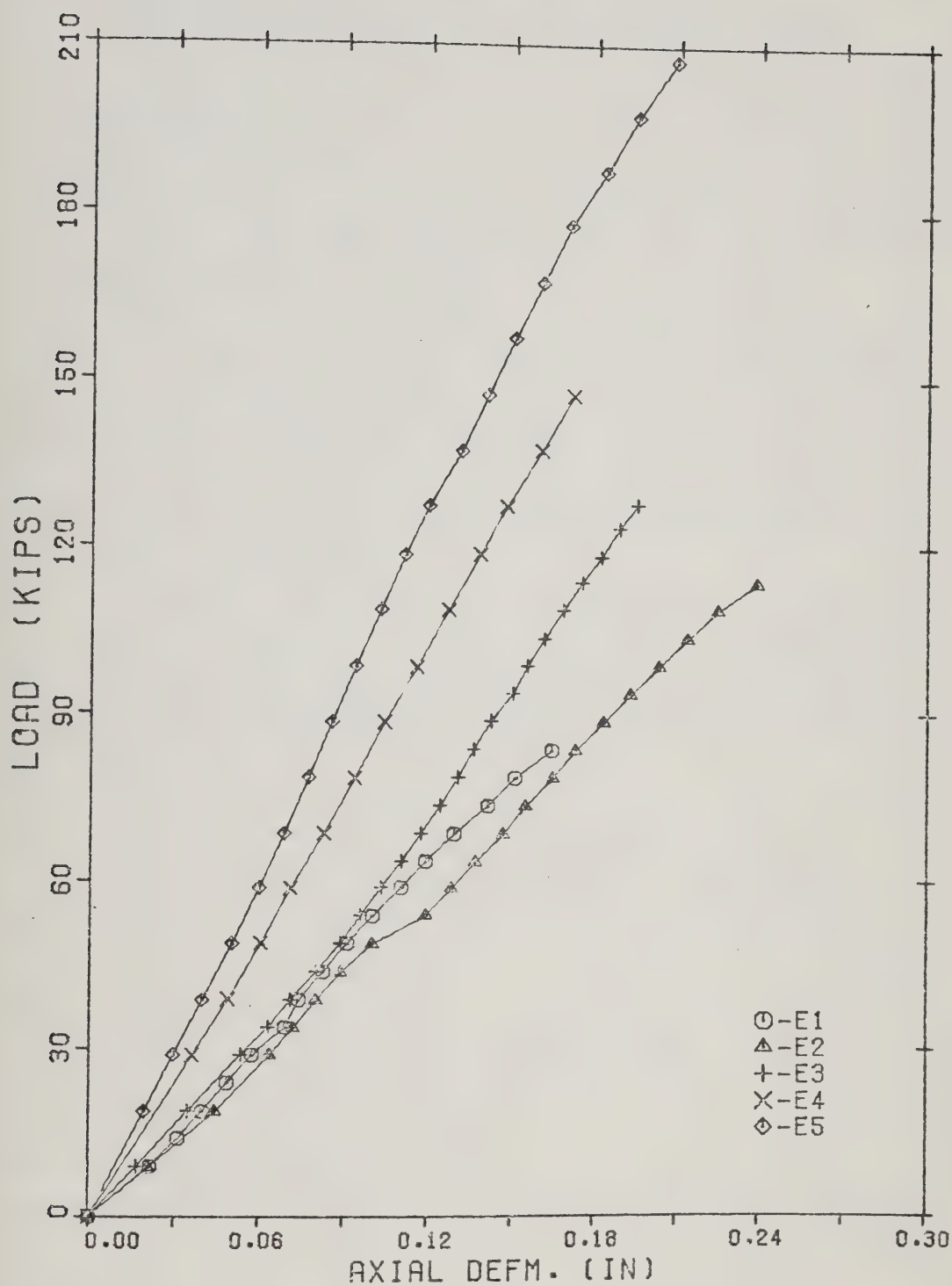


FIG. 7.10 Axial Deformation vs Vertical Load for Series E

7.3.3 Vertically Reinforced Walls, Single Curvature Bending

Twenty-four walls, each with one reinforcing bar in each of the three grouted cores, were tested in single curvature with equal end eccentricities. The walls varied in height from 12 to 22 blocks. Three bar sizes were used, namely #9, #6, and #3. Test results were listed in Table 7.4. In the table, test conditions such as eccentricities and actual slenderness ratios, are given. Failure moments were adjusted to account for the $P-\Delta$ effect based on the deflection at the point of maximum moment obtained from measurements taken during the test. A typical load deflection relation for Wall L3 is shown in Figure 7.11.

In general, large deformations were observed before failures. The walls failed when the compressive strength of the unit was reached on the compression side. It was observed that when the strength of the mortar was exceeded, particles of mortar fell to the floor but the walls supported additional load before failing.

Plate 7.9 shows Wall L5 during the test. The mid-height deflection is in the order of 3.5", as can be seen from the plumb line attached to the wall at the top. At failure the crushing of the compression side was accompanied simultaneously by separation of the blocks on the opposite side, as shown in Plate 7.10. For walls tested with load eccentricities equal or smaller to $t/3$, vertical cracks were formed through the ungrouted cores. This type of failure is shown in Plates 7.11 and 7.12. Strains in the reinforcing bars, measured at mid-height, indicated that the load was distributed evenly over the cross-section. Typical strain measurements are shown in Figures 7.12 and 7.13. The variation in

TABLE 7.4 Test Results for Vertically Reinforced Walls
Tested in Single Curvature Bending

Wall Designation	h/t Nominal	h/t Actual	Reinforcement		Eccentricities		Failure Load kips	Moment at Failure	
			Vertical	Horizontal	Top in.	Bottom in.		P_e max kip-in.	Including P- Δ Effect kip-in.
B2	12	13.77	3#9	plain	+1.27	+1.27	320.0	406.4	627.2
B3	12	13.77	3#9	"	+2.54	+2.54	140.0	355.6	660.9
B4	12	13.77	3#9	"	+3.00	+3.00	155.0	465.0	558.6
B5	12	13.77	3#9	"	+3.50	+3.50	114.9	402.1	497.7
C3	14	15.87	3#9	plain	+1.27	+1.27	249.6	316.9	476.7
C4	14	15.87	3#9	"	+2.54	+2.54	125.0	317.5	524.0
C5	14	15.87	3#9	"	+3.00	+3.00	122.5	367.5	618.0
C6	14	15.87	3#9	"	+3.50	+3.50	90.0	315.0	490.3
D3	16	17.97	3#9	plain	+1.27	+1.27	200.0	254.0	426.0
D4	16	17.97	3#9	"	+2.54	+2.54	108.8	276.3	466.8
D5	16	17.97	3#9	"	+3.00	+3.00	94.5	283.5	468.9
D6	16	17.97	3#9	"	+3.50	+3.50	83.0	290.5	516.0
L2	22	24.26	3#9	plain	+1.27	+1.27	150.0	190.5	320.7
L3	22	24.26	3#9	"	+2.54	+2.54	90.0	228.6	543.8
L4	22	24.26	3#9	"	+3.00	+3.00	80.0	240.0	512.0
L5	22	24.26	3#9	"	+3.50	+3.50	73.3	256.5	542.0
H2	16	17.97	3#6	plain	+1.27	+1.27	259.5	329.5	500.8
H3	16	17.97	3#6	"	2.54	+2.54	86.3	219.2	424.4
H4	16	17.97	3#6	"	+3.00	+3.00	65.1	195.3	374.0
H5	16	17.97	3#6	"	+3.50	+3.50	56.0	196.0	406.0
I2	16	17.97	3#3	plain	+1.27	+1.27	217.0	275.5	479.2
I3	16	17.97	3#3	"	+2.54	+2.50	54.0	137.1	149.8
I4	16	17.97	3#3	"	+3.00	+3.00	32.9	98.7	105.3
I5	16	17.97	3#3	"	+3.50	+3.50	24.3	85.0	94.8

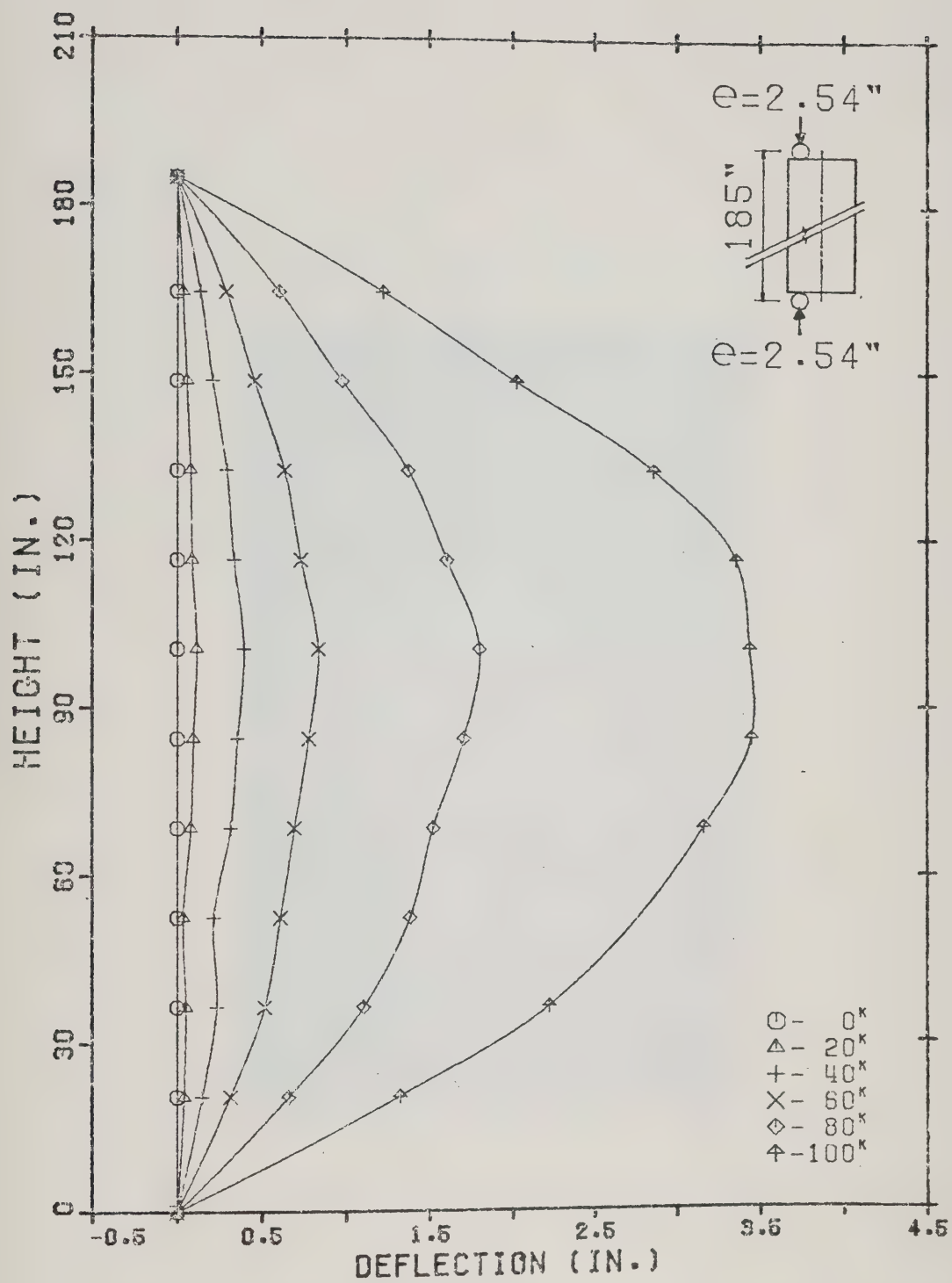


FIG. 7.11 Deflected Shape of Wall L3

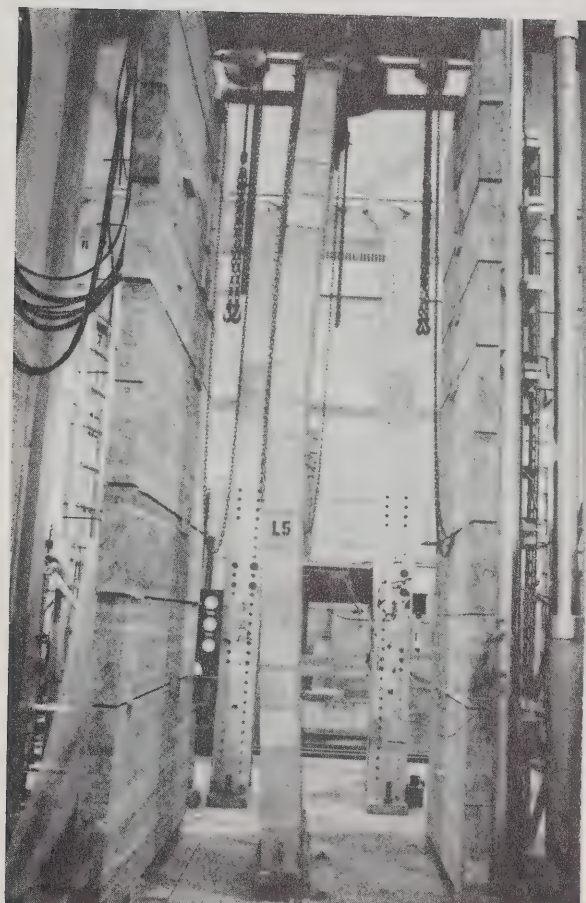


PLATE 7.9 Wall L5 During Testing

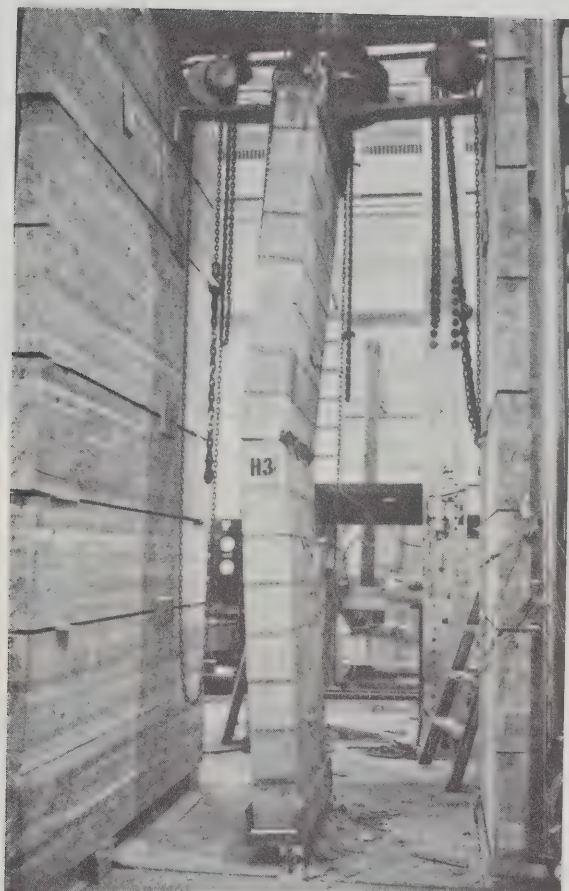


PLATE 7.10 Typical Failure of Reinforced Wall
Tested in Single Curvature With
Eccentricities Larger Than $t/3$

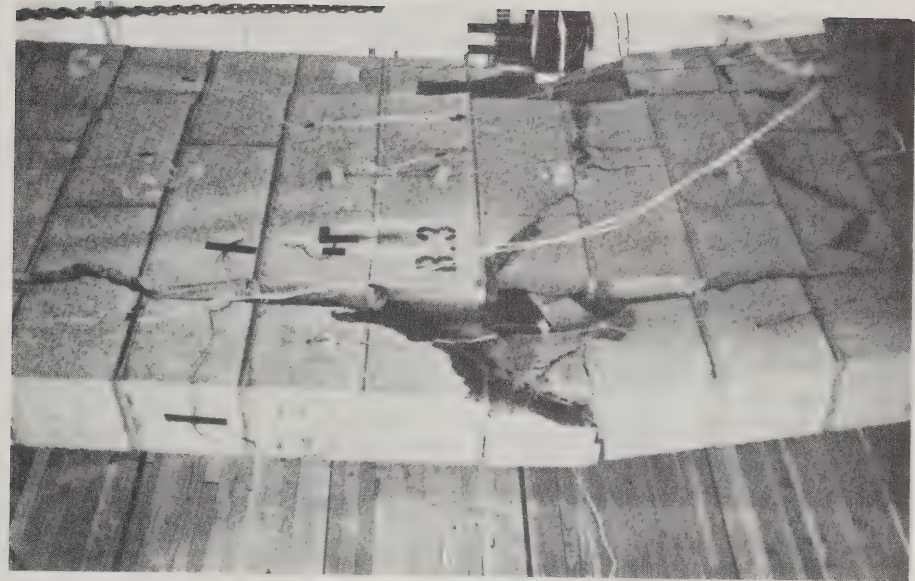


PLATE 7.12 Failure of Wall B3

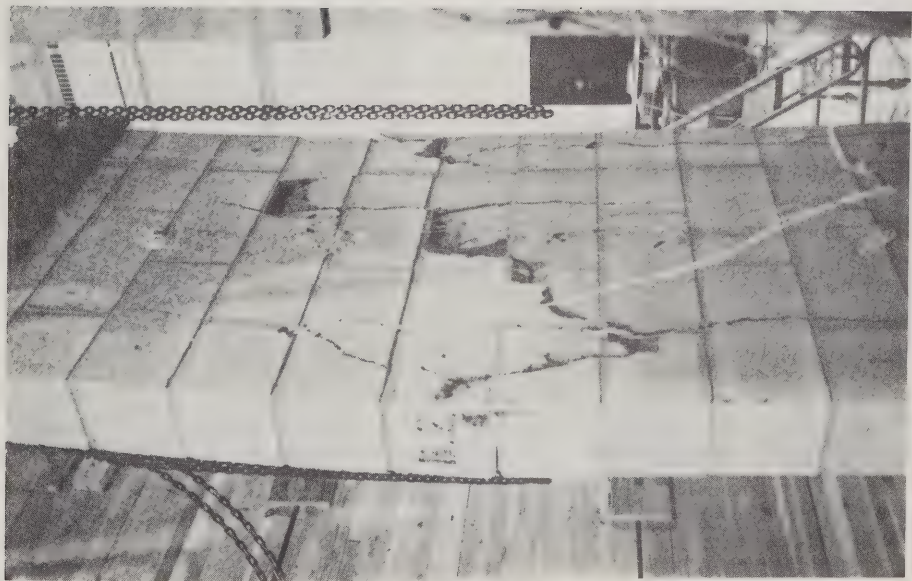


PLATE 7.11 Failure of Wall B2

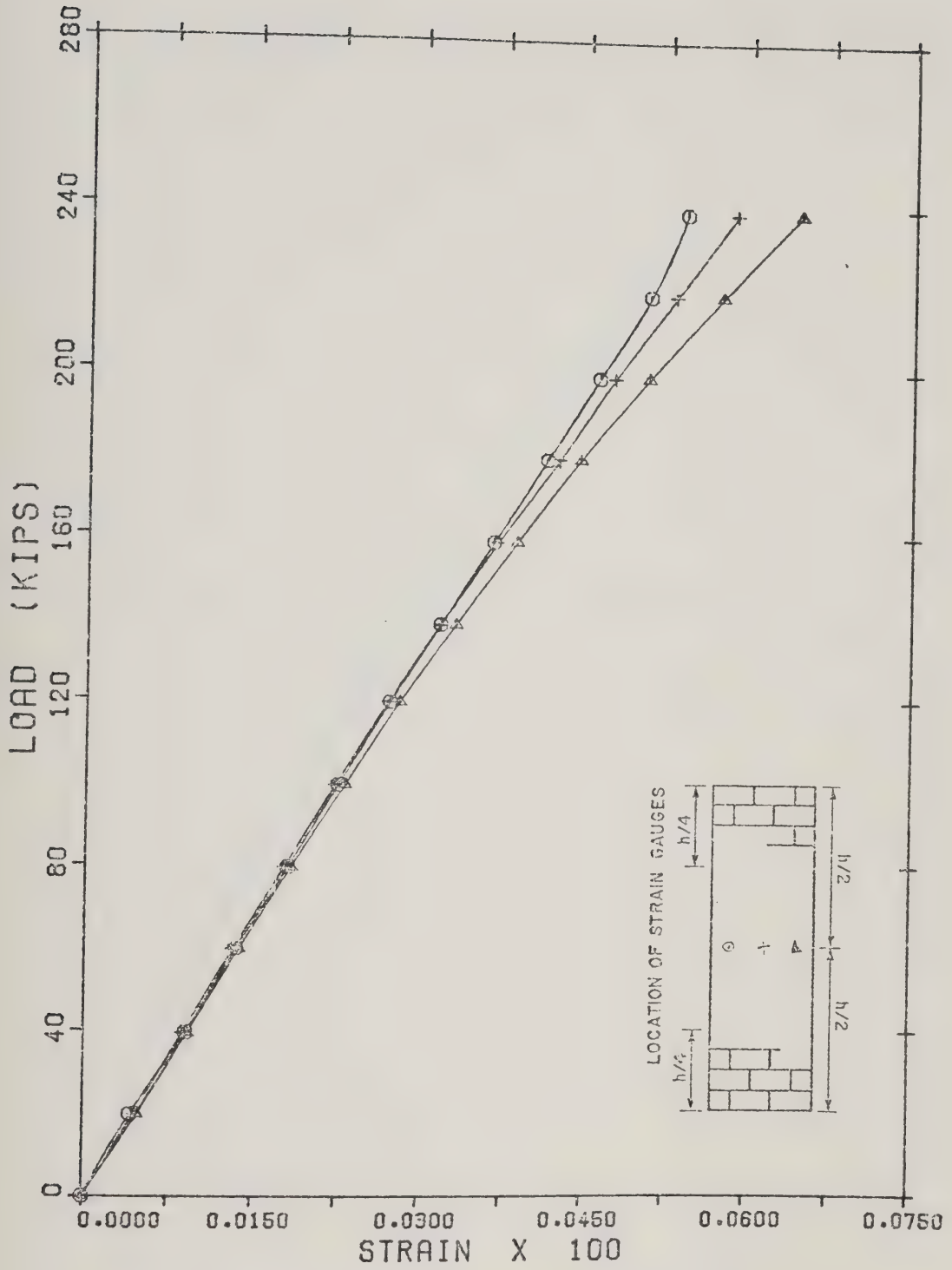


FIG. 7.12 Reinforcement Strains at Mid-height for Wall C3

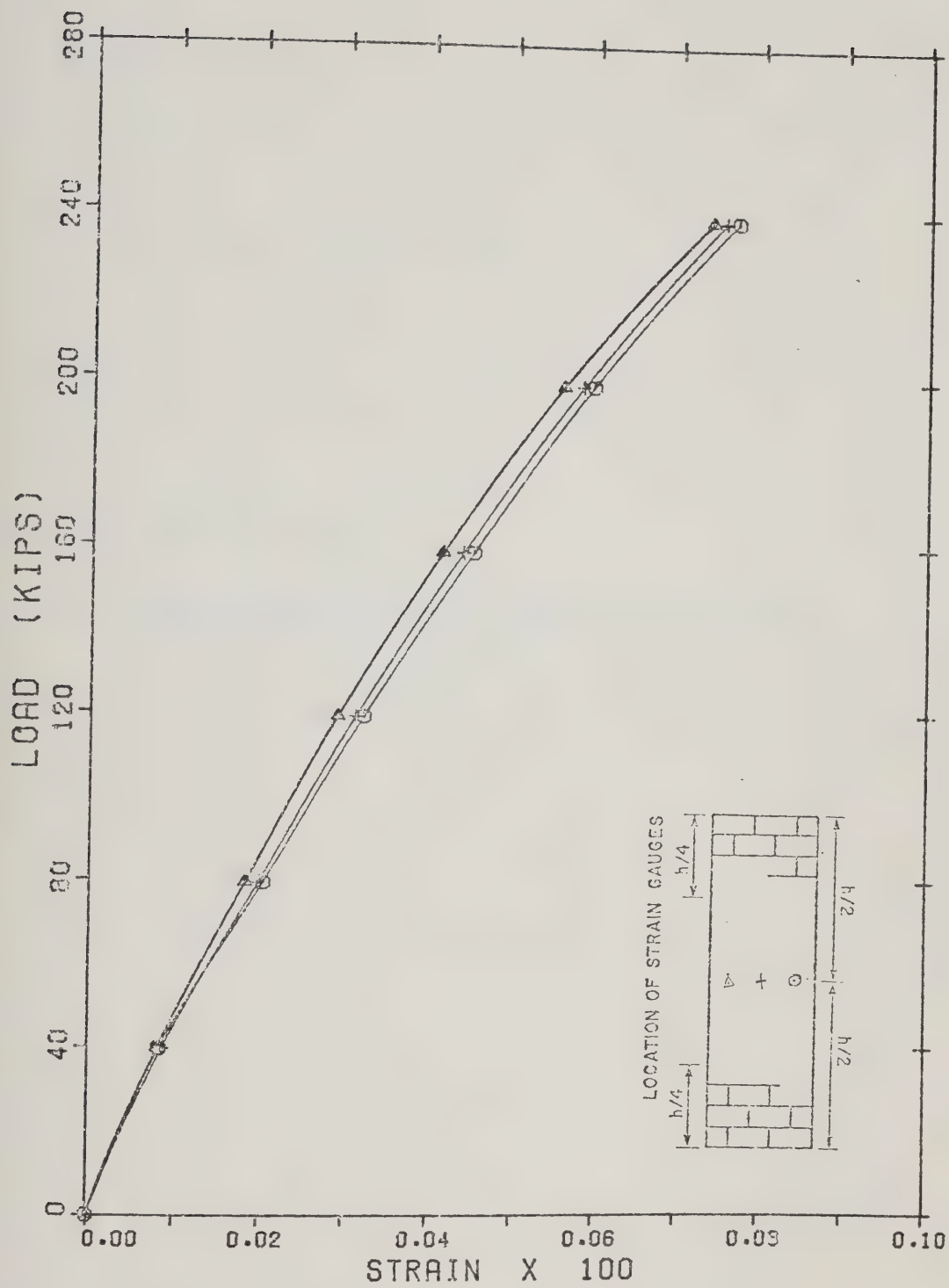


FIG. 7.13 Reinforcement Strains at Mid-height for Wall H2

strains in the three bars is attributed to the position of the strain gauge on the face of the bars. Figure 7.14 shows the influence of location of the strain gauge to the measured strain. For larger bar sizes this latter aspect can contribute significantly to the measured strain. From the strain measurements it is observed that in the case of eccentric loading, as in the case of axial loading, the reinforcing steel does not reach its yield strain. The maximum tensile strain for walls reinforced with 3-#9 bars was 9×10^{-4} in/in. as measured in Wall L5. For Series H the maximum tensile strain in the reinforcement was 1.8×10^{-3} in/in. which is 87% of the yield strain.

7.3.4 Vertically Reinforced Walls Double Curvature Bending

Five walls, each reinforced with one number three bar in each of the three grouted cores, were tested with eccentricities producing double curvature bending. The results are listed in Table 7.5, in which the eccentricities and wall properties are also given. Wall J1, tested with load eccentricities of $+t/6$ and $-t/6$, failed when its compressive capacity was reached at mid-height. The failure mode, as demonstrated in Plates 7.13 and 7.14 was splitting of the blocks in a similar manner to that in short specimens. All other walls failed when the strength of the material on the compression side was reached. Plates 7.15 and 7.16 show failures of Walls J3 and K1. The deflected shape of all walls, monitored during the tests, indicated that reinforced walls with double curvature imperfections have a tendency to buckle in their first mode, an observation made previously for plain walls.

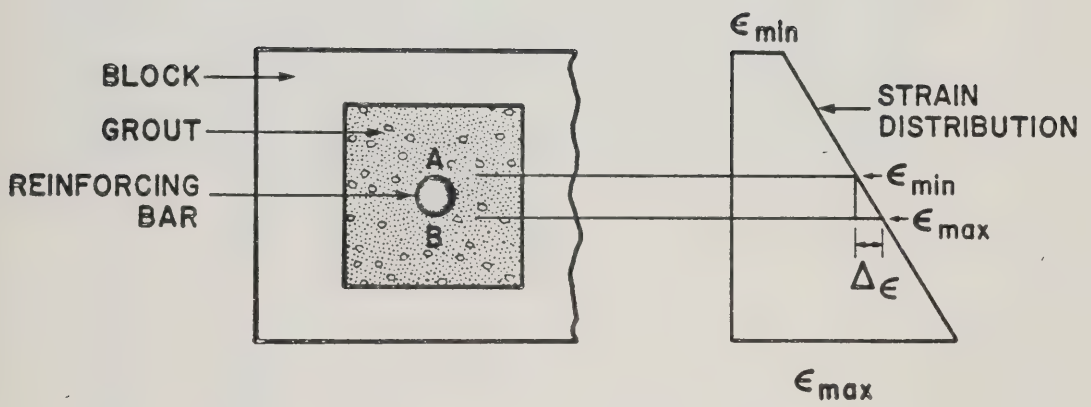


FIG. 7.14 Influence of Location of Strain Gauge on the Measured Strain

TABLE 7.5 Test Results for Reinforced Walls
Tested in Double Curvature

Wall Designation	h/t Nominal	h/t Actual	Reinforcement		Eccentricities		Failure Load kips	Moment at Failure kip-in.
			Vertical	Horizontal	Top in.	Bottom in.		
J1	16	17.97	3#3	plain	+1.27	-1.27	305.00	387.30
J2	16	17.97	3#3	"	+2.54	-2.54	263.30	668.70
J3	16	17.97	3#3	"	+3.00	-3.00	244.80	734.40
J4	16	17.97	3#3	"	+3.50	-3.50	157.60	551.60
K1	16	17.97	3#3	"	+2.54	-1.27	230.20	584.70

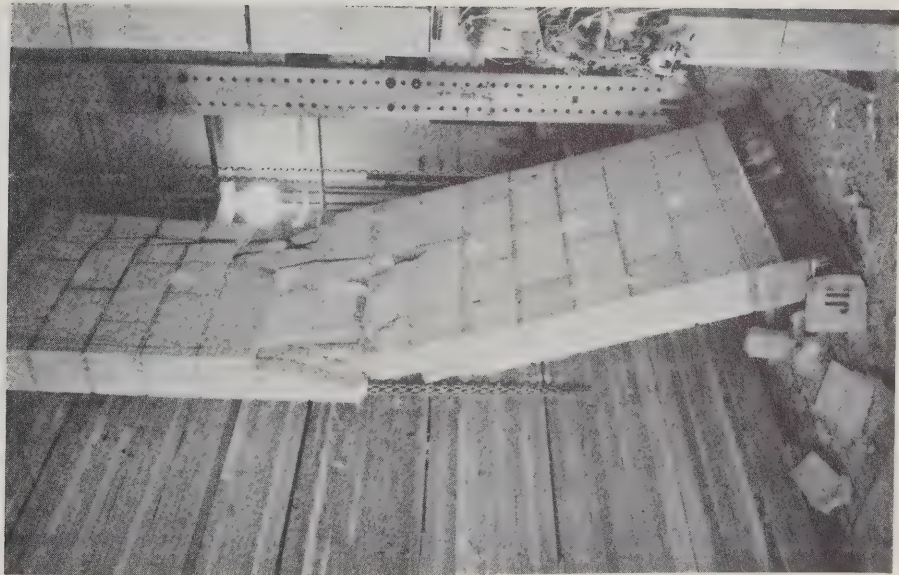


PLATE 7.13 Failure of Wall J1 (Crushing
at Mid-Height)

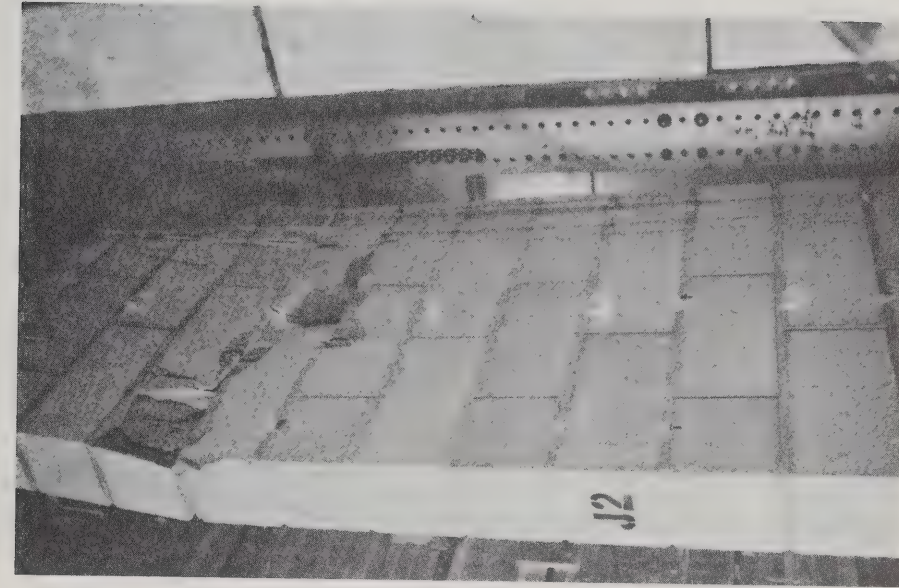


PLATE 7.14 Failure of Wall J2
(Bending in Upper Portion)

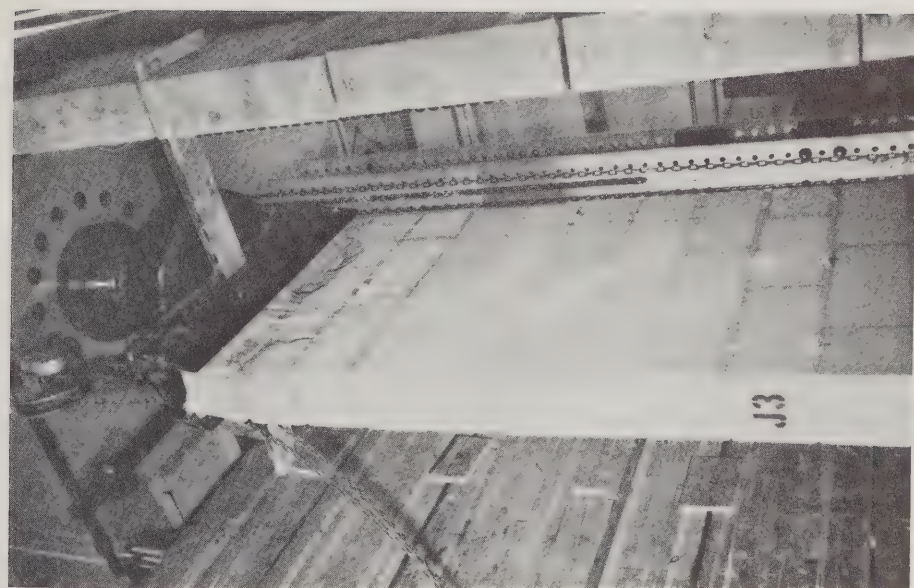


PLATE 7.15 Failure of Wall J3
(Bending at Upper Portion)

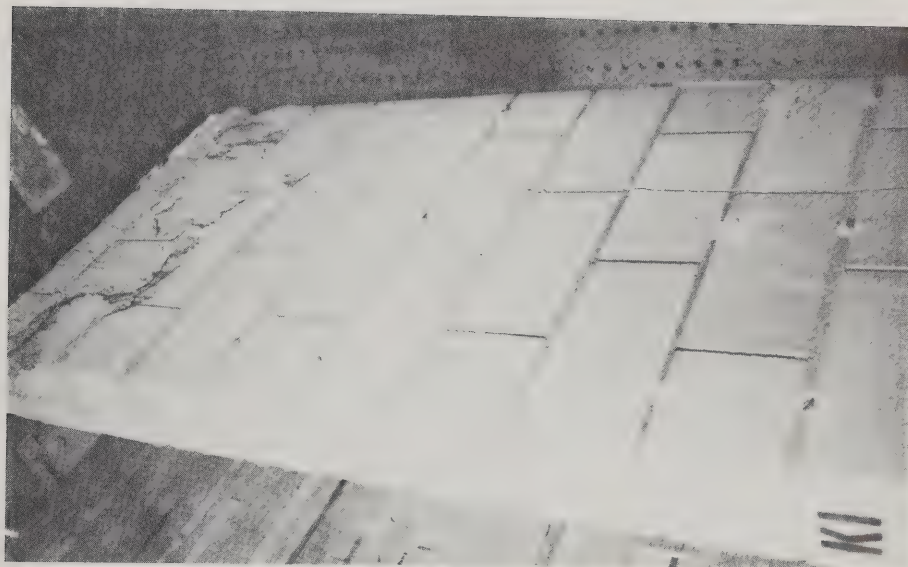


PLATE 7.16 Failure of Wall K1
(Bending of Upper Portion)

Figure 7.15 shows the load deflection curve of Wall J4 at 20 kip load increments during testing. On the same figure the migration of the point of inflection from mid-height towards the lower support is clearly shown. Deflected shapes for the other walls are given in Structural Engineering Report No. 71 of the Department of Civil Engineering, University of Alberta.

Strain measurements at 1/4 points along the wall height for Series J indicated that the steel remained in compression throughout the test and that maximum strain occurred in the lower portion of the walls as expected from the observation of the movement of the point of inflection. Figure 7.16 shows the average of three strain measurements taken during testing. Maximum strain observed was 6.2×10^{-4} in/in.

7.4 Effect of Eccentricities on the Load Carrying Capacity of Masonry Walls

The test data indicated, as expected, a reduction in load capacity with increasing eccentricity for all cases tested.

The reduction in axial load was also influenced by the slenderness ratio as it relates to increased deflection which, in effect, magnified the moment on the section. Axial load versus eccentricity is plotted in Figure 7.17 for plain and reinforced walls with a nominal slenderness ratio of 16 and tested with equal end eccentricities. The shape of the relations is similar to that for buckling loads for masonry walls in single and double curvature as derived in Chapter IV.

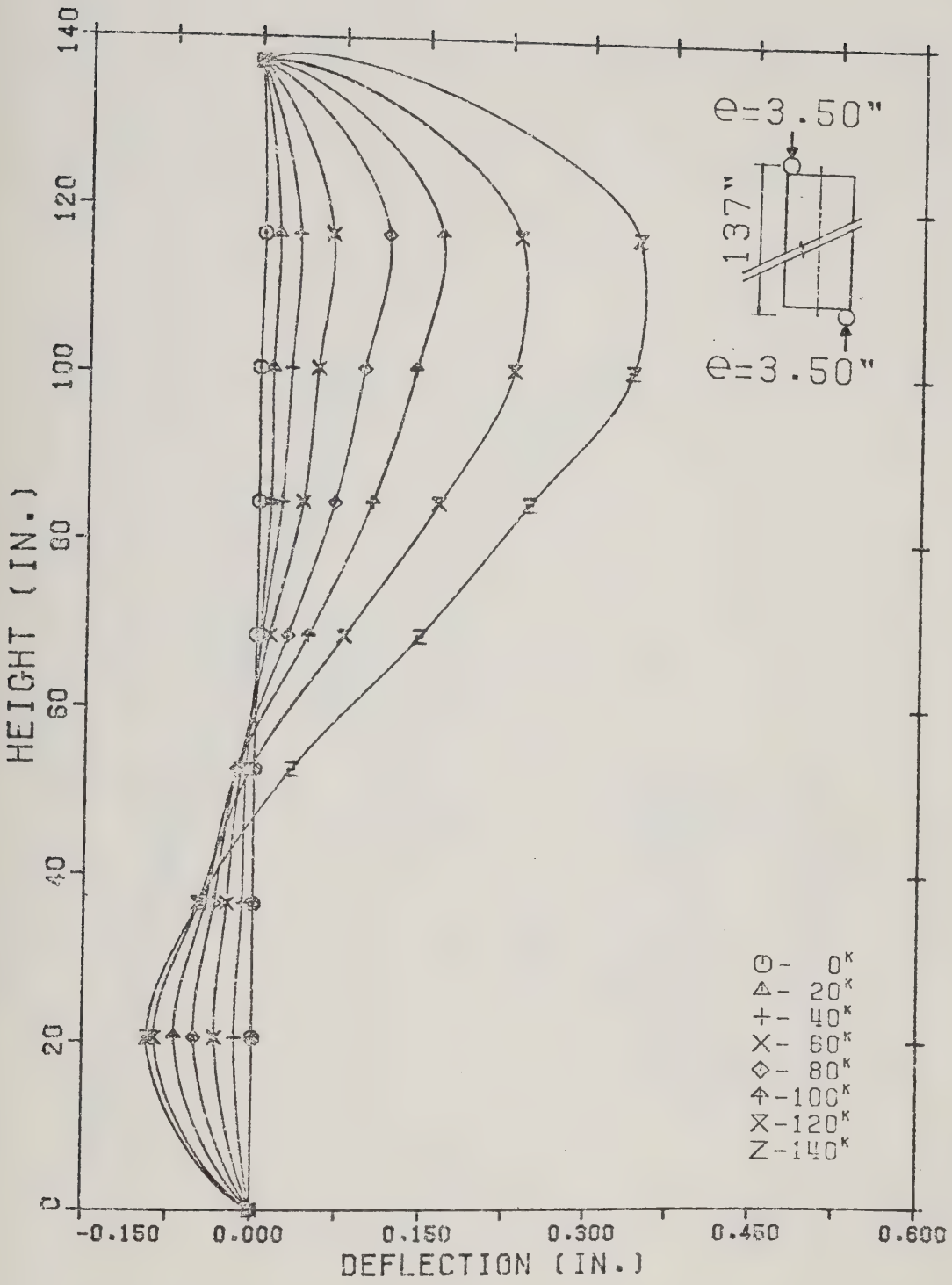


FIG. 7.15 Deflected Shape of Wall J4

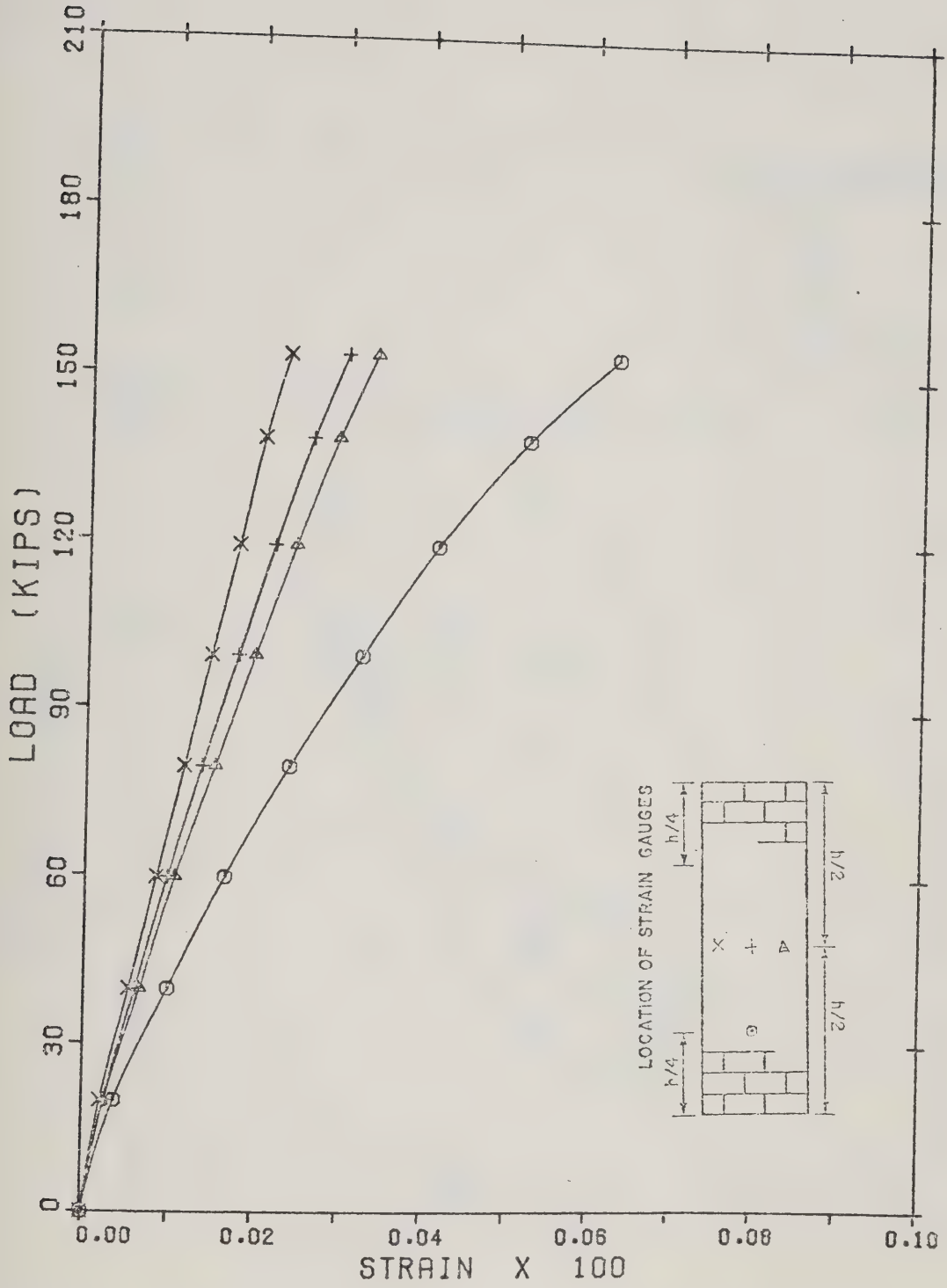


FIG. 7.16 Reinforcement Strains in Wall J4

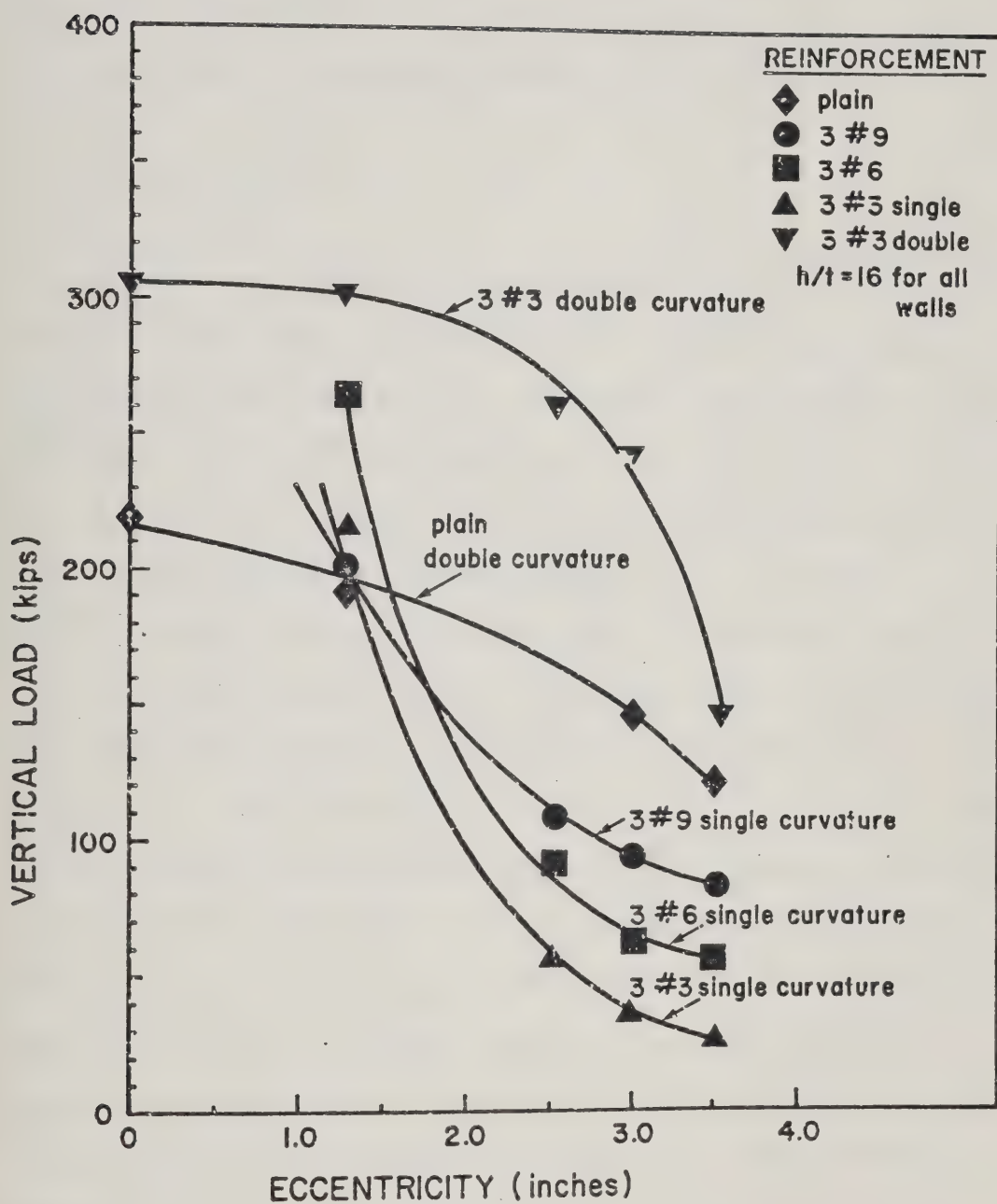


FIG. 7.17 Vertical Load vs Eccentricity for Plain and Reinforced Walls in Double and Single Curvature

Figure 7.17 indicates that the amount of reinforcement influences, in a predictable manner, the capacity of the section for eccentricities outside the kern. For eccentricities within the kern, the steel utilization is not very efficient as shown in the test results and as discussed in previous sections.

7.5 Masonry Strains

Strain measurements on the compression and tension side at mid-height, were taken during loading for a number of walls using 4 in. long concrete strain gauges. Because of shape variation along the height of the block unit (thicknesses vary from 1.25 in. at bottom to 1.75 in. at the top) strain measurements are only indicative of the stress-strain relation of the assembly. The 4 in. gauge length included a mortar joint in all cases. Compressive strains at failure were between 0.002 and 0.003 in/in. Tensile strains were of the same order; however, joint separation resulted in gauge damage at loads much lower than the failure load. A typical relation between vertical load and compressive and tensile masonry strains is given in Figure 7.18 for Wall B5. It has been observed previously that the stress-strain relation on the compression side is almost linear up to failure. The same observation is also true for most tensile strain measurements. Deviations from the straight line can be attributed to the breaking of the bond at the joints. Masonry strains for the axially loaded Wall F1, measured on both sides of the wall at mid-height, are plotted in Figure 7.19. From this figure, and based on active mortared area of 122.35 in.² the modulus of elasticity of the wall is of the order of 1.0×10^6 psi.

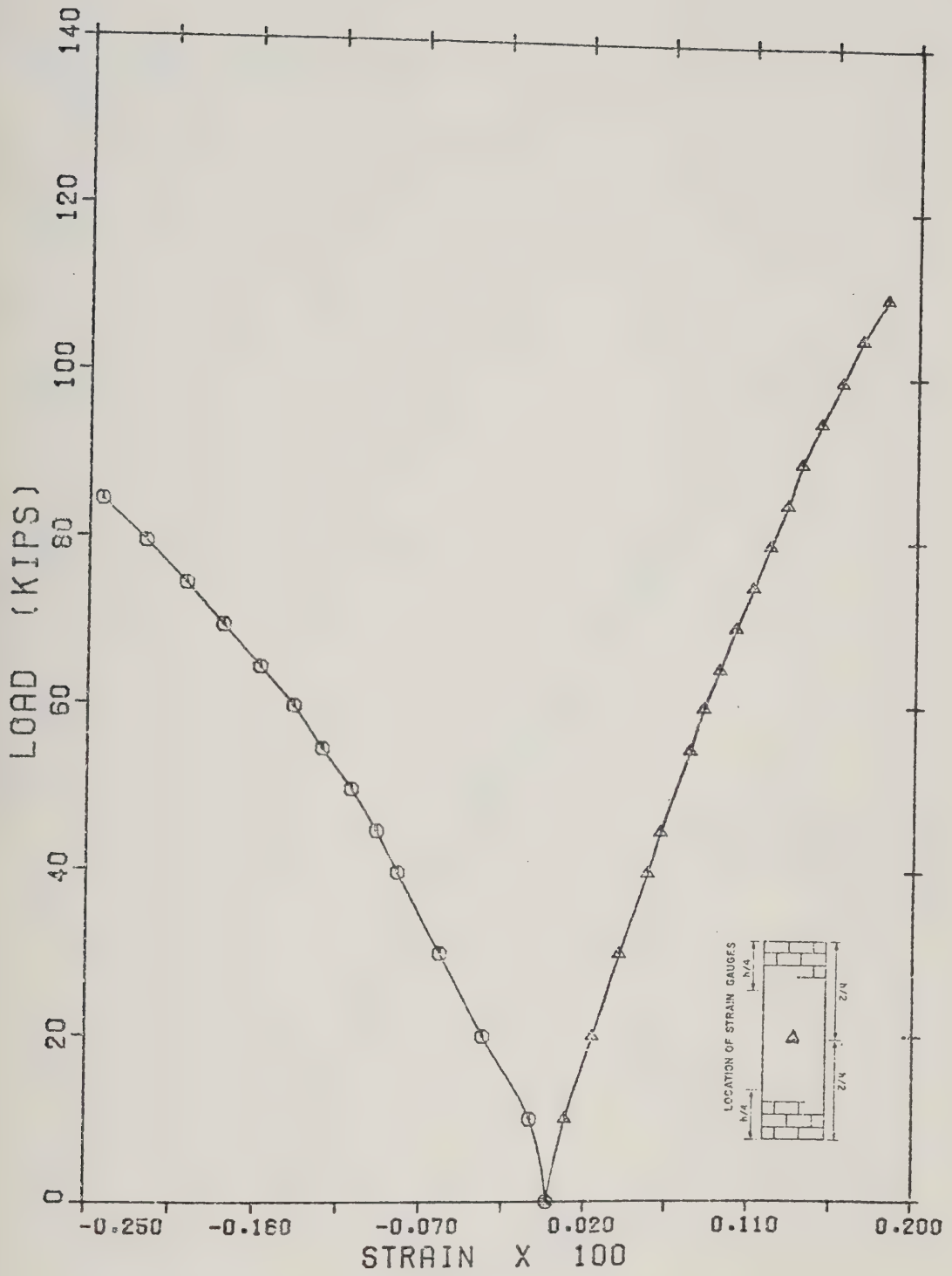


FIG. 7.18 Masonry Strains for Wall B5

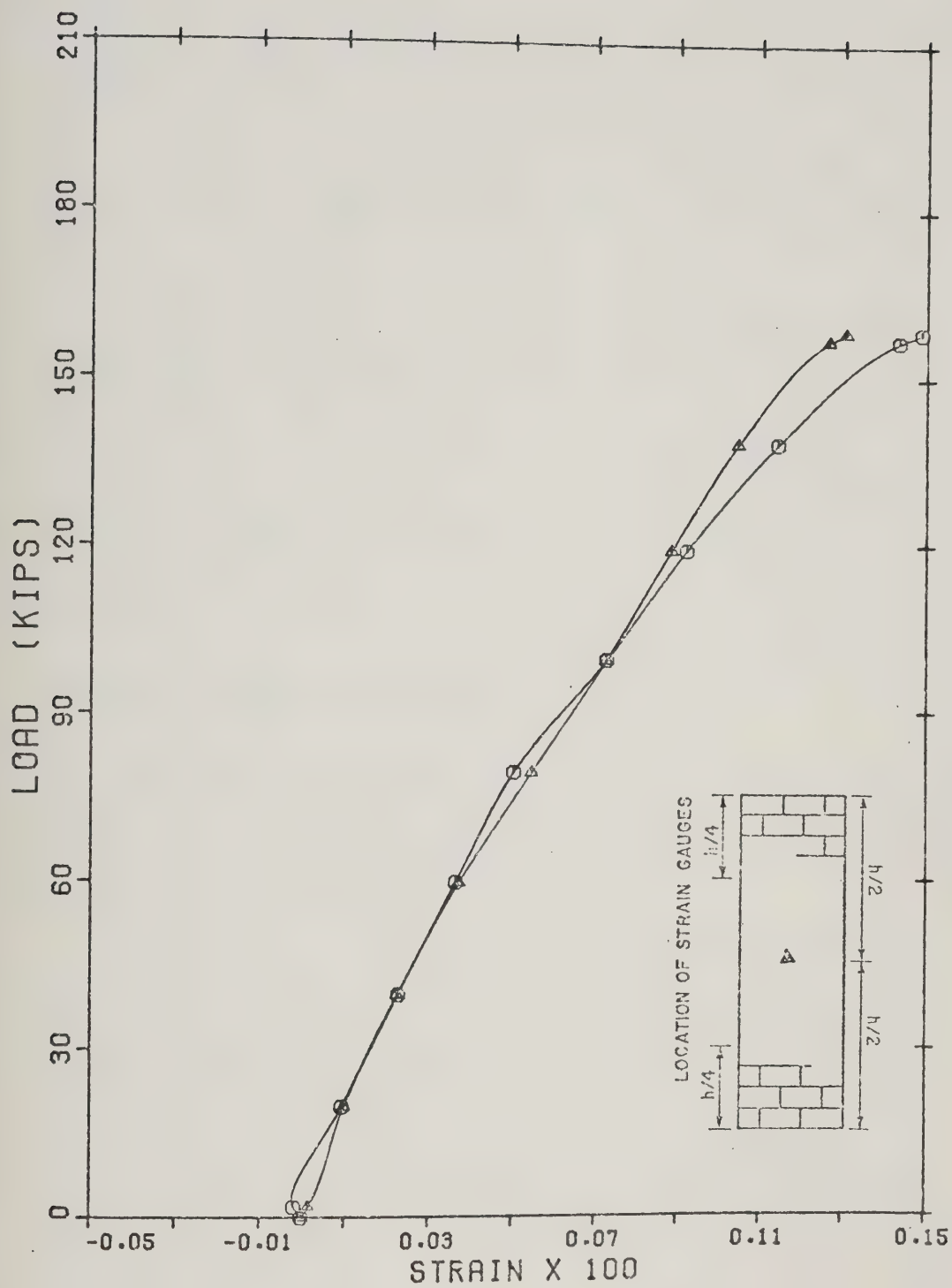


FIG. 7.19 Masonry Strains for Wall F1

However the strains were measured over length of 4 inches including a mortar joint where the average thickness of the two block portions involved was 1.5 in. Based on an approximate minimum load bearing area of 100 in.² the modulus of elasticity is 1.2×10^6 psi. This value is in close agreement with that obtained in tests on small specimens.

Figure 7.20 shows masonry strains for Wall H1 which was axially loaded and reinforced with three number six bars. Based on 210 in.² minimum load bearing area, the modulus of elasticity calculated for Wall H1 is 1.10×10^6 psi. This value is within the two limiting values for modulus of elasticity calculated previously for plain ungrouted walls.

7.6 Flexural Rigidity of Masonry

A reliable evaluation of axial rigidity EA and the flexural rigidity EI of the masonry section is essential in the analysis and design of masonry structures.

The flexural rigidity depends on the intensity and the distribution of stresses on the cross-section, as it relates to the moment of inertia which decreases with flexural cracking. It was observed from tests that, for all practical purposes, the load deformation characteristics of masonry are linear for stress levels up to the ultimate load, if creep and other time effects are neglected. It is therefore desirable to relate the variation in flexural rigidity to the eccentricity of the load and allow for the time dependent effects by means of a factor similar to that used for concrete.

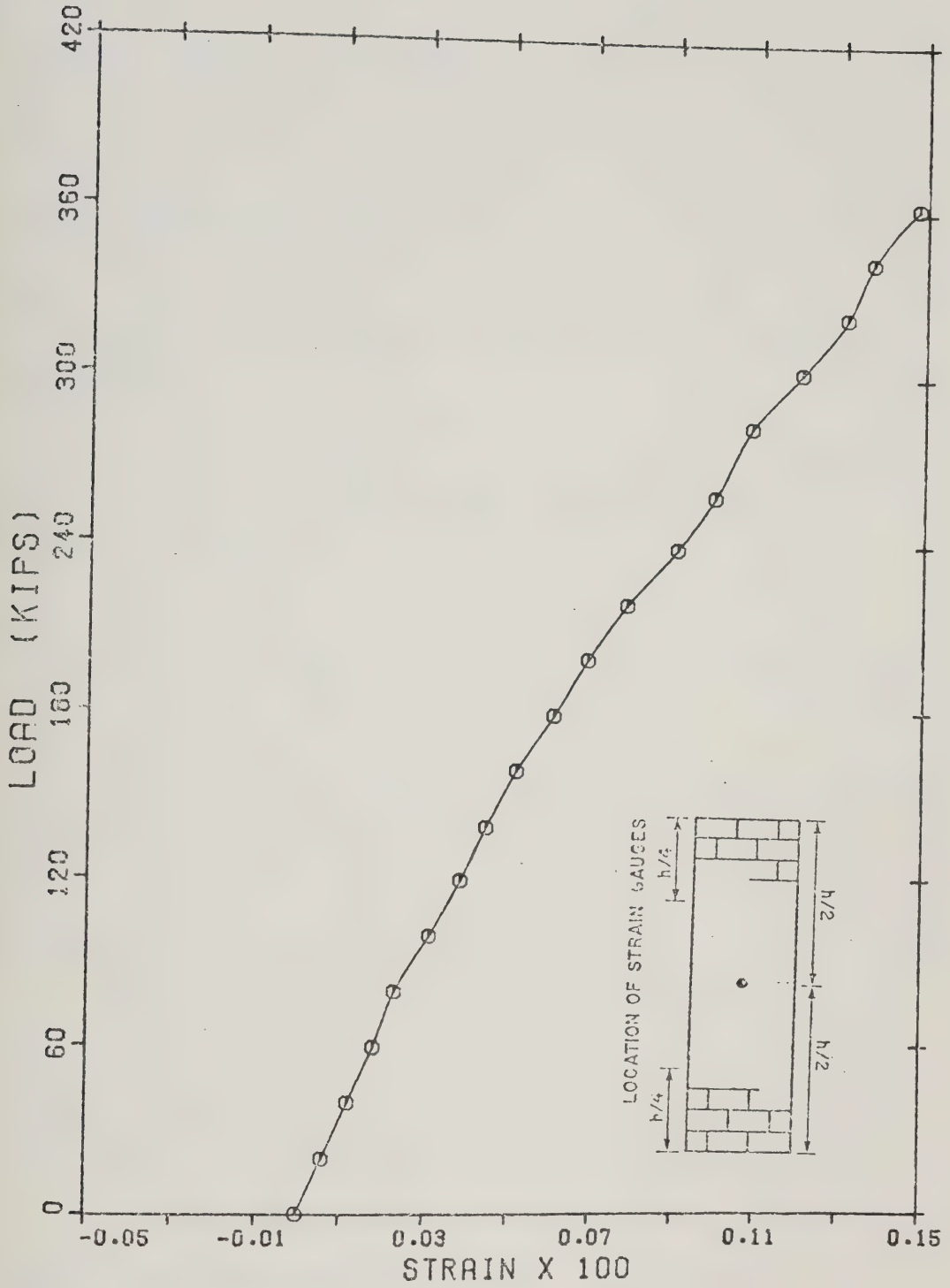


FIG. 7.20 Masonry Strains for Wall H1

Exact calculation of the moment of inertia for masonry members is affected by such factors as type of construction as it relates to mortared area, type of masonry units as it relates to cross-sectional areas, and other factors. These factors include mortar penetration and mortar overhang in the cores. The effect of these factors is cumulative over the member as a whole. It is for these reasons that the rigidity of masonry should be evaluated experimentally.

It was shown in Chapter IV that the moment of inertia for the evaluation of the critical buckling load is given by the following equation:

$$I = 8 \left[\frac{1}{2} - \frac{e}{t} \right]^3 I_0 \dots\dots\dots 7.1$$

To allow for the influence of the tensile bond a factor ζ was introduced. This factor, calculated using procedures given in Chapters II and IV, will increase the moment of inertia and thus influence the buckling load.

Relation 7.1 however, is only valid for buckling cases and it will be very conservative for strength problems. When strength governs, the section will fail prior to reaching its buckling load and as a result cracks will not reach their maximum penetration.

From the load deflection curves obtained from tests, the rigidity EI was calculated for a number of load intervals. In Figure 7.21 the ratio of the calculated rigidity prior to failure, to that obtained from the first load increment when the section was uncracked, is plotted versus the ratio of the eccentricity to the

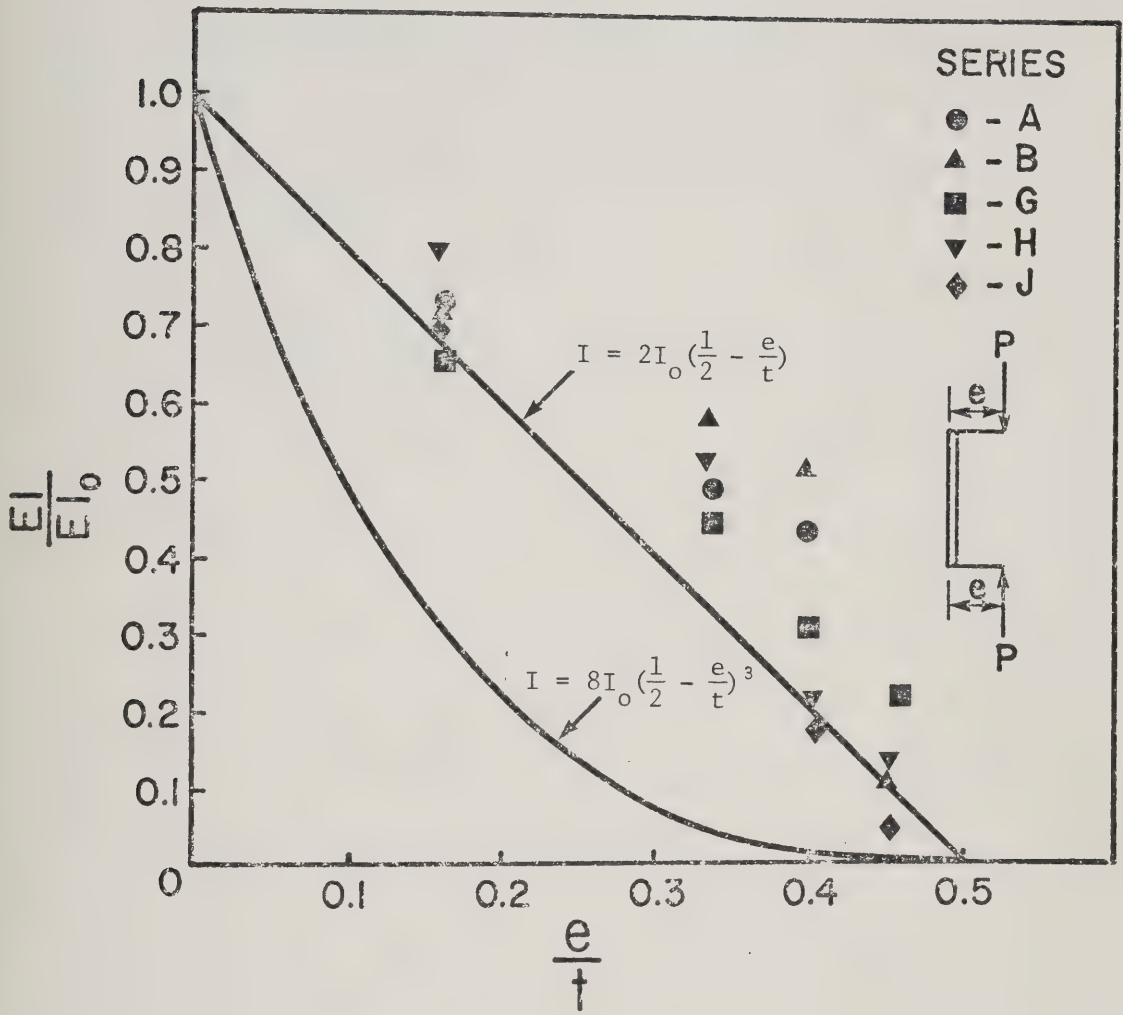


FIG. 7.21 Variation of Flexural Rigidity with Eccentricity

thickness. On the same figure Equation 7.1 is plotted. It is obvious that Equation 7.1 is very conservative for all cases. A straight line relation given by $EI = EI_0 (1/2 - e/t)$ appears to give a good estimate of the flexural rigidity for all types of loading of plain and reinforced walls. From the experimental evidence it appears that, for design purposes, one can safely use the following relation for estimating the moment of inertia of eccentrically loaded masonry walls.

$$I = \left[\frac{1}{2} - \frac{e}{t} \right] I_0 \dots\dots\dots 7.2$$

CHAPTER VIII

Analysis and Synthesis of Test Results

8.1 Introduction

In this chapter, the experimental results are interpreted and compared with analytical results based on theoretical considerations of previous chapters. Emphasis is placed on applying a rational analysis based on established theory in predicting the strength of masonry under axial load and bending.

8.2 Constitutive Relations

The capacity of a masonry cross-section subjected to a combination of vertical load and moment can be determined if the compressive and tensile strengths, as well as the stress distribution over the cross-section at failure, are known. The stress distribution, in turn, depends on the stress-strain properties of the masonry. In previous chapters it has been shown that a linear stress-strain relationship gives a close approximation of the load deformation characteristics of masonry.

Stress distributions over the cross-section were also assumed linear for various load-moment combinations. It was observed that the failure mode of masonry depends on the loading conditions. Splitting failure governs for axially loaded sections, and crushing governs for axial load plus moment. Crushing failures were accompanied

by an apparent increase in calculated normal stress at failure. This phenomenon is attributed to the presence of shear and the fact that most of the rotation occurs in the mortar joint when the wall deflects. Shear and lateral forces in the joint, as they relate to the rotation, counteract the splitting force allowing the section to reach the compressive strength of the masonry unit, provided that the mortar joint is not thick enough for failure to occur when the compressive strength of the mortar is reached.

In the following sections the flexural rigidity is based on the gross moment of inertia and a modulus of elasticity equal to 1.125×10^6 psi. The value of the elastic modulus was experimentally evaluated in Chapter VI and it is a mean value for all specimens tested. The lower and upper bounds for the elastic modulus from Figure 7.9 are 0.875×10^6 psi and 1.35×10^6 psi.

CSA Standard S-304-M¹³ recommends calculation of the elastic modulus on the basis of the ultimate strength of the masonry. The recommended value is $1000 f'_m$. Based on this recommendation there are two possible values for the modulus of elasticity:

- a) $E = 1.5 \times 10^6$ psi based on f'_m calculated as recommended by CSA Standard S-304-M¹³.
- b) $E = 1.9 \times 10^6$ psi based on experimental evaluation of the ultimate compressive strength and multiplied by the same factor as recommended by CSA Standard S-304-M¹³.

In both cases the values are much higher than the observed ones and their use will lead to an overestimation of both flexural and axial rigidity.

8.3 Analysis for Slender Column Effects

While the capacity of a "short" wall is dependent only on the strength of section, the strength of "high" walls is dependent also on slenderness. When a wall is loaded with an eccentric vertical load the moment along the wall height is magnified due to deflection. For walls in single curvature bending, the moment is maximum at mid-height, where the deflection is maximum. The magnified moment for any combination of loading was shown in Chapter IV to be:

$$M_m = P e_{\max} \left(\frac{C_m}{1 - \frac{P}{P_{cr}}} \right) \dots\dots\dots 8.1$$

It has been shown in Chapter IV that the buckling load for masonry walls is a function of the reduced moment of inertia and the tensile strength. For an axially loaded wall the tensile strength has no effect on the buckling load. For an eccentrically loaded wall the stress level at buckling decreases as the eccentricity increases, resulting in an increase in the effect of the tensile strength as it relates to the depth of cracks.

The magnification factor in Equation 8.1, is a function of the applied vertical load and the critical load. The critical load depends on the effective moment of inertia, which in turn depends on the magnitude of the load and its eccentricity. As a result, an iterative procedure must be used to evaluate the effect of slenderness on the load carrying capacity of masonry walls. In the following sections the procedure is presented in a step by step form and then applied in examples.

Step 1 For a given eccentricity, find the section capacity from a short wall [$h/t = 0$] interaction diagram.

Step 2 Calculate the critical load using Equation 4.26, repeated here for clarity:

$$P_{cr} = \frac{\pi^2 E}{12h^2} \left[\left(1 - \frac{2e}{t} \right) t + \zeta \right]^3 b \dots\dots\dots 8.2$$

In the above relation ζ is evaluated using Equations 2.6, 2.8 and 4.25. These equations are:

$$f_{max} = \frac{4}{3} - \frac{P}{A(1 - 2e/t)} \dots\dots\dots 8.3$$

$$\zeta = \frac{2tP}{Af_{max}} \dots\dots\dots 8.4$$

and

$$\zeta = \frac{\zeta f' t}{f_{max}} \dots\dots\dots 8.5$$

Step 3 Calculate P from Equation 8.1 using the moment and the eccentricity from Step 1. For this new vertical load find the corresponding moment from the strength interaction diagram.

Step 4 Repeat Steps 2 and 3 until the calculated vertical load converges.

8.4 Application of the Moment Magnifier Method to Plain Masonry Walls

8.4.1 Single Curvature Bending, Equal End Eccentricities

The strength interaction diagram for a cross-section as

obtained using a computer program developed for this purpose, is shown in Figure 8.1. To account for slenderness effects, the basic strength interaction diagram is modified using the iterative procedure of Section 8.2. The reduced capacities for slenderness ratios of 6.5 and 14 are shown in the figure. These reduced capacities are found to be in good agreement with test data. In the same figure, the design provision of the CSA Standard S-304-M¹³ are plotted, excluding the safety factor applied to the strength.

The iterative procedure used in modifying the strength interaction diagram for slenderness effects is illustrated in the following example. Consider a plain wall 40 in. wide and 7.625 in. thick with slenderness ratio of 6.5, loaded in single curvature with an eccentricity of $t/3$ top and bottom. It is required to determine the capacity of the wall.

Step 1 The capacity of a short wall ($h/t = 0$) of the same cross-section, loaded at an eccentricity of $t/3$, is a vertical load 135 kips with a corresponding moment of 343 kip-in. (Figure 8.1).

Step 2 The maximum compressive stress at this load level, based on Equation 8.3, is:

$$f_{\max} = \frac{135}{305} \left[\frac{4}{3 \left(1 - \frac{2 \times 2.54}{7.625} \right)} \right] = 1.77 \text{ ksi}$$

The approximate point on the cross-section where the stress is zero is found using Equation 8.4.

$$\xi = \frac{2 \times 7.625}{305 \times 1.77} = 3.8 \text{ in.}$$

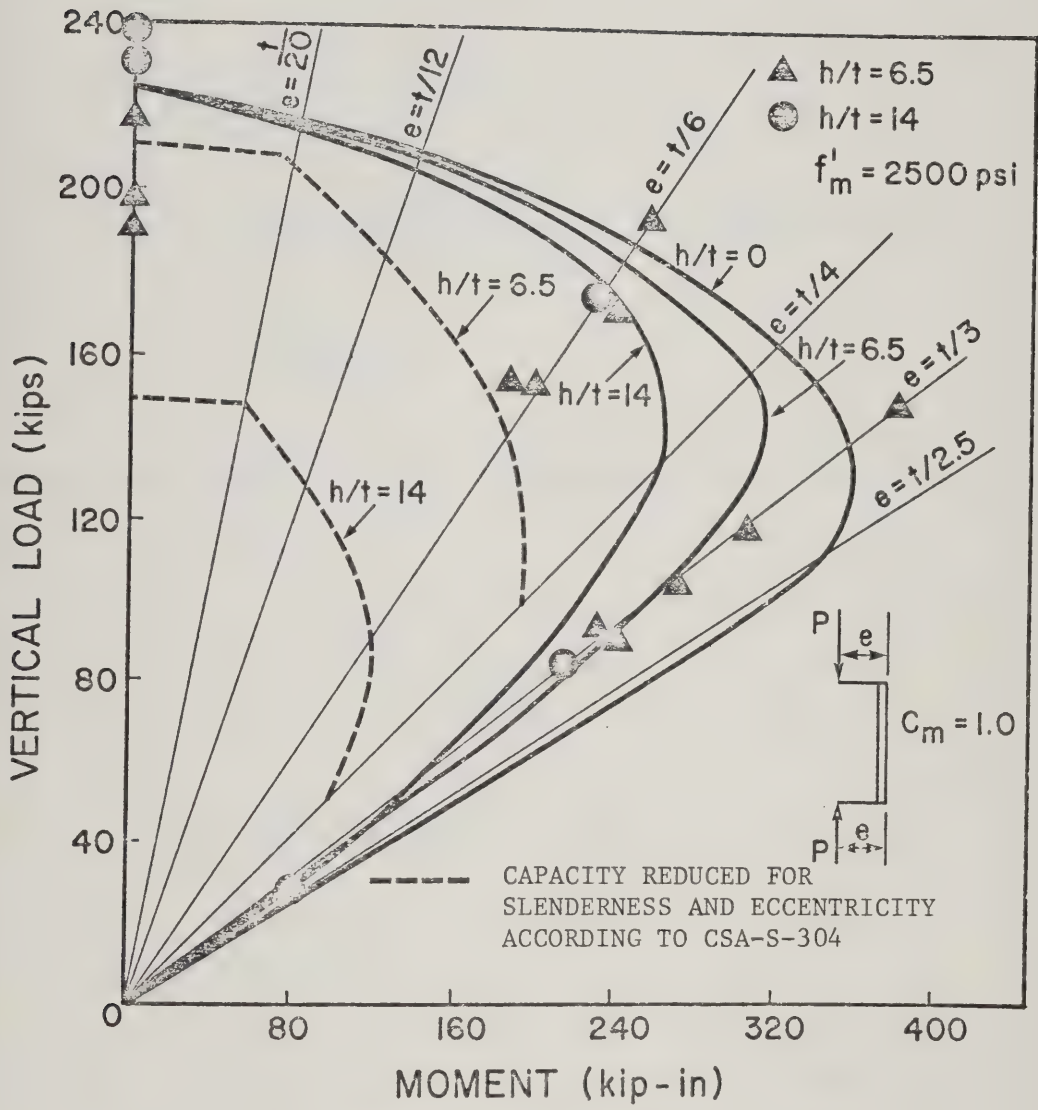


FIG. 8.1 Effects of Slenderness on the Strength of Masonry Walls in Single Curvature Bending

The reduction due to the crack penetration, attributed to the tensile strength of the masonry, is found using Equation 8.5. (Figures 2.4 and 4.12 define the parameters ξ and ζ .)

$$\zeta = \frac{3.8 \times 0.2}{1.77} = 0.43 \text{ in.}$$

From Equation 8.2 the critical load is

$$\begin{aligned} P_{cr} &= \frac{\pi^2 \times 1.125 \times 10^6}{12 \times [6.5 \times 7.625]^2} \left[\left(1 - \frac{2 \times 2.54}{7.625} \right) 7.625 + 0.43 \right]^3 40 \\ &= 396 \text{ kips} \end{aligned}$$

Step 3 The reduced vertical load capacity is evaluated using Equation 8.1.

$$343 = 2.54 \times P \left[\frac{1}{1 - \frac{P}{396}} \right] \quad \text{or}$$

$$343 \left[1 - \frac{P}{396} \right] = 2.54 P \quad \text{and}$$

$$P = 100 \text{ kips}$$

This load is lower than the one obtained in Step 1 and therefore the maximum moment that the section can carry under this vertical load is 320 kip-in. The procedure is repeated with $P = 100$ kips and $M_m = 320$ kip-in as the corresponding values of Step 1. With $P = 100$ Step 2 gives

$\zeta = 0.59$ in. and $P_{cr} = 464$ kips. Repeating Step 3 with $M_m = 320$ kip-in. and $P_{cr} = 464$ kips, the vertical load is calculated to be 99 kips which is close to the previously calculated load, indicating a rapid convergence in the iterative procedure.

In all the above calculations the gross section area and gross moment of inertia were used. To account for the fact that at least two blocks at the end are not cracked and that the tensile strength of the units influences the crack penetration, a tensile bond strength of 200 psi was used. This is an approximation of the average tensile strength of the masonry units and tensile bond.

8.4.2 Single Curvature Bending, Unequal End Eccentricities

When the top and bottom eccentricities are not equal, initial moments along the height of the wall are not constant. As a result, crack penetration decreases with decrease in moment and the evaluation of the critical load must be carried out using the average of the two eccentricities. This accounts for an increased moment of inertia at the end which has the smaller eccentricity. Although this is an approximation, it is found to give satisfactory results. The remaining procedure for determining the reduced capacity is similar to the one previously described for walls in single curvature and with equal end eccentricities.

Figure 8.2 is an interaction diagram on which the test data and the reduction for bending have been plotted. The results are those for walls G1 to G5 which are specimens with joint reinforcement which has been shown to reduce the capacity of the section,

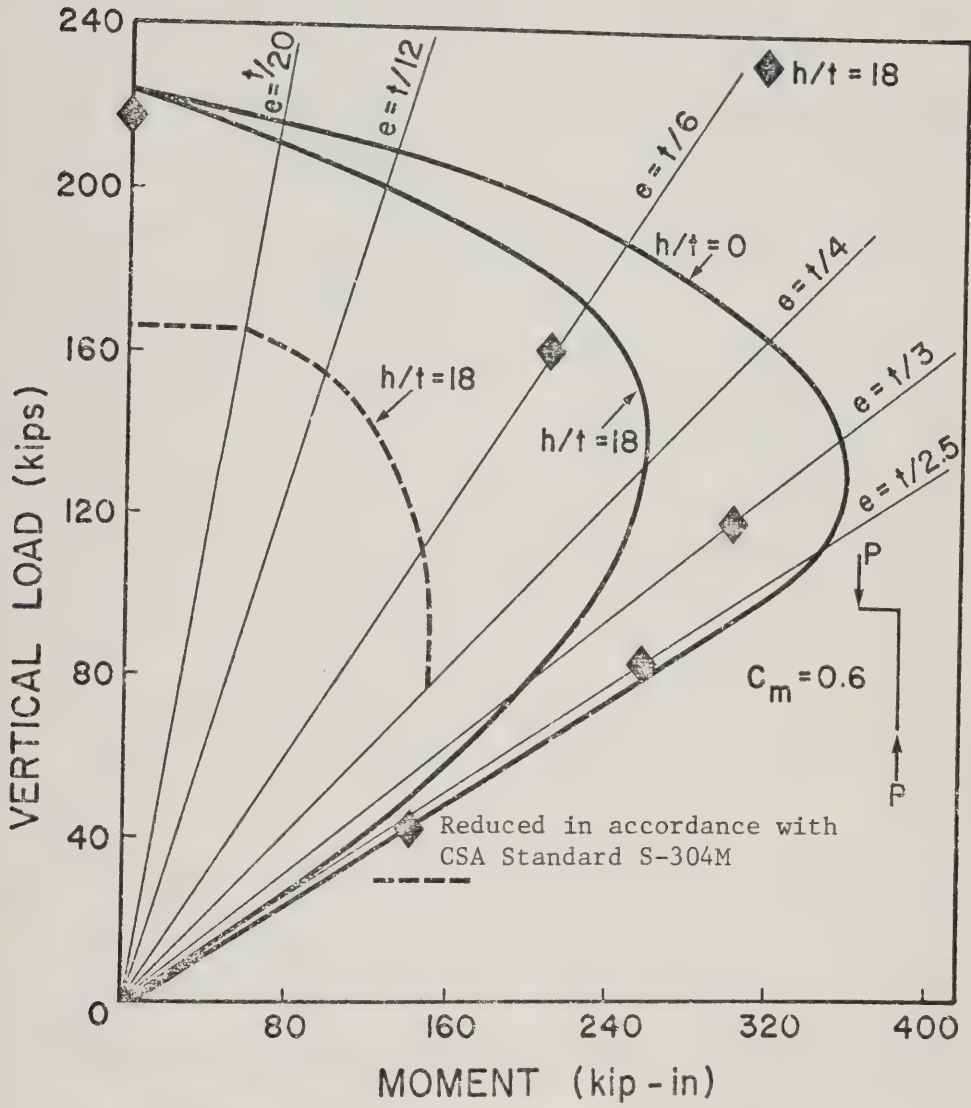


FIG. 8.2 Effects of Slenderness on the Strength of Masonry Walls in Single Curvature Eccentricity

especially at small eccentricities.

8.4.3 Double Curvature Bending

The critical load for masonry walls with initial double curvature imperfections was theoretically investigated in Chapter IV. The effect of slenderness and loading conditions can be evaluated in a manner similar to that for walls in single curvature by using the critical load as evaluated in Section 4.5. In Chapter VII, it was shown that masonry walls loaded in double curvature buckle in the first buckling mode.

The strength of a cross-section similar to that of the plain walls tested is shown in Figure 8.3. On the same figure the results obtained from the tests of Series N($h/t = 18$) are plotted.

The reduced capacity of the section resulting from slenderness effects is calculated as follows for $h/t = 18$ and $e = t/6$.

Step 1 For $e = t/6$ the short section ($h/t = 0$), can carry a vertical load of 190 kips. The corresponding moment is 241.3 kip-in.

Step 2 The critical load for the wall is 571 kips, evaluated using Table 4.1 with $\alpha = 0.5$ and $\beta = 0.329$.

Step 3 For $P = 190$ kips and $P_{cr} = 571$ kips and $C_m = 0.4$, the magnification factor is 0.59 which indicates that maximum moment occurs at the top or bottom of the wall.

If the weight of the wall is increased the magnification factor will increase as the critical load decreases. For a given eccentricity there is a particular h/t ratio for which the magnification factor is 1.0. For larger eccentricities there will be a

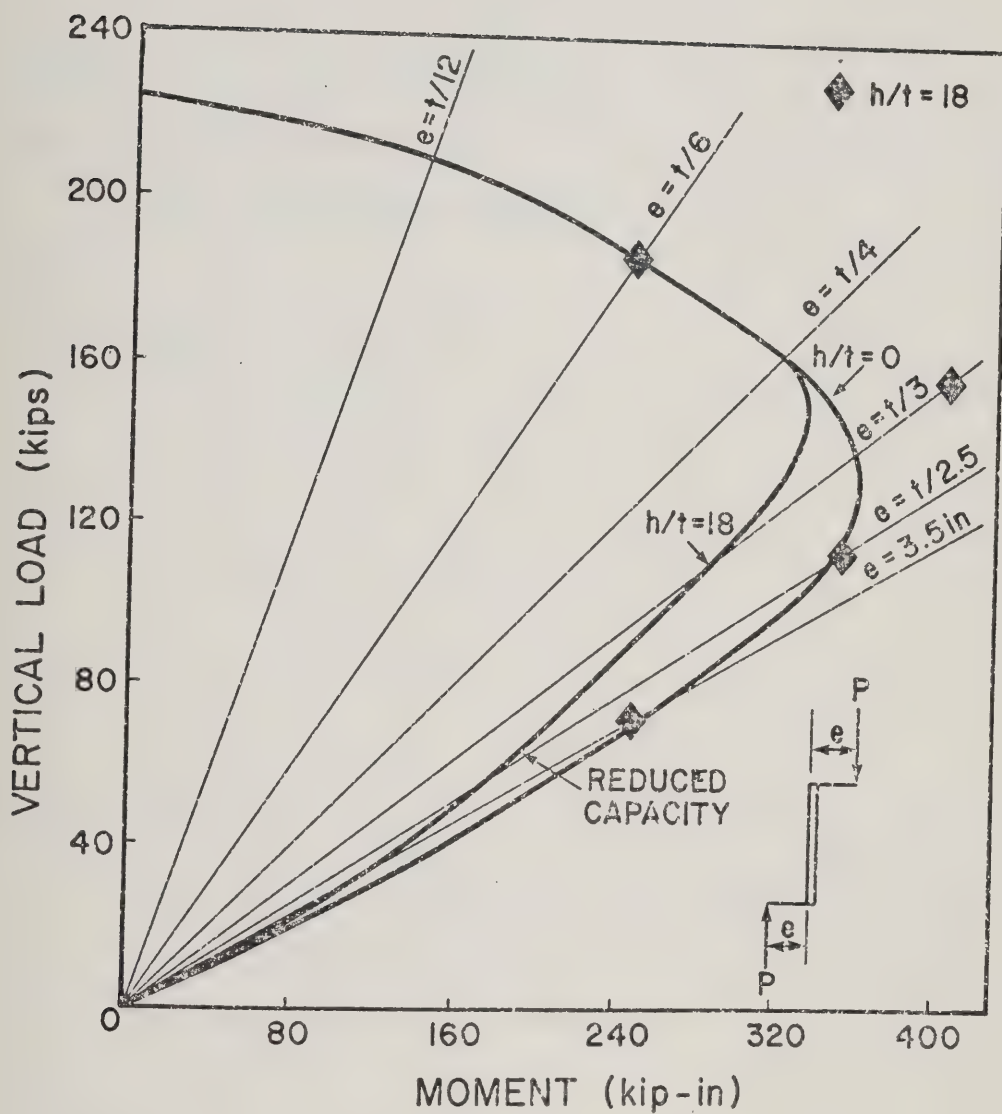


FIG. 8.3 Effect of Slenderness on the Strength of Masonry Walls in Double Curvature Bending

reduction due to slenderness effects. For $e = t/6$, the magnification factor is 1.0 for a critical load of 316 kips and slenderness ratio of 21.5. Examples of calculating the reduced capacity of the section resulting from slenderness effects are presented below for $e_1 = -e_2 = t/4$ and $e_1 = e_2 = t/3$ for $h/t = 18$.

Example 1: $e_1 = -e_2 = t/4$, $h/t = 18$

Step 1 The short section capacity for this eccentricity is 165 kips with a corresponding moment of 314.5 kip-in.

Step 2

$$f_{\max} = 1.433 \text{ ksi}$$

$$\xi = 5.75 \text{ in.}$$

$$\zeta = 0.802 \text{ in.}$$

$$I = 330 \text{ in.}^4$$

$$\beta = I/I_o = 0.223$$

$$\alpha = e_1/e_2 + e_1 = 0.5$$

$$\lambda = 3.918$$

$$P_{cr} = 437 \text{ kips}$$

Step 3 The amplification factor for this value of P_{cr} and $C_m = 0.4$ is 0.64 which indicates that maximum moment occurs at the ends. Failure of this wall will occur when the section capacity at one end is reached.

Example 2: $E_1 = -e_2 = t/3$

Step 1 The short section capacity is $P = 135$ kips with a corresponding moment of 342.9 kip-in.

Step 2 The critical load, calculated in a similar manner to that for $e = t/4$, is 148.7 kips.

Step 3 For $M_m = 342.9$ kip-in, $e = t/3$, $C_m = 0.4$ and $P_{cr} = 148$ kips, Equation 8.1 is solved for P :

$$342.9 = 2.54 P \left[\frac{0.4}{1 - \frac{P}{148.7}} \right] \quad \text{and}$$

$$P = 103 \text{ kips}$$

Since this load is lower than the section capacity, the procedure has to be repeated.

Step 1 From the interaction diagram the corresponding moment for $P = 103$ kip is 335 kip-in.

Step 2 For

$$P = 103 \text{ kips}$$

$$\zeta = 0.56 \text{ in.} \quad \text{and}$$

$$P_{cr} = 159 \text{ kips}$$

Step 3 Solving Equation 8.1 for P with $M_m = 335$ kip-in, $e = t/3$, $C_m = 0.4$ and $P_{cr} = 159$, the vertical load capacity is found to be 107 kips.

Repeating the cycle once again P is calculated to be 105 kips. A horizontal line at $P = 105$ kips intercepts the $t/3$ line at the modified interaction diagram. Therefore the capacity of this wall is 105 kips vertical load.

For other eccentricities the procedure is repeated to find the reduced capacities. For walls with unequal end eccentricities

a similar procedure gives a lower bound interaction diagram. The test results obtained from Series G, follow the trend suggested in this analysis. (Table 7.3 gives a detailed account of test results). Load deflection curves such as shown in Figure 7.14 indicate that the moment is maximum at a point away from the end for eccentricities greater than $t/4$ and for slenderness ratios greater than 18. Deflection curves for other walls tested in double curvature are given in Structural Engineering Report No. 71 of the Department of Civil Engineering, the University of Alberta.

8.5 Application of the Moment Magnifier Method to Vertically Reinforced Masonry Walls

8.5.1 Single Curvature Bending, Equal End Eccentricities

The strength of a cross-section reinforced with 3-#3 deformed bars is shown in Figure 8.4. To account for slenderness this interaction diagram is modified using the moment magnifier method. Consider a wall segment with $h/t = 18.0$. (Test series I1 to I5). For these walls $A_n \approx 305 \text{ in.}^2$ and $I_o \approx 1477 \text{ in.}^4$. The procedure used in reducing the capacity of the section to allow for slenderness effects follows the same steps as for plain walls.

The reduced moment of inertia is evaluated using Equations 4.24 and 4.26.

$$I = \left(\frac{1}{2} - \frac{e}{t} \right) I_o \geq 0.10 I_o \quad \dots\dots\dots 8.6$$

$$I = \frac{b}{12} \left[\left(1 - \frac{2e}{t} \right) t + \zeta \right]^3 \quad \dots\dots\dots 8.7$$

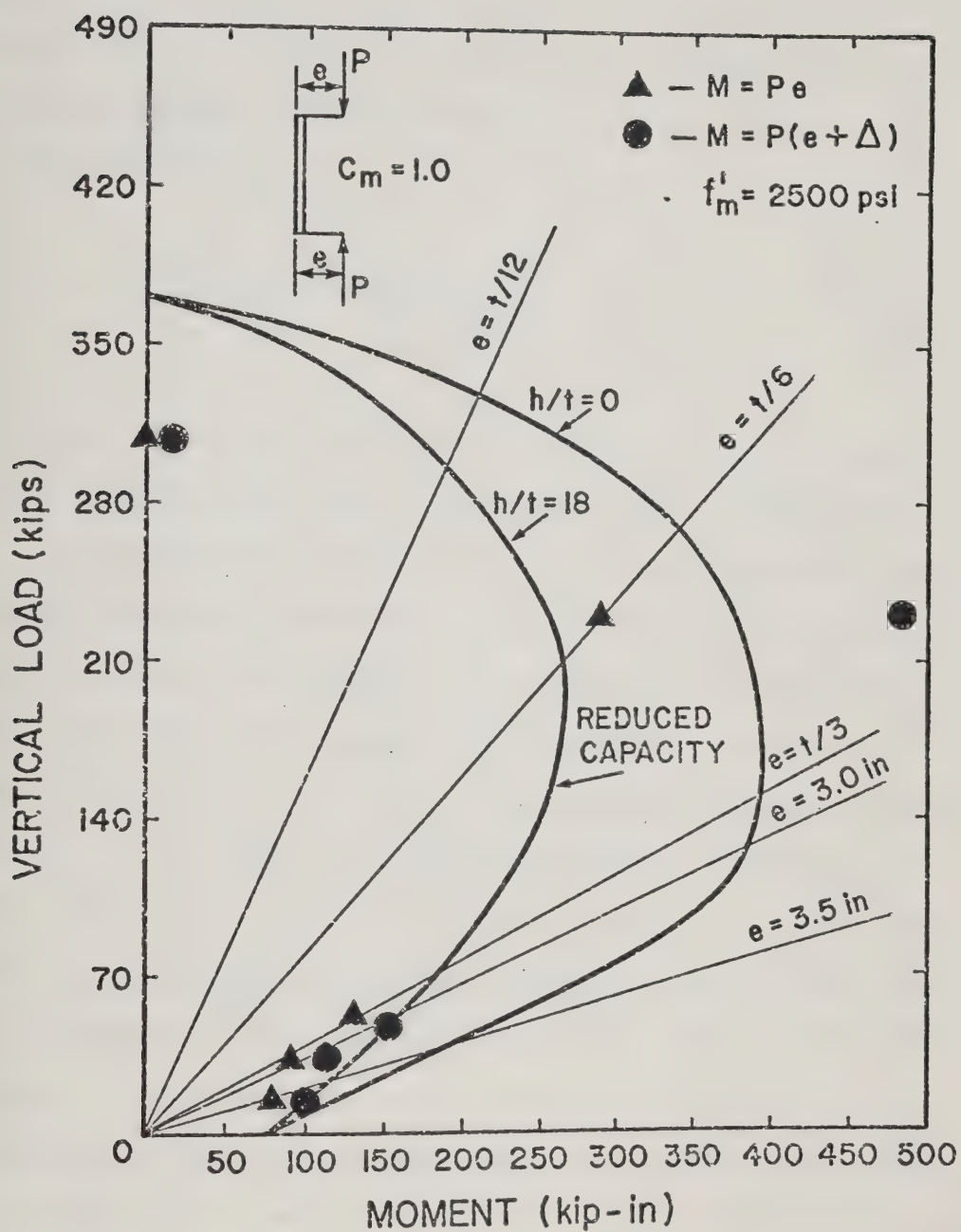


FIG. 8.4 Interaction Diagram Modified for Slenderness
for a Cross-Section Reinforced with 3-#3 Bars

From Figure 8.4, for $e = t/12$ the section capacity is $P = 328$ kips and $M = 207$ kip-in. Using Equation 8.1, the reduced capacity is found to be 237 kips. However at this vertical load level the moment capacity is 362 kip-in. Reducing the vertical load to 300 kips the magnified moment from Equation 8.1 for the same eccentricity is

$$M_f = 0.635 \times 300 \left[\frac{1}{1 - \frac{300}{874}} \right] = 390 \text{ kip-in.}$$

At this load level the section moment capacity is close to this value indicating that there is no need to repeat the iteration.

Repeating the procedure for $e = t/6$ and evaluating ζ and P_{cr} as for plain walls, the reduced capacity is found to be 210 kips. The interaction diagram modified for slenderness is plotted in Figure 8.4 where the results for Test Series I are also plotted. The reduced capacity for walls reinforced with 3-#9 bars is shown in Figure 8.5 for slenderness ratios corresponding to those used in test Series B, C, D and L. From Figure 8.4 and 8.5 it can be seen that the method gives satisfactory results although for axial loads the experimental data do not compare favorably with the theoretical values. As the slenderness ratio increases the critical load decreases and Figure 8.5, indicates that for a wall with h/t ratio of 24 the critical load is less than the strength of the cross-section. The calculated axial load capacity is larger than the experimental value due to the change in failure mode when moment is introduced and inefficient development of vertical steel reinforcement. The reasons for this discrepancy have been discussed in previous chapters.

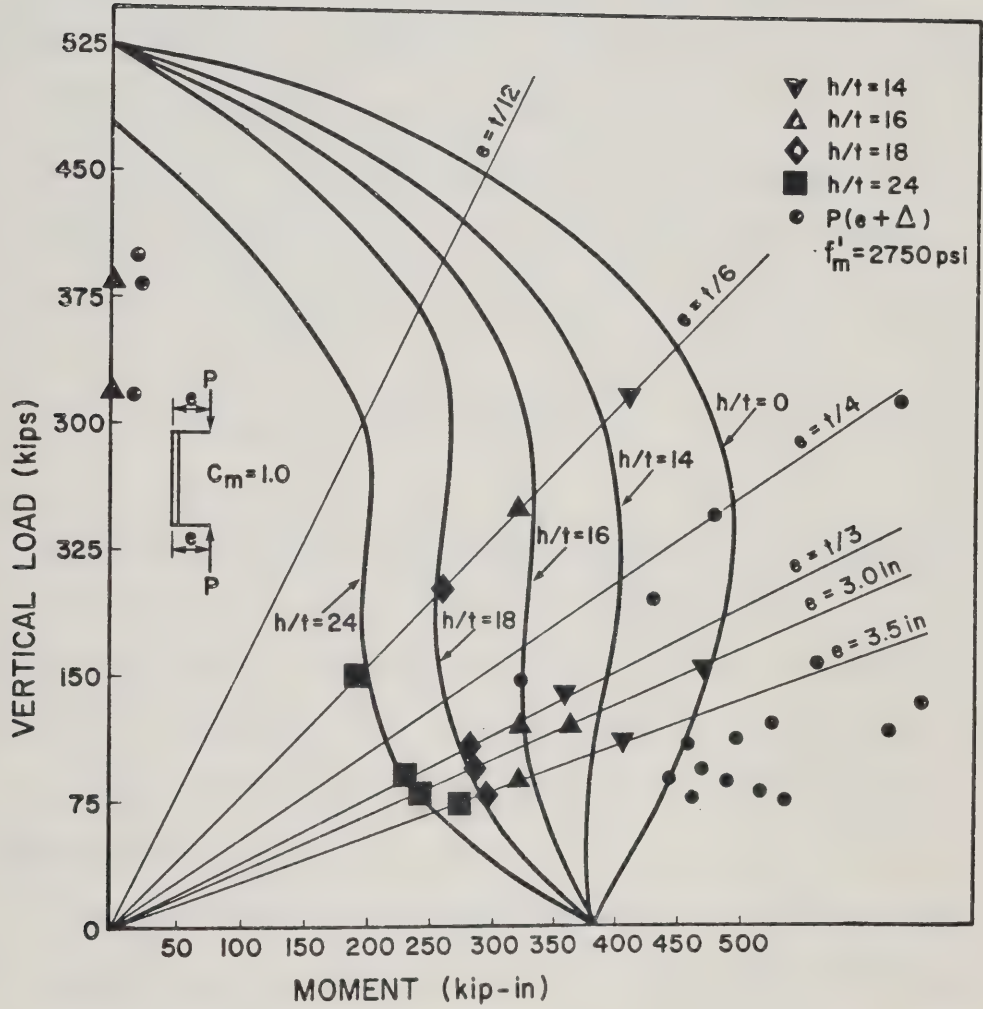


FIG. 8.5 Interaction Diagram Modified for Slenderness for a Cross-Section Reinforced with 3-#9 Bars

8.5.2 Double Curvature Bending, Equal End Eccentricities

Application of the magnifier method to vertically reinforced walls with double curvature end moments is similar to that for plain walls. In evaluating the critical load Table 4.1 is used and the limiting moment of inertia is calculated using Equation 8.6. The strength interaction for walls with 3-#3 bars in double curvature is the same as for single curvature (Figure 8.4).

Using Equation 8.1 with C_m equal to 0.4 it can be shown that for h/t ratios of 18 [Test Series J1 - J5] maximum moment occurs at the ends for all eccentricities. For Wall J1

$$e_{\text{top}} = e_{\text{bottom}} = t/6 = 1.27 \text{ in.}$$

From the short wall interaction diagram of Figure 8.4, $P = 265$ kips and $M = 336$ kip-in. The moment of inertia calculated using Equation 8.6 is 709 in.^3 . With $\alpha = 0.5$ and $\beta = 0.48$, $\lambda = 6.488$ from Table 4.1. Therefore $P_{cr} = 6.488 \times 1.125 \times 10^3 \times 1477/137^2 = 574$ kips. The corresponding magnifier factor is 0.74, indicating that the maximum moment occurs at the ends.

For $e = t/3$ the critical load calculated in a similar manner is 286 kips and the magnifier factor is 0.84, indicating that maximum moment still occurs at the ends. Similar calculations for eccentricities of 3.0 and 3.54 inches yield magnification factors of 0.97 and 0.48. This analysis shows that, for reinforced walls in double curvature with slenderness h/t ratios less than 18, maximum moment occurs at the ends, and that there is no reduction in capacity due to slenderness.

Test data obtained from Series J fall outside the theoretical strength interaction diagram of Figure 8.4. Load deflection curves obtained from the tests reconfirm that maximum moment occurs at the ends in accordance with the previous calculations. The slenderness ratio at which maximum moment will occur along the height of the wall can be easily obtained for any eccentricity. Consider for example the case of equal and opposite eccentricities of $t/6$. The magnification factor will be equal to unity for $P_{cr} = 411$ kips. If all conditions are the same as for Wall J1, the wall must be 156 inches long, or the slenderness ratio must be 20.5.

CHAPTER IX

Summary, Conclusions and Recommendations

9.1 Summary

This investigation was devoted to the study of the behavior of masonry walls under combined vertical load and bending, and factors affecting their strength. The experimental phase of the study consisted of tests of small specimens to determine physical and material properties, types of construction and reinforcement, and tests of full scale specimens to evaluate the effects of slenderness, grouting procedures and types of loading. The analytical phase of the study included prediction of strength and material properties, evaluation of buckling loads and application of theoretical considerations to the experimental data.

9.2 Conclusions

- 1) The behavior of masonry is a function of the individual materials involved, the type of construction and the loading conditions.
- 2) The physical properties of masonry can be approximated from the properties of the materials involved. However, experimental investigation is essential in order to account for factors, such as variation in thickness, vertical joints, mortar penetration, etc.

- 3) The evaluation of strength of individual units is affected by the testing procedure, end conditions and the shape of the unit.
- 4) The tensile and shear bond strength of masonry can be satisfactorily evaluated using the centrifugal testing system developed in this study.
- 5) Strength evaluation based on prism testing is not always representative of actual field conditions. Fully bedded two block - one mortar joint prisms fail at substantially higher loads than similar prisms with face-shell bedding only. However, walls constructed in running bond have the same ultimate capacity as fully bedded ones. Because of web misalignment the bearing area is the same in both cases. A five block prism is more representative of the strength of masonry assemblages.
- 6) Axially loaded masonry fails in a splitting mode caused by differences in the physical properties of the materials involved, such as Poisson's ratio and modulus of elasticity.
- 7) With the addition of moment the failure mode of masonry changes from splitting to crushing.
- 8) Joint reinforcement creates stress concentrations which reduce the axial capacity of masonry. These stress concentrations result from the large difference between the elastic modulus of steel and that of mortar. The mortar directly above and below the joint reinforcement fails before the capacity of the section is reached, causing an increase in volume which, as a result, increases the splitting force.

- 9) Grouting of hollow masonry should be carried out in one lift. This will eliminate the creation of voids in the hardened grout by revibrating after initial setting. Also by grouting in more than one lift, particles sitting on mortar and block protrusions reduce the cavity and create air pockets in the grouted core.
- 10) The bond between grout and masonry units can be satisfactorily evaluated using the centrifugal testing system developed in this study.
- 11) The contribution of grout in carrying vertical load is not directly additive to the capacity of the masonry because of possible splitting failure before the grout strength is completely developed. The effective grouted area is less than the smaller block cavity due to mortar penetration into the core.
- 12) Vertical reinforcement is not fully developed in resisting axial loads in reinforced masonry. The efficiency of vertical reinforcement decreases with increasing bar size.
- 13) The modulus of elasticity of masonry can be approximated if the moduli of the mortar and masonry units are known. However, experimental evaluation of the modulus of elasticity for hollow block masonry is more reliable than theoretical evaluation because of variation in block thickness and type of construction.
- 14) Vertically reinforced walls under combined vertical load and moment behave in a manner similar to reinforced concrete walls.

- 15) Plain walls under axial load fail by splitting of the flanges and webs of the individual masonry units. Failures are complete and with little or no warning. The vertical failure load at which failure occurs can be predicted by theoretical considerations provided that the strength and properties of the material involved are accurately evaluated.
- 16) Plain walls in single curvature bending fail when the compressive strength of the units is reached on the compression side. Failures of plain walls under combined loading are complete with very little or no warning prior to failure, especially for large eccentricities of loading.
- 17) Plain walls loaded in double curvature have a tendency to fail in their first buckling mode. Failures of such walls are explosive but the capacity of such walls is substantially increased as compared to walls loaded in single curvature. Splitting failures occur for small eccentricities and compressive failures occur for eccentricities larger than $t/6$.
- 18) The effect of slenderness on the capacity of masonry walls can be evaluated using the moment magnifier method. The critical load to be used in such an evaluation must account for:
 - a) the effect of loading conditions,
 - b) tensile bond strength,
 - c) type of construction (reinforced or plain).

Application of the moment magnifier method to concrete block masonry gives satisfactory results when the buckling

loads are evaluated using the procedures developed in this study.

9.3 Recommendations

- 1) It is recommended that the modulus of elasticity allowed by CSA Standard S-304 M be reduced to $750 f'_m$ for concrete block masonry and that a research project be undertaken to evaluate elastic modulus for other forms of masonry.
- 2) It is recommended that the function of horizontal joint reinforcement be re-examined. The liberal distribution of total reinforcement between the horizontal and vertical directions allowed by the CSA Standard S-304 M, should be investigated. It is recommended that a research project be carried out to thoroughly investigate the effect of joint reinforcement in load bearing masonry, with emphasis on pilasters, and masonry columns.
- 3) It is recommended that the reductions for slenderness and eccentricities given by CSA-S-304-M be re-evaluated using the procedures developed in this study.
- 4) As flexural rigidity and axial rigidity are of great importance in the analysis and design of masonry structures, it is recommended that research be carried out to evaluate these important parameters for commonly used masonry units and types of construction.

REFERENCES

1. Angervo: "Über Knickung and Tragfähigkeit eins exzentrisch gedrückten Pfeilers ohne Zugfestigkeit" [On the buckling and bearing capacity of an eccentrically compressed pillar with no tensile strength] Staatliche Technische Forschungsunstalt, Finnland, Publication 26, Helsinki, 1954.
2. Chapman, J.C., and Slatford, J.: "The elastic buckling of brittle columns". Paper No. 6147, Proceedings of the Institution of Civil Engineers, London, Vol. 6, pp. 107-125, January, 1957.
3. Hilsdorf, H.K.: "Investigation into the failure mechanism of brick masonry loaded in axial compression". International Conference on Masonry Structural Systems, University of Texas, Austin, 1967.
4. Francis, A.J., Horman, C.B. and Jerrems, L.E.: "The effect of joint thickness and other factors on the compressive strength of brickwork". Proceedings of the 2nd International Brick Masonry Conference, Stoke-on-Trent, April, 1970.
5. Hendry, A.W. and Khoo, C.L.: "Strength tests on brick and mortar under complex stresses for the development of a failure criterium for brickwork in compression". Proceedings of the British Ceramic Society, No. 21, April, 1973, p. 51.
6. Hendry, A.W. and Hassan, S.S.: "The effect of slenderness and eccentricity on the compressive strength of walls". 4th International Brick Masonry Conference, Brugge, April, 1976.
7. Fattal, S.G. and Cattaneo, L.E.: "Structural performance of masonry walls under compression and flexure". U.S. Department of Commerce, June, 1976.
8. Yokel, F.Y. and Mathey, R.G. and Dikkers, R.D.: "Compressive strength of slender concrete masonry walls". National Bureau of Standards, Building Science Series 33, December, 1970.
9. Shahlin, S.: "Structural masonry". Englewood Cliffs, N.J., Prentice Hall, 1971.
10. Smith, B.S. and Rahman, K.M.K.: "The variations of stress in vertically loaded brickwork walls". Proceedings of the Institution of Civil Engineers, Vol. 51, pp. 689-700, April, 1972.

11. Yokel, F.Y. and Dikkers, R.D.: "Strength of load bearing masonry walls". Journal of the Structural Division, Proceedings of the American Society of Civil Engineers, pp. 1593-1609, May, 1971.
12. Drysdale, R.G., Sallam, Saad, E.A. and Karaluk, E.: "Design of masonry walls and columns for combined axial load and bending moment". Proceedings First Canadian Masonry Symposium, E.L. Jessop, M.A. Ward, Editors, The University of Calgary, June, 1976.
13. CSA Standard S304 , Masonry design and construction for buildings. Canadian Standards Association, Ontario, Canada, May 1977.
14. Cranston, W.B. and Roberts, J.J.: "The structural behavior of concrete masonry-reinforced and unreinforced". The Structural Engineer, No. 11, Volume 54, November, 1976.
15. Yorkdale, A.H. and Allen, M.H.: "Compressive strength of brick walls with load eccentricities greater than one-third". Research report number 18, Brick Institute of America, February, 1973.
16. Turkstra, C.J.: "The capacity of masonry walls under eccentric vertical loads". Structural Mechanics Series No. 71-3. Department of Civil Engineering and Applied Mechanics, McGill University, Montreal, August, 1971.
17. Polyakov, S.V.: "Masonry in frame buildings", Gosudatst Vennoe Izdatel Stro Literature Po Stractel stru i Arkhitekture". Moscow, 1956. [translated by Building Research Station and Published by National Lending Library for Science and Technology, Boston, Spa. England].
18. Pearson, J.C.: "Measurement of bond between bricks and mortar". Proceedings, American Society for Testing Materials, 43, 1963.
19. Kampf, L.: "Factors affecting bond between bricks and mortar". Symposium of masonry testing, ASTM, S.T.P. 320, Feb. 1963.
20. Murthy, C.K. and Hendry, A.W.: "Preliminary investigation of the shear strength of one-sixth scale model brickwork". Technical Note No. 65, British Ceramic Research Association, Feb., 1965.
21. Sinha, B.P. and Hendry, A.W.: "Further investigation of bond tension, bond shear and the effect of precompression on the shear strength of model brick masonry couplets". British Ceramic Research Association, Technical Note No. 80, 1966.

22. Hatzinikolas, M.: "Shear behaviour of masonry walls subdivided by floor slabs". M.Sc. Thesis, University of Manitoba, Winnipeg, October, 1975.
23. "Uniform building code", 1973. Edition published by the International Conference of Building Officials, Whittier, California, 1973.
24. CP111, Part 2: 1970 Structural recommendations for load bearing walls, Published by British Standards, London.
25. Macchi, G.: "Safety considerations for a limit-state design of brick masonry". SIBMAC Proceedings, Proceedings of the Second International Brick Masonry Conference held in Stoke-on-Trent, England, April, 1970.
26. Yokel, F.Y.: "Stability and load capacity of members with no tensile strength". Journal of the Structural Division, Proceedings of the American Society of Civil Engineers, July, 1971.
27. MacGregor, J.G., Oelhafen, V.H. and Hage, S.: A re-examination of the EI value for slender columns". Draft Paper for ACI Column Symposium, Ottawa, Canada, 1974.
28. McGuire, W.: "Steel structures". Prentice-Hall International Series, 1968.
29. MacGregor, J.G., Breen, J.E. and Pfrang, E.O.: "Design of slender concrete columns". Journal American Concrete Inst. 57, (1), 6, 1970.
30. Galambos, T.V.: "Structural members and frames". Prentice-Hall International Series in Theoretical and Applied Mechanics, Prentice-Hall, Inc., Englewood Cliffs, New Jersey, U.S.A., 1968.
31. "American Concrete Institute Building Code Requirements, ACI 318-71". American Concrete Institute, Detroit, Michigan, U.S.A.
32. MacGregor, J.G. and Mathews, G.: "The second-order analysis and design of reinforced concrete frames". Structural Engineering Report #60, Civil Engineering Department, the University of Alberta.
33. "Mortar and grout for unit masonry". CSA Standard A179M-1976.
34. "Portland Cements". CSA Standard A5-1961.
35. "Hydrated lime for masonry purposes". CSA Standard - A82.43-1950.
36. "Aggregate for masonry mortar". CSA Standard A82.56M-1970.

37. "Methods of test for concrete". CSA Standard A23.2-1973.
38. "Aggregates for masonry grout". ASTM Standard-C595-74.
39. Richart, F.E., Brandtzaeg, A. and Brown, R.L.: "A study of the failure of concrete under combined compressive stresses". University of Illinois, Engineering Experimental Station Bulletin No. 185, 1928, 104 pp.
40. Lekhniskii, S.G.: "Anisotropic plates". Translated for the second edition by Tsai, S.W. and Cheron, T., Gordon and Breach Science Publishers, New York, London, Paris.
41. Yokel, F.Y., Mathey, R.G., Dikkers, R.D.: "Compressive strength of slender concrete masonry walls". National Bureau of Standards (U.S.) Bldg. Science Series, pp. 32-33, 1970.
42. Larson, L.E.: "Bearing capacity of plain and reinforced concrete walls". Docktorsavhandlingar vid Chalmers Tekniska Hogskolu, No. 19, Goteborg, 1950.
43. Benjamin, J.R. and Williams, H.A.: "The behaviour of one-storey brick shear walls". Proceedings ASCE, Journal of Structural Division, V84, No. ST4, 1958.
44. Hognestad, E.: "A study of combined bending and axial load in reinforced concrete members". University of Illinois, Engineering Experimental Station, Bulletin Series No. 399, November 1951, 128 pp.

APPENDIX A

Solution of the Differential Equations for Wall Without Tensile Strength

It was shown in Chapter IV, Section 4.4 that:

$$\frac{d^2y}{dx^2} = \frac{k}{(u_0 + y)^2} \dots\dots\dots A.1$$

where

$$k = \frac{2P}{9Eb}$$

The boundary conditions of the differential Equation A.1

$$\text{at } x = 0 \quad y = 0 \quad \text{and} \quad \frac{dy}{dx} = 0$$

$$\text{at } x = \frac{h}{2} \quad y = u_1 - u_0$$

with this condition the solution of the covering differential equation can be expressed in terms of u_1 , where $u_1 = (t/2 - e)$.

Equation A.1 can be written as:

$$2 \frac{dy}{dx} \frac{d^2y}{dx^2} = \frac{2k}{(u_0 + y)^2} \frac{dy}{dx} = \frac{d}{dx} \left(\frac{dy}{dx} \right)^2$$

$$\left(\frac{dy}{dx} \right)^2 = 2k \int \frac{dy}{(u_0 + y)^2} = -2k \frac{1}{(u_0 + y)} + C_0$$

$$\text{at } y = 0 \quad \frac{dy}{dx} = 0 \quad \text{and} \quad C_0 = \frac{2k}{u_0}$$

$$\left(\frac{dy}{dx} \right)^2 = 2k \left(\frac{1}{u_0} - \frac{1}{u_0 + y} \right) = \frac{2k}{u_0} \left(\frac{y}{u_0 + y} \right)$$

$$\frac{dy}{dx} = \pm \sqrt{\frac{2k}{u_0}} \left(\frac{y}{u_0 + y} \right)^{1/2}$$

$$x = \pm \frac{1}{k_1} \left[\sqrt{y(u_0 + y)} + u_0 \ln \frac{\sqrt{y} + \sqrt{u_0 + y}}{\sqrt{u_0}} \right]$$

Since

$$k_1 = \frac{2}{3} \sqrt{\frac{P}{Ebu_0}}$$

$$x = \pm \frac{3}{2} \sqrt{\frac{Ebu_0}{P}} \left[\sqrt{y(u_0 + y)} + u_0 \ln \left(\frac{\sqrt{y} + \sqrt{u_0 + y}}{\sqrt{u_0}} \right) \right]$$

at

$$x = \frac{h}{2} \quad y = u_1 - u_0$$

$$\frac{h}{2} = \pm \frac{3}{2} \sqrt{\frac{Ebu_0}{P}} \left[\sqrt{u_1(u_1 - u_0)} + u_0 \ln \left(\sqrt{\frac{u_1 - u_0}{u_0}} + \sqrt{\frac{u_1}{u_0}} \right) \right]$$

Solving for P:

$$P = \frac{9Ebu_0}{h^2} \left[\sqrt{u_1(u_1 - u_0)} + u_0 \ln \left(\sqrt{\frac{u_1 - u_0}{u_0}} + \sqrt{\frac{u_1}{u_0}} \right) \right]^2$$

Substituting $\alpha = \frac{u_0}{u_1}$

$$P = \frac{9Ebu_1^3}{h^2} \alpha \left[\sqrt{1 - \alpha} + \alpha \ln \left[\sqrt{\frac{1 - \alpha}{\alpha}} + \sqrt{\frac{1}{2}} \right] \right]^2$$

Let

$$\frac{9Ebu_1^3}{4h^2} = P_{\text{equiv}} = \text{equivalent critical load} = P_{\text{ec}}$$

Let

$$K_1 = \sqrt{\frac{2k}{u_0}} = \frac{2}{3} \sqrt{\frac{P}{Ebu_0}}$$

then

$$\frac{dy}{dx} = \pm k_1 \left(\frac{y}{u_0 + y} \right)^{1/2}$$

and

$$dx = \pm \frac{1}{k_1} \left(\frac{u_0 + y}{y} \right)^{1/2} dy$$

$$x = \pm \frac{1}{k_1} \int \left(\frac{u_0 + y}{y} \right)^{1/2} dy \dots$$

$$\int \left(\frac{u_0 + y}{y} \right)^{1/2} dy = \sqrt{y(u_0 + y)} + \frac{u_0}{2} \int \frac{dy}{\sqrt{y(u_0 + y)}} =$$

$$= \sqrt{y(u_0 + y)} + u_0 \ln \sqrt{y} + \sqrt{u_0 + y} \dots$$

Therefore

$$x = \pm \frac{1}{k_1} \left[\sqrt{y(u_0 + y)} + u_0 \ln \left(\sqrt{y} + \sqrt{u_0 + y} \right) \right] + C_1$$

at

$$x = 0 \quad y = 0$$

for positive x

$$C_1 = -\frac{u_0}{k_1} \ln \sqrt{u_0}$$

Then

$$\frac{P}{P_{ec}} = 0.040528\alpha \left[\sqrt{1-\alpha} + \alpha \ln \left[\sqrt{\frac{1-\alpha}{\alpha}} + \sqrt{\frac{1}{\alpha}} \right] \right]^2$$

A plot of P/P_{ec} versus $\alpha = u_0/u_1$ is shown in Figure A.1. From this figure instability occurs when

$$P_{cr} = 0.285 P_{ec}$$

or

$$P_{cr} = 0.285 \frac{9}{4} \pi^2 E b u_1^3 \times \frac{1}{L^2} =$$

or

$$= 0.64125 \pi^2 E b u_1^3 / L^2$$

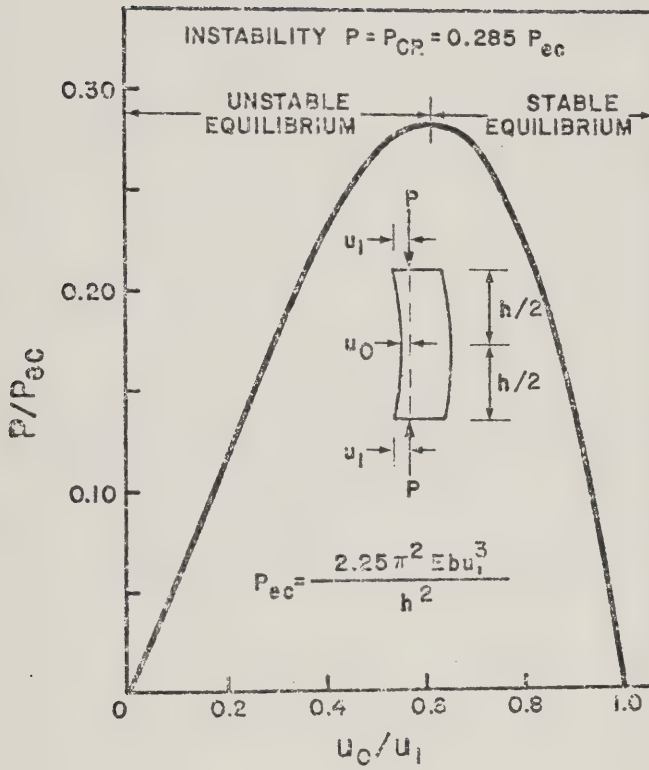


FIG. A-1 Instability Failure of Column Without Tensile Strength

APPENDIX B

Evaluation of Interpolating Functions and
Computer Program for Evaluating the
Buckling Load for Stepped Columns

Since deflections are zero at both ends ϕ_1 and ϕ_4 are zero. The remaining four functions are shown schematically in Figure B.1. The boundary conditions to be satisfied by these functions ($\phi_2, \phi_3, \phi_5, \phi_6$) are as follows:

η	y	y'	y''	Functions
0	0	1	0	ϕ_2
1	0	0	0	
0	0	0	1	ϕ_3
1	0	0	0	
0	0	0	0	ϕ_5
1	0	1	0	
0	0	0	0	ϕ_6
1	0	0	1	

The functions which satisfy these conditions are:

$$\phi_2 = -3\eta^5 + 8\eta^4 - 6\eta^3 + \eta$$

$$\phi_3 = -1/2 (\eta^5 - 3\eta^4 + 3\eta^3 - \eta^2)$$

$$\phi_5 = -3\eta^5 + 7\eta^4 - 4\eta^3$$

$$\phi_6 = 1/2 (\eta^5 - 2\eta^4 + \eta^3)$$

Differentiating these functions once yields

$$[\Phi'] = \begin{bmatrix} \phi_2' & \phi_2' & \phi_2' & \phi_3' & \phi_2' & \phi_5' & \phi_2' & \phi_6' \\ & & \phi_3' & \phi_3' & \phi_3' & \phi_5' & \phi_3' & \phi_6' \\ \text{symmetric} & & & \phi_5' & \phi_5' & \phi_5' & \phi_6' & \\ & & & & & \phi_6' & \phi_6' & \end{bmatrix}$$

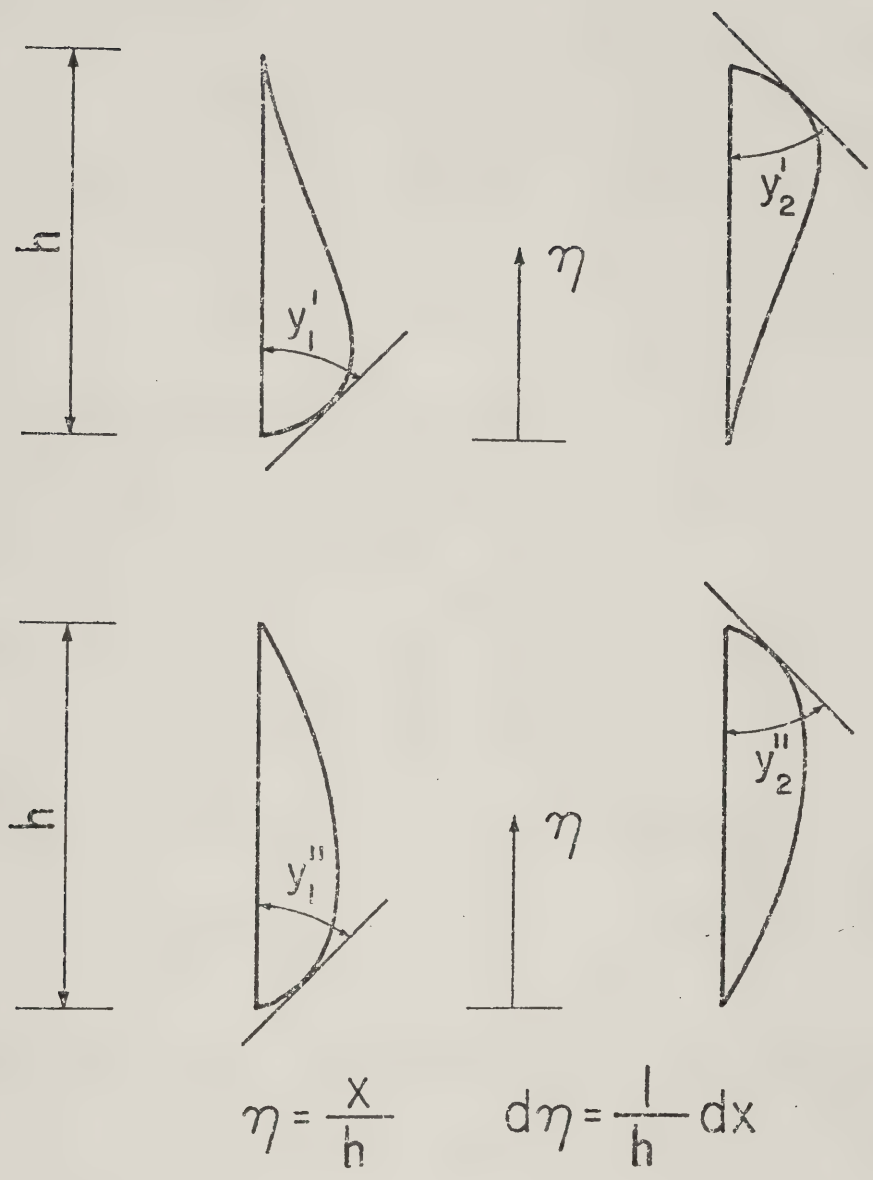


FIG. B-1 Interpolating Functions

Substitution of the functions and integration of the above matrix from 0 to 1 results in

$$\int_0^1 [\Phi'] dn = \begin{bmatrix} 0.22857 & 0.016666 & -0.014285 & 0.004762 \\ & 0.0015873 & -0.004762 & 0.000793 \\ \text{symmetric} & & 0.228571 & -0.016667 \\ & & & 0.001587 \end{bmatrix} = [K_g]$$

where $[K_g]$ is the geometric stiffness matrix.

The interpolating functions are then differentiated twice and the matrix $[\Phi'']$ is obtained as:

$$[\Phi''] = \begin{bmatrix} \phi_2'' & \phi_2'' & \phi_2'' & \phi_3'' & \phi_2'' & \phi_5'' & \phi_2'' & \phi_6'' \\ & & \phi_3'' & \phi_3'' & \phi_3'' & \phi_5'' & \phi_3'' & \phi_6'' \\ \text{symmetric} & & & \phi_5'' & \phi_5'' & \phi_5'' & \phi_6'' \\ & & & & & \phi_6'' & \phi_6'' \end{bmatrix}$$

After substitution of the corresponding functions, integrating this matrix and evaluating $[\Phi'']_0^\alpha + C[\Phi'']_\alpha^1$, the bending stiffness matrix, $[K]$, is obtained.

For the case of a column with constant EI_1 ($\alpha = 0$) this matrix is

$$[K] = \begin{bmatrix} 5.4857 & 0.3143 & +3.0857 & -0.11428 \\ & 0.0857 & 0.1143 & 0.01428 \\ & & 5.4857 & -0.31428 \\ & & & 0.00857 \end{bmatrix}$$

Solving the relation

$$[K] \{\theta\} = P_{cr} \frac{h^2}{EI_0} [K_g] \{\theta\}$$

for

$$\frac{h^2}{EI_0} = 1$$

and the geometric and bending stiffness matrices, $[K_g]$ and $[K]$ as evaluated above, using the power sweep method, $P_{cr} = 9.8734354$ which compares very closely with the exact value of π^2 . Table B.1 is obtained by evaluating $[K]$ and solving relations for various values of α and β from 0.0 to 1. All mathematical operations involving interpolating functions and the solution of the buckling problem were carried out using a computer program. This program with a sample input and output is given in the following pages. The input data consists of the coefficients of the interpolating function.


```

C      This is a program that solves for critical
C      buckling load.

      IMPLICIT REAL*8 (A-H,O-Z)
      DIMENSION PPFI(4,4),PFI(4,4),C(4,6),AA(100),BPPFI(4,4)
*,PCRIT(20,21)
      REAL VAL(21)
C      Initialize values to evaluate the root
      IA=100
      AA(1)=0.1D0
      DO 1 I=2,100
1      AA(I)=AA(I-1)+0.1D0
C      Initialize the values of alpha and beta to be used.
      VAL(1)=0.0
      N=4
C      Initailize the number of coefficients
C      in the poynomial.
      N1=6
C      Initialize the number of polynomials.
      NDF=4
C      Read in the coefficients.
      READ(5,6)((C(I,J),J=1,N1),I=1,NDF)
C      Evaluate the geometric stiffness.
      CALL PHI1(1.,0.,C,PFI,N1,NDF)
C      Calculate the critical load for various values of
C      alpha and beta.
      DO 4 IJ1=2,21
      VAL(IJ1)=VAL(IJ1-1)+0.05
C      Calculate beta - the ratio of the EI's.
      BETA=DFLOAT(IJ1-1)*0.05D0
      DO 3 IJ=1,21
C      Calculate alpha - the ratio of lengths.
      ALPHA=DFLOAT(IJ-1)*0.05D0
C      Integrate polynomials from 0.0 to alpha.
      CALL PHI2(ALPHA,0.0,C,1.0,PPFI,N1,NDF)
C      Integrate polynomials fromm alpha to 1.0.
      CALL PHI2(1.0,ALPHA,C,BETA,BPPFI,N1,NDF)
C      Formulate stiffness matrix.
      DO 2 I=1,4
      DO 2 J=1,4
2      BPPFI(I,J)=BPPFI(I,J)+PPFI(I,J)
C      Solve for critical buckling load, Pcrit.
      CALL STAR(BPPFI,PFI,AA,IA,N,N1,NDF,PCRIT(IJ1-1,IJ))
3      CONTINUE
4      CONTINUE
C      Print table of critical loads.
      WRITE(4,7)
      WRITE(4,8)
      WRITE(4,9)
      WRITE(4,10) VAL
      WRITE(4,9)
      WRITE(4,8)
      WRITE(4,9)

```



```

DO 5 I=2,21
WRITE(4,11) VAL(I),(PCRIT(I-1,J),J=1,21)
5  WRITE(4,9)
   WRITE(4,8)
   STOP
6  FORMAT(6F12.7)
7  FORMAT('1'////////)
8  FORMAT(20X,40('-'))
9  FORMAT(20X,'|',31X,'|')
10 FORMAT(20X,'|',6F5.2,'|')
11 FORMAT(20X,'|',F5.2,'|',6F5.2,'|')
END

```

```

SUBROUTINE STAR(SB,SG,AA,IA,N,N1,NDF,A3)

```

```

IMPLICIT REAL*8 (A-H,O-Z)
DIMENSION AA(100),SB(4,4),SG(4,4),SBG(4,4),B(4)
DIMENSION IC(4)
DO 1 I=1,IA
II=I
A1=AA(I)
A2=AA(I+1)
IF(A1.EQ.A2) GO TO 1
CALL RSFORM(A1,SB,SG,SBG,N)
CALL DELTA(N,SBG,DET1,IC)
IF(DET1.EQ.0) GO TO 5
CALL RSFORM(A2,SB,SG,SBG,N)
CALL DELTA(N,SBG,DET2,IC)
IF(DET2) 2,6,1
1  CONTINUE
2  A3=(A2*DET1-A1*DET2)/(DET1-DET2)
   CALL RSFORM(A3,SB,SG,SBG,N)
   CALL DELTA(N,SBG,DET3,IC)
   D1=DABS(A3-A2)
   D2=DABS(A3-A1)
   IF(D1.LT.1.0D-4) GO TO 8
   IF(D2.LT.1.0D-4) GO TO 8
   IF(DET3) 3,8,4
3  DET2=DET3
   A2=A3
   GO TO 2
4  DET1=DET3
   A1=A3
   GO TO 2
5  DET3=DET1
   A3=A1
   GO TO 8
6  DET3=DET2
   A3=A2
   GO TO 8
7  WRITE(6,9)
   STOP
8  RETURN
9  FORMAT(' SECTION DID NOT BOCKLE')

```


END

SUBROUTINE RSFORM (EA,SB,SG,SBG,N)

```

IMPLICIT REAL*8 (A-H,O-Z)
DIMENSION SB (4,4), SG (4,4), SBG (4,4)
DO 1 I=1,N
DO 1 J=1,N
1 SBG (I,J) = SB (I,J) - EA*SG (I,J)
RETURN
END

```

C DETERMINANT BY PIVOTAL CONDENSATION

SUBROUTINE DELTA(N,A,DETERM,IC)

```

IMPLICIT REAL*8 (A-H,O-Z)
DIMENSION A (N,N), IC (N)
KK=0
K=1
DO 1 I=1,N
1 IC (I) = I
CALL CHANGE (K,A,N,KK,IC)
K=2
L=1
2 DO 3 I=K,N
RATIO=A (I,L) /A (L,L)
DO 3 J=K,N
3 A (I,J) = A (I,J) - A (L,J) *RATIO
DO 4 J=K,N
A (L,J) = A (L,J) /A (L,L)
4 A (J,L) = 0.0
CALL CHANGE (K,A,N,KK,IC)
IF (K-N) 5,6,6
5 L=K
K=K+1
GO TO 2
6 DETERM=1.0D0
DO 7 L=1,N
7 DETERM=DETERM*A (L,L)
DETERM= (-1.0D0) **KK*DETERM
RETURN
END

```

SUBROUTINE THETA (N,A,B)

```

IMPLICIT REAL*4 (A-H,O-Z)
DIMENSION A (4,4), B (4)
B (N) = 1.0D0
N1=N-1
DO 1 I=1,N1
II=N-I
SUM=0.0D0
II1=II+1

```



```

DO 1 J=II1,N
SUM=SUM+A (II,J) *B (J)
1 B (II)=-SUM
RETURN
END

```

SUBROUTINE CHANGE (K,A,N,KK,IC)

```

IMPLICIT REAL*8 (A-H,O-Z)
DIMENSION A (N,N) ,COLREP (4) ,ROWREP (4) ,IC (N)
ACC=DABS (A (K,K) )
IROW=K
JCOL=K
DO 1 I=K,N
DO 1 J=K,N
BCC=DABS (A (I,J) )
IF (ACC.GE.BCC) GO TO 1
ACC=BCC
IROW=I
JCOL=J
1 CONTINUE
IF (JCOL.EQ.K) GO TO 3
KK=KK+1
IIC=IC (K)
IC (K)=IC (JCOL)
IC (JCOL)=IIC
DO 2 I=1,N
COLREP (I)=A (I,K)
A (I,K)=A (I,JCOL)
2 A (I,JCOL)=COLREP (I)
3 CONTINUE
IF (IROW.EQ.K) GO TO 5
KK=KK+1
DO 4 I=1,N
ROWREP (I)=A (K,I)
A (K,I)=A (IROW,I)
4 A (IROW,I)=ROWREP (I)
5 CONTINUE
END

```

SUBROUTINE PHI1 (B,A,C,CC,N1,NDF)

```

IMPLICIT REAL*8 (A-H,O-Z)
DIMENSION HC (6,4) ,C (4,6) ,H (10) ,CC (4,4)
CALL EXPO (B,A,H)
DO 2 I=1,N
DO 2 J=1,NDF
SUM=0.0
DO 1 K=1,N1
II=K+I-3
IF (I.EQ.1.ORK.EQ.1) GO TO 1
SUM=SUM+ (I-1) * (K-1) *H (II) *C (J,K)
1 CONTINUE
1 HC (I,J)=SUM

```



```

2      CONTINUE
      DO 4 I=1,NDF
      DO 4 J=1,NDF
      SUM=0.0
      DO 3 K=1,N1
3      SUM=SUM+C(I,K)*HC(K,J)
      CC(I,J)=SUM
4      CC(J,I)=CC(I,J)
      RETURN
      END

      SUBROUTINE PHI2(B,A,C,BETA,CC,N1,NDF)

      IMPLICIT REAL*8 (A-H,O-Z)
      DIMENSION HC(6,4),C(4,6),H(10),CC(4,4)
      CALL EXPO(B,A,H)
      DO 2 I=3,N
      DO 2 J=1,NDF
      SUM=0.0
      DO 1 K=3,N1
      II=K+I-5
      SUM=SUM+(I-1)*(I-2)*(K-1)*(K-2)*H(II)*C(J,K)
1      CONTINUE
      HC(I,J)=SUM
2      CONTINUE
      DO 4 I=1,NDF
      DO 4 J=1,NDF
      SUM=0.0
      DO 3 K=3,N1
3      SUM=SUM+C(I,K)*HC(K,J)
      CC(I,J)=SUM
4      CC(J,I)=CC(I,J)
      RETURN
      END

```

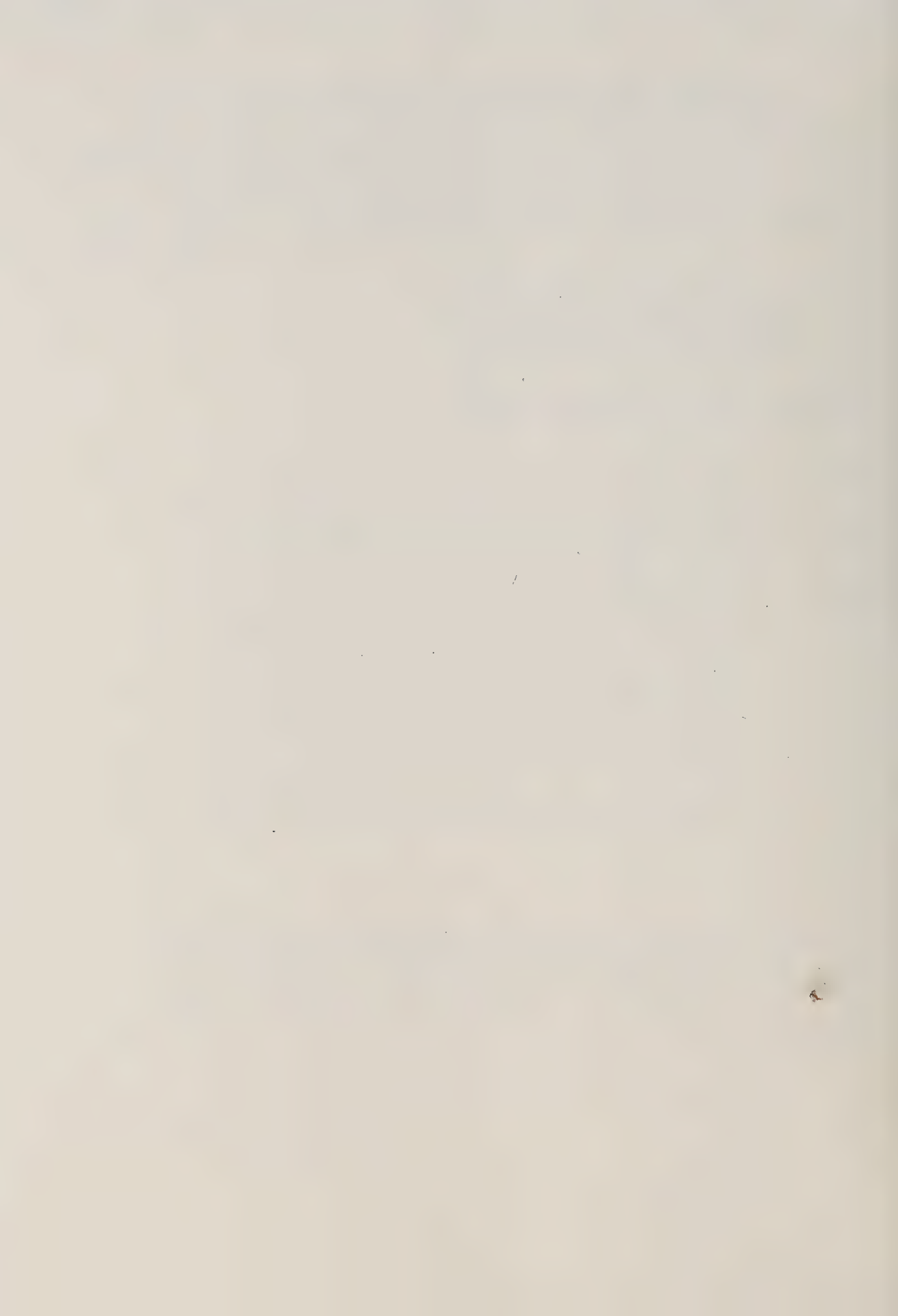

The input data consists of the coefficients of the interpolating function entered in increasing order of power of the parameter eta. The following is an example of a typical set of data for calculating critical buckling loads:

```
0.0,1.0,0.0,-6.0,8.0,-3.0,
0.0,0.0,0.5,-1.5,1.5,-0.5,
0.0,0.0,0.0,-4.0,7.0,-3.0,
0.0,0.0,0.0,0.5,-1.0,0.5,
```

Example output from above data:

$\alpha \backslash \beta$	0.0	0.01	0.02	0.03	0.04	0.05
0.01	0.10	0.10	0.20	0.20	0.09	0.12
0.02	0.20	0.20	0.20	0.10	0.15	0.18
0.03	0.20	0.10	0.30	0.30	0.22	0.25
0.04	0.10	0.10	0.10	0.20	0.30	0.40
0.05	0.10	0.10	0.10	0.10	0.10	0.10

Note that the range of alpha and beta for which the buckling coefficients are evaluated is controlled in the program.



APPENDIX C

The Use of Centrifugal Force for Determining the
Tensile and Shear Bond of Masonry

C.1 Introduction

The bond between the mortar and the masonry unit consists of two major components; the tensile bond and the shear bond. The tensile bond is developed when a tensile load is applied normal to the bonded face and the shear bond is developed when a mortar joint is subjected to a shear load. In this Appendix, a new method of evaluating tensile and shear bond strength is presented. The method makes use of centrifugal force to apply a tensile or a shearing force to the specimen.

C.2 Existing Methods of Testing

A number of different tests are presently employed for evaluating tensile and shear bond strengths. They can be divided into four categories depending on the manner in which the load is applied to the test specimen.

a) Modulus of Rupture

This method utilizes the beam theory to evaluate the stress at the extreme fibres of plain masonry beams loaded at mid-span or third points. A linear stress distribution is assumed.

b) Direct Tension

Specimens consisting of two or three masonry units are placed in tension using end clamps or glued connections.

c) Direct shear

Specimens with 1 of 2 mortar joints are subjected to a pushout test.

d) Combined Test

Single joint specimens are subjected to loads inclined to the axis of the specimen.

Results of a number of experimental programs using the above methods are available in the literature. A number of authors have reported problems encountered in applying these methods. These problems include the following:

- 1) In the modulus of rupture test the stress distribution is not linear as assumed.
- 2) Difficulties exist in aligning and fixing the direction of load in the center of the couplet in the direct tension test.
- 3) The stress distribution resulting from direct shear force applied at the outer face of the specimen is not uniform over the total area of contact.
- 4) In the combined test the same problems occur as in 2 and 3 above.

C.3 Development of Centrifugal Testing Procedure

If a mass is rotated about a fixed axis at a constant angular velocity, it is subjected to a force in the radial direction, known as a centrifugal force. This force is a function of the mass m , the radius of rotation R and the angular velocity ω . If the mass accelerates, an additional component of force, proportional to the acceleration, is introduced in the tangential direction.

If a test specimen is mounted on a rotating disc the magnitude and direction of the force acting on the specimen is dependent on the specimen shape and orientation, the angular velocity and acceleration. By increasing the angular velocity sufficient force may be developed to cause failure of the specimen. A schematic diagram of such an apparatus is shown in Figure C.1.

Consider the case of a tensile bond specimen mounted on a rotating disc and clamped at one end (Figure C-1). The disc is driven by a variable speed motor starting from rest and accelerating with a constant acceleration to an angular velocity, ω . The force acting at any section of the specimen is given by the well known equation:

$$F = m \omega^2 R \quad \dots\dots\dots C.1$$

where

F = centrifugal force

m = mass of section considered

ω = angular velocity

R = distance to the center of mass of the portion of the specimen where the force is calculated.

Assume further that the bonded area is $A = 2.5 \text{ in.} \times 2.5 \text{ in.}$ and that the weight of the separated portion of the test specimen is 4.0 lbs. If the distance to the center of mass is 18.0 in. and the tensile bond, σ_b , is 100 psi then the angular velocity required to break the specimen in direct tension can be calculated. At failure the system rotates at an angular velocity given by:

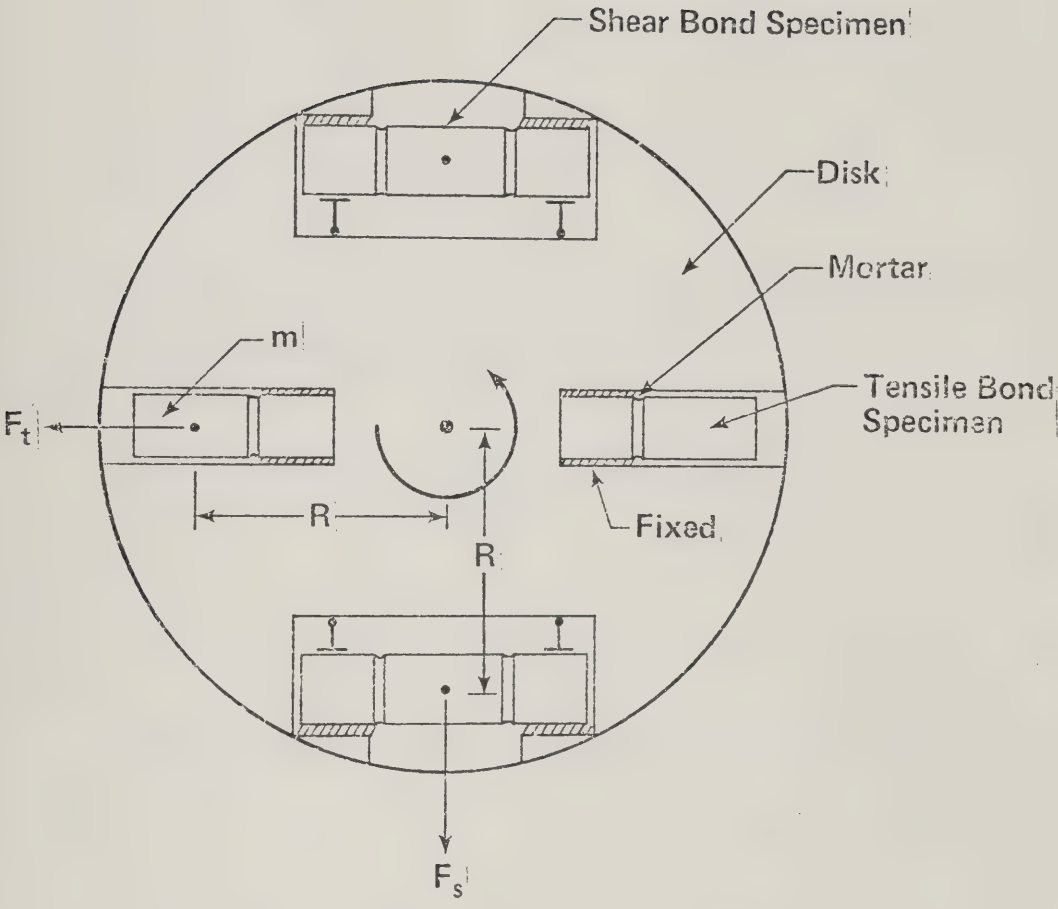


FIG. C-1 Schematic Diagram of
Test Apparatus

$$\omega = \sqrt{\frac{F}{R_m}} = \sqrt{\frac{\sigma_b A}{R_m}} \dots\dots\dots C.2$$

$$\omega = \sqrt{\frac{100 \times 2.5^2 \times 32.2 \times 12}{18 \times 4}} = 58 \text{ radians/sec}^2$$

or

$$58 \times \frac{60}{2\pi} = 553.8 \text{ R.P.M.}$$

If the system accelerates from rest to the speed of 553.8 rpm in 5 minutes, the tangential acceleration a_t will be

$$a_t = \frac{dv}{dt} = \frac{\omega R}{t} = \frac{58 \times 18}{60 \times 5} = 3.48 \text{ in./sec}^2$$

where

t = time required to reach the speed at failure.

The shearing force on the specimen due to this acceleration will be

$$Fv_t = ma_t = \frac{4}{32.3} \times 3.48 = 0.43 \text{ lb.}$$

This force will cause a shearing stress of 0.07 psi which is 0.14% of an assumed mean tensile bond strength of 50 psi. By decreasing the acceleration this shearing stress may be reduced even further if desired. The effects of tangential acceleration therefore may be neglected.

To evaluate the shear bond strength the procedure is the same as for tensile bond, except for the orientation of the specimen on the disc. The placement of the shear specimen is illustrated in Figure C.1

C.4 Limitations

The uniformity of the force distribution on the specimen depends on the shape of the specimen and the distribution of the mass throughout the volume of the body. If the mass is not uniformly distributed, then center of mass and the geometric center will not coincide and as a result moment will develop which will cause a non-uniform stress distribution. This factor is not considered to be significant in masonry units because of the degree of quality control in the manufacturing process.

C.5 Testing

C.5.a Test Equipment

The test apparatus is shown in Plate C.1 and part of it is shown in Plate C.2. In these photographs the compartment for the tensile bond test is shown. The flywheel is driven by an AC/DC motor and the acceleration is controlled by regulating the voltage input. In the compartment for the tensile bond test, bolts attached to a rubber padded steel plate are provided for clamping the test specimen in position. Plate C.2 illustrates the clamping device. The angular velocity of the flywheel is monitored in r.p.m. by an electronic sensor attached to the apparatus. Two compartments for

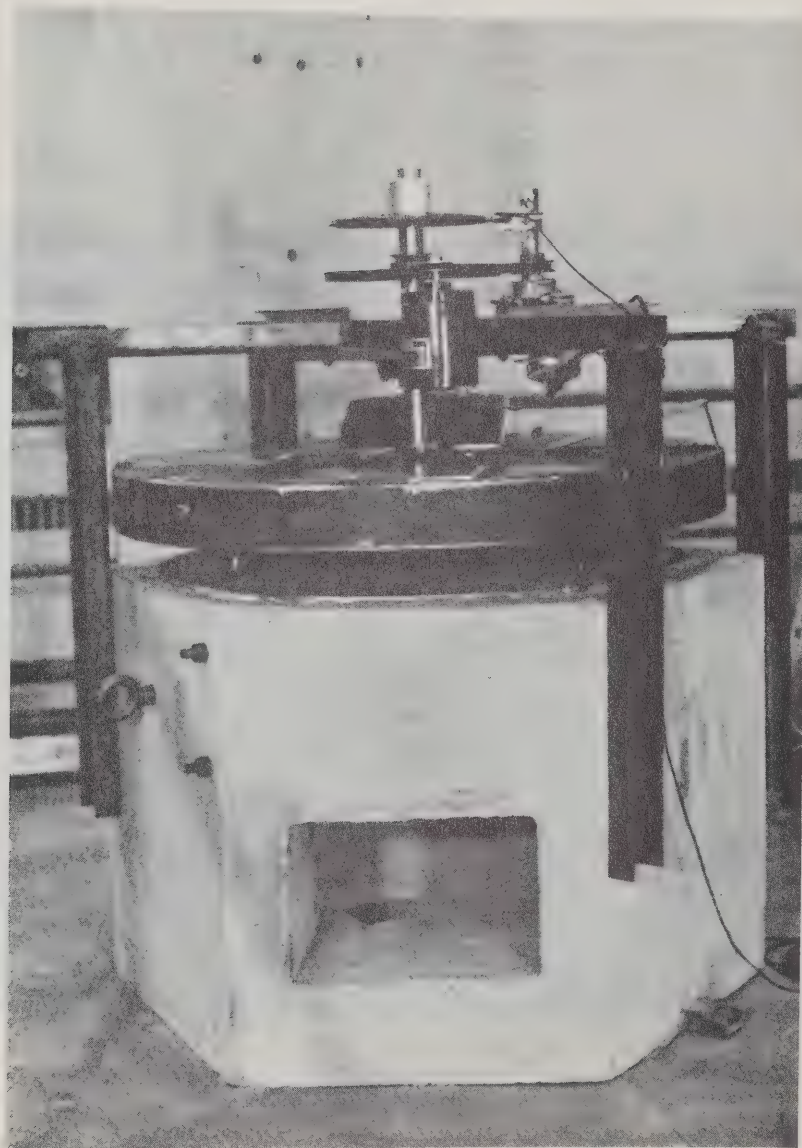


PLATE C.1 View of the Testing Machine

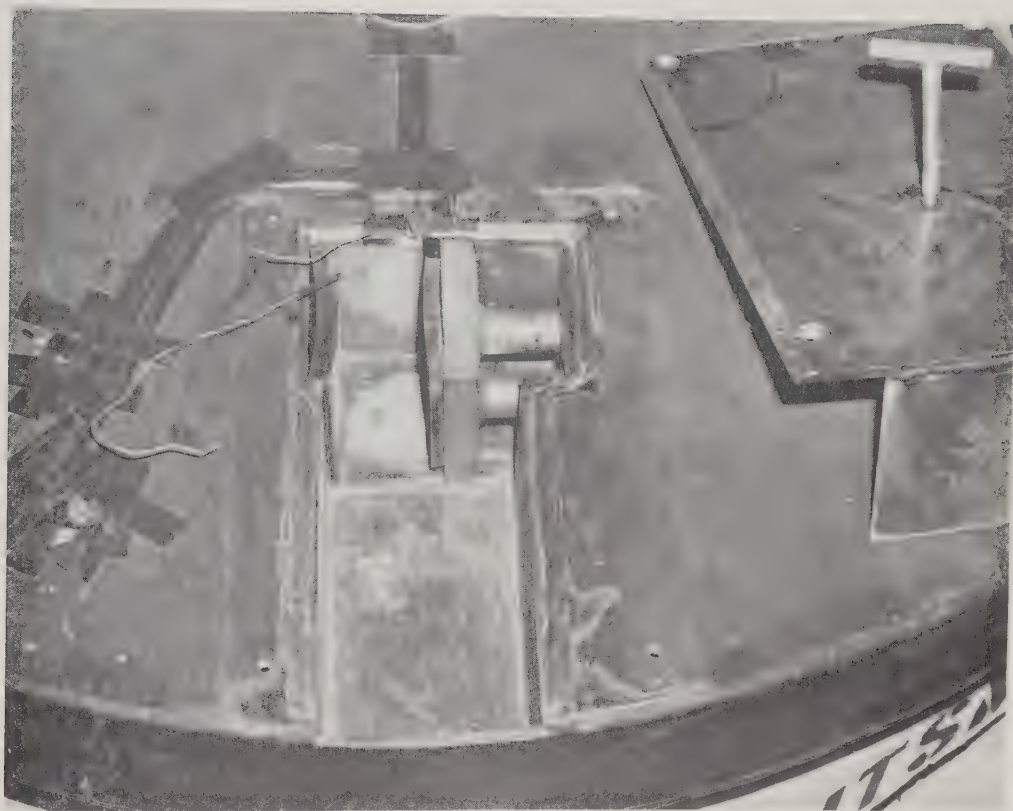


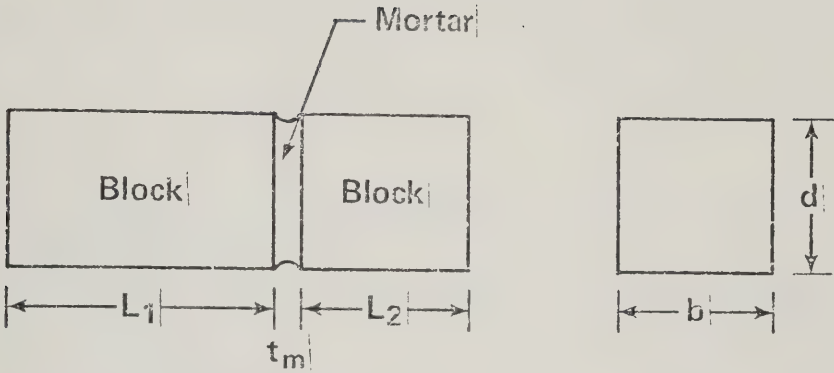
PLATE C.2 Compartment for Tensile Bond Test

tensile bond and two compartments for shear bond strength are provided. Two specimens can be tested simultaneously.

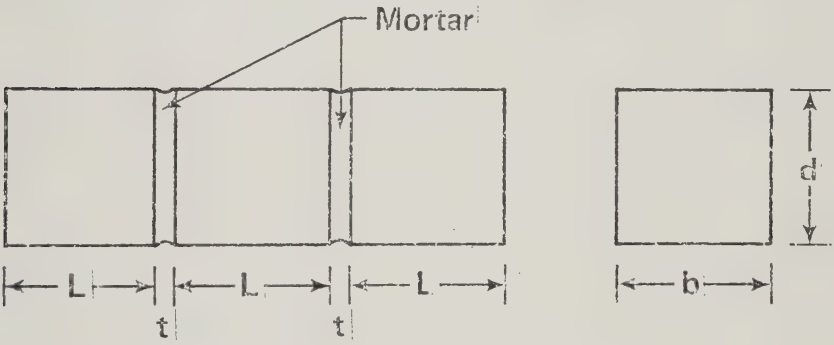
C.5.b Test Specimens

A total of 90 tensile bond specimens were manufactured using 2.5 x 2.5 x 2.5 in. rectangular cubes cut from 4 x 8 x 16 in. solid concrete block. Mortar was placed on the factory produced face and not on the saw-cut face in order to simulate actual field conditions. Fifty specimens were prepared by one mason using standard construction practice and forty were prepared by another mason who was constantly supervised in order to obtain the best workmanship possible. Type S mortar was used in both cases. For the 40 specimens, the mortar was used 90 minutes after mixing in order to observe the effect of retempering. The mortar was mixed by volume using the following proportions: 1 part normal cement, 1/2 part hydrated lime, 4-1/2 parts masonry sand. All specimens were air cured for a minimum of 28 days. 2 x 2 x 2 in. mortar cubes were also prepared for mortar compressive strength tests. Forty-five shear specimens, as shown schematically in Figure C.2, were prepared and cured in a similar manner as the tensile specimens.

In order to determine the variability in test results which might be ascribed to the characteristics of the machine, 18 special specimens were tested. These specimens were prepared by pouring a cube of grout on top of a block section with the same dimensions as in the mortar jointed specimens. As a result of this procedure the effects of workmanship and elapsed time on the quality of the mortar were eliminated. The grout was mixed by volume in



a) Tensile bond specimen



b) Shear bond specimen

FIG. C-2 Test Specimens

accordance to CSA Standard A179 M-1970 and the specimens were rodded 25 times in each of the three layers poured. The compressive strength of the grout was 2380 psi.

These specimens not only provided a check on the variability of the testing procedure, but they also were used to evaluate the bond between grout and concrete block. Test specimens are illustrated in Plates C.3, C.4 and C.5.

C.5.c Test Procedure

The test specimens were placed in the compartment and clamped into position in such a way that the mortar joint and one of the two block parts are air suspended. The clamping force was applied through soft rubber pads which bind into the rough surface of the block. The applied clamping force was small and applied at a distance of 2 cm from the mortar joint in order to avoid possible damage to the bond. The flywheel accelerated from the rest. When failure occurred a circuit breaker caused a signal light to go off. At failure the speed was recorded, and the center of mass of the separated portion of the specimen was calculated to account for the mortar joint which might remain attached to the mixed end of the specimen or to the separated part.

The bonded area was also determined after failure. From these data the tensile bond was calculated using Equation C.1. The shear bond test was carried out by placing the specimen in the shear compartment as shown in Figure C.1. The two end portions of the specimen were supported in such a way as to avoid bending stresses at the mortar joints.

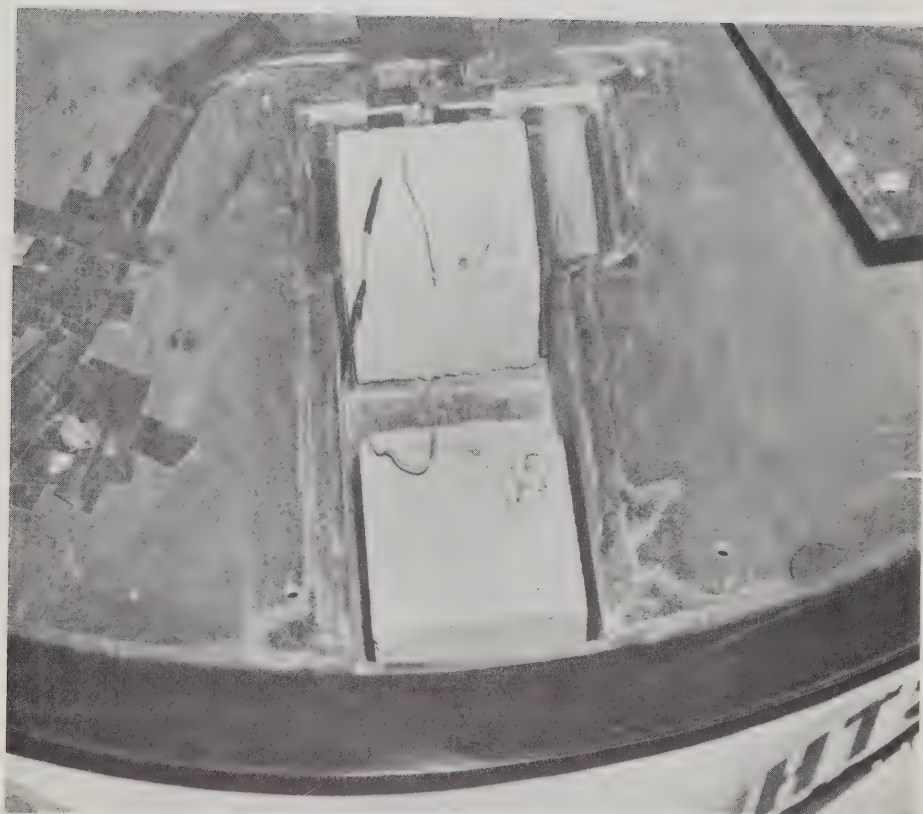


PLATE C.3 Tensile Bond Specimen After Failure



PLATE C.4 Specimen for Tensile Bond Strength Test

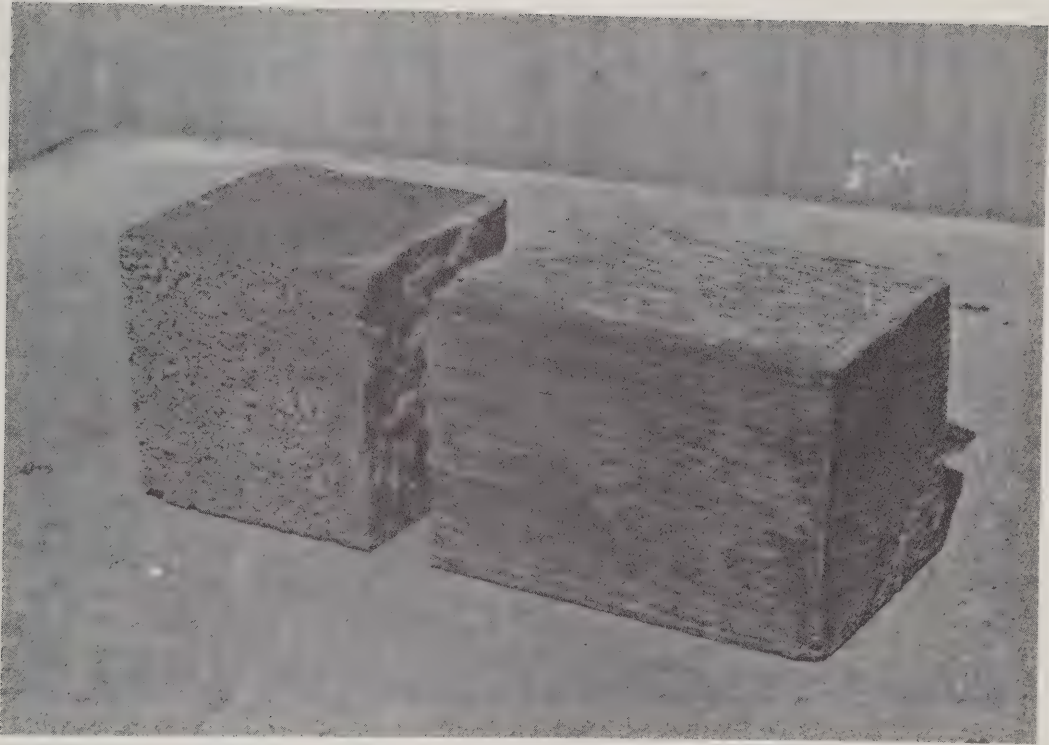


PLATE C.5 Specimen for Grout Tensile Bond
After Testing

At failure the centrifugal force was calculated as for the tensile test by considering only the mass of the separated portion of the specimen and the shear bond strength was evaluated using the beam theory.

C.6 Test Results

The mean value of the tensile bond for all specimens tested was 42 psi, the standard deviation was 20 psi and the coefficient of variation was 0.48. The specimens with poor workmanship had a mean value of 50 psi, a standard deviation of 22.7 and a coefficient of variation of 0.448. Corresponding values for the results of specimens with good workmanship were: mean 31.3 psi, standard deviation of 8.6 psi and a coefficient of variation of 0.274. The reduction in the mean strength is attributed to the 90 minute delay in manufacturing the specimens after mixing the mortar. Poor workmanship increased the coefficient of variation by 17%.

Table C.1 summarizes the results of the 90 mortar tensile bond tests. Table C.2 shows the results of the grout bond tests. Results of a statistical analysis of the data are summarized in Table C.3. This analysis indicates that the tensile bond strength for type S mortar and concrete block has a large coefficient of variation, and that workmanship influences bond strength by 15% - 20%.

Although a large scatter of test results for mortar tensile bond strength was observed, whereas the tensile bond between grout and concrete block was very consistent. The coefficient of variation for the grout bond tests data was 5.0%.

TABLE C.1 Tensile Bond Strength of Type S
Mortar and Concrete Block

No.	Area of Contact in ²	Angular Velocity r.p.m.	Weight of Separated Portion lb.	Calculated Tensile Bond Strength psi
1*	13.14	474	3.13	27.3
2	13.68	425	3.12	21.0
3	14.44	770	2.85	59.6
4	14.05	406	2.80	16.8
5	13.49	531	2.93	35.0
6	14.00	437	3.03	21.1
7	13.31	657	2.90	53.7
8	13.48	512	3.08	30.6
9	13.50	744	3.02	63.2
10	13.49	862	3.00	84.4
11	13.32	669	2.92	50.1
12	13.68	869	3.15	89.0
13	13.67	782	3.11	71.1
14	13.67	640	3.04	46.5
15	14.15	750	3.11	63.3
16	13.32	781	2.84	66.3
17	13.50	545	3.07	34.5
18	13.51	900	2.94	90.0
19	13.50	680	2.97	52.0
20	14.05	807	2.92	69.1
21	14.53	650	3.02	44.8
22	13.68	961	2.95	101.8
23	12.96	659	2.94	50.4
24	13.32	745	2.95	62.9
25	13.13	417	2.98	20.1
26	14.56	804	3.22	73.2
27	13.13	523	2.90	30.9
28	13.86	415	3.11	19.7
29	14.46	708	3.03	53.7
30	14.04	626	2.82	40.2
31	13.25	480	2.83	25.2
32	13.68	981	2.83	101.9
33	13.14	780	2.97	70.2
34	14.04	516	3.24	31.4
35	12.92	540	3.08	35.5
36	12.96	687	3.00	55.9
37	13.32	776	2.95	68.2
38	13.05	397	2.94	18.1
39	13.87	801	3.07	72.6
40	13.68	574	2.83	34.9
41	13.14	627	2.87	43.9
42	13.69	603	2.97	40.3
43	13.31	616	2.85	41.6

Table C.1 Cont'd

No.	Area of Contact in ²	Angular Velocity r.p.m.	Weight of Separated Portion lb.	Calculated Tensile Bond Strength psi
44	12.60	850	2.83	83.0
45	13.59	480	3.14	27.2
46	14.24	696	3.17	55.1
47	12.25	646	2.68	46.7
48	12.96	463	2.86	24.2
49	13.68	583	3.00	38.1
50	13.50	805	3.00	73.5
51**	13.87	401	2.459	34.7
52	13.69	401	2.376	34.5
53	13.88	302	2.471	20.0
54	13.88	357	2.461	27.7
55	14.06	338	2.313	23.3
56	13.51	393	2.509	35.4
57	13.87	388	2.470	34.9
58	13.51	330	2.543	23.1
59	13.51	321	2.340	21.9
60	14.24	303	2.944	23.3
61	13.32	326	2.484	24.5
62	13.14	296	2.518	20.7
63	13.88	368	2.427	29.2
64	14.05	384	2.558	33.3
65	13.51	423	2.398	39.1
66	12.96	322	2.720	27.3
67	13.69	350	2.421	26.7
68	13.51	310	2.504	21.9
69	13.87	393	2.461	33.5
70	13.64	377	2.405	30.7
71	13.87	330	2.377	22.9
72	13.87	364	2.565	30.4
73	13.87	336	2.379	24.0
74	14.04	315	2.966	26.3
75	14.22	375	3.126	38.8
76	13.51	505	2.496	57.9
77	14.05	370	5.505	30.1
78	13.51	426	2.384	39.3
79	13.87	368	2.388	28.6
80	14.81	347	2.335	25.5
81	13.87	436	2.605	40.6
82	13.68	454	2.518	46.5
83	13.69	336	2.597	26.6
84	13.69	509	2.337	54.6
85	13.51	393	2.564	35.8
86	13.69	386	2.609	35.8
87	13.87	352	2.591	29.2
88	13.87	330	2.472	24.3
89	13.69	439	2.431	42.5
90	13.69	380	2.611	34.0

* Specimens 1 - 50 considered of poor workmanship

** Specimens 51 - 90 considered of good workmanship

TABLE C.2 Tensile Bond Strength of
Grout and Concrete Block

No.	Velocity at Failure in r.p.m.	Weight of Separated Grout Kg	Bond Strength psi
1	804	2.914	147
2	764	2.848	133
3	765	2.896	134
4	796	3.808	140
5	798	2.830	140
6	737	2.989	125
7	758	2.945	133
8	774	2.752	135
9	808	2.799	146
10	760	2.901	134
11	811	2.873	153
12	775	2.887	137
13	797	2.864	143
14	797	2.971	149
15	795	2.920	146
16	806	2.682	141
17	795	2.738	138
18	772	2.741	134

TABLE C.3 Statistical Analysis of Test Results

Type of Specimen	Number of Data	Mean Value psi	Standard Deviation psi	Coef. of Variation
Tensile bond of C-Block and type S Mortar	50*	50.0	22.7	0.44
	40**	31.3	8.6	0.274
	90***	42.0	20.0	0.480
Tensile bond of C-Block and Grout	18	139.0	7.0	0.050
Compressive Strength of Mortar Cubes	50	254.5	212.0	0.083

* Specimens considered of poor workmanship

** Specimens considered of excellent workmanship

*** Both series of test data together

TABLE C.4 Tensile Bond Test Data

Mortar Proportions	Test Conditions						Bond Strength psi
	Mortar Flow	Mortar Retentivity	Brick Type	Brick Suction 8 bm.	Reference	Number Specimens	
1C:0.25F.C.:3S	95-100	77	1	Corrected to zero by 1/2 hr. soaking	Stanford Project	10	high 42.5 low 24.7 avg. 37.1
1C:0.25L:3S	95-100	not measured	1	Corrected to zero by 1/2 hr. soaking	"	9	high 36.2 low 18.3 avg. 25.1
1C:0.25L:3S	95-100	77	1	Corrected to zero by 24 hrs. soaking	"	10	high 51.3 low 33.0 avg. 43.5
1C:0.25L:3S	100-110	56	2	10-20	V.P.I. Tests	8	high 36.0 low 1.0 avg. 18.7
1C:0.50L:4.5S	100-110	63	2	10-20	"	8	high 52.0 low 23.0 avg. 40.3
1C:1L:6S	100-110	73	2	10-20	"	8	high 54.0 low 22.0 avg. 35.2
1C:0.50L:4.5S	95-105	66	3	10-20	"	12	high 59.0 low 26.0 avg. 40.8
1C:0.15L:3S	---	---	4	brick set wet	Canadian Tests	5	high 88.0 low 43.0 avg. 65.0
1C:0.5L:4.5S	95-100	not measured	concrete block	not measured	this study	90	high 102.0 low 17.0 avg. 42.2

Adapted from Benjamin^{4,3}.

APPENDIX D

Computer Interaction Diagram

D.1 General

The Fortran program entitled Theory pm has been developed to provide theoretical interaction diagrams for masonry block walls. This program will handle walls rectangular cross-section, with or without reinforcement. Load-moment relationships can also be computed for masonry block walls with all cavities grouted or ungrouted.

The main program in Theory pm relies upon subroutines Prop, Axial, Fsteel and Inerta to obtain information, balance the loads, calculate the maximum moment for a given load and calculate the eccentricity of load required to produce such a moment. In analyzing walls with $h/t > 1.0$ the program calculates the deflection at mid-height using reduced flexural rigidity. The calculated moment includes $P-\Delta$ effects.

Output information provided includes the load and moment relationship for maximum stress on a section.

D.2 Basic Assumptions for Analysis

The following basic assumptions were used for analysis:

- 1) Cross-sections which were plane before loading the member remain plane after the load is applied. Accurate measurements have shown that minor deviations from the plane section occur when the load approaches the failure load. However, theoretical considerations based on this assumption predict test results satisfactorily.

- 2) The stress-strain relationship for steel is linear until the yield strength of the steel is reached after which it is plastic.
- 3) Sufficient bonding of the reinforcing bars to the grout is developed to prevent slipping between the two materials. This ensures that the strain in the embedded bar is the same as that of the surrounding grout.
- 4) The stress-strain relationship of masonry follows a second degree parabola proposed by Hognestad⁴⁴.
- 5) Since the masonry units or the mortar bond may be cracked, due to shrinkage or other reasons, even before a load is applied, it is unsafe to take into account their tensile strength.
- 6) The deflection calculated by the program is based on the wall bending in single curvature.

D.3 Limitations

- 1) The program does not recognize any strength properties given to the section by placing "tie-bars" around the reinforcement.
- 2) The masonry is considered to have strength only in compression. Any tensile strength is neglected.
- 3) When calculating the deflection of the wall, the modulus of elasticity of the wall is taken as that of the masonry unit. The effect of the reinforcement is neglected.
- 4) For reinforced walls the maximum reinforcement should be equal to the balanced reinforcement for flexure.

D.4 Input Data

Figure D.1 shows the required dimensions and physical properties of the materials to be included in the input data involved.

The following data refer to a wall reinforced with 3-#6 bars, 121 in. in height. The strength of the masonry is 2500 psi, the yield strength of steel is 60 ksi and the modulus of elasticity of steel is 29×10^6 psi. The modulus of elasticity of masonry is taken as $1000 f'_m$.

D.5 List of Data

BB = 40 in.	ASC = 0.0 in. ²
H = 7.63 in.	FC = 2500 psi
DD = 3.81 in.	FY = 60,000 psi
AS = 1.33 in. ²	ES = 29×10^6 psi
DC = 3.81 in.	
NB = 3	
AS(1) = .44 in. ²	DS(1) = 3.81 in.
AS(2) = .44 in. ²	DS(2) = 3.81 in.
AS(3) = .44 in. ²	DS(3) = 3.81 in.
DH = 1.25 in.	
HN = 2.	
WH = 5.13	
WL = 5.5	
RL = 121.	

DATA FILE

1] 40., 7.63, 3.81, 3.81, 1.33, 0.,
2] 2500., 60000., 29000000.,
3] 3,
4] .44, 3.81,
5] .44, 3.81,
6] .44, 3.81,
7] 1.25, 2., 5.13, 5.5, 121.,

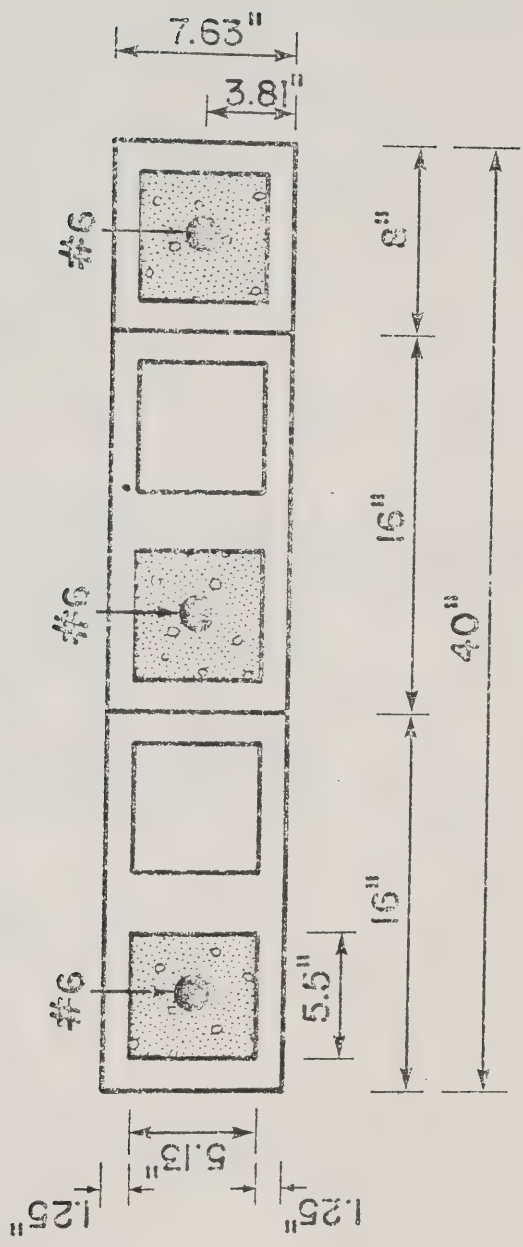


FIG. D-1 Input Dimensions

C PROGRAM THEORY

C THIS PROGRAM CALCULATES THE THEORETICAL P-M DIAGRAM

```

DIMENSION ECN(40),DELTA(40),COR(40),STA(40),YBAR(40)
COMMON N,EOH1(13),PO,BMO,DCS,DTS,RC
COMMON FC,FY,ES,BB,H,DC,DD,AS,NRU,DH,HN,WH,WL,RL
COMMON PHI,EO,J,Z,ECC,EY,FCONCC(20),ASC,EOH(40)
&,FCONST(25)
COMMON X(16000),EC(20),B(20),P(40),BMM(1000),BM(40)
&,FCS(20)
COMMON FST,E(20),NB,DS(20),ASB(20),FSS(20),SBM(20)
COMMON CC(40),XAXIS(40),RIX(40)
2 CALL PROP
FC=FC*0.85
IF (FC.EQ.1000.0) FC=1000.1
ECC = 750. * FC
EO = 0.0038
EY=FY/ES
PO = FC*BB*H +AS*FY - AS*FC - FC*HN*WL*WH
J=0
1 J=J+1
IF (J.EQ.1) GO TO 5
IF (P(J-1).LE.(0.6*PO)) P(J)=P(J-1)-0.034*PO
IF (P(J-1).LE.(0.1*PO)) P(J)=P(J-1)-0.04*PO
IF (P(J-1).GT.(0.6*PO)) P(J)=P(J-1)-0.08*PO
IF(J.EQ.35)P(J) = 0.0
IF (P(J).LE.0.0) P(J)=0.0
IF (J.EQ.2) P(J)=P(J-1)-0.08*PO
CALL AXIAL
IF (P(J).EQ.0.0) BMO=BM(J)
IF(P(J).EQ.0.0)EOH(J) = 0.0
IF (P(J).EQ.0.0) GO TO 7
GO TO 6
5 P(J)=PO
BM(J)=0.0
6 EOH(J)=BM(J)/(P(J))
GO TO 1
7 N=J-1
M=N
NJ=N-1
DO 8 IJ=3,NJ
IF (BM(IJ).GE.BM(IJ-1)) GO TO 8
IF (BM(IJ+1).LE.BM(IJ-1)) GO TO 8
M=M-1
DO 9 JJJ=IJ,NJ
P(JJJ)=P(JJJ+1)
BM(JJJ)=BM(JJJ+1)
9 EOH(JJJ)=EOH(JJJ+1)
8 CONTINUE
N=M+1
DO 10 J=1,N
CALL INERTA

```



```

      STA(J) = SQRT(P(J)/(ECC*RIX(J)))
      COR(J) = COS(STA(J)*RL/2.)
      ECN(J) = EOH(J)*COR(J)
      DELTA(J) = EOH(J) - ECN(J)
      RMEI = BM(J)/(1500000.*RIX(J))
      IF(P(J).EQ.0.0) DELTA(J)=RMEI *(RL**2.)/2.
10  CONTINUE
      WRITE(6,100)
100  FORMAT('1',////////23X,
&'****THEORY INTERACTION DIAGRAM****')
      WRITE(6,101)
101  FORMAT(//19X,'P(O) LBS',6X,'M(O) LB-IN')
      WRITE(6,102) PO,BMO
102  FORMAT(/16X,3E15.7)
      WRITE(6,103)
103  FORMAT(//,19X,'P(J)',15X,'M(J)',10X,'ECN(J)',6X
&,'DELTA(J)')
      DO 20 J=1,N
20  WRITE(6,104) P(J),BM(J),ECN(J),DELTA(J)
104  FORMAT(/16X,4E15.7)
      WRITE(4,105) N
105  FORMAT(I2,',')
      DO 106 J=1,N
106  WRITE(4,107) P(J),BM(J)
107  FORMAT(/2E15.7)
      GO TO 2
      END

      SUBROUTINE PROP

C THIS SUBROUTINE READS AND WRITES THE COLUMN PROPERTIES

      COMMON N,EOH1(13),PO,BMO,DCS,DTS,RC
      COMMON FC,FY,ES,BB,H,DC,DD,AS,NRU,DH,HN,WH,WL,RL
      COMMON PHI,EO,J,Z,ECC,EY,FCONCC(20),ASC,EOH(40)
&,FCONST(25)
      COMMON X(16000),EC(20),B(20),P(40),BMM(1000),BM(40)
&,FCS(20)
      COMMON FST,E(20),NB,DS(20),ASB(20),FSS(20),SBM(20)
      COMMON CC(40),XAXIS(40),RIX(40)
C      FC=CONCRETE STRENGTH
C      FY=STEEL STRENGTH (PSI)
C      ES=STEEL MODULUS OF ELASTICITY (PSI)
C      BB=CROSS SECTION WIDTH (IN)
C      H=CROSS SECTION DEPTH (IN)
C      DC=DISTANCE TO THE COMPRESSION STEEL (IN)
C      DD=DISTANCE TO THE TENSION STEEL (IN)
C      ASC=AREA OF COMPRESSION STEEL (SQ IN)
C      AST=AREA OF TENSION STEEL (SQ IN)
C      AS=TOTAL AREA OF STEEL (SQ IN)
C      DH=DISTANCE TO CLOSE EDGE OF HOLE
C      HN=NUMBER OF HOLES IN WALL
C      WH=WIDTH OF EACH HOLE
C      WL=LENGTH OF EACH HOLE

```



```

C      RL=TOTAL HEIGHT OF COLUMN(IN)
      READ (5,100,END=115) BB,H,DD,DC,AS,ASC
100    FORMAT (6F15.2)
      READ (5,101) FC,FY,ES
101    FORMAT(3F15.7)
      READ (5,102) NB
102    FORMAT (1I3)
      DO 1 I=1,NB
      READ (5,103) ASB(I),DS(I)
103    FORMAT (2F15.7)
      1 CONTINUE
      READ(5,104) DH,HN,WH,WL,RL
104    FORMAT(5F15.3)
      WRITE (6,105)
105    FORMAT ('1',////////30X,'COLUMN CROSS SECTION PROPERTIES
&')
      WRITE (6,106)
106    FORMAT (16X,'FC (PSI)',3X,'FY (PSI)',5X,'ES (PSI)')
      WRITE (6,107) FC,FY,ES
107    FORMAT (/16X,1F6.1,5X,1F7.1,4X,1F10.1)
      WRITE (6,108)
108    FORMAT (//16X,'B(IN)',5X,'H(IN)',5X,'D(IN)',4X,
1'DC(IN)',4X,'AS(SQIN)',3X,'ASC(SQIN)')
      WRITE (6,109) BB,H,DD,DC,AS,ASC
109    FORMAT (/12X,6F10.2)
      WRITE (6,110)
110    FORMAT (//16X,'DH(IN)',5X,'HN(#)',5X,'WH(IN)',5X,
&'WL(IN)',5X,'RL')
      WRITE (6,111) DH,HN,WH,WL,RL
111    FORMAT (/12X,5F10.2)
      WRITE (6,112)
112    FORMAT (//16X,'NB',4X,'ASB(I)',5X,'DS(I)')
      DO 114 I=1,NB
      WRITE (6,113) NB,ASB(I),DS(I)
113    FORMAT (15X,1I3,2F10.2)
114    CONTINUE
      RETURN
115    STOP
      END

```

SUBROUTINE AXIAL

C THIS SUBROUTINE CALCULATES THE MOMENT AFTER BALANCING P

```

COMMON N,EOH1(13),PO,BMO,DCS,DTS,RC
COMMON FC,FY,ES,BB,H,DC,DD,AS,NRU,DH,HN,WH,WL,RL
COMMON PHI,EO,J,Z,ECC,EY,FCONCC(20),ASC,EOH(40)
&,FCONST(25)
COMMON X(16000),EC(20),B(20),P(40),BMM(1000),BM(40)
&,FCS(20)
COMMON FST,E(20),NB,DS(20),ASB(20),FSS(20),SBM(20)
COMMON CC(40),XAXIS(40),RIX(40)
DIMENSION CCC(1000)
PHI=0.0000001

```



```

    PHIH=PHI*H
    II=1
    TEMP = 0.
    CTEMP = 0.
14  E4=0.002
    EINCR=0.002
15  E4=E4-EINCR
    EINCR=EINCR/2.0
16  E4=E4+EINCR
    FCCONC=0.0
    IF (PHI.GT.0.) C=E4/PHI
    IF (PHI.EQ.0.) C=H
    ECO=(C-H)*PHI
    IF (C.GE.H) C=H
    IF (C.LT.H) ECO=0.0
    ASC=0.0
    DO 17 I=1,NB
    IF (DS(I).LE.C) ASC=ASC+ASB(I)
17  CONTINUE
    DX=C/10.
C  CALCULATE THE CONCRETE COMPRESSION BLOCK FORCE
    DO 24 I=1,10
    AI=I
    X(I)=C-AI*DX+DX/2.
    EC(I)=PHI*X(I)+ECO
    ABH = DH + WH
    IF (C.LT.ABH) GO TO 18
    BH=C - (DH + WH)
    IF (X(I).LT.BH) GO TO 20
    DDH=C - DH
    IF (X(I).GT.DDH) GO TO 20
    GO TO 19
18  IF (C.LT.DH) GO TO 20
    AH = C - DH
    IF (X(I).GT.AH) GO TO 20
19  B(I) = BB - (HN * WL)
    GO TO 21
20  B(I) = BB
21  CONTINUE
C  MAXIMUM STRAIN FOR UNCONFINED COMPRESSION EO=0.0038
    IF (EC(I).GT.0.003) GO TO 22
    FCC=FC*(2.0*EC(I)/.003-(EC(I)/.003)**2)
    GO TO 23
22  FCC = FC*(1.-(EC(I) - .003)*18.65)
    IF (EC(I).GT..0038) FCC = 0.0
23  FCONCC(I)=FCC*DX*B(I)
24  FCCONC=FCCONC+FCONCC(I)
    RC=C
    CALL FSTEEL (E4)
C  CHECK FORCE COMPATIBILITY
    PAXIAL = FCCONC + FST
    TOLA=P(J)*0.025
    IF (P(J).EQ.0.0) TOLA=0.001*PO
    TOL=P(J)-PAXIAL

```



```

      IF (TOL.LT.-TOLA) GO TO 15
      IF (TOL.GT.TOLA) GO TO 25
      GO TO 26
25  IF (EC(1).GE.EO) GO TO 30
      IF(EINCR.GE.0.0000001) GO TO 16
26  COMPM=0.0
C   CALCULATE THE MOMENT DUE TO CONCRETE COMPRESSION FORCE
      CC(J) = C
      DO 27 I=1,10
27  COMPM=COMPM+FCONCC(I)*(H/2.-C+X(I))
      SM=0.0
C   CALCULATE THE MOMENT DUE TO THE STEEL FORCES
      DO 28 I=1,NB
      SBM(I)=(FSS(I)-FCS(I)*ASB(I))*ABS(H/2.-DS(I))
28  SM=SM+SBM(I)
C   SUM THE MOMENTS ABOUT THE TENSION STEEL
      BMM(II) = COMPM - SM
      CCC(II) = C
      IF (II.EQ.1) GO TO 29
      IF(BMM(II).LE.0.0) GO TO 31
      TOLBMA=ABS(BMM(II-1)*0.01)
      TTOL = BMM(II-1)*0.0001
      BMTOL=BMM(II)-BMM(II-1)
      BMA = -TOLBMA
      IF(BMTOL.LT.TTOL) GO TO 34
      IF(BMTOL.GT.0.0) GO TO 32
34  IF(BMTOL.GT.BMA) GO TO 33
      IF(TEMP.EQ.0.)CTEMP = CCC(II-1)
      IF(TEMP.EQ.0.)TEMP = BMM(II-1)
      IF (TEMP.LT.BMM(II-1))CTEMP = CCC(II-1)
      IF(TEMP.LT.BMM(II-1))TEMP=BMM(II-1)
      II = II - 2
      PHIH = PHIH - 2*PHINCR
      PHINCR = 4.*(PHINCR/5.)
      GO TO 32
29  PHINCR=0.001
      GO TO 32
30  E4=0.001
      PHIH=PHIH-PHINCR
      PHINCR=PHINCR/5.0
      PHIH=PHIH+PHINCR
      PHI=PHIH/H
      EINCR=EINCR/2.0
      GO TO 16
31  PHIH=PHIH-PHINCR
      PHINCR= (PHINCR/5.0)
32  PHIH=PHIH+PHINCR
      PHI=PHIH/H
      II = II + 1
      GO TO 14
33  BM(J)=BMM(II-1)
      IF(TEMP.GT.BMM(II-1))BM(J)=TEMP
      CC(J) = CCC(II-1)
      IF(TEMP.GT.BMM(II-1))CC(J) = CTEMP

```



```

CONTINUE
RETURN
END

```

SUBROUTINE FSTEEL (E4)

C THIS SUBROUTINE CALCULATES THE THEORY FORCES IN THE STEEL

```

COMMON N,EOH1(13),PO,BMO,DCS,DTS,RC
COMMON FC,FY,ES,BB,H,DC,DD,AS,NRU,DH,HN,WH,WL,RL
COMMON PHI,EO,J,Z,ECC,EY,FCONCC(20),ASC,EOH(40)
&,FCONST(25)
COMMON X(16000),EC(20),B(20),P(40),BMM(1000),BM(40)
&,FCS(20)
COMMON FST,E(20),NB,DS(20),ASB(20),FSS(20),SBM(20)
COMMON CC(40),XAXIS(40),RIX(40)
FST=0.0
C=RC
DO 4 I=1,NB
E(I)=E4-PHI*DS(I)
IF (DS(I).GE.C) GO TO 5
IF (E(I).GT.EO) GO TO 5
FCS(I)=FC*(2.0*E(I)/EO-(E(I)/EO)**2)
FSC=-FCS(I)*ASB(I)
GO TO 8
5 FSC=0.0
FCS(I)=0.0
8 IF(E(I).GE.EY) GO TO 1
IF (E(I).LE.-EY) GO TO 2
GO TO 3
1 FSS(I)=FY*ASB(I)
GO TO 4
2 FSS(I)=-FY*ASB(I)
GO TO 4
3 FSS(I)= E(I)*ES*ASB(I)
4 FST=FST+FSS(I)+FSC
RETURN
END

```

SUBROUTINE INERTA

C THIS SUBROUTINE CALCULATES THE MOMENT OF INERTIA OF
C THE CRACKED SECTION

```

COMMON N,EOH1(13),PO,BMO,DCS,DTS,RC
COMMON FC,FY,ES,BB,H,DC,DD,AS,NRU,DH,HN,WH,WL,RL
COMMON PHI,EO,J,Z,ECC,EY,FCONCC(20),ASC,EOH(40)
&,FCONST(25)
COMMON X(16000),EC(20),B(20),P(40),BMM(1000),BM(40)
&,FCS(20)
COMMON FST,E(20),NB,DS(20),ASB(20),FSS(20),SBM(20)
COMMON CC(40),XAXIS(40),RIX(40)
DIMENSION XJ(1600)
AH = DH + WH

```



```

IF (J.EQ.1) CC(J)=7.63
DX = CC(J)/20.
RIX(J) = 0.
DO 30 I=1,20
AI = I
XJ(I) = CC(J) - AI*DX+DX/2.
ABH = DH + WH
IF(CC(J).LE.DH) GO TO 25
IF(CC(J).GT.ABH) GO TO 12
ABC = CC(J) - DH
IF(XJ(I).GT.ABC) GO TO 25
GO TO 24
12 ABD = CC(J) - ABH
IF(XJ(I).LT.ABD) GO TO 25
ABY = CC(J) - DH
IF(XJ(I).GT.ABY) GO TO 25
GO TO 24
24 B(I) = BB - WL*HN
GO TO 26
25 B(I) = BB
26 RIXX = XJ(I)*XJ(I)*B(I)*DX
RIX(J) = RIX(J) +RIXX
30 CONTINUE
RIX2 = 0.
DO 40 I =1,NB
RNR = ES/ECC -1.
IF(DS(I).GT.CC(J)) RNR=ES/ECC
RM = ABS(DS(I) - CC(J))
RIX2 = RIX2 +ASB(I)*RNR*RM*RM
40 CONTINUE
RIX(J) = RIX(J) + RIX2
RETURN
END

```


B30226